diagnostics

Special Issue Reprint

Lung Cancer

Screening, Diagnosis and Management

Edited by
Fu-Zong Wu

mdpi.com/journal/diagnostics

MDPI

Lung Cancer: Screening, Diagnosis and Management

Lung Cancer: Screening, Diagnosis and Management

Guest Editor

Fu-Zong Wu

MDPI

Basel • Beijing • Wuhan • Barcelona • Belgrade • Novi Sad • Cluj • Manchester

Guest Editor
Fu-Zong Wu
Department of Radiology
Kaohsiung Veterans General
Hospital
Kaohsiung
Taiwan

Editorial Office
MDPI AG
Grosspeteranlage 5
4052 Basel, Switzerland

This is a reprint of the Special Issue, published open access by the journal *Diagnostics* (ISSN 2075-4418), freely accessible at: https://www.mdpi.com/journal/diagnostics/special_issues/Z2JCIURNGF.

For citation purposes, cite each article independently as indicated on the article page online and as indicated below:

Lastname, A.A.; Lastname, B.B. Article Title. *Journal Name* **Year**, *Volume Number*, Page Range.

ISBN 978-3-7258-4483-8 (Hbk)
ISBN 978-3-7258-4484-5 (PDF)
https://doi.org/10.3390/books978-3-7258-4484-5

Contents

About the Editor

Fu-Zong Wu

Fu-Zong Wu, M.D., is the Director of Medical Imaging at Kaohsiung Veterans General Hospital and an Associate Professor at National Yang Ming Chiao Tung University, Taiwan. His expertise includes thoracic imaging, LDCT lung cancer screening, radiomics, and AI-assisted diagnostics. He has led several key studies on risk-adapted LDCT screening strategies in non-smoking Asian populations, contributing to improved early detection while minimizing unnecessary procedures and overtreatment/overdiagnosis. Dr. Wu currently leads interdisciplinary projects integrating imaging biomarkers with deep learning to predict nodule malignancy. He has published widely in leading journals and received multiple research and innovation awards, including recognition from Taiwan's Ministry of Health and Welfare for his contributions to cancer screening policy. Actively engaged in international academic forums, Dr. Wu collaborates with global experts to promote innovation and quality assurance in precision cancer screening.

Preface

Lung cancer remains a critical global health challenge, representing the leading cause of cancer mortality worldwide. Despite advances in therapeutic strategies, the overall prognosis for lung cancer patients remains poor, primarily due to late-stage diagnosis. This Special Issue, "Lung Cancer—Screening, Diagnosis, and Management," brings together a series of innovative studies and comprehensive reviews that aim to address the most urgent needs in lung cancer care—early detection, accurate diagnosis, and personalized management. The scope of this Special Issue spans multiple disciplines, incorporating cutting-edge developments in low-dose computed tomography (LDCT) screening, radiomics, artificial intelligence-assisted diagnostics, and molecular and biomarker-guided tools, in addition to evolving treatment paradigms including immunotherapy and targeted therapy. It also considers the implementation of risk-based and population-tailored screening strategies, especially relevant for non-smoking individuals and underrepresented high-risk groups. The purpose of this collection is to present a curated body of work that reflects the dynamic and collaborative efforts of clinicians, researchers, and public health professionals working to reduce lung cancer burden. The contributing authors, drawn from leading institutions and diverse clinical settings, provide valuable insights based on real-world data, translational research, and multidisciplinary clinical experience. This Special Issue is intended for an audience that includes medical professionals, oncologists, pulmonologists, radiologists, epidemiologists, health policymakers, and researchers dedicated to cancer prevention and care. I extend my sincere gratitude to all of the authors for their contributions and the editorial and peer-review teams for their meticulous efforts in ensuring the scientific integrity and relevance of this issue. It is my hope that the findings and discussions presented herein will support better decision-making, inspire further research, and ultimately contribute to improving outcomes for patients with or at risk of lung cancer.

Fu-Zong Wu
Guest Editor

diagnostics

MDPI

Editorial

Editorial: Advancements and Challenges in Lung Cancer Screening, Diagnosis, and Management

Yi-Chi Hung †, Yun Lin † and Fu-Zong Wu *

Department of Radiology, Kaohsiung Veterans General Hospital, Kaohsiung 813414, Taiwan; ychuang@vghks.gov.tw (Y.-C.H.); ylin@vghks.gov.tw (Y.L.)
* Correspondence: cmvwu1029@gmail.com; Tel.: +886-7-3422121 (ext. 76256)
† Yi-Chi Hung and Yun Lin contributed equally as first authors.

1. Diagnostic Challenges and Innovations

1.1. High Incidence of False Positives in EGFR S768I Mutation Detection Using the Idylla qPCR System in NSCLC Patients

The study highlights a significant issue in detecting the EGFR S768I mutation using the Idylla qPCR system, with a high false-positive rate. This calls for additional validation using alternative methods, such as next-generation sequencing (NGS), to avoid misclassification and ensure appropriate targeted therapy.

1.2. Real-Life Pre-Operative Nodal Staging Accuracy in Non-Small Cell Lung Cancer and Its Relationship with Survival

This multicenter cohort study evaluated the accuracy of preoperative mediastinal nodal staging in NSCLC and its impact on two-year survival. Among the 973 patients, pre- and postoperative staging were concordant in 80%, while 13% were under-staged and 7% were over-staged. Invasive mediastinal staging with EBUS was found to improve staging accuracy. Preoperative understaging was independently associated with higher lung cancer-specific mortality, whereas overstaging had no adverse impact on survival. Accurate nodal staging is crucial for optimal treatment and improved outcomes in patients with potentially curable NSCLC.

1.3. Effectiveness of Apparent Diffusion Coefficient (ADC) Values in Predicting Pathologic Subtypes and Grades in NSCLC

Diffusion-weighted MRI results, particularly ADC values, show promise for differentiating NSCLC subtypes and tumor grades. Higher ADC values were linked to lower tumor aggressiveness, which suggests their potential utility in noninvasive tumor characterization.

1.4. Rare Driver Mutations in Advanced, Oncogene-Addicted NSCLC: A North Italian Real-World Experience

This registry-based study underscores the importance of comprehensive molecular profiling in advanced NSCLC, as rare driver mutations were identified in a substantial subset of patients. These findings support the expansion of targeted therapy beyond common EGFR, ALK, and ROS1 alterations.

2. Advancements in Lung Cancer Screening and Risk Assessment

2.1. A Retrospective Analysis: Investigating Factors Linked to High Lung-RADS Scores in a Nonsmoking, Non-Family History Population

This study provides valuable insights into high-risk nodule characteristics among non-smokers without a family history of lung cancer. Identifying novel risk factors could refine the lung-RADS criteria and improve risk stratification in this patient subgroup.

2.2. Managing Persistent Subsolid Nodules in Lung Cancer: Education, Decision Making, and Impact of Interval Growth Patterns

Persistent subsolid nodules pose a clinical dilemma, and this study emphasizes the role of patient education and shared decision making. The growth patterns of the nodules influence management strategies and balance early interventions against overdiagnosis.

2.3. Predicting the Invasiveness of Pulmonary Adenocarcinomas in Pure Ground-Glass Nodules Using the Nodule Diameter: A Systematic Review, Meta-Analysis, and Validation in an Independent Cohort

The study validated nodule diameter as a predictive marker for invasiveness in pure ground-glass nodules (GGNs), thus, supporting a more individualized follow-up and intervention approach for such lesions.

3. Emerging Therapeutic Strategies

3.1. Early Effects of Bronchoscopic Cryotherapy in Metastatic NSCLC Patients Receiving Immunotherapy: A Single-Center Prospective Study

The study reports that bronchoscopic cryotherapy provides symptomatic relief and potential synergy with immunotherapy in patients with metastatic NSCLC. Further research is needed to validate the long-term survival benefits.

3.2. Improving Outcomes of CT-Guided Malignant Lung Lesion Microwave Ablation by Tract Sealing Using Venous Blood Clot

A novel technique of using autologous venous blood clots for tract sealing post-microwave ablation shows promise in reducing complications such as air leaks and hemorrhage. This approach may improve post-procedural recovery and treatment efficacy.

3.3. Usefulness of Saline Sealing in Preventing Pneumothorax After CT-Guided Biopsies of the Lung

The study highlights the effectiveness of saline sealing in reducing pneumothorax incidence post-CT-guided lung biopsies. This simple yet effective technique can enhance procedural safety in routine clinical practice.

4. Surgical and Radiation Therapy Considerations

4.1. Predictive Value of Clinicopathological Factors to Guide Post-Operative Radiotherapy in Completely Resected pN2-Stage III NSCLC

Identifying patients who benefit most from post-operative radiotherapy (PORT) remains a challenge. This study provides a predictive model that incorporates clinicopathological factors to guide PORT decisions in patients with stage III NSCLC after resection.

4.2. Comparison of Outcomes Between Systematic Lymph Node Dissection and Lobe-Specific Lymph Node Dissection for Stage I NSCLC

This comparative analysis of lymph node dissection techniques in early-stage NSCLC suggests that lobe-specific lymph node dissection may offer comparable oncologic outcomes to systematic dissection while reducing surgical morbidity.

5. Future Directions in Lung Cancer Research

AI-assisted CAD (Computer-Aided Detection): Advanced artificial intelligence algorithms are utilized to enhance the detection of lung nodules in imaging, reduce inter-reader variability among radiologists, and improve overall diagnostic accuracy. By integrating AI-assisted CAD into routine clinical workflows, early detection rates can be optimized while minimizing false positives and unnecessary follow-up procedures [1,2].

Precision Medicine: expanding comprehensive genomic profiling to tailor personalized treatment plans based on individual tumor characteristics. This approach enables the identification of novel biomarkers, facilitates more effective patient stratification, and improves therapeutic outcomes. By incorporating precision medicine strategies, oncologists can optimize targeted therapies, enhance response rates, and minimize the adverse effects in patients with NSCLC and other malignancies [3].

Strategies to Mitigate Overdiagnosis in the Asian Population: developing and implementing risk-adapted lung cancer screening guidelines tailored to the unique epidemiological characteristics of Asian populations, particularly nonsmokers. This includes refining screening criteria based on genetic predisposition, environmental risk factors, and biomarker-based risk stratification to reduce unnecessary interventions and psychological distress, while ensuring that high-risk individuals receive appropriate early detection and management [4].

6. Conclusions

The studies summarized here reflect rapid progress in lung cancer screening, diagnosis, and management shown in Figure 1 and Table 1. However, significant gaps remain, particularly in optimizing screening for nonsmokers, integrating AI into diagnostic workflows, and refining minimally invasive therapies. Future research should focus on precision medicine approaches, AI-driven diagnostics, and balancing early detection while minimizing harm. By addressing these challenges, lung cancer outcomes can be improved, while reducing unnecessary interventions and ultimately enhancing patient care globally. In recent years, Western countries have begun to recognize the importance of lung cancer screening for never-smoking women, as the prevalence of lung cancer in this population continues to rise [5]. Current research on lung cancer screening for never-smokers is primarily conducted in East Asian countries such as Taiwan, China, Japan, and South Korea [6,7]. However, there is a lack of direct evidence from randomized controlled trials (RCTs) on lung cancer screening in Asian never-smokers. Nevertheless, recent evidence-based literature has revealed a significant shift in lung cancer detection among never-smokers undergoing screening [8]. Prior studies have also observed a higher likelihood of overdiagnosis, particularly in never-smokers. Therefore, it is crucial to optimize the effectiveness and quality of lung cancer screening in never-smokers through personalized precision medicine policies and strategies. Future developments are expected to advance clinical lung cancer screening, diagnosis, and treatment toward a more individualized and precision medicine approach [9,10].

The 12 key topics explore the latest advancements and challenges in lung cancer management, including innovations and limitations in diagnostics, emerging risk assessment factors, surgical and radiation therapy strategies, and novel therapeutic approaches like cryotherapy and blood clot sealing. Additionally, future directions emphasize AI-assisted cancer detection, precision medicine, and efforts to reduce overdiagnosis risks, particularly in Asian populations.

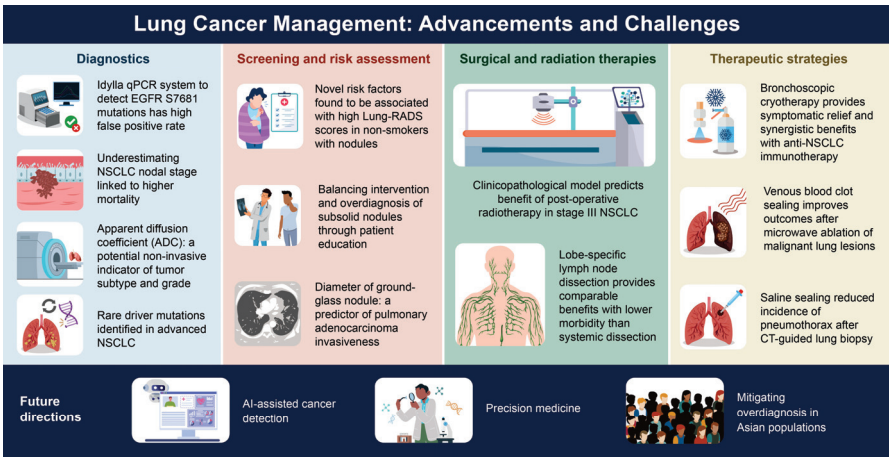

Figure 1. The advancements and challenges in lung cancer management across 12 different domains.

Table 1. Overview of 12 studies on lung cancer: screening, diagnosis, and management.

Category	Study Title	DOI	Key Findings	Clinical Implications
Diagnostic challenges and innovations	High incidence of false positives in EGFR S7681 mutation detection using the idylla qPCR system in NSCLC patients	10.3390/diagnostics15030321	High false-positive rate in detecting EGFR S768l mutation using idylla qPCR	Validation with NGS is necessary to avoid misclassification and ensure proper targeted therapy
	Real-life pre-operative nodal staging accuracy in non-small cell lung cancer and its relationship with survival	10.3390/diagnostics15040430	Pre-operative nodal staging accuracy was 80%, with 13% under-staged and 7% over-staged. Under-staging linked to higher lung cancer-specific mortality	Emphasizes the importance of invasive mediastinal staging (EBUS) for accurate staging and treatment optimization
	Effectiveness of apparent diffusion coefficient values in predicting pathologic subtypes and grade in NSCLC	10.3390/diagnostics14161795	ADC values correlate with NSCLC subtypes and tumor grades, with higher values linked to lower aggressiveness	Suggests ADC values as a potential non-invasive imaging biomarker for NSCLC characterization
Surgical and radiation therapy considerations	Predictive value of clinicopathological factors to guide post-operative radiotherapy in completely resected pN2-stage III NSCLC	10.3390/diagnostics13193095	Developed a predictive model for guiding PORT decisions in stage III NSCLC	Helps identify patients who would benefit most from PORT.
	Comparison of the outcomes between systematic lymph node dissection and lobe-specific lymph node dissection for stage I NSCLC	10.3390/diagnostics13081399	Lobe-specific lymph node dissection showed comparable oncologic outcomes to systematic dissection with lower morbidity	Supports a more tailored surgical approach to reduce complications

Table 1. *Cont.*

Category	Study Title	DOI	Key Findings	Clinical Implications
	Predicting the invasiveness of pulmonary adenocarcinomas in pure ground-glass nodules using the nodule diameter: a systematic review, meta-analysis, and validation in an independent cohort	10.3390/diagnostics14020147	Meta-analysis validated nodule diameter as a predictor of invasiveness in GGNs	Supports individualized follow-up and intervention strategies for GGNs
Emerging therapeutic strategies	Early effects of bronchoscopic cryotherapy in metastatic NSCLC patients receiving immunotherapy: a single-center prospective study	10.3390/diagnostics15020201	Demonstrated symptomatic relief and potential synergy with immunotherapy in metastatic NSCLC	Requires further research to validate long-term survival benefits
	Improving outcomes of CT-guided malignant lung lesion microwave ablation by tract sealing using venous blood clot	10.3390/diagnostics14232631	Autologous venous blood clot sealing reduced air leaks and hemorrhage post-microwave ablation	Enhances safety and recovery post-procedure
	Usefulness of saline sealing in preventing pneumothorax after CT-guided biopsies of the lung	10.3390/diagnostics13233546	Saline sealing effectively reduced pneumothorax incidence post-CT-guided biopsy	Simple, cost-effective technique to improve procedural safety
	Rare driver mutations in advanced, oncogene-addicated NSCLC: a north Italian, real-world, registry experience	10.3390/diagnostics14101024	Identified rare driver mutations beyond common EGFR, ALK, and ROS1 mutations in advanced NSCLC	Supports the need for comprehensive molecular profiling to expand targeted therapy options
Advancements in lung cancer screening and risk assessment	A retrospective analysis: investigating factors linked to high lung-RADS scores in a nonsmoking, non-family history population	10.3390/diagnostics14080784	Identified novel risk factors contributing to high lung-RADS scores in non-smokers	Helps refine risk stratification and improve screening strategies fot this subgroup
	Managing persistent subsolid nodules in lung cancer: education, decision making, and impact of interval growth patterns	10.3390/diagnostics13162674	Highlights the importance of shared decision making and monitoring interval growth in persistent subsolid nodules	Balances early intervention and overdiagnosis concerns to optimize patient outcomes

Author Contributions: Conceptualization, F.-Z.W.; writing—original draft preparation, Y.-C.H., Y.L. and F.-Z.W.; writing—review and editing, Y.-C.H., Y.L. and F.-Z.W.; visualization, F.-Z.W.; supervision, F.-Z.W.; project administration, F.-Z.W. All authors have read and agreed to the published version of the manuscript.

Funding: This study was supported by grants from Kaohsiung Veterans General Hospital, KSVGH-114-062; KSVGH-114-D03-1, National Science and Technology Council, NSTC 113-2314-B-075B-005.

Conflicts of Interest: The authors declare no conflicts of interest.

References

1. Liang, C.H.; Liu, Y.C.; Wu, M.T.; Garcia-Castro, F.; Alberich-Bayarri, A.; Wu, F.Z. Identifying pulmonary nodules or masses on chest radiography using deep learning: External validation and strategies to improve clinical practice. *Clin. Radiol.* **2020**, *75*, 38–45. [CrossRef] [PubMed]
2. Wu, J.; Li, R.; Gan, J.; Zheng, Q.; Wang, G.; Tao, W.; Yang, M.; Li, W.; Ji, G.; Li, W. Application of artificial intelligence in lung cancer screening: A real-world study in a Chinese physical examination population. *Thorac. Cancer* **2024**, *15*, 2061–2072. [CrossRef] [PubMed]
3. Kästner, A.; Kron, A.; van den Berg, N.; Moon, K.; Scheffler, M.; Schillinger, G.; Pelusi, N.; Hartmann, N.; Rieke, D.T.; Stephan-Falkenau, S.; et al. Evaluation of the effectiveness of a nationwide precision medicine program for patients with advanced non-small cell lung cancer in Germany: A historical cohort analysis. *Lancet Reg. Health Eur.* **2024**, *36*, 100788. [CrossRef] [PubMed]
4. Kim, S.Y.; Silvestri, G.A.; Kim, Y.W.; Kim, R.Y.; Um, S.W.; Im, Y.; Hwang, J.H.; Choi, S.H.; Eom, J.S.; Gu, K.M.; et al. Screening for Lung Cancer, Overdiagnosis, and Healthcare Utilization: A Nationwide Population-Based Study. *J. Thorac. Oncol.* **2024**. [CrossRef]
5. Kauczor, H.U.; von Stackelberg, O.; Nischwitz, E.; Chorostowska-Wynimko, J.; Hierath, M.; Mathonier, C.; Prosch, H.; Zolda, P.; Revel, M.P.; Horváth, I.; et al. Strengthening lung cancer screening in Europe: Fostering participation, improving outcomes, and addressing health inequalities through collaborative initiatives in the SOLACE consortium. *Insights Imaging* **2024**, *15*, 252. [CrossRef] [PubMed]
6. Goo, J.M.; Jung, K.W.; Kim, H.Y.; Kim, Y. Potential Overdiagnosis with CT Lung Cancer Screening in Taiwanese Female: Status in South Korea. *Korean J. Radiol.* **2022**, *23*, 571–573. [CrossRef] [PubMed]
7. Hsin-Hung, C.; En-Kuei, T.; Yun-Ju, W.; Fu-Zong, W. Impact of annual trend volume of low-dose computed tomography for lung cancer screening on overdiagnosis, overmanagement, and gender disparities. *Cancer Imaging* **2024**, *24*, 73. [CrossRef] [PubMed]
8. Yang, C.Y.; Lin, Y.T.; Lin, L.J.; Chang, Y.H.; Chen, H.Y.; Wang, Y.P.; Shih, J.Y.; Yu, C.J.; Yang, P.C. Stage Shift Improves Lung Cancer Survival: Real-World Evidence. *J. Thorac. Oncol.* **2023**, *18*, 47–56. [CrossRef] [PubMed]
9. Liu, Y.C.; Liang, C.H.; Wu, Y.J.; Chen, C.S.; Tang, E.K.; Wu, F.Z. Managing Persistent Subsolid Nodules in Lung Cancer: Education, Decision Making, and Impact of Interval Growth Patterns. *Diagnostics* **2023**, *13*, 2674. [CrossRef] [PubMed]
10. Zhou, F.; Zhou, C. Lung cancer in never smokers-the East Asian experience. *Transl. Lung Cancer Res.* **2018**, *7*, 450–463. [CrossRef] [PubMed]

diagnostics

MDPI

Article

Real-Life Pre-Operative Nodal Staging Accuracy in Non-Small Cell Lung Cancer and Its Relationship with Survival

Ahmed Alkarn [1,2], Liam J. Stapleton [1], Dimitra Eleftheriou [3], Laura Stewart [3], George W. Chalmers [1], Ahmad Hamed [2], Khaled Hussein [2], Kevin G. Blyth [4,5], Joris C. van der Horst [1] and John D. Maclay [1,4,*]

[1] Glasgow Royal Infirmary, Glasgow G4 0SF, UK; ahmed.alkarn@mft.nhs.uk (A.A.); liamstapleton@nhs.net (L.J.S.); george.chalmers@nhs.scot (G.W.C.); joris.vanderhorst@nhs.scot (J.C.v.d.H.)
[2] Faculty of Medicine, Assiut University, Assiut 71515, Egypt; prof.ahmad.hamed.assiut@gmail.com (A.H.); khaldhussein@yahoo.com (K.H.)
[3] Department of Statistics, University of Glasgow, Glasgow G4 0SF, UK; d.eleftheriou@lacdr.leidenuniv.nl (D.E.); laura.stewart@ed.ac.uk (L.S.)
[4] Institute of Cancer Sciences, University of Glasgow, Glasgow G4 0SF, UK; kevin.blyth@glasgow.ac.uk
[5] Glasgow Pleural Disease Unit, Queen Elizabeth University Hospital, Glasgow G4 0SF, UK
* Correspondence: john.maclay2@nhs.scot

Abstract: Background/Objectives: The precise staging of non-small cell lung cancer (NSCLC) determines its initial treatment and provides more accurate prognostic information for patients. The aim of this cohort study was to determine pre- and post-operative mediastinal nodal staging agreement and its effect on 2-year survival. **Methods:** A retrospective multi-centre cohort study was performed, using prospectively collected and pre-defined data from weekly lung cancer multidisciplinary team (MDT) meetings in 11 hospitals. Consecutive patients who underwent surgical resection of NSCLC between 2015 and 2017 were eligible. Pre-operative under-staging was defined as a lower pre-operative than post-operative nodal stage, and pre-operative over-staging as a higher pre-operative than post-operative nodal stage. Disparities between pre-operative nodal staging established at MDT and post-surgical nodal staging were determined and associations with subsequent lung cancer-specific 2-year mortality were identified using univariate and multivariate regression. **Results:** A total of 973 patients fulfilled the eligibility criteria. Concordant pre- and post-operative nodal staging was observed in 783/973 (80%), 123/973 (13%) were under-staged pre-operatively and 67/973 (7%) were over-staged. In 173 patients with clinical N1 or N2 disease (in whom invasive mediastinal staging was indicated), staging EBUS was performed in 55/173 (32%). In these patients, younger age and use of staging EBUS were independent predictors of concordant pre- and post-operative staging. In all patients, pre-operative under-staging was independently associated with increased lung cancer-specific 2-year mortality. There was no increased mortality associated with pre-operative nodal over-staging. **Conclusions:** Invasive mediastinal staging with EBUS was independently associated with more accurate pre-operative staging. Pre-operative nodal under-staging was associated with increased lung cancer-specific mortality. Nodal staging accuracy in potentially curable NSCLC is of fundamental importance to ensure patients receive the correct first-line treatment and to improve survival.

Keywords: non-small cell lung cancer; mediastinal staging; endobronchial ultrasound (EBUS); thoracic surgery; survival

1. Introduction

Although the national and international guidelines for the diagnosis and management of lung cancer differ, they all mandate mediastinal staging with endobronchial ultrasound (EBUS), endoscopic ultrasound (EUS) and/or mediastinoscopy for non-small cell lung cancer (NSCLC) if any intrathoracic node is 10 mm or greater or shows FDG uptake on PET-CT scanning [1–3].

In the UK, pre-surgical induction chemotherapy is not common practice due to concerns regarding patients' subsequent fitness for surgery and a similar survival benefit from adjuvant chemotherapy [4]. As such, a common suggestion is that multimodal treatment could be determined by post-operative stage. However, the recent publication of the CheckMate 816 study has fundamentally changed the landscape of treatment for resectable but locally advanced NSCLC [5]. Pre-treatment staging is of fundamental importance to select patients suitable for neoadjuvant chemotherapy plus nivolumab followed by surgery, which confers a significant survival benefit in stage IB-3 disease, irrespective of PD-L1 status. Furthermore, in patients with unresectable stage 3 disease, the PACIFIC study demonstrated a survival benefit in treating stage 3 patients with concurrent chemoradiotherapy plus durvalumab [6]. As such, ensuring the pre-treatment stage is correct will ensure that these patients embark on the correct treatment path from the outset.

Comparing pre-operative clinical staging with post-operative surgical staging based on lymph node resection allows the accuracy of the pre-treatment nodal staging work-up to be objectively assessed. More importantly, such comparisons also allow the impact of discordant pre-operative staging to be quantified and the factors associated with this identified and addressed. A recent Dutch audit reported an agreement between pre- and post-surgical nodal staging of 79% [7]. In recent years, staging EBUS +/− EUS alone has been used in place of mediastinoscopy and has been shown to be non-inferior to both procedures combined in diagnosing unforeseen N2 disease with less morbidity [8].

The aim of this retrospective cohort study was to determine the level of concordance between pre- and post-operative mediastinal nodal staging in a cohort of surgically resected NSCLC patients assessed using modern staging investigations. We also sought to identify any impact of discordant nodal staging on lung cancer-specific 2-year mortality.

2. Patients and Methods

2.1. Patients

Consecutive patients diagnosed in the West of Scotland (a region including 11 centres with a mix of both university teaching and district general hospitals comprising 7 multidisciplinary teams) were included. Cases were eligible if they were diagnosed with NSCLC between 1 January 2015, and 31 December 2017 and underwent surgical resection as first treatment. Cases were excluded if pre-operative staging was not recorded and/or no PET-CT was performed (Figure 1). These data were prospectively collected locally by clinical audit staff in each NHS Board from diagnosis to definitive treatment in accordance with the nationally agreed-upon Quality Performance Indicator dataset and definitions, and storage of these data for future analysis is approved nationally. These routine data were then matched with cause-of-death data from death certification held by NHS National Services Scotland. The Caldicott Guardian oversees the storage and use of these patient identifiable data for audit and research purposes. Permissions for specific analyses were sought a priori and were approved by the local Caldicott Guardian. Patients' electronic clinical records were reviewed to identify lung cancer recurrence in all patients at two years post-surgery. In patients deemed to have died of other causes, electronic clinical records were reviewed to confirm this. Patients who died either during their admission for lung cancer resection or within 30 days of their discharge were excluded from the survival anal-

yses. Details regarding invasive mediastinal staging and any missing data were extracted from electronic patient records. Performance status was defined according to the Eastern Cooperative Oncology Group scale [9]. For statistical analyses, patients were classified into 3 histopathological groups: squamous cell carcinoma, adenocarcinoma and other. Wait-time until surgery was defined as the number of days between the first radiological diagnosis by CT and resection. The follow-up period for survival was 2 years from the date of surgery.

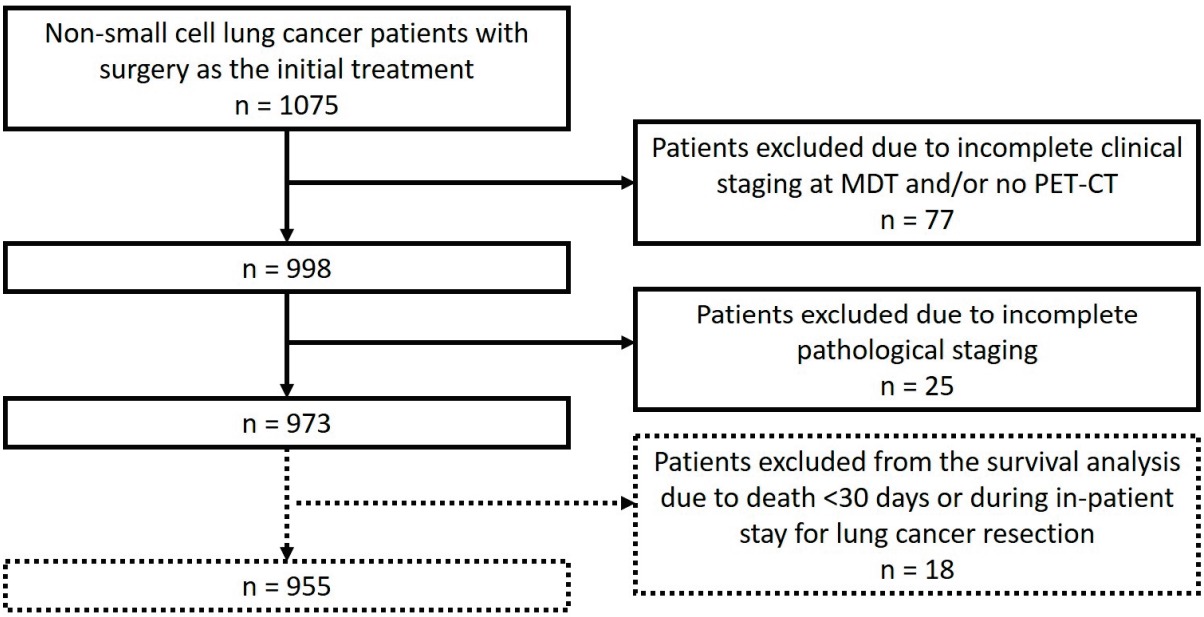

Figure 1. Patients included in the analyses.

The pre-operative stage was defined as the stage determined prior to surgery after all pre-operative staging investigations were complete, including PET-CT and any invasive mediastinal staging procedures e.g., EBUS, EUS or mediastinoscopy, usually established at multi-disciplinary team meetings. In general, only patients with N0, N1 or single-station N2 disease were deemed suitable for surgery. Post-operative stage was based on the pathological examination of the resected tumour and lymph nodes. Patients were staged using the TNM Classification of Malignant Tumours, 7th Edition [10]. Concordant (or accurate) staging was defined as identical pre- and post-operative nodal stages. Regarding discordant or inaccurate staging, pre-operative under-staging was defined as a lower pre-operative than post-operative nodal stage and pre-operative over-staging was defined as a higher pre-operative than post-operative nodal stage.

2.2. Statistical Analyses

The data are reported as simple proportions (%), mean (SD) if normally distributed or median (IQR) if not. A univariate analysis for factors associated with discordant clinical N staging was performed in a pre-planned sub-group analysis of patients with pre-operative N1 and N2, in whom invasive mediastinal staging was indicated according to international guidelines [1–3], using Chi-squared and Mann–Whitney U tests as appropriate; variables with a $p < 0.1$ were subsequently entered into a binary logistic regression analysis focussed on the same outcome measure.

A competing relative risk analysis (Fine and Gray) was performed to examine cancer-specific 2-year mortality in all patients, as a proportion of patients in our cohort had died of non-cancer-related causes [11]. This allowed us to determine the factors independently

associated with mortality, including nodal staging concordance and post-operative staging, presented with hazard ratios with 95% confidence intervals.

IBM® SPSS® Statistics 25.0 (Armonk, NY, USA) and R 4.1.1 (Vienna, Austria) were used for the statistical analyses. $p < 0.05$ was considered to indicate significance.

3. Results

The study flowchart is presented in Figure 1. A total of 973 patients with clinical stage IA to IIIB NSCLC underwent surgical resection as an initial treatment between 2015 and 2017 and fulfilled all eligibility criteria. The exclusions are documented in Figure 1. Eighteen patients were excluded from the survival analyses as they died in the immediate post-operative period. The baseline characteristics of the study population are summarized in Table 1. The mean (SD) age was 69 (8.7), and there was a slight female predominance (Table 1).

Table 1. Patient characteristics.

	Total	Accurate Nodal Staging	Pre-Operative Over-Staging	Pre-Operative Under-Staging
Number of patients	973	783 (80%)	67 (7%)	123 (13%)
Mean age (SD)	69 (9)	68 (9)	69 (8)	69 (8)
Sex, n (%)				
Male	443 (46%)	360 (46%)	27 (40%)	56 (46%)
Female	530 (54%)	423 (54%)	40 (60%)	67 (54%)
Site of the tumour, n (%)				
Main bronchus	13 (1%)	7 (1%)	1 (1%)	5 (4%)
Upper lobe	586 (60%)	475 (61%)	39 (58%)	72 (58%)
Middle lobe	39 (4%)	32 (4%)	2 (3%)	5 (4%)
Lower lobe	335 (34%)	269 (34%)	25 (37%)	41 (33%)
Median (IQR) days from CT to surgery	74 (56–97)	75(56–98)	69(53–84)	70(54–96)
Surgical procedure, n (%)				
Lobectomy	836 (86%)	679 (87%)	58 (87%)	99 (80%)
Pneumonectomy	42 (4%)	18 (3%)	6 (9%)	18 (15%)
Sublobar resection	95 (10%)	86 (11%)	3 (4%)	6 (5%)
Histology, n (%)				
Squamous	337 (35%)	261 (33%)	32 (48%)	44 (36%)
Adenocarcinoma	553 (57%)	463 (60%)	29 (43%)	61 (50%)
Other	83 (9%)	59 (8%)	6 (9%)	18 (15%)
Pre-operative TNM stage, n (%)				
Stage I	655 (67%)	587 (75%)	0	68 (55%)
Stage II	227 (23%)	146 (19%)	36 (54%)	45 (37%)
Stage III	91 (9%)	50 (6%)	31 (46%)	10 (8%)
Pre-operative T stage, n (%)				
T1	528 (54%)	453 (58%)	21 (31%)	54 (44%)
T2	321 (33%)	245 (31%)	28 (42%)	48 (39%)
T3	102 (11%)	72 (9%)	14 (21%)	16 (13%)
T4	22 (2%)	13 (2%)	4 (6%)	5 (4%)
Pre-operative N stage, n (%)				
N0	800 (82%)	708 (90%)	0	92 (75%)
N1	119 (12%)	44 (6%)	44 (66%)	31 (25%)
N2	54 (6%)	31 (4%)	23 (34%)	0
2-year lung cancer mortality, n (%)				
Alive	752 (77%)	633 (81%)	52 (78%)	67 (54%)
Died due to lung cancer	146 (15%)	91 (12%)	11 (16%)	44 (36%)
Post-operative death	18 (2%)	11 (1%)	2 (3%)	5 (4%)
Died due to other causes	57 (6%)	48 (6%)	2 (3%)	7 (6%)

NSCLC: non-small cell lung cancer.

3.1. Accuracy of Pre-Operative Nodal (N) Stage Compared to Post-Operative (N) Stage

Pre- and post-operative N stages were concordant in 783/973 of patients (80%, Table 2). Pre-operative stage N0 was associated with the most accurate pre-operative staging, with 89% concordance, in comparison to stages N1 and N2 (37% and 58%, respectively). There was a higher rate of pre-operative nodal under-staging in patients undergoing pneumonectomy than in those treated by lobectomy or sublobar resection (40% vs. 14% vs. 2%; χ^2 51.2, $p < 0.001$). More patients had three or more N2 nodes resected at pneumonectomy, compared to lobar or sublobar resections (98% vs. 85% vs. 38%, respectively; χ^2 273.3, $p < 0.001$).

Table 2. Agreement between clinical and pathologic nodal stage.

		Post-Operative N Stage				
		pN0	**pN1**	**pN2**	**Total**	**Accuracy of Pre-Operative Staging**
Pre-operative N stage	N0	708	54	38	800	89%
	N1	44	44	31	119	37%
	N2	15	8	31	54	58%
Total		767	106	100	973	

White: accurately staged; light grey: pre-operative over-staging; dark grey: pre-operative under-staging.

3.2. Factors Affecting Nodal Staging Accuracy in Patients with Pre-Operative N1/N2 Staging

173/973 (18%) patients had pre-operative N1 or N2 suitable for invasive mediastinal staging. While all patients had PET-CT scans performed, among those patients, staging EBUS was performed in 55/173 (32%) patients and mediastinoscopy was performed in 5/173 (3%) patients. In these 173 patients, after adjusting for covariates, younger age (OR 1.05, 95% CI = 1.01–1.09, $p = 0.02$, Table 3) and staging EBUS (OR 2.0, 95% CI = 1.01–4.05, $p < 0.05$) were independent predictors of staging accuracy. In this analysis, sex, performance status, location of the primary tumour, type of surgical procedure, histology, waiting time until surgery and the diagnosis year were not significant on the univariate analysis.

Table 3. Regression analysis of factors affecting lung cancer-related mortality in patients undergoing surgery for non-small cell lung cancer.

		Hazard Ratio	**95% Confidence Interval**	***p*-Value**
Age		1.01	0.99–1.03	0.28
Sex	Female	1 (ref)		
	Male	1.17	0.83–1.62	0.37
Pathological T stage	T1	1 (ref)		
	T2	1.26	0.83–1.90	0.28
	T3	2.74	1.71–4.38	<0.001
	T4	7.57	4.04–14.17	<0.001

Table 3. *Cont.*

			Hazard Ratio	95% Confidence Interval	*p*-Value
Pathological N stage by post-operative nodal staging concordance	N0	pre-operative stage concordant	1 (ref)		
		pre-operative over-staging	1.17	0.58–2.37	0.65
	N1	pre-operative stage concordant	1.79	0.85–3.78	0.13
		pre-operative over-staging	1.43	0.20–10.36	0.72
		pre-operative under-staging	2.85	1.57–5.18	<0.001
	N2	pre-operative stage concordant	2.26	1.02–4.97	0.04
		pre-operative under-staging	5.24	3.33–8.27	<0.001
Adjuvant chemotherapy		Yes	1 (ref)		
		No	1.58	0.96–2.61	0.07

Performance status, type of surgical procedure, number of nodes sampled at surgery, time to surgery and pathological subtype were not significant.

3.3. Association of Pre-Operative Nodal Under- and Over-Staging on Survival

Of the patients with concordant pre- and post-operative stages, 81% were alive and 12% died due to lung cancer (Table 1). In the patients with pre-operative under-staging, 54% were alive and 36% died due to lung cancer. In the survival analysis, as expected, the hazard ratio increased with a higher T stage ($p < 0.001$; Table 3). In patients with post-operative N1 and N2 disease, pre-operative nodal under-staging conferred an increased risk of lung cancer-related mortality in comparison to those with accurate pre-operative staging, independent of T stage (N0 concordant as reference; N1 staging concordance HR 1.8, 95%CI 0.8–3.8, $p = 0.13$ vs. N1 nodal under-staging HR 2.9, 95%CI 1.6–5.2, $p < 0.001$; N2 staging concordance HR 2.3, 95%CI 1.02–5.0, $p = 0.04$ vs. N2 nodal under-staging HR 5.2, 95%CI 3.3–8.3, $p < 0.001$; Figure 2). Using adjusted estimates, pre-surgical N2 nodal under-staging had increased mortality in comparison to concordant pre- and post-operative N2 nodal staging (HR 2.33, 95%CI 1.01–5.3, $p < 0.05$). Not receiving adjuvant chemotherapy was associated with a trend suggesting increased mortality (HR 1.6, 95%CI 0.96–2.6, $p = 0.07$). Age, sex, performance status, type of surgical procedure, number of nodes sampled at surgery, time to surgery and pathological subtype had no association with lung cancer-specific mortality on the univariate analysis. There was no association between pre-operative over-staging and lung cancer-specific mortality (Table 3).

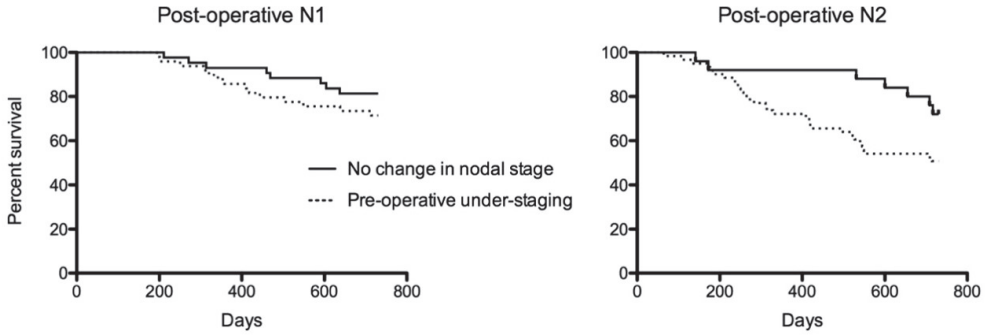

Figure 2. Post-operative survival by nodal staging accuracy.

4. Discussion

Invasive mediastinal staging for radically treatable non-small cell lung cancer (NSCLC) is recommended by all international guidelines, yet its utility remains in question by some respiratory physicians and surgeons. A recent survey of pulmonologists and thoracic surgeons in the USA reported barriers to the application of these guidelines. The predominant reasons for this lack of guideline adherence appearedto be either perceived lack of evidence for systematic staging or inadequate technical expertise [12]. Other barriers to invasive mediastinal staging included potential time delays for additional investigations prior to treatment and institutional reliance on imaging alone for mediastinal staging. Certainly, in this cohort, there was marked variability in practice, with only 35% of patients undergoing surgery with pre-operative N1 or N2 disease and having this confirmed with EBUS or mediastinoscopy, with the majority of patients staged using staging CT and PET-CT alone. These differences in practice may be explained by issues with technical expertise which may in turn influence multidisciplinary team (MDT) decision making with over-reliance on imaging for staging; this would explain the nodal over-staging in this cohort. Whilst MDT meetings allow for shared decision making across specialties in terms of making choices regarding treatment, specialty-specific expertise may influence diagnosis, staging and treatment choices. This heterogeneity may be reduced with regular education, audit of quality performance indicators and external peer review of MDT meetings [13].It is recognized however that there are circumstances in which accurate mediastinal nodal staging is more challenging. In Asian countries, where the proportion of patients with adenocarcinoma is higher both in screened and non-screened populations [14], the sensitivity of PET-CT is lower, with increased specificity in comparison with western countries [15].

We have found that patients with inaccurate pre-operative nodal staging have increased lung cancer-related mortality at 2 years in comparison to those with pre- and post-operative nodal staging concordance. Therefore, our data add to the evidence base supporting invasive staging in patients planned for treatment with radical intent with possible nodal disease on imaging. In addition, with the recent publication and recommendation of neo-adjuvant treatment in patients with stage 1B-3 NSCLC, accurate pre-operative staging is essential to ensure patients with resectable disease receive the optimum treatment. While the introduction of lung cancer screening will result in more early-stage lung cancers being diagnosed, the NELSON study has indicated that there will be a reduction in stage 4 presentations and unchanged proportions of stage 2 and 3 patients who would require mediastinal staging [16].

4.1. Accuracy of Pre-Operative Nodal Staging

In this study, the agreement between pre- and post-operative nodal staging was 80%; 13% of patients had a higher post-operative nodal stage, and 7% had unforeseen N2. In a similar study from the Netherlands, Heineman reported very similar findings to those presented in this manuscript using the Dutch Lung Surgery Audit, with an accuracy of nodal staging of 79%, 15% pre-operative nodal under-staging and 6% unforeseen N2, using modern staging techniques [7]. In the era of neo-adjuvant and adjuvant systemic treatment in the context of radical treatment, the importance of pre-operative staging accuracy in confirming (or excluding) nodal involvement prior to surgery will alter a patient's treatment strategy.

Whilst 89% of patients with pre-operative N0 status had concordant post-operative staging, in the patients with pre-operative N1 and N2, concordant staging was only present in 37% and 58%, respectively. Younger age and the utilisation of staging EBUS were independently associated with staging accuracy. Pneumonectomy was associated with a higher proportion of discordant staging in comparison to lobectomy and sublobar resection.

This is important as generally patients with known pre-operative N2 disease are considered unattractive candidates for pneumonectomy. On closer review of the 18 patients upstaged at pneumonectomy, 10 were upstaged from N0 to N1. Of these, all 10 were N1 by direct extension with a N1 node found in the main specimen. Eight were upstaged from N1 to N2, and all eight had occult N2 disease (not FDG-avid). This highlights the importance of systematic staging EBUS, particularly in patients undergoing a planned pneumonectomy. In addition, a higher number of lymph nodes were resected at pneumonectomy in comparison to lobectomy and sublobar resection, thus increasing the likelihood of discovering occult nodal disease. Similar to our cohort, Edwards et al. described that a higher proportion of patients who underwent pneumonectomy had at least three N2 nodal stations sampled, in comparison to lobectomies and sublobar resections [17]. Therefore, pre-operative under-staging may be underestimated in patients undergoing lobectomy and sublobar resection due to less thorough lymph node resection. It is important to note that, although patients undergoing pneumonectomy had proportionally higher-stage disease, neither type of surgery nor number of lymph nodes dissected were associated with increased lung cancer-specific mortality.

Pre-operative over-staging occurs when FDG-avid lymph nodes on PET-CT are not confirmed to be malignant pathologically. The false-positive rate of PET-CT for mediastinal lymph nodes is up to 40%. Consistent with this, in this cohort, there was no increased mortality between pre-operative nodal over-staging and patients with concordant staging, confirming it is not acceptable to rely on the results of the PET-CT alone. Given the gold standard of neo-adjuvant treatment of patients with resectable locally advanced lung cancer, assuming lymph node involvement due to FDG uptake will result in over-staging and patients receiving potentially toxic and expensive pre-operative treatment that is not indicated. In the SEISMIC study, Steinfort et al. reported a reduction in the volume of mediastinal disease in 25% of patients planned for radical radiotherapy who underwent systematic EBUS staging, which resulted in either a smaller volume treated or a switch of treatment to surgery. In addition, occult N2 nodes were discovered in 12% of patients, resulting in a change in treated volume [18]. As such, nodal over-staging will result in patients either being considered for inappropriate neo-adjuvant or adjuvant treatment in the radical treatment setting or could deem patients unsuitable for radical treatment at all.

4.2. Effect of Nodal Staging Accuracy on Lung Cancer-Specific Mortality

We have found that pre-operative under-staging is independently associated with increased risk of lung cancer-specific mortality at two years in comparison with pre-operative concordant nodal staging for the same pathological nodal stage. This is an important finding for several reasons. Principally, it confirms the relevance and importance of the recommendations of international guidelines, specifically regarding the application of invasive mediastinal staging when indicated.

The increased risk of mortality was present in patients with both unexpected N1 and N2 disease, and on the regression analysis, the effect size was greater in patients with unexpected N2 after adjusting for other relevant variables. Two recent studies from the Netherlands also highlighted the importance of systematic staging to guide appropriate treatment. Bousema et al. found evidence of significant unexpected N2 disease in patients with nodal imaging appearances that would indicate invasive mediastinal staging [19]. In addition, the SCORE study found that systematic mediastinal staging was more effective than targeted staging based on CT and PET-CT appearances [20]. As regards survival, in Lung-BOOST, a post hoc analysis of 133 patients with NSCLC, the group randomized to undergo EBUS-TBNA as their first test had an improvement in overall survival in comparison to patients undergoing conventional diagnosis and staging [21]. However, in a

meta-analysis, Navani and colleagues found that there was no independent association between inaccurate clinical TNM staging and all-cause mortality [22]. In the current radical treatment landscape for NSCLC, identifying patients appropriate for neo-adjuvant and adjuvant treatment by determining an accurate stage is essential to improve survival, particularly in patients with locally advanced disease.

The reasons that pre-operative under-staging may be associated with increased mortality remain unclear. One explanation is that patients with disease clearly defined on PET and mediastinal staging are more straightforward to treat in comparison with occult disease that is not delineated using current staging techniques. It is currently not known if patients with occult N2 disease have a poorer prognosis in comparison to patients with clearly evident N2 disease. Alternatively, it is possible that in centres where staging is more thorough, the delivery of treatment may also be more appropriate. Typically, in patients proven to have multi-station N2 disease, patients are more appropriately treated with radical chemoradiotherapy than surgical resection. In addition, if a surgeon is aware of specific nodal involvement prior to resection, then they will be more likely perform a more thorough lymphadenectomy to try and ensure complete clearance of disease.

4.3. Strengths and Limitations

One of the major strengths of this study is completeness of data. Consecutive patients diagnosed with lung cancer across multiple hospital sites and treated with surgery in 2015–2017 were included. However, there was a lower than recommended use of invasive staging modalities in our study; this may be representative of the variability of adherence to international guidelines on mediastinal staging outside of large teaching centres. Indeed, this is likely to explain the proportion of patients who were over-staged pre-operatively. This variability did enable us to demonstrate that staging with EBUS-TBNA is an independent predictor of pre- and post-operative intrathoracic nodal staging concordance.

There are well-described limitations of using routine death certificate data for cause-specific mortality. However, using electronic patient records, we were able to establish evidence of lung cancer recurrence in all patients with lung cancer recorded as cause of death, and the non-lung cancer causes of deaths were also reviewed and confirmed. In our study, around a third of patients who died within 2 years of surgery were confirmed to have a cause of death other than lung cancer.

5. Conclusions

Mediastinal staging with EBUS was independently associated with pre- and post-operative staging concordance. Pre-operative under-staging was associated with higher risk of lung cancer-specific mortality in comparison to concordant pre-and post-operative nodal staging. Pre-operative nodal staging accuracy in potentially curable non-small cell lung cancer is of fundamental importance to ensure patients receive the correct first-line treatment and to improve survival.

Author Contributions: Conception and design: A.A., K.G.B., J.C.v.d.H. and J.D.M. Acquisition, analysis or interpretation of data: A.A., D.E., L.S., L.J.S., J.D.M. and J.C.v.d.H. Drafting and revision of the manuscript: A.A., D.E., L.S., L.J.S., G.W.C., A.H., K.H., K.G.B., J.C.v.d.H. and J.D.M. All authors have read and agreed to the published version of the manuscript.

Funding: This research received no external funding.

Institutional Review Board Statement: These data were prospectively collected locally by clinical audit staff in each NHS Board from diagnosis to definitive treatment in accordance with the nationally agreed Quality Performance Indicator dataset and definitions, and storage of these data for future analysis is approved nationally. These routine data were then matched with cause-of-death data from

death certification held by NHS National Services Scotland. The Caldicott Guardian oversees the storage and use of these patient-identifiable data for audit and research purposes. Permissions for specific analyses were sought a priori and were approved by the local Caldicott Guardian. Formal ethical approval was not necessary.

Informed Consent Statement: Formal informed consent was waived as the data used in this manuscript were routinely collected for audit purposes, historic and retrospective. Approval for the analyses was granted by the Calidicott Guardian.

Data Availability Statement: The datasets presented in this article are not readily available because they are only available on application to the West of Scotland Cancer Network (WOSCAN). Requests to access the datasets should be directed to the WOSCAN audit team.

Acknowledgments: J.M. is an NRS Senior Research Fellow funded by the Chief Scientist Office, and A.A. received support from the Egyptian Government to undertake a research fellowship in the UK.

Conflicts of Interest: There are no specific conflicts of interest related to this manuscript. J.M. has received fees for lectures and advisory boards from Astra Zeneca. J.V.D.H. has received fees for lectures and an advisory board from Astra Zeneca and for teaching and travel from Fujinon. The other authors have no conflicts of interest to declare.

References

1. National Institute for Health and Care Excellence. Lung Cancer: Diagnosis and Management (NICE Guideline 122). 2019. Available online: https://www.nice.org.uk/guidance/NG122 (accessed on 25 October 2022).
2. De Leyn, P.; Dooms, C.; Kuzdzal, J.; Lardinois, D.; Passlick, B.; Rami-Porta, R.; Turna, A.; Van Schil, P.; Venuta, F.; Waller, D.; et al. Revised ESTS guidelines for preoperative mediastinal lymph node staging for non-small-cell lung cancer. *Eur. J. Cardio-Thorac. Surg.* **2014**, *45*, 787–798. [CrossRef] [PubMed]
3. Silvestri, G.A.; Gonzalez, A.V.; Jantz, M.A.; Margolis, M.L.; Gould, M.K.; Tanoue, L.T.; Harris, L.J.; Detterbeck, F.C. Methods for staging non-small cell lung cancer: Diagnosis and management of lung cancer, 3rd ed: American College of Chest Physicians evidence-based clinical practice guidelines. *Chest* **2013**, *143*, e211S–e250S. [CrossRef]
4. Lim, E.; Harris, G.; Patel, A.; Adachi, I.; Edmonds, L.; Song, F. Preoperative versus postoperative chemotherapy in patients with resectable non-small cell lung cancer: Systematic review and indirect comparison meta-analysis of randomized trials. *J. Thorac. Oncol.* **2009**, *4*, 1380–1388. [CrossRef] [PubMed]
5. Forde, P.M.; Spicer, J.; Lu, S.; Provencio, M.; Mitsudomi, T.; Awad, M.M.; Felip, E.; Broderick, S.R.; Brahmer, J.R.; Swanson, S.J.; et al. Neoadjuvant Nivolumab plus Chemotherapy in Resectable Lung Cancer. *N. Engl. J. Med.* **2022**, *386*, 1973–1985. [CrossRef]
6. Antonia, S.J.; Villegas, A.; Daniel, D.; Vicente, D.; Murakami, S.; Hui, R.; Yokoi, T.; Chiappori, A.; Lee, K.H.; de Wit, M.; et al. Durvalumab after Chemoradiotherapy in Stage III Non–Small-Cell Lung Cancer. *N. Engl. J. Med.* **2017**, *377*, 1919–1929. [CrossRef] [PubMed]
7. Heineman, D.J.; Berge, M.G.T.; Daniels, J.M.; Versteegh, I.; De Mheen, P.J.M.-V.; Wouters, M.W.; Schreurs, W.H. The Quality of Staging Non-Small Cell Lung Cancer in the Netherlands: Data From the Dutch Lung Surgery Audit. *Ann. Thorac. Surg.* **2016**, *102*, 1622–1629. [CrossRef] [PubMed]
8. Bousema, J.E.; Dijkgraaf, M.G.; van der Heijden, E.H.; Verhagen, A.F.; Annema, J.T.; van den Broek, F.J. MEDIASTrial Study Group. Endosonography With or Without Confirmatory Mediastinoscopy for Resectable Lung Cancer: A Randomized Clinical Trial. *JCO* **2023**, *41*, 3805–3815. [CrossRef]
9. Oken, M.M.; Creech, R.H.; Tormey, D.C.; Horton, J.; Davis, T.E.; McFadden, E.T.; Carbone, P.P. Toxicity and response criteria of the Eastern Cooperative Oncology Group. *Am. J. Clin. Oncol.* **1982**, *5*, 649–655. [CrossRef]
10. Groome, P.A.; Bolejack, V.; Crowley, J.J.; Kennedy, C.; Krasnik, M.; Sobin, L.H.; Goldstraw, P. The IASLC Lung Cancer Staging Project: Validation of the proposals for revision of the T, N, and M descriptors and consequent stage groupings in the forthcoming (seventh) edition of the TNM classification of malignant tumours. *J. Thorac. Oncol.* **2007**, *2*, 694–705. [CrossRef] [PubMed]
11. Fine, J.P.; Gray, R.J. A Proportional Hazards Model for the Subdistribution of a Competing Risk. *J. Am. Stat. Assoc.* **1999**, *94*, 496–509. [CrossRef]
12. Henderson, L.M.; Farjah, F.; Detterbeck, F.; Smith, R.A.; Silvestri, G.A.; Rivera, M.P. Pretreatment Invasive Nodal Staging in Lung Cancer: Knowledge, Attitudes, and Beliefs Among Academic and Community Physicians. *Chest* **2022**, *161*, 826–832. [CrossRef] [PubMed]
13. Winters, D.A.; Soukup, T.; Sevdalis, N.; Green, J.S.A.; Lamb, B.W. The cancer multidisciplinary team meeting: In need of change? History, challenges and future perspectives. *BJU Int.* **2021**, *128*, 271–279. [CrossRef] [PubMed]

14. Wu, F.Z.; Kuo, P.L.; Huang, Y.L.; Tang, E.K.; Chen, C.S.; Wu, M.T.; Lin, Y.P. Differences in lung cancer characteristics and mortality rate between screened and non-screened cohorts. *Sci. Rep.* **2019**, *9*, 19386. [CrossRef] [PubMed]
15. Schmidt-Hansen, M.; Baldwin, D.R.; Hasler, E.; Zamora, J.; Abraira, V.; Roqué IFiguls, M. PET-CT for assessing mediastinal lymph node involvement in patients with suspected resectable non-small cell lung cancer. *Cochrane Database Syst. Rev.* **2014**, *11*, CD009519. [CrossRef]
16. de Koning, H.J.; van der Aalst, C.M.; de Jong, P.A.; Scholten, E.T.; Nackaerts, K.; Heuvelmans, M.A.; Lammers, J.J.; Weenink, C.; Yousaf-Khan, U.; Horeweg, N.; et al. Reduced Lung-Cancer Mortality with Volume CT Screening in a Randomized Trial. *N. Engl. J. Med.* **2020**, *382*, 503–513. [CrossRef] [PubMed]
17. Edwards, T.; Balata, H.; Elshafi, M.; Foden, P.; Bishop, P.; Fontaine, E.; Jones, M.; Krysiak, P.; Rammohan, K.; Shah, R.; et al. Adequacy of Intraoperative Nodal Staging during Surgical Resection of NSCLC: Influencing Factors and Its Relationship to Survival. *J. Thorac. Oncol.* **2017**, *12*, 1845–1850. [CrossRef]
18. Steinfort, D.P.; Kothari, G.; Wallace, N.; Hardcastle, N.; Rangamuwa, K.; Dieleman, E.M.T.; Lee, P.; Li, P.; Simpson, J.A.; Yo, S.; et al. Systematic endoscopic staging of mediastinum to guide radiotherapy planning in patients with locally advanced non-small-cell lung cancer (SEISMIC): An international, multicentre, single-arm, clinical trial. *Lancet Respir. Med.* **2024**, *12*, 467–475. [CrossRef]
19. Bousema, J.E.; Heineman, D.J.; Dijkgraaf, M.G.W.; Annema, J.T.; van den Broek, F.J.C. Adherence to the mediastinal staging guideline and unforeseen N2 disease in patients with resectable non-small cell lung cancer: Nationwide results from the Dutch Lung Cancer Audit–Surgery. *Lung Cancer* **2020**, *142*, 51–58. [CrossRef] [PubMed]
20. Crombag, L.M.M.; Dooms, C.; Stigt, J.A.; Tournoy, K.G.; Schuurbiers, O.C.J.; Ninaber, M.K.; Buikhuisen, W.A.; Hashemi, S.M.S.; Bonta, P.I.; Korevaar, D.A.; et al. Systematic and combined endosonographic staging of lung cancer (SCORE study). *Eur. Respir. J.* **2019**, *53*, 1800800. [CrossRef] [PubMed]
21. Navani, N.; Nankivell, M.; Lawrence, D.R.; Lock, S.; Makker, H.; Baldwin, D.R.; Stephens, R.J.; Parmar, M.K.; Spiro, S.G.; Morris, S.; et al. Lung cancer diagnosis and staging with endobronchial ultrasound-guided transbronchial needle aspiration compared with conventional approaches: An open-label, pragmatic, randomised controlled trial. *Lancet Respir. Med.* **2015**, *3*, 282–289. [CrossRef]
22. Navani, N.; Fisher, D.J.; Tierney, J.F.; Stephens, R.J.; Burdett, S.; Rydzewska, L.H.M.; Auperin, A.; Le Chevalier, T.; Le Pechoux, C.; Pignon, J.P.; et al. The Accuracy of Clinical Staging of Stage I-IIIa Non-Small Cell Lung Cancer: An Analysis Based on Individual Participant Data. *Chest* **2019**, *155*, 502–509. [CrossRef] [PubMed]

diagnostics

MDPI

Article

High Incidence of False Positives in *EGFR* S768I Mutation Detection Using the Idylla qPCR System in Non-Small Cell Lung Cancer Patients

Miguel Carnero-Gregorio [1,2,*], Enzo Perera-Gordo [1], Vanesa de-la-Peña-Castro [3], Jesús María González-Martín [4], Julio José Delgado-Sánchez [1] and Carmen Rodríguez-Cerdeira [2,5,6,*]

[1] Department of Pathological Anatomy, Hospital Universitario de Gran Canaria Dr. Negrín, Barranco de la Ballena, s/n, 35010 Las Palmas de Gran Canaria, Spain; epergor@gobiernodecanarias.org (E.P.-G.); jdelsanr@gobiernodecanarias.org (J.J.D.-S.)
[2] Fundación Vithas, Grupo Hospitalario Vithas, 28043 Madrid, Spain
[3] Fundación Canaria Instituto de Investigación Sanitaria de Canarias (FIISC), Barranco de la Ballena, s/n, Edf. Anexo al Hospital Universitario de Gran Canaria Dr. Negrín, 35019 Las Palmas de Gran Canaria, Spain; nesa206@gmail.com
[4] Research Unit, Hospital Universitario de Gran Canaria Dr. Negrín, C/Barranco de la Ballena, s/n, 35010 Las Palmas de Gran Canaria, Spain; josu.estadistica@gmail.com
[5] Dermatology Department, Grupo Hospitalario (CMQ Concheiro), Manuel Olivié 11, 36203 Vigo, Spain
[6] Department of Health Sciences, University of Vigo, Campus of Vigo, As Lagoas, 36310 Vigo, Spain
* Correspondence: miguel.carnero.gregorio@hotmail.com or mcargre@gobiernodecanarias.org (M.C.-G.); carmencerdeira33@gmail.com (C.R.-C.); Tel.: +34-600538114 (C.R.-C.)

Abstract: Background/Objectives: The accurate detection of *EGFR* mutations, particularly the rare S768I variant, is crucial for guiding treatment decisions in non-small cell lung cancer (NSCLC) patients. This study investigated the incidence of false positives in S768I mutation detection using the Idylla™ qPCR system and compared results with next-generation sequencing (NGS). **Methods:** A prospective observational study was conducted at the Dr. Negrín University Hospital between July 2023 and July 2024. Six NSCLC patient samples with S768I variant detection by Idylla™ were analyzed from all NSCLC cases tested during the study period. Initial testing was performed on tissue samples (Idylla1), followed by replicate analysis using extracted DNA (Idylla2). Results were compared with NGS as the reference method. Statistical analysis included the calculation of sensitivity, specificity, accuracy, and Kappa concordance index. **Results:** Initial Idylla testing showed an 80% false positive rate, with only one of five positive results confirmed by NGS. The first analysis demonstrated high sensitivity (100%) but low specificity (20%), with an accuracy of 0.333 and poor concordance with NGS (Kappa = 0.077). Repeat testing using extracted DNA showed improved performance, with increased accuracy (0.833) and better agreement with NGS (Kappa = 0.571). Analysis of amplification curves revealed that false positives typically showed normalized fluorescence values below 12 points, with no clear correlation between false positives and factors such as sample quantity or tumor content. **Conclusions:** While the Idylla™ system shows high sensitivity for S768I detection, its initial specificity is problematic, leading to frequent false positives. These findings emphasize the importance of confirming positive S768I results through alternative methods like NGS, particularly when these results could influence therapeutic decisions. Results suggest the need to refine the system's interpretation algorithms to improve specificity.

Keywords: molecular diagnostics; non-small cell lung cancer; EGFR mutation testing; S768I variant; false positives; qPCR; next-generation sequencing

1. Introduction

In 2020, 19.3 million new cancer cases were diagnosed worldwide, with 10 million cancer-related deaths recorded. Lung cancer (LC) is the leading cause of cancer death, with an incidence of 2.5 million cases and approximately 1.8 million deaths per year, ranking first in both incidence and mortality and accounting for 18.4% of all cancer deaths globally [1–3]. LC is divided into two major groups: non-small cell lung cancer (NSCLC), which is the most common and represents approximately four out of five cases, and small cell lung cancer (SCLC), which accounts for approximately 15% of cases [4–6].

In the last two decades, advances in understanding the molecular biology of NSCLC have enabled the identification of genetic alterations that play a crucial role in disease pathogenesis and progression [7]. Some of these variants are found in the *EGFR* gene, which codes for the epidermal growth factor receptor, and have emerged as one of the most significant findings, with direct implications for patient therapeutic management [7–9]. The *EGFR* gene is altered in approximately 10% to 15% of NSCLC patients in Western populations and up to 40% to 50% in Asian populations [9,10]. These alterations result in the constitutive activation of the *EGFR* receptor, promoting cell proliferation and tumor survival [9]. Their identification has revolutionized NSCLC treatment and is key to its personalization, as patients with *EGFR*-activating variants show a greater response to tyrosine kinase inhibitors (TKIs) compared to conventional chemotherapy [10].

The S768I variant, found in exon 20 of the EGFR gene, is one of the less common but clinically significant alterations, representing approximately 1% of all mutations occurring in this gene [11]. This variant involves the substitution of a serine residue (polar amino acid) with an isoleucine residue (nonpolar amino acid) at codon 768 of the protein encoded by this gene and has been associated with both sensitivity and resistance to different TKIs [12–14]. Despite its lower frequency compared to other mutations, such as L858R or exon 19 deletions, the detection of S768I is equally important due to its specific therapeutic implications [12,15].

The identification of this variant is commonly performed using real-time polymerase chain reaction (qPCR) techniques or through next-generation sequencing (NGS). One of the qPCR-based tests used in healthcare centers is the Idylla™ *EGFR* Mutation Test (CE-IVD) (Biocartis, Mechelen, Belgium). This system performs all necessary steps automatically, reducing errors, handling time, and risk of cross-contamination, allowing for a rapid and reproducible evaluation of *EGFR* variants, comparable to other techniques, offering high sensitivity and specificity [10,16,17]. However, the Idylla™ *EGFR* Mutation Test based on qPCR is not free from errors, and cases of false negatives or false positives can occur.

Given the importance of precision in molecular diagnosis to guide treatment decisions in NSCLC patients, it is necessary to investigate and understand the underlying causes of false positives and negatives for the S768I mutation in the Idylla™ system. This will help improve diagnostic accuracy and contribute to optimizing the use of this platform in clinical practice.

The objective of this article is to explore the prevalence of false positives in the detection of the *EGFR* gene S768I mutation after one year of using the Biocartis qPCR Idylla™ platform at the Dr. Negrín University Hospital of Gran Canaria (Gran Canaria, Spain), analyzing the possible causes contributing to these incorrect results and discussing possible solutions.

2. Materials and Methods

2.1. Study Design and Patient Selection

This prospective observational study was conducted between 1 July 2023 and 1 July 2024 in the Department of Pathological Anatomy at the Dr. Negrín University Hospital

of Gran Canaria (HUGCDN) in Las Palmas de Gran Canaria, Spain. Patients with non-small cell lung cancer (NSCLC) diagnosed in this department were included, regardless of their pathological stage. During the evaluation period, all NSCLC cases diagnosed in our Pathology Department underwent comprehensive molecular testing as part of routine clinical practice, with each sample analyzed in parallel using both the Idylla™ system and NGS for a complete panel of actionable mutations, including *EGFR*, *KRAS*, *ALK*, *ROS1*, *MET*, and *RET*. This parallel testing strategy was implemented as part of an ongoing departmental project.

2.2. Sample Collection and Processing

Previously extracted paraffin-embedded (FFPE) biopsy samples were used. The tumor area and tumor content of the samples were determined by pathologists from the Department of Pathological Anatomy. *EGFR* gene variant determination was performed using two methods: qPCR and next-generation sequencing (NGS).

2.3. Idylla™ System Analysis

The determination of pathogenic variants in *EGFR* by qPCR was performed using the Idylla™ *EGFR* Mutation Test cartridge (Biocartis, Mechelen, Belgium) on the Idylla™ Platform. This fully automated system integrates multiple steps of molecular testing into a single cartridge-based process. The technology combines automated sample preparation and mutation detection through three key steps: tissue processing using a combination of chemical reagents, enzymes, heat, and high-intensity focused ultrasound; multiplexed PCR amplification with allele-specific primers; and real-time detection using fluorescence-labeled probes. The system can detect 51 *EGFR* mutations in exons 18, 19, 20, and 21, offering a comprehensive coverage of clinically relevant variants.

The procedure was carried out according to the manufacturer's instructions [18], with a total processing time of approximately 2.5 h and an actual handling time of less than 2 min. Briefly, one or more tissue sections totaling between 5 and 10 µm in thickness, all with a minimum of 20% tumor cells, were loaded into the Idylla™ *EGFR* Mutation Test cartridges. The cartridges were inserted into the Idylla™ instrument, which automatically performed DNA extraction, real-time PCR, and results analysis. Deparaffinization, tissue disruption, and cell lysis are achieved through a combination of chemical reagents, enzymes, heat, and high-intensity focused ultrasound. Real-time PCR uses allele-specific primers and fluorescence-labeled probes for variant detection [19]. For DNA analyses extracted via Idylla™, the recommendations of Bocciarelli et al. (2020) were followed, where they recommend that the minimum quantity should be greater than 25 ng of DNA [20]. Results are shown directly on the Idylla™ console in report form and classified as positive, negative, or invalid. Each run included internal control checks for sample processing and amplification to ensure result validity. Amplification curves and Cq values were reviewed for all samples. This was performed by connecting to the Idylla™ Explore web application (https://idyllaexplore.biocartis.com/ (accessed on 1 July 2023)), where these results can be viewed and curves analyzed. Another parameter to consider is the ΔCq, which is the difference between the control sample Cq values and the S768I variant Cq values. Lower ΔCq values typically indicate a higher abundance of the target mutation, while higher values suggest a lower abundance or potential false positive signals. According to the manufacturer's specifications, the Limit of Detection (LOD) for the S768I mutation varies depending on the total *EGFR* Cq value. With 1000 input copies (Total *EGFR* Cq = 21.3), the LOD is 2.5%, while with 2500 copies (Total *EGFR* Cq = 19.8), it improves to 1.4%. Results should be interpreted considering these analytical sensitivity thresholds.

2.4. Next-Generation Sequencing Analysis

For NGS analysis, DNA was extracted from the same tissue samples. Nucleic acids were extracted and purified using the RecoverAll™ Total Nucleic Acid Isolation Kit for FFPE (Invitrogen™, ThermoFisher Scientific, Waltham, MA, USA), according to manufacturer specifications and guidelines and quantified using the Qubit™ 4 Fluorometer (Invitrogen™, San Diego, CA, USA). Prior to NGS analysis, tumor cell content was assessed for each sample by a pathological review of adjacent sections. The same tumor area evaluated for Idylla™ testing was used for DNA extraction for NGS to ensure comparable tumor content between both methods. All samples met the minimum requirement of 20% tumor cellularity for reliable variant detection. Library preparation, sequencing, and data analysis were carried out using the Ion GeneStudio™ S5 System platform (ThermoFisher™ Scientific Inc.) and the Oncomine™ Focus Assay panel (ThermoFisher™ Scientific Inc.). Only one sample was sequenced and analyzed using the Ion Torrent™ Genexus™ System platform (ThermoFisher™ Scientific Inc.) and the Oncomine™ Focus Assay panel (ThermoFisher™ Scientific Inc.) due to equipment updates performed in our laboratory in January 2024. In this case, library preparation was conducted using the Ion Torrent™ Genexus™ System itself in an automated manner. Both panels have coverage for *EGFR* exons 18, 19, 20, and 21, including the S768I variant [21,22].

For all samples, a minimum coverage depth of 1000 reads at the S768I locus was required for reliable variant calling. The mean coverage achieved across samples at this specific locus was approximately 2000 reads, ensuring robust mutation detection capability.

2.5. Statistical Analysis

Statistical analysis was performed to evaluate the concordance between results obtained by Idylla™ and NGS in detecting the *EGFR* S768I variant. Two Idylla datasets were used, corresponding to the first analysis (Idylla1) and the duplicate (Idylla2), to compare with the results obtained by NGS as the reference method. To evaluate the concordance between the two variables, the following statistics were calculated: Kappa index, accuracy, prevalence, sensitivity, specificity, positive predictive value, and negative predictive value. The ROC curve was calculated between a quantitative variable and a dichotomous one (NGS) to obtain the optimal cutoff point to discriminate between positive and negative. The statistical program used was R Core Team 2024, version 4.3.3 (https://www.r-project.org/ (accessed on 1 September 2024)).

3. Results

3.1. Patient Characteristics

Among all *EGFR* mutations detected, the distribution of variant types was consistent with published frequencies, with the S768I variant representing a small fraction of cases, in line with its reported frequency of approximately 1% of all *EGFR* mutations.

From all cases analyzed, six patients were identified in whom Idylla™ detected the S768I variant of the *EGFR* gene. These cases were further analyzed using the Idylla™ system in duplicate (Idylla1 and Idylla2) and NGS for detailed evaluation. Among these six patients, the mean age was 67.5 $\pm$ 6.08 years, with five males (M) and one female (F). Tumor histological types included large cell neuroendocrine carcinoma (n = 1), adenocarcinoma (n = 2), squamous cell carcinoma (n = 2), and unspecified lung neoplasm (n = 1). All patients were metastatic (stage IVa or IVb) (Table 1).

Table 1. Clinical and pathological characteristics of patients with S768I detected by Idylla™.

Sample	Age	Gender	Tumor Area	% Tumor Cells	Tumor Type	Stage
95	75	M	17 mm^2	60%	High-grade neuroendocrine tumor, suspicious for large cell neuroendocrine carcinoma	T4N2M1b (IVA)
107	72	M	24 mm^2	80%	NSCLC, most likely adenocarcinoma	T4N2M1a (IVA)
132	59	F	4 mm^2	65%	NSCLC, compatible with adenocarcinoma	T4N3M1c (IVB)
142	73	M	4 mm^2	25%	Lung neoplasm	Unknown (IVA)
143	64	M	15 mm^2	80%	NSCLC, most likely squamous cell carcinoma	T4N0M1a (IVA)
195	62	M	44 mm^2	20%	NSCLC, most likely squamous cell carcinoma	T3N3M1c (IVB)

3.2. Performance of the Idylla™ System Detection

As part of our routine molecular diagnostic workflow, all *EGFR* mutation results from Idylla™ testing were cross-validated by NGS analysis. Prior to this systematic evaluation, our laboratory had no experience with S768I variant detection using the Idylla™ system, as this technique was incorporated into our lab routine in June 2023. The concordance between Idylla™ and NGS for other common *EGFR* mutations (such as exon 19 deletions and L858R) was high, with discrepancies primarily observed in S768I variant detection.

The Idylla™ system identified a total of seven S768I alterations (seven in 2023 and one in 2024) in six samples analyzed in duplicate: five in the first analysis (Idylla1) and two in the replicates (Idylla2). Tissue samples (biopsies or cell blocks) were analyzed using the Idylla™ system in duplicate (Idylla1 and Idylla2). For Idylla2 replicates, the same extracted DNA that was used for NGS sequencing was used due to either a lack of additional tissue sample or insufficient tumor representation in the remaining block (except for sample 107, where more material was available) (Table 2).

Table 2. Results of the Idylla™ analysis.

Sample	Sample Type	Quantity	Result	Cq (Total *EGFR*)	Cq (S768I)	ΔCq
95	Biopsy	2 slides (3 µm each)	Positive	24.04	32.12	8.08
95-R1	Extracted DNA	100 ng	Negative	21.59	-	-
107	Biopsy	1 slide (5 µm)	Positive	22.65	27.89	5.24
107-R1	Biopsy	1 slide (5 µm)	Positive	22.47	27.01	4.54
132	Cell block	2 slides (3 µm each)	Positive	24.04	30.57	6.53
132-R1	Extracted DNA	126 ng	Negative	22.29	-	-
142	Biopsy	1 slide (5 µm)	Negative	30.44	-	-
142-R1	Extracted DNA	40.8 ng	Positive	24.90	34.97	10.07
143	Biopsy	2 slides (5 µm each)	Positive	24.52	34.23	9.71
143-R1	Extracted DNA	155.2 ng	Negative	22.22	-	-
195	Biopsy	2 slides (3 µm each)	Positive	21.94	31.54	9.60
195-R1	Extracted DNA	101.16 ng	Negative	21.30	-	-

The Cq values for total *EGFR* (control) were relatively consistent between samples, being 24.6 ± 3.02 (range: 21.94–30.44) for Idylla1 and 22.46 ± 1.27 (range: 21.3–24.9) for Idylla2, suggesting similar DNA quantity in all samples and generally good for analysis, with only one value far from the mean (Sample 142-Cq 30.44). According to established LOD parameters, optimal detection sensitivity (2.5%) requires a minimum total *EGFR* Cq

of 21.3. While some of our samples met this threshold, others showed higher Cq values, potentially affecting the reliability of mutation detection. The ΔCq values for samples called positive for S768I ranged from 5.24 to 9.71, with the confirmed true positive case (sample 107) showing the lowest ΔCq values.

During the study period, S768I amplification curves were observed in samples ultimately classified as negative. In these cases, while some amplification was detected, the curves typically showed normalized fluorescence values below 12 points. This pattern was consistently observed across negative samples, suggesting it may represent background amplification rather than true mutation detection. The amplification curves obtained by the Idylla™ system for the detection of the *EGFR* gene S768I variant were analyzed in all samples. Figure 1 shows the results for the six samples analyzed.

In all samples, except for 142, the amplification of the S768I curve was observed when tissue was used, although with variations in its profile and Cq values. When repeating the test using extracted DNA, all gave negative results, except for sample 142. Sample 107 was repeated with a biopsy sample, as more material was available for analysis.

Although tumor cell content varied between samples (20% to 80%), there was no clear correlation between tumor cellularity and the occurrence of false positive results. Both high tumor content samples (e.g., sample 143 with 80%) and lower tumor content samples (e.g., sample 195 with 20%) showed discrepant results between Idylla and NGS, suggesting that variations in tumor content alone do not explain the observed discrepancies.

3.3. Comparison with NGS Results

Concerning NGS sequencing, all samples were analyzed using the Ion GeneStudio™ S5 System sequencer and the OFA panel, except for sample 195, which was analyzed using the Ion Torrent™ Genexus™ System platform and the OPA panel. The DNA concentration of the samples for NGS use ranged between 1.02 ng/μL and 19.4 ng/μL. NGS detected only one S768I alteration in the same analyzed samples (Table 3).

Table 3. NGS analysis parameters and results. Sample 195 shows higher read depth due to analysis on the Ion Torrent™ Genexus™ System platform versus the Ion GeneStudio™ S5 System used for other samples.

Sample	[DNA]	Read Depth	Result
95	3.18 ng/μL	1995	Negative
107	9.40 ng/μL	1944	Positive
132	4.20 ng/μL	1995	Negative
142	1.02 ng/μL	1993	Negative
143	19.4 ng/μL	1996	Negative
195	5.62 ng/μL	4739	Negative

To better visualize the concordance between methods, a direct comparison of results obtained by both Idylla runs and NGS is presented in Table 4.

Table 4. Comparison of results between detection methods for each sample analyzed.

Sample	Sample Type	Idylla1 Result	Idylla2 Result	NGS Result	Method Concordance
95	Biopsy	Positive	Negative	Negative	Idylla2 = NGS
107	Biopsy	Positive	Positive	Positive	Both = NGS
132	Cell Block	Positive	Negative	Negative	Idylla2 = NGS
142	Biopsy	Negative	Positive	Negative	Idylla1 = NGS
143	Biopsy	Positive	Negative	Negative	Idylla2 = NGS
195	Biopsy	Positive	Negative	Negative	Idylla2 = NGS

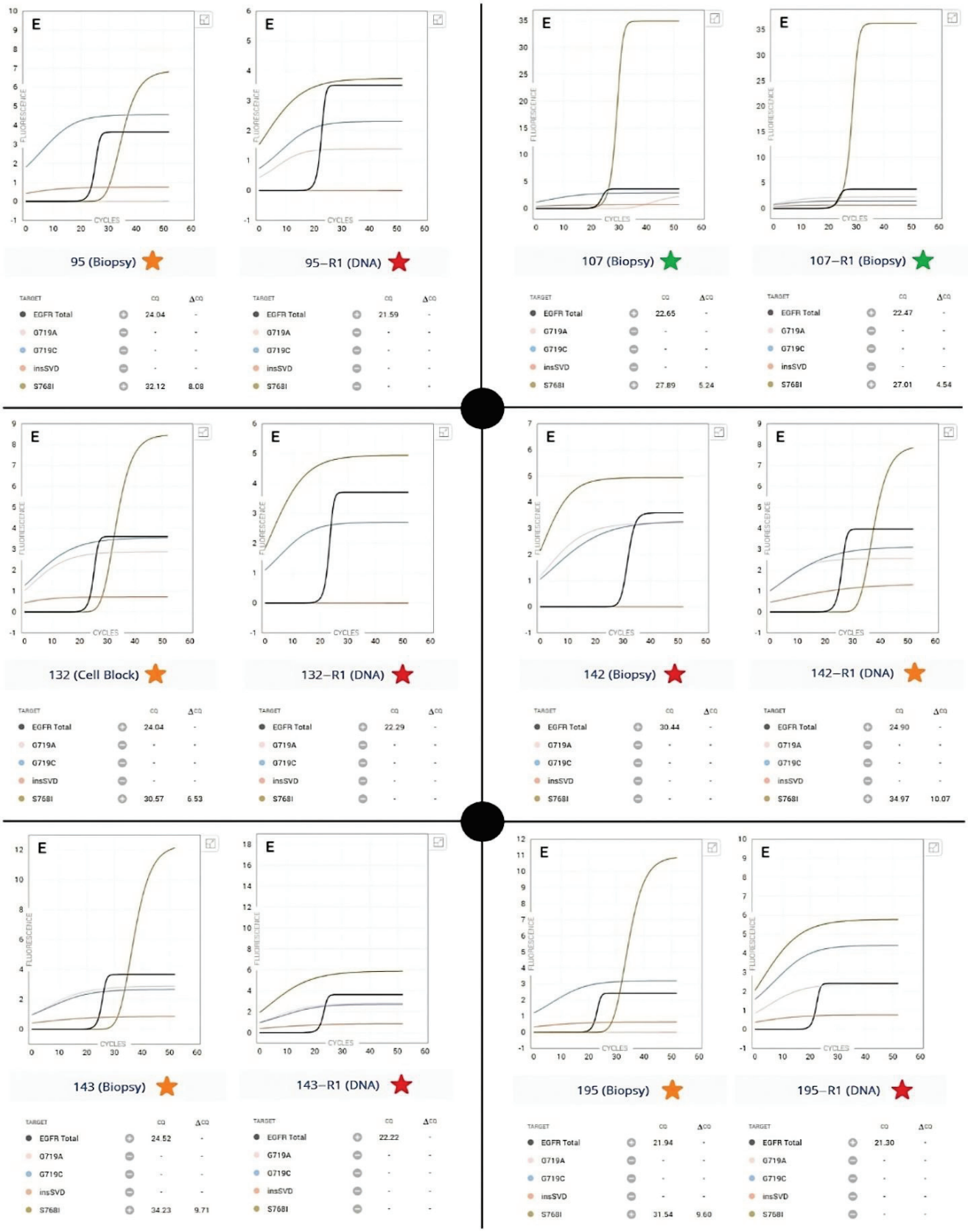

Figure 1. Amplification curves for EGFR S768I variant detection in six samples analyzed by Idylla1 and Idylla2 (R1). Curves show total EGFR (control), G719A, G719C, insSVD, and S768I amplification. Green stars are true positives, orange stars are false positives, and red stars are negative results. Sample types are indicated in parentheses.

A low ΔCq could suggest a higher relative abundance of the S768I variant, although this should be interpreted with caution given that most of these detections turned out to be false positives in the NGS validation. The only sample in which both Idylla™ and NGS detected the S768I variant corresponded to sample 132.

3.4. Statistical Analysis and False Positive Rates

The statistical analysis performed on the results obtained by Idylla™ and NGS in detecting the *EGFR* S768I variant revealed significant findings. For Idylla1, of the six samples in which the S768I variant was detected, only one was confirmed by NGS. This suggests a false positive rate of 80% (4/5) for S768I detection by Idylla™ in our case series. The accuracy was 0.333 (95% CI: 0.04–0.78). The Kappa concordance index was 0.077, indicating very weak concordance with NGS, suggesting a substantial discrepancy between both methods.

The high sensitivity (100%; 95% CI: 0.03–1) but low specificity (20%; 95% CI: 0.01–0.72) of Idylla1 implies that the system effectively detects all positive cases but also produces a considerable number of false positives. This is reflected in the low positive predictive value (PPV), which was 0.2 (95% CI: 0.01–0.72), indicating that only 20% of Idylla1 positive results are true positives, according to NGS. The high negative predictive value (NPV), which was 1 (95% CI: 0.03–1), suggests that Idylla1's negative results are reliable, although these data should be interpreted with caution, given the small sample size. The ROC curve analysis for Idylla1 (Figure 2A), with an area under the curve (AUC) of 0.8 and an optimal cutoff point of 23.345, indicates good overall test performance but also suggests that adjusting the positivity threshold could improve its specificity.

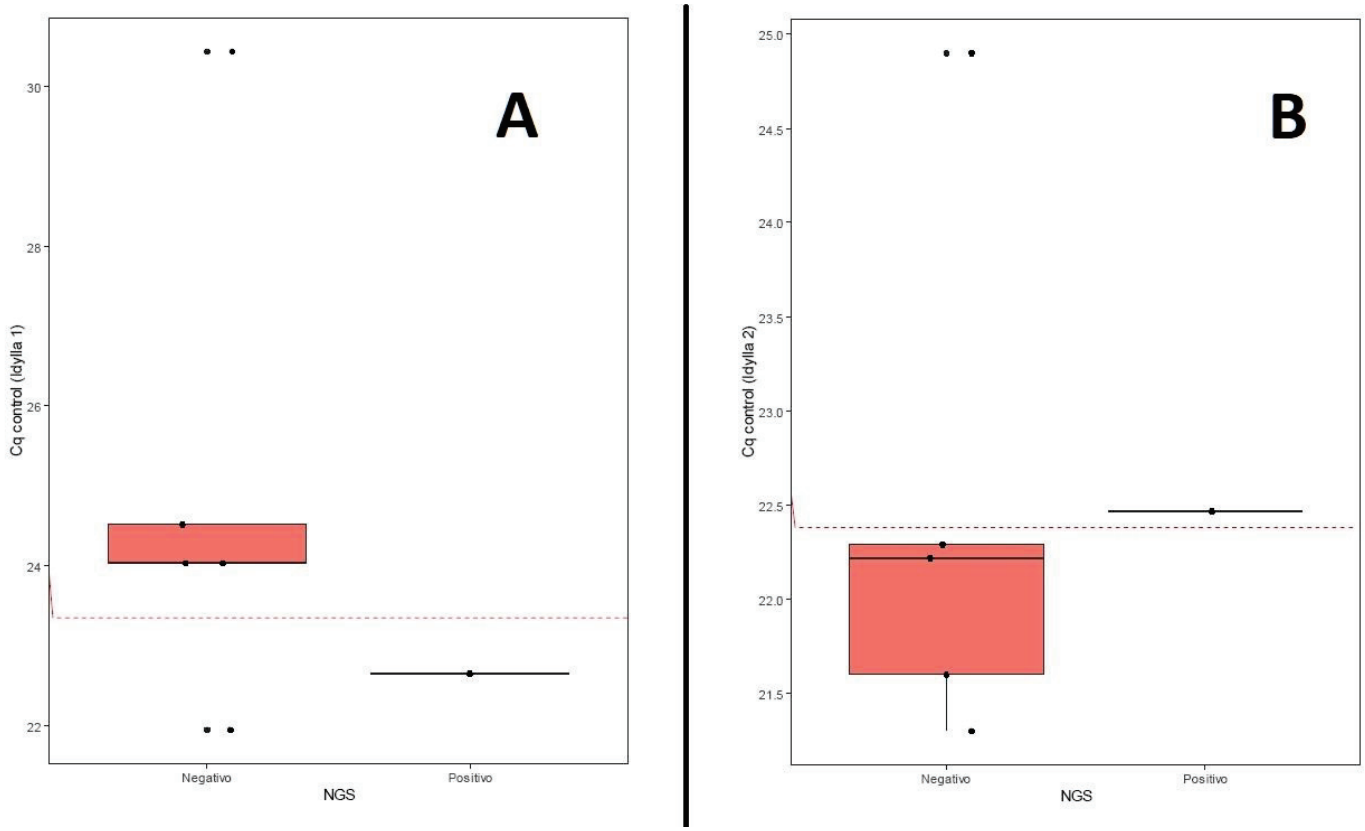

Figure 2. ROC curve analysis comparing Idylla™ and NGS results. (**A**) ROC curve for Idylla1 (AUC = 0.8, optimal cutoff = 23.345). (**B**) ROC curve for Idylla2 (AUC = 0.8, optimal cutoff = 22.38).

For Idylla2, a notable improvement in diagnostic performance was observed. The increase in the Kappa index to 0.571 indicates moderate agreement with NGS, representing a substantial improvement compared to Idylla1. Accuracy increased from 0.333 to 0.833 (95% CI: 0.36–1), and specificity improved to 80% (95% CI: 0.28–0.99) while maintaining 100% sensitivity (95% CI: 0.03–1). The PPV increased to 0.5 (95% CI: 0.01–0.99), while the NPV remained at 1 (95% CI: 0.4–1). The optimal cutoff point for Idylla2 was 22.38, with an AUC of 0.8 and identical sensitivity, specificity, and accuracy values to those of Idylla1 (Figure 2B). This suggests that the modifications introduced in Idylla2 (performing the test with extracted DNA instead of tissue) succeeded in significantly reducing false positives without compromising the detection of true positive cases. The increase in positive predictive value to 0.5 indicates that, in this case, half of Idylla2's positive results are confirmed by NGS, representing a considerable improvement in the reliability of positive results.

The ROC curve analysis yielded an AUC of 0.8 for both Idylla1 and Idylla2, indicating good discriminatory ability. This value suggests that the test can effectively distinguish between true positive and negative cases 80% of the time. However, the clinical implications of this performance metric should be considered carefully, particularly given our small sample size. The identical AUC values between Idylla1 and Idylla2, despite their different specificity profiles, suggest that while both versions have the similar overall diagnostic capability, the improved specificity in Idylla2 makes it more suitable for clinical implementation.

The descriptive statistics revealed that the control Cq values for Idylla1 had a mean of 24.6 ($\pm$3.02), with a range from 21.94 to 30.44, while for Idylla2, the mean was 22.46 ($\pm$1.27), with a range from 21.3 to 24.9. This reduction in the variability of Cq values in Idylla2 could partially explain the improvement in diagnostic performance. It is important to note that due to the small sample size (n = 6), the confidence intervals are wide, which limits the precision of the estimates and underscores the need to interpret these results with caution.

4. Discussion

Alterations occurring in the *EGFR* gene, especially those in exons 18 to 21, are determinants for response to tyrosine kinase inhibitors (TKIs), a class of targeted therapies that have significantly improved prognosis in NSCLC patients [9,10,23,24]. The S768I mutation, although less common, has important clinical implications [12,25], which highlights the need for accurate detection to select appropriate treatment. However, a precise detection of these mutations is critical, as false positives can lead to incorrect therapeutic decisions and suboptimal patient management [26,27].

qPCR is a widely used technique for mutation detection due to its high sensitivity and specificity. Nevertheless, each qPCR platform and method can have different levels of precision and propensity for errors [28]. The Biocartis Idylla^{TM} system is an automated molecular diagnostic instrument designed to facilitate the rapid and accurate detection of genetic mutations, including those in *EGFR*. This system is valued for its ability to provide quick and reliable results, allowing real-time results without the need for complex sample preparation, which is particularly useful in clinical settings where time is a critical factor [29,30]. The Idylla^{TM} system, while offering significant advantages in terms of automation and rapid turnaround time, has several important limitations that need to be considered. The reliability and validity of results depend heavily on sample quality and preparation, with multiple preanalytical factors potentially affecting performance. These include suboptimal sample collection, handling procedures, variations in tissue fixation methods, and the use of stained tissues. Additionally, paraffin samples with high melting temperatures may interfere with proper DNA extraction. The system also has specific

requirements for minimum tumor content and DNA quantity that must be met for reliable results, as evidenced by our findings about Cq values and sample adequacy. These technical limitations, combined with the observed specificity issues for S768I detection in our study, suggest that the system's performance should be carefully monitored and validated. The high prevalence of false positives observed specifically in the S768I detection indicates that a more cautious approach is necessary, including mandatory cross-validation with other detection methods such as NGS. Given these limitations, we recommend against using the Idylla™ system as a sole detection method for the S768I mutation, particularly when these results could influence critical therapeutic decisions.

Some studies have reported cases of false positives in S768I mutation detection using the Idylla platform. In a multicenter study evaluating Idylla's performance, a false positive for S768I was observed that was not confirmed by reference methods [29]. Similarly, another study analyzing decalcified bone metastasis samples also reported a false positive for this mutation [31]. The occurrence of these false positives raises important concerns. First, it can lead to an overestimation of this mutation's prevalence in the NSCLC patient population. More critically, it can result in inappropriate therapeutic decisions, potentially exposing patients to unnecessary or ineffective treatments. False positives (and false negatives) in S768I detection can arise for various reasons, including nonspecific amplification, cross-contamination, and technical problems inherent to the assay design [26,32,33]. The incidence of false positives not only compromises diagnostic accuracy but can also lead to erroneous therapeutic decisions, such as an inappropriate administration of TKIs, which can result in adverse effects and treatment resistance [11].

The Idylla™ System showed a high sensitivity for S768I signal detection, as evidenced by amplification in all samples. However, the low specificity (high false positive rate) suggests that signal detection does not always correspond to the actual presence of the variant. It is important to note that all S768I curves crossed the positivity threshold established by the Idylla™ System, which led to the classification of these samples as positive for the variant. This highlights the need to reevaluate the positivity criteria to reduce false positives.

Regarding the possible causes of the false positives found, there was no clear relationship between the amount of sample used or the *EGFR* control Cq value and the likelihood of obtaining a false positive. For example, patient 195, with the lowest Cq (21.8), indicative of good sample quality, also turned out to be a false positive. Additionally, false positives were observed in various histological types, including adenocarcinoma, squamous cell carcinoma, and large cell neuroendocrine carcinoma, suggesting that tumor type would not be a determining factor in the appearance of false positives. As for tumor cell content, it varied widely between samples (from 25% to 80%), with no apparent correlation with the probability of false positives.

The S768I curves showed different patterns of exponential growth and plateau between samples, reflecting differences in amplification efficiency and/or the amount of variant present. It was observed that amplification curves for S768I, in cases of false positives, tended to show a normalized fluorescence of fewer than 12 points, which could be a parameter to consider for determining false positives. Notably, this high rate of false positives appears to be specific to the S768I variant, as concordance between Idylla™ and NGS was substantially better for other *EGFR* mutations tested in our laboratory in the study period. This suggests that the technical challenges in accurate detection may be particularly relevant to this specific variant. The presence of low-level amplification curves in confirmed negative samples suggests that the S768I detection may be particularly susceptible to background noise. This observation, combined with our findings about false positives, indicates that a careful evaluation of amplification patterns and fluorescence

thresholds is crucial for accurate mutation calling. A study with more samples would be necessary to determine if this is a value that can be established as a cutoff point.

Taken together, these results suggest that although Idylla™ shows high sensitivity in detecting the S768I variant, its initial specificity (Idylla1) was problematic, leading to a high false positive rate. The improvements observed in Idylla2 are promising, indicating that with appropriate adjustments, the system could achieve more balanced and reliable diagnostic performance using extracted DNA from samples. However, given the persistent discrepancy with NGS, especially in the first analysis (Idylla 1), these findings highlight the importance of confirming positive *EGFR* S768I results obtained by Idylla™ through alternative methods such as NGS, especially in cases where the detection of this variant could influence critical therapeutic decisions.

It is also important to consider the economic and resource implications of false positives in diagnostic testing. Errors in molecular diagnosis can lead to unnecessary treatments, additional follow-ups, and potential delays in the administration of more appropriate therapies. This not only affects the quality of patient care but also has implications for efficiency and resource allocation in healthcare systems [30].

To further validate these findings, multicenter studies would be valuable. Such studies could determine whether the high false positive rates for S768I detection are consistently observed across different laboratories using the Idylla™ platform or if they are influenced by local factors such as sample processing variations or environmental conditions.

5. Conclusions

In conclusion, although the Idylla™ system demonstrates high sensitivity for detecting signals associated with S768I, the high rate of false positives observed in this study underscores the need to interpret these results with caution. Confirmation by alternative methods, such as NGS, is recommended, especially in cases where the detection of this variant could influence important therapeutic decisions. Furthermore, these findings suggest the need to refine the Idylla™ system's interpretation algorithms to improve its specificity in detecting the S768I variant of the *EGFR* gene in NSCLC samples.

Author Contributions: Conceptualization, M.C.-G.; methodology, M.C.-G.; statistical analysis, J.M.G.-M.; resources, V.d.-l.-P.-C. and J.J.D.-S.; data curation, E.P.-G.; writing—original draft preparation, M.C.-G.; writing—reviewing and editing, M.C.-G. and C.R.-C.; supervision, C.R.-C. All authors have read and agreed to the published version of the manuscript.

Funding: This research received no external funding.

Institutional Review Board Statement: The study was conducted in accordance with the Declaration of Helsinki of 1975. The number of the request to the Ethics Committee (CEI/CEIm HUGCDN) was 452 (Servicio Canario de Salud, Gobierno de Canarias).

Informed Consent Statement: Informed consent from patients is not required due to the retrospective nature of the study, the anonymization/dissociation of patient data, and that the results will not affect the clinical management of patients.

Data Availability Statement: The original contributions presented in this study are included in the article. Further inquiries can be directed to the corresponding author(s).

Conflicts of Interest: The authors declare no conflicts of interest.

References

1. World Health Organization. Cancer. Available online: https://www.who.int/news-room/fact-sheets/detail/cancer (accessed on 24 July 2024).
2. Sung, H.; Ferlay, J.; Siegel, R.L.; Laversanne, M.; Soerjomataram, I.; Jemal, A.; Bray, F. Global Cancer Statistics 2020: GLOBOCAN Estimates of Incidence and Mortality Worldwide for 36 Cancers in 185 Countries. *Cancer J. Clin.* **2021**, *71*, 209–249. [CrossRef] [PubMed]
3. International Agency for Research on Cancer. World Health Organization. Available online: https://gco.iarc.who.int/media/globocan/factsheets/cancers/15-trachea-bronchus-and-lung-fact-sheet.pdf (accessed on 24 July 2024).
4. Siegel, R.L.; Miller, K.D.; Wagle, N.S.; Jemal, A. Cancer statistics, 2023. *CA: Cancer J. Clin.* **2023**, *73*, 17–48. [CrossRef] [PubMed]
5. Alduais, Y.; Zhang, H.; Fan, F.; Chen, J.; Chen, B. Non-small cell lung cancer (NSCLC): A review of risk factors, diagnosis, and treatment. *Medicine* **2023**, *102*, e32899. [CrossRef] [PubMed]
6. Rudin, C.M.; Brambilla, E.; Faivre-Finn, C.; Sage, J. Small-cell lung cancer. *Nat. Rev. Dis. Primers* **2021**, *7*, 3. [CrossRef]
7. Herbst, R.S.; Morgensztern, D.; Boshoff, C. The biology and management of non-small cell lung cancer. *Nature* **2018**, *553*, 446–454. [CrossRef] [PubMed]
8. Hirsch, F.R.; Suda, K.; Wiens, J.; Bunn, P.A. New and emerging targeted treatments in advanced non-small-cell lung cancer. *Lancet* **2016**, *388*, 1012–1024. [CrossRef]
9. Lynch, T.J.; Bell, D.W.; Sordella, R.; Gurubhagavatula, S.; Okimoto, R.A.; Brannigan, B.W.; Harris, P.L.; Haserlat, S.M.; Supko, J.G.; Haluska, F.G.; et al. Activating mutations in the epidermal growth factor receptor underlying responsiveness of non-small-cell lung cancer to gefitinib. *N. Engl. J. Med.* **2004**, *350*, 2129–2139. [CrossRef]
10. Mok, T.S.; Wu, Y.L.; Thongprasert, S.; Yang, C.H.; Chu, D.T.; Saijo, N.; Sunpaweravong, P.; Han, B.; Margono, B.; Ichinose, Y.; et al. Gefitinib or carboplatin-paclitaxel in pulmonary adenocarcinoma. *N. Engl. J. Med.* **2009**, *361*, 947–957. [CrossRef] [PubMed]
11. Paik, P.K.; Arcila, M.E.; Fara, M.; Sima, C.S.; Miller, V.A.; Kris, M.G.; Ladanyi, M.; Riely, G.J. Clinical characteristics of patients with lung adenocarcinomas harboring BRAF mutations. *J. Clin. Oncol.* **2011**, *29*, 2046–2051. [CrossRef]
12. Wu, S.G.; Liu, Y.N.; Tsai, M.F.; Chang, Y.L.; Yu, C.J.; Yang, P.C.; Yang, J.C.-H.; Wen, Y.-F.; Shih, J.-Y. The mechanism of acquired resistance to irreversible *EGFR* tyrosine kinase inhibitor-afatinib in lung adenocarcinoma patients. *Oncotarget* **2016**, *7*, 12404–12413. [CrossRef]
13. Zhang, H.; Shao, Y.W.; Xia, Y. Responsiveness to Full-Dose Afatinib in a Patient with Lung Adenocarcinoma Harboring *EGFR* S768I and V769L Mutations. *J. Thorac. Oncol.* **2019**, *14*, e25–e27. [CrossRef] [PubMed]
14. Niogret, J.; Coudert, B.; Boidot, R. Primary Resistance to Afatinib in a Patient with Lung Adenocarcinoma Harboring Uncommon *EGFR* Mutations: S768I and V769L. *J. Thorac. Oncol.* **2018**, *13*, e113. [CrossRef] [PubMed]
15. Oxnard, G.R.; Lo, P.C.; Nishino, M.; Dahlberg, S.E.; Lindeman, N.I.; Butaney, M.; Jackman, D.M.; Johnson, B.E.; Jänne, P.A. Natural history and molecular characteristics of lung cancers harboring *EGFR* exon 20 insertions. *J. Thorac. Oncol.* **2013**, *8*, 179–184. [CrossRef] [PubMed]
16. Ilie, M.; Butori, C.; Lassalle, S.; Heeke, S.; Piton, N.; Sabourin, J.C.; Tanga, V.; Washetine, K.; Long-Mire, E.; Maitre, P.; et al. Optimization of *EGFR* mutation detection by the fully-automated qPCR-based Idylla system on tumor tissue from patients with non-small cell lung cancer. *Oncotarget* **2017**, *8*, 103055–103062. [CrossRef] [PubMed]
17. Uguen, A.; Troncone, G. A review on the Idylla platform: Towards the assessment of actionable genomic alterations in one day. *J. Clin. Pathol.* **2018**, *71*, 757–762. [CrossRef]
18. Idylla EGFR. Mutation Test. Available online: https://www.biocartis.com/en/meet-idylla/idylla-oncology-tests/idylla-egfr-mutation-test (accessed on 9 October 2024).
19. Tan, L.Y.; Walker, S.M.; Lonergan, T.; Lima, N.E.; Todd, A.V.; Mokany, E. Superior Multiplexing Capacity of PlexPrimers Enables Sensitive and Specific Detection of SNPs and Clustered Mutations in qPCR. *PLoS ONE* **2017**, *12*, e0170087. [CrossRef] [PubMed]
20. Bocciarelli, C.; Cohen, J.; Pelletier, R.; Tran Van Nhieu, J.; Derman, J.; Favre, L.; Bourgogne, A.; Monnet, I.; Chouaid, C.; Pujals, A. Evaluation of the Idylla system to detect the *EGFR* T790M mutation using extracted DNA. *Pathol. Res. Pract.* **2020**, *216*, 152773. [CrossRef] [PubMed]
21. Thermo Fisher Scientific Inc. Oncomine Focus Assay-ES. Available online: https://www.thermofisher.com/es/es/home/clinical/preclinical-companion-diagnostic-development/oncomine-oncology/oncomine-focus-assay.html (accessed on 9 October 2024).
22. Thermo Fisher Scientific Inc. Oncomine Precision Assay-ES. Available online: https://www.thermofisher.com/es/es/home/clinical/preclinical-companion-diagnostic-development/oncomine-oncology/oncomine-precision-assay.html.html (accessed on 9 October 2024).
23. Sequist, L.V.; Yang, J.C.-H.; Yamamoto, N.; O'Byrne, K.; Hirsh, V.; Mok, T.; Geater, S.L.; Orlov, S.; Tsai, C.-M.; Boyer, M.; et al. Phase III Study of Afatinib or Cisplatin Plus Pemetrexed in Patients with Metastatic Lung Adenocarcinoma With *EGFR* Mutations. *J. Clin. Oncol.* **2023**, *41*, 2869–2876. [CrossRef]
24. Heeke, S.; Hofman, P. *EGFR* Mutation Analysis in Non-small Cell Lung Carcinoma from Tissue Samples Using the Fully Automated Idylla™ qPCR System. *Methods Mol. Biol.* **2019**, *2054*, 147–155.

25. Duan, H.; Peng, Y.; Cui, H.; Qiu, Y.; Li, Q.; Zhang, J.; Shen, W.; Sun, C.; Luo, C. Effectiveness of afatinib after ineffectiveness of gefitinib in an advanced lung adenocarcinoma patient with a single *EGFR* exon 20 S768I mutation: A case report. *OncoTargets Ther.* **2018**, *11*, 2303–2309. [CrossRef]
26. Ellison, G.; Donald, E.; McWalter, G.; Knight, L.; Fletcher, L.; Sherwood, J.; Cantarini, M.; Orr, M.; Speake, G. A comparison of ARMS and DNA sequencing for mutation analysis in clinical biopsy samples. *J. Exp. Clin. Cancer Res.* **2010**, *29*, 132. [CrossRef] [PubMed]
27. Lee, C.K.; Man, J.; Lord, S.; Cooper, W.; Links, M.; Gebski, V.; Herbst, R.S.; Gralla, R.J.; Mok, T.; Yang, J.C.-H. Clinical and Molecular Characteristics Associated with Survival Among Patients Treated with Checkpoint Inhibitors for Advanced Non-Small Cell Lung Carcinoma: A Systematic Review and Meta-analysis. *JAMA Oncol.* **2018**, *4*, 210–216. [CrossRef] [PubMed]
28. Zhao, F.; Maren, N.A.; Kosentka, P.Z.; Liao, Y.Y.; Lu, H.; Duduit, J.R.; Huang, D.; Ashrafi, H.; Zhao, T.; Huerta, A.I.; et al. An optimized protocol for stepwise optimization of real-time RT-PCR analysis. *Hortic. Res.* **2021**, *8*, 179. [CrossRef] [PubMed]
29. Evrard, S.M.; Taranchon-Clermont, E.; Rouquette, I.; Murray, S.; Dintner, S.; Nam-Apostolopoulos, Y.-C.; Bellosillo, B.; Varela-Rodriguez, M.; Nadal, E.; Wiedorn, K.H.; et al. Multicenter Evaluation of the Fully Automated PCR-Based Idylla *EGFR* Mutation Assay on Formalin-Fixed, Paraffin-Embedded Tissue of Human Lung Cancer. *J. Mol. Diagn.* **2019**, *21*, 1010–1024. [CrossRef]
30. Huang, H.; Springborn, S.; Haug, K.; Bartow, K.; Samra, H.; Menon, S.; Mackinnon, A.C. Evaluation, Validation, and Implementation of the Idylla System as Rapid Molecular Testing for Precision Medicine. *J. Mol. Diagn.* **2019**, *21*, 862–872. [CrossRef]
31. Boureille, A.; Ferraro-Peyret, C.; Pontarollo, G.; Confavreux, C.; Pialat, J.-B.; Isaac, S.; Forest, F.; Yvorel, V.; Watkin, E.; Girard, N.; et al. Rapid detection of *EGFR* mutations in decalcified lung cancer bone metastasis. *J. Bone Oncol.* **2020**, *21*, 100277. [CrossRef] [PubMed]
32. Delgado-García, M.; Weynand, B.; Gómez-Izquierdo, L.; Hernández, M.J.; Blanco, Á.M.; Varela, M.; Matias-Guiu, X.; Nadal, E.; Márquez-Lobo, B.; Alarcão, A.; et al. Clinical performance evaluation of the Idylla™ *EGFR* Mutation Test on formalin-fixed paraffin-embedded tissue of non-small cell lung cancer. *BMC Cancer* **2020**, *20*, 275. [CrossRef] [PubMed]
33. Xu, Y.; Zhang, L.; Jia, L.; Ren, M.; Xue, T.; Bai, Q.; Yao, Q.; Wei, R.; Zhou, X.; Zhu, X. Evaluation of the Idylla™ *EGFR* Mutation Test on formalin-fixed, paraffin-embedded tissue of human lung cancer. *J. Thorac. Dis.* **2024**, *16*, 40–50. [CrossRef] [PubMed]

diagnostics

MDPI

Article

Early Effects of Bronchoscopic Cryotherapy in Metastatic Non-Small Cell Lung Cancer Patients Receiving Immunotherapy: A Single-Center Prospective Study

Gediminas Vasiliauskas [1,*], Evelina Žemaitė [2], Erika Skrodenienė [2], Lina Poškienė [3], Gertrūda Maziliauskienė [4], Aurimas Mačionis [4], Skaidrius Miliauskas [1], Donatas Vajauskas [4] and Marius Žemaitis [1]

[1] Department of Pulmonology, Lithuanian University of Health Sciences, 44307 Kaunas, Lithuania; skaidrius.miliauskas@lsmu.lt (S.M.); marius.zemaitis@lsmu.lt (M.Ž.)
[2] Department of Laboratory Medicine, Lithuanian University of Health Sciences, 44307 Kaunas, Lithuania; evelina.zemaite@lsmu.lt (E.Ž.); erika.skrodeniene@lsmu.lt (E.S.)
[3] Department of Pathology, Lithuanian University of Health Sciences, 44307 Kaunas, Lithuania; lina.poskiene@lsmu.lt
[4] Department of Radiology, Lithuanian University of Health Sciences, 44307 Kaunas, Lithuania; gertruda.maziliauskiene@lsmu.lt (G.M.); aurimas.macionis@lsmu.lt (A.M.); donatas.vajauskas@lsmu.lt (D.V.)
* Correspondence: gediminas.vasiliauskas@lsmu.lt

Abstract: Background/Objectives: Cryotherapy is used for local tissue destruction through rapid freeze–thaw cycles. It induces cancer cell necrosis followed by inflammation in the treated tumor microenvironment, and it stimulates systemic adaptive immunity. Combining cryotherapy with immunotherapy may provide a sustained immune response by preventing T cell exhaustion. **Methods:** Fifty-five patients with metastatic non-small cell lung cancer who had received no prior treatment were randomized into two groups in a 1:1 ratio: the bronchoscopic cryotherapy group or the control group. Patients received up to four cycles of pembrolizumab as monotherapy or in combination with platinum-based chemotherapy. Immune-related adverse events (irAEs), complications, tumor size changes, overall response rate (ORR), and disease control rate (DCR) were evaluated. **Results:** Lung tumors, treated with cryotherapy, demonstrated continuous reduction from the baseline (22.4 cm^2 vs. 14.4 cm^2 vs. 10.2 cm^2, $p < 0.001$). Similar changes were observed in pulmonary tumors in the control group (19.0 cm^2 vs. 10.0 cm^2, $p < 0.001$). The median change in pulmonary tumors between two groups was not significant (−42.9% vs. −27.7%, $p = 0.175$). No significant differences were observed in the ORR (28.6% vs. 23.1%, $p = 0.461$) or target lesion decrease (−24.0% vs. −23.4%, $p = 0.296$) between the groups. However, the DCR was significantly higher in the cryotherapy group (95.2% vs. 73.1%, $p = 0.049$). No cases of serious bleeding during cryotherapy or pneumothorax were observed. Six patients (25.0%) in the cryotherapy group and eight (26.7%) in the control group experienced irAEs. **Conclusions:** Our study demonstrated that combined bronchoscopic cryotherapy and immunotherapy with or without chemotherapy may reduce the rate of progressive disease in metastatic non-small cell lung cancer patients while maintaining a satisfactory safety profile.

Keywords: lung cancer; cryotherapy; immunotherapy

1. Introduction

Lung cancer remains the most frequently diagnosed form of cancer, with nearly 2.5 million new cases in 2022, and it is a leading cause of cancer-related mortality, responsible for an estimated 1.8 million deaths worldwide [1]. The overall survival rate

for non-small cell lung cancer (NSCLC) remains low, largely due to late diagnosis, as 45% of patients present with stage IV disease [2]. Since systemic treatment remains the cornerstone in these cases, the continued development and refinement of targeted therapies and immunotherapies is imperative to improve patient survival.

The tumor immune microenvironment is a heterogeneous and dynamic landscape that influences cancer pathogenesis and response to therapy [3]. An inflamed or "hot" tumor microenvironment has been associated with better prognosis and response to immunotherapy compared to immunologically "cold" tumors [4]. These differences help explain the observed objective response rate of only about 45% in NSCLC patients treated with immunotherapy, also highlighting the need for further studies aimed at transforming "cold" tumors into "hot" ones [5–7].

Cryotherapy is used for local tissue destruction via rapid freeze–thaw cycles [8,9]. This process leads to the formation of intracellular ice crystals, which damage cell membranes and organelles, as well as freezing extracellular water, causing fluid shifts and cell dehydration [9,10]. As malignant cells die in this manner, their neoantigens remain in the body, acting as a form of vaccination. These neoantigens are absorbed by antigen-presenting cells, stimulating adaptive immunity. While this process may induce inflammation in the treated tumor microenvironment, creating a more favorable environment for an anti-tumor immune response, reports have also noted the shrinking of distant untreated metastases. However, subsequent research has shown that cryotherapy alone does not reliably create or sustain this effect [11].

Murine models have demonstrated that cryotherapy can cause the upregulation of programmed cell death protein 1 (PD-1) on T cells and programmed death-ligand 1 (PD-L1) on cancer cells, which ultimately inhibits the systemic anti-tumor response [12,13]. The addition of immune checkpoint inhibitors may counteract this mechanism and induce a stronger anti-tumor immune response. However, current clinical research investigating the synergistic mechanisms of cryotherapy and immunotherapy consists only of a few case reports and small studies [14–17].

The clinical benefits of combining cryotherapy with immune checkpoint inhibitor therapy remain underexplored. This study aims to evaluate the safety and effectiveness of this treatment combination for metastatic NSCLC, in search of more effective therapeutic options.

2. Materials and Methods

2.1. Study Design

Patients with metastatic non-small cell lung cancer and eligible for first-line systemic treatment including immunotherapy were enrolled. Consenting men and women who were at least 18 years old were eligible if they had histologically confirmed metastatic non-small cell lung cancer; no activating EGFR or ALK gene mutations; known PD-L1 expression on tumor cells; scored 0 to 1 according to Eastern Cooperative Oncology Group (ECOG) performance status score [18]; at least one pulmonary lesion, measurable according to the Response Evaluation Criteria in Solid Tumors, version 1.1 (RECIST 1.1) criteria [19] and reachable via flexible bronchoscopy; received no surgical treatment, radiotherapy, or chemotherapy for at least 12 months before the study and no prior immunotherapy. Patients with brain metastases were permitted to enroll after Gamma Knife radiosurgery.

Patients were excluded if they were unable or unwilling to undergo bronchoscopy, were previously diagnosed with autoimmune or immunosuppressive diseases, were currently treated with immunosuppressive drugs or systemic corticosteroids (with prednisolone equivalent doses exceding 10 mg daily), were positive for hepatitis B

virus surface antigen or hepatitis C virus antibody, had active HIV, or had pulmonary tuberculosis infection.

Informed consent was obtained from all subjects involved in the study. Patients were randomized in a 1:1 ratio to receive bronchoscopic cryotherapy. As per standard care, patients further received pembrolizumab monotherapy (for PD-L1 tumor proportion score equal to or greater than 50%) or pembrolizumab and platinum-based chemotherapy (for PD-L1 tumor proportion score less than 50%). Patients who were assigned to the cryotherapy group were offered to continue as controls if the procedure was not technically successful.

This study was conducted in accordance to the guidelines of the Declaration of Helsinki and approved by the Kaunas Regional Biomedical Research Ethics Committee. This study was registered in the United States National Institute of Health trial registry (https://clinicaltrials.gov/) under identifier NCT06000358.

2.2. Procedure

The cryotherapy procedure was performed 7 ($\pm$1) days before the start of systemic treatment via a flexible bronchoscope (Olympus Corporation, Tokyo, Japan), under conscious sedation and visual (for endobronchial cryotherapy) or radial endobronchial ultrasound (EBUS) and fluoroscopy control (for transbronchial cryotherapy), ensuring the correct position of the cryoprobe in the tumor. After being placed in the correct position, the cryoprobe was cooled for at least 30 s, using an ERBECRYO® 2 (Erbe Elektromedizin GmbH, Tübingen, Germany) system and 1.7, 1.9, or 2.4 mm cryoprobes, with smaller diameter cryoprobes used for tumors located in the upper lobes or more peripherally. Carbon dioxide (CO_2) was used as the cryogenic gas. Afterwards, passive cryoprobe thawing for 60 s followed. The cooling–thawing stages were repeated for a total of 3 times to maximize tumor cell destruction in the treated area.

2.3. Assessment

Patients were followed up for up to 4 cycles of systemic therapy. Immune-related adverse events (irAEs) were evaluated using the National Cancer Institute Common Terminology Criteria for Adverse Events, version 5.0 (CTCAE v5.0) [20]. Grade 1 and 2 irAEs were attributed to immunotherapy by the treating physician or a consultant, specializing in the affected system, while grade 3 or higher irAEs were diagnosed only by the consultant.

Tumor imaging was performed using computed tomography (CT) during the time of the fourth cycle, which was 9 to 12 weeks from the beginning of systemic therapy. Tumor response was assessed according to RECIST 1.1 criteria [19]. Cases where a clear response could not be interpreted by radiologist were discussed in a multidisciplinary tumor board meeting. Patients who underwent bronchoscopic cryotherapy procedure also had a chest CT scan at the time of second cycle of systemic therapy. The three scans in cryotherapy group were evaluated for cavitation, necrosis, and surface area (defined as the product of its largest width and length on axial images).

2.4. Statistical Analysis

Due to the size of the study population, continuous variables such as patient age, treated tumor size, and target lesion changes are presented as medians with lower and upper quartiles. Categorical variables are described using frequencies and percentages for each group. The 95% confidence intervals (CI) for the overall response (ORR), described as the proportion of patients with complete (CR) or partial response (PR), and disease control rates (DCR), or the proportion of patients with CR, PR, or stable disease, were calculated using the Clopper–Pearson exact method. Differences in continuous variables between groups were assessed with the Mann–Whitney U test, while repeated measurements were

analyzed using the Wilcoxon signed rank test. Categorical variables were evaluated using Fisher's exact test and chi-square tests. Statistical analyses were conducted using SPSS version 29.0.1.0 (IBM Corp., Armonk, NY, USA). Exact tests were employed, with two-sided *p*-values below 0.05 considered statistically significant for population statistics and continuous variables, whereas one-sided *p*-values below 0.05 were deemed significant for overall response and disease control rates.

3. Results

Between 27 February 2023 and 9 September 2024, a total of 55 patients were enrolled. Out of the 28 patients who were randomized to the cryotherapy group at first, 24 had a successful procedure, resulting in a technical success rate of 85.7%. Of all treated tumors, 11 (45.8%) tumors were treated via transbronchial cryotherapy and 13 (54.2%) with endobronchial cryotherapy. Of all patients treated via the transbronchial approach, only one had achieved the best cryoprobe location excentrically in relation to the tumor. Out of the four unsuccessful procedures, two failed due to inability to locate the pulmonary lesion via radial EBUS, and two failed due to the inability to position the cryoprobe within the tumor. As per protocol, these patients were offered to continue in the control group, with three agreeing and one patient withdrawing their consent to further participate in the study. The patient groups at the beginning and end of the study are provided in Figure 1.

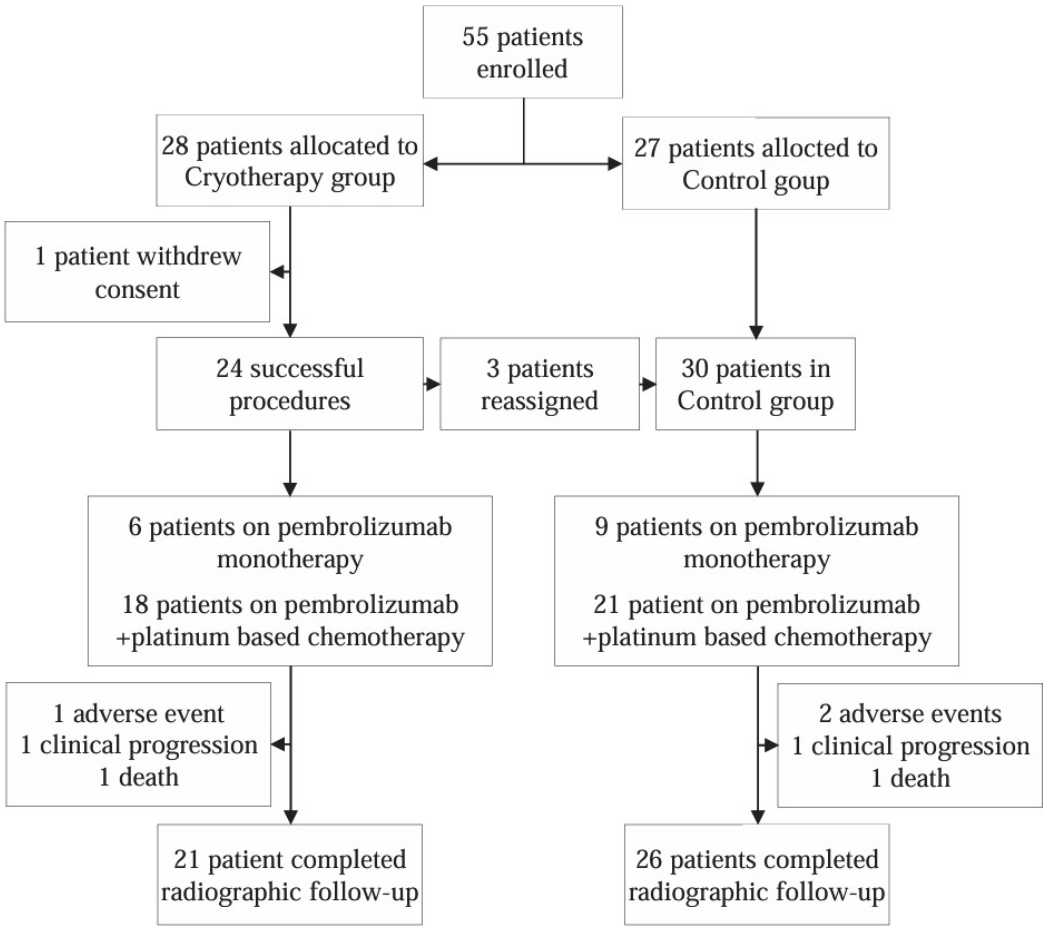

Figure 1. Enrollment and assignment to cryotherapy and control groups.

The majority of patients were male (77.8%) and former or current smokers (88.9%). In total, 36 (66.7%) patients had at least one extrathoracic metastasis, with 16 (66.7%) patients in the cryotherapy group and 20 (66.7%) in the control group (p = 1.000). All patients received systemic treatment with pembrolizumab, although 39 (72.2%) patients received

it with platinum-based chemotherapy. Carboplatin was the drug of choice for 34 (87.2%) of all the patients receiving chemotherapy—16 (88.9%) patients in the cryotherapy group and 18 (85.7%) in the control group ($p = 1.000$). Detailed population statistics are provided in Table 1.

Table 1. Demographic, disease, and treatment characteristics of patients.

	Cryotherapy (*n* = 24)	**Control (*n* = 30)**	**Exact Significance**
Median age—years (range)	64 (62–71)	64 (60–72)	0.841
Male—*n* (%)	19 (79.2)	23 (76.7)	1.000
Smokers—*n* (%)	21 (87.5)	27 (90.0)	1.000
Performance status—*n* (%)			
0	5 (20.8)	7 (23.3)	1.000
1	19 (79.2)	23 (76.7)	
Histology—*n* (%)			
Squamous	11 (45.8)	13 (43.3)	1.000
Adenocarcinoma	13 (54.2)	17 (56.7)	
PD-L1 tumor proportion score—*n* (%)			
<1%	11 (45.8)	12 (40.0)	0.940
1–49%	7 (29.2)	9 (30.0)	
≥50%	6 (25.0)	9 (30.0)	
Brain metastases—*n* (%)	3 (12.5)	5 (16.7)	0.720
Pembrolizumab monotherapy—*n* (%)	6 (25.0)	9 (30.0)	0.766

n—number of patients; PD-L1—programmed death-ligand 1.

Of the 24 patients in the cryotherapy group, 20 underwent CT scans both before and during the second and fourth cycles of systemic treatment. The excluded patients were those who did not complete the treatment course, as well as one patient who missed the second scan.

The median surface area of the treated tumors showed continuous shrinking from the baseline to the time of the fourth cycle, measuring 22.4 (10.1–62.3), 14.4 (10.6–26.6), and 10.2 (6.1–19.1) cm^2 ($p < 0.001$). Additionally, 3 out of 20 (15.0%) patients had signs of cavitation in the tumor treated with cryotherapy at the baseline. This number increased to seven (35.0%) and eight (40.0%) during subsequent scans. Meanwhile, necrosis was observed in 12 (60.0%), 13 (65.0%), and 8 (40.0%) patients at the baseline, second, and fourth cycles, respectively. A pair of representative cases showing tumor reduction and cavitation are shown in Figures 2 and 3.

As a pragmatic comparison, we also measured lung tumors in the control group with signs of being the primary tumor (e.g., single pulmonary tumor, signs of spiculation, etc.). The median surface area of these tumors decreased from 19.0 (7.8–34.9) to 10.0 (4.9–23.1) cm^2 during treatment ($p < 0.001$). Cavitation was observed in four (15.4%) and six (23.1%) patients at the baseline and at the time of the fourth cycle, respectively. Meanwhile, necrosis was present in 9 (34.6%) and 11 (42.3%) cases.

Finally, we measured the surface area change of pulmonary tumors between the two groups. While the change appeared greater in the cryotherapy group, measuring at −42.9% (−16.4% to −73.6%), compared to −27.7% (−6.9% to −57.8%) in the control group, the difference was not statistically significant ($p = 0.175$).

Out of 47 patients who completed radiological follow-up, 12 (25.5%) showed a partial response after four cycles of systemic therapy. A total of 27 patients (57.5%) had stable

disease. Meanwhile, eight patients had progressive disease (17.0%). The distribution of radiological outcomes in different study groups is provided in Table 2.

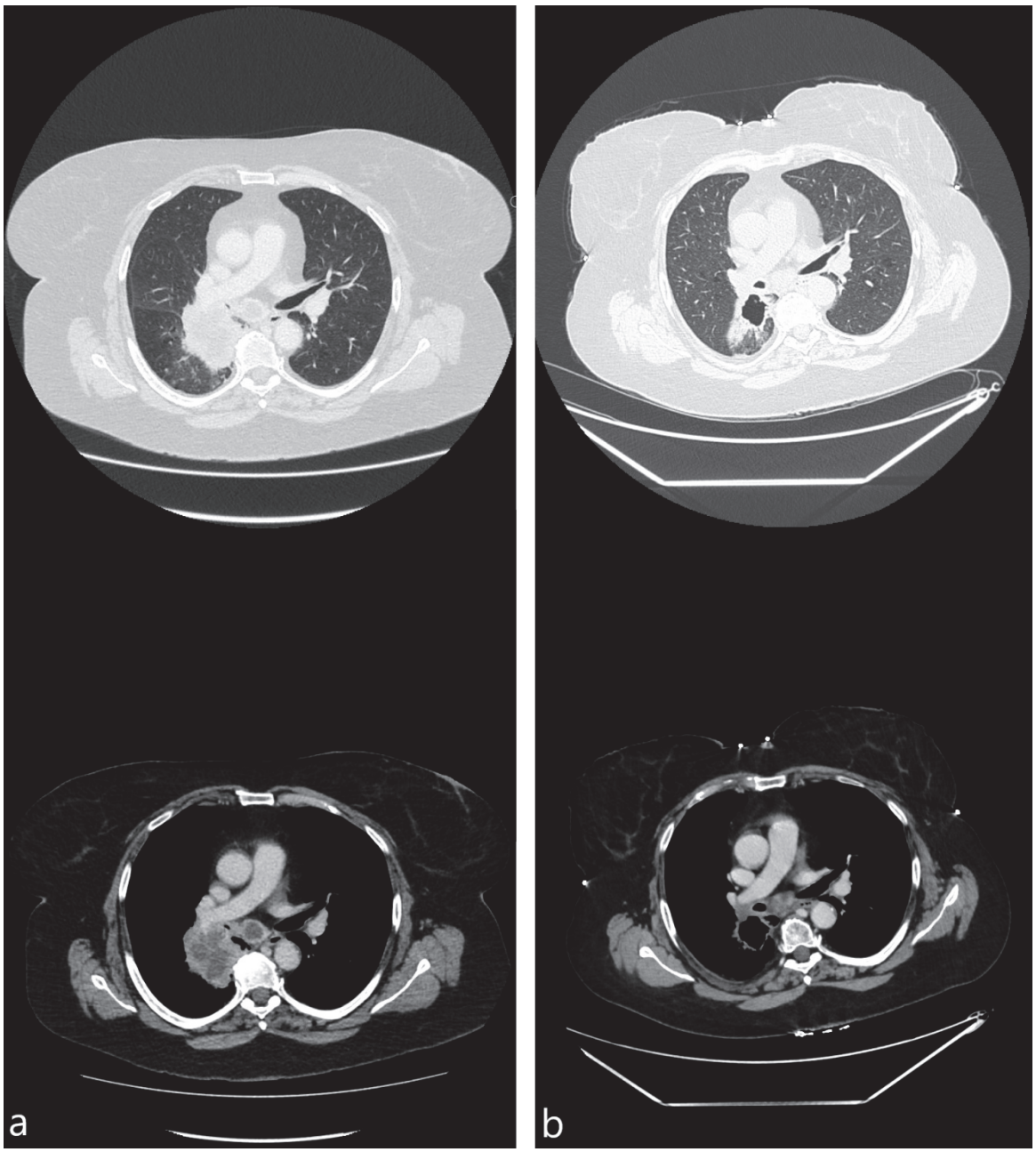

Figure 2. CT images, obtained 1 week before (**a**) and 4 weeks after (**b**) bronchoscopic cryotherapy (59 y.o. female with stage IV squamous cell carcinoma, PD-L1 expression 3%).

Table 2. Comparison of radiological response between study groups.

	Partial Response	**Stable Disease**	**Progressive Disease**
Cryotherapy—*n* (%)	6 (28.6)	14 (66.7)	1 (4.7)
Control—*n* (%)	6 (23.1)	13 (50.0)	7 (26.9)
Total—*n* (%)	12 (25.5)	27 (57.5)	8 (17.0)

n—number of patients.

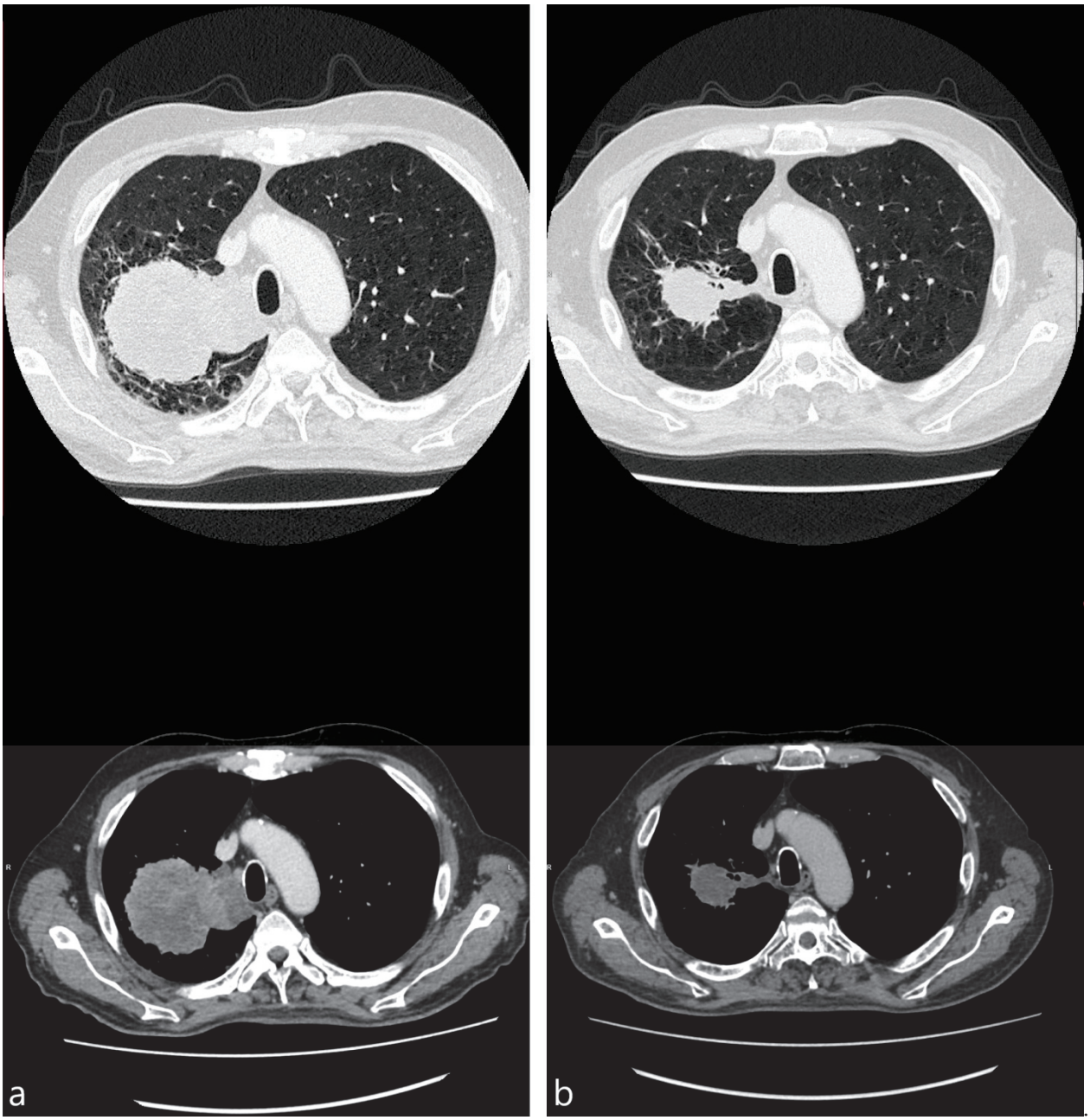

Figure 3. CT images, obtained almost 2 weeks before (**a**) and 4 weeks after (**b**) bronchoscopic cryotherapy (65 y.o. male with stage IV adenocarcinoma, PD-L1 expression 20%).

The ORR was 28.6% (95% CI, 11.3% to 52.2%) in the cryotherapy group and 23.1% (95% CI, 9.0% to 43.6%) in the control group (p = 0.461). Patients in the cryotherapy group had a relative risk of 0.81 (95% CI, 0.31 to 2.14) for no response compared to the control group. Meanwhile, patients in the cryotherapy group had a markedly better DCR. Only one patient in the cryotherapy group experienced progressive disease, resulting in a DCR of 95.2% (95% CI, 76.2% to 99.9%), compared to 73.1% (95% CI, 52.2% to 88.4%) in the control group (p = 0.049). The risk of disease progression in the cryotherapy group was 0.77 (95% CI, 0.60 to 0.99) times that of the control group.

No significant difference in the median change in target lesions between the groups was observed. The median change was −24.0% (−13.8% to −44.1%) in the cryotherapy group and −23.4% (−5.3% to −39.8%) in the control group (p = 0.296). Target lesion changes for both groups are shown in Figures 4 and 5.

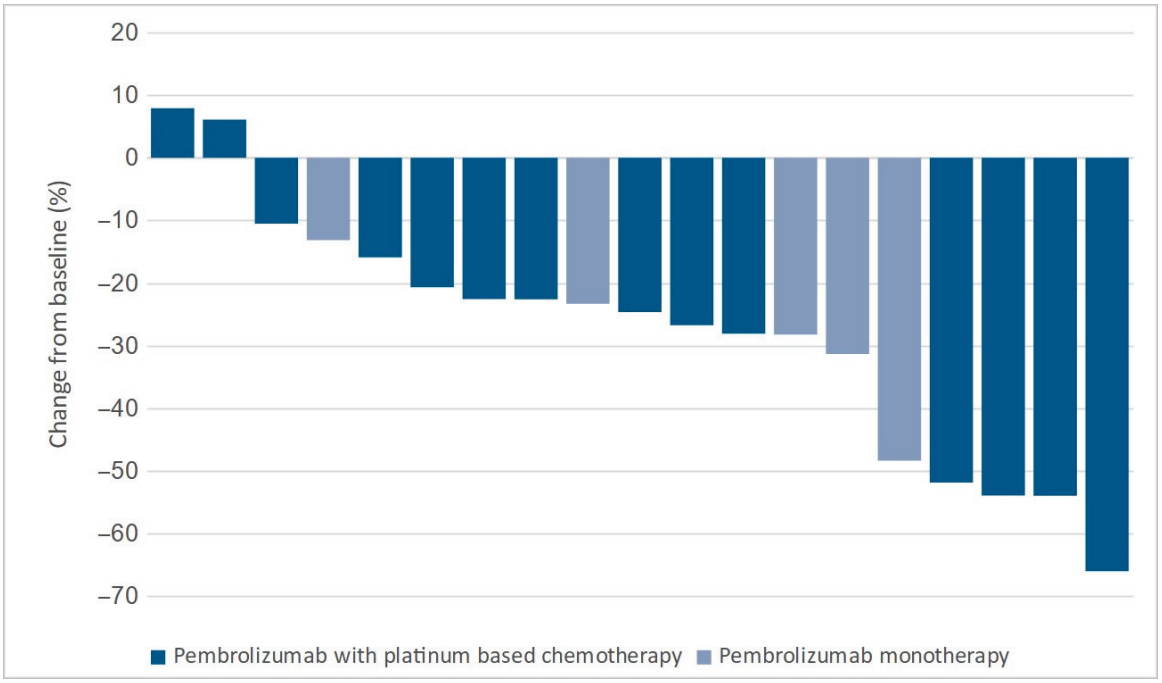

Figure 4. Changes in target lesion size in the cryotherapy group.

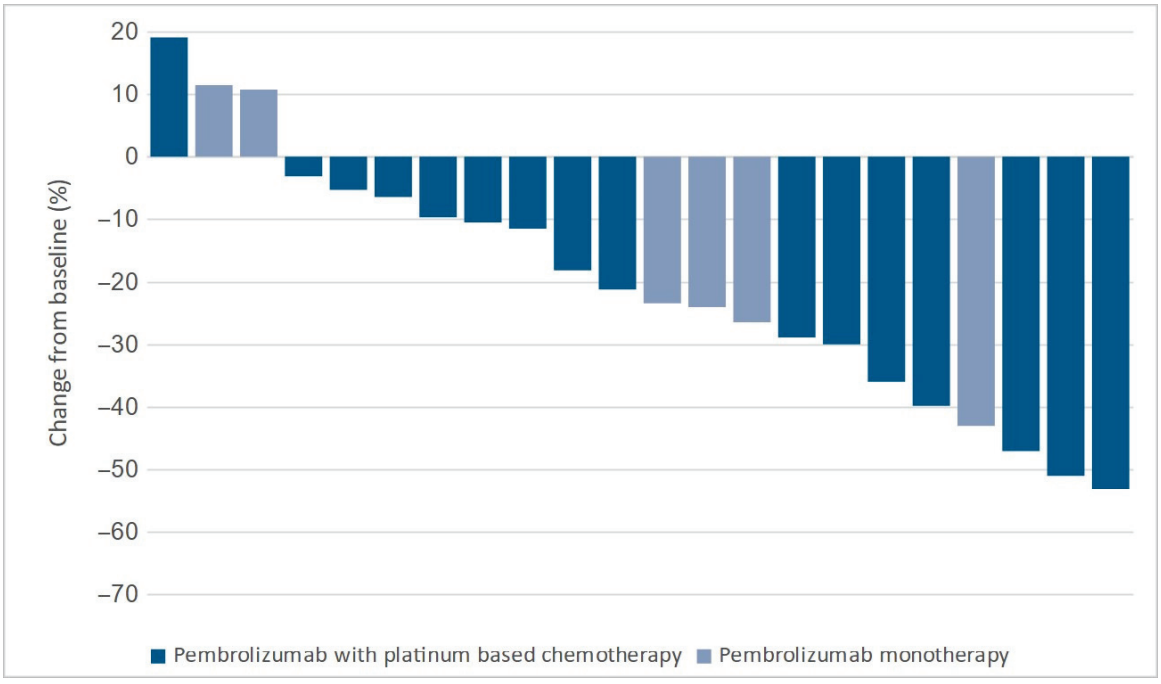

Figure 5. Changes in target lesion size in the control group.

The period following the bronchoscopic therapy procedure was relatively uneventful. Two of the patients experienced subfebrile fever and one experienced mild hemoptysis, all successfully managed conservatively. One patient developed bacterial pneumonia, for which intravenous antibiotics had to be administered. No cases of serious bleeding during procedure or pneumothorax were observed.

The total number of patients who developed irAEs was 14 (25.9%), with 6 (25.0%) being in the cryotherapy group and 8 (26.7%) being in the control group ($p = 1.000$). One patient in the control group experienced two irAEs, those being hyperthyroidism and neuropathy. A total of three cases (5.6%) of grade 3 or higher irAEs were observed, with

one in the cryotherapy group and two in the control group. The most frequent irAEs among both groups were hepatitis, hyperthyroidism, and nephritis, reported in four (7.4%), three (5.6%), and three (5.6%) patients, respectively. Despite premedication, there was a single grade 3 allergic reaction, which was found to be caused by paclitaxel. The distribution of irAEs between groups is provided in Table 3.

Table 3. Immune-related adverse events.

	Cryotherapy (*n* = 24)		**Control (*n* = 30)**		**Total (*n* = 54)**	
Immune-related adverse events	Any grade	Grade ≥ 3	Any grade	Grade ≥ 3	Any grade	Grade ≥ 3
	Number of patients (%)					
Any	6 (25.0)	1 (4.2)	9 (30.0)	2 (6.7)	15 (27.3)	3 (5.5)
Hepatitis	2 (8.3)	1 (4.2)	2 (6.7)	1 (3.3)	4 (7.3)	2 (3.6)
Hyperthyroidism	2 (8.3)	0 (0.0)	1 (3.3)	1 (3.3)	3 (5.5)	1 (1.8)
Hypophysitis	1 (4.2)	0 (0.0)	0 (0.0)	0 (0.0)	1 (1.8)	0 (0.0)
Nephritis	1 (4.2)	0 (0.0)	2 (6.7)	0 (0.0)	3 (5.5)	0 (0.0)
Colitis	0 (0.0)	0 (0.0)	2 (6.7)	0 (0.0)	2 (3.6)	0 (0.0)
Hyperparathyroidism	0 (0.0)	0 (0.0)	1 (3.3)	0 (0.0)	1 (1.8)	0 (0.0)
Neuropathy	0 (0.0)	0 (0.0)	1 (3.3)	0 (0.0)	1 (1.8)	0 (0.0)

The median time to the first irAE did not differ between groups, being 45.5 (23–52.5) days in the cryotherapy group and 34 (25–45.5) days in the control group ($p = 0.607$). The single grade 3 irAE in the cryotherapy group occurred after 49 days, whereas the median time for the two patients in the control group was 31.5 days.

In total, seven patients, three from cryotherapy and four from the control group, discontinued systemic treatment due to adverse events, deteriorating ECOG performance status or, in the case of two patients, death.

4. Discussion

To our knowledge, this is one of the first studies examining the effects of cryotherapy and immunotherapy in metastatic NSCLC patients. The rationale for our research stems from the potential for these treatment modalities to overcome the shortfalls of one another.

Contact cryotherapy with a cryoprobe induces both immediate and delayed effects, resulting in tissue destruction. The immediate effect of cryotherapy is direct cell injury near the probe, caused by intracellular and extracellular ice crystal formation. The delayed effects arise from vasoconstriction and thrombosis, leading to tissue ischemia [9,21,22]. Meanwhile, cells located farther from the probe are not exposed to lethal temperatures and instead undergo apoptosis [21,22]. Necrosis results in the release of cancer cell neoantigens and damage-associated molecular patterns (DAMPs), which facilitate dendritic cell infiltration and maturation. Mature dendritic cells transport neoantigens to regional lymph nodes, presenting them to CD4 and CD8 T lymphocytes via major histocompatibility complex (MHC) class I and II molecules. The dendritic cells also co-present stimulatory proteins, such as CD80 and CD86 and secrete interleukins that are critical for Th1 immune responses, activating specific antitumor lymphocytes [23,24]. Conversely, the uptake of apoptotic cells does not lead to dendritic cell maturation. Instead, it induces a tolerogenic state in dendritic cells, resulting in T cell anergy [22,25]. As necrosis promotes immune activation and apoptosis-immune tolerance, the systemic effects of cryotherapy arise from the balance between these two processes.

An activated immune system has intrinsic mechanisms, such as immune checkpoints, that are in place to prevent prolonged inflammation and minimize damage to healthy tissues. Cancer cells exploit these checkpoints as escape mechanisms, blocking further T cell proliferation and suppressing the continuation of the antitumor immune response. Several studies using murine models have reported increased numbers of PD-1-expressing T cells and the upregulation of PD-L1 expression on tumor cells following tumor cryoablation [12,16,26]. The addition of PD-1/PD-L1 axis inhibitors enables T cells to sustain the antitumor response, effectively destroying both residual tumor tissue after cryoablation and distant metastases [12,16].

In our study, both the pulmonary lesions treated with cryotherapy and those in the control group showed a significant decrease in surface area. This finding suggests that the antitumor immune response, rather than direct cell destruction by cryotherapy, was the primary driving factor behind this effect, and cryotherapy had an insignificant additional effect against established tumors. Conversely, tissue destruction in the cryotherapy group might have been offset by increased infiltration of immune cells. While we did not perform repeat biopsies after cryotherapy to evaluate this possibility, a recent study of eight metastatic NSCLC patients by Desilets et al. found significant upregulation of tumor-infiltrating CD8 T cells in cases where a clinical benefit from immunotherapy with pembrolizumab was observed [27].

Interestingly, our study observed an apparent increase in cavitation in tumors treated with cryotherapy. Cavitation in treatment-naive NSCLC has been associated with a worse prognosis by some authors [28,29]. While Nguyen et al. did not report a similar association with survival, they noted that cavitating NSCLCs were associated with a larger size and greater metabolism on PET/CT scans [30]. Interestingly, Chaudhry et al. found that patients who underwent percutaneous cryoablation for primary stage I lung cancer and developed cavitation did not experience disease recurrence [31]. Cavitation in treatment-naive tumors appears to indicate more aggressive cancer growth, whereas in treated tumors, it seems to represent treatment success and is associated with better outcomes.

While we observed no significant differences between the studied groups in terms of objective response, the cryotherapy group demonstrated increased resistance to disease progression. A robust molecular basis underpins these findings. The potential of cryotherapy to induce a systemic immune response and prevent metastasis was demonstrated by Sabel et al. in a study using 4T1 mammary carcinoma-bearing Balb/c mice [32]. In their study, primary tumors were treated with cryoablation using either a low or high freeze rate, removed surgically, or left untreated. High freeze rate cryoablation resulted in the lowest count of pulmonary metastases (4.89 nodules per mouse), compared to surgical excision (9 nodules per mouse) and untreated controls (47.2 nodules per mouse). Subsequently, lymphocytes from tumor-draining lymph nodes were extracted and cultured with either 4T1 or RENCA tumor cells as a control. Lymphocytes from mice treated with high-freeze-rate cryoablation exhibited increased IFN-γ production after co-culture with 4T1 cells but not RENCA cells, suggesting a tumor-specific immune response. Notably, low freeze rates did not produce a similar effect.

However, the transience of the antitumor response elicited by cryotherapy alone was highlighted by Zhu et al. [12]. In their study, mice inoculated with RENCA cells on bilateral flanks received cryoablation on one side. Examination of the contralateral tumor revealed upregulation of IFN-γ and GZMB on day 3, followed by a decline by day 7. Concurrently, PD-L1 mRNA expression increased. Combining cryoablation with anti-PD-1 therapy significantly decreased distant tumor growth compared to either treatment alone. Similar results were reported by Liu et al. in a murine Lewis lung adenocarcinoma model [13]. In addition to reduced abscopal tumor growth, the combination of cryoablation and anti-PD-1

therapy induced immune memory, resulting in resistance to rechallenge with Lewis lung carcinoma cells but not MC38 colon cancer cells.

The translation of combined cryotherapy and immunotherapy's effectiveness seen in murine models to a clinical setting is mainly limited to several case reports and small studies [14–16,27]. Additionally, one retrospective study examined combined effect of argon–helium cryoablation and monoclonal anti-PD-1 antibody nivolumab immunotherapy in patients with stage IIIb-IV NSCLC, who had a relapse after radiotherapy, surgical resection or radical radiotherapy, or disease progression after chemotherapy [17]. While the comparator was cryoablation alone and not immunotherapy, that study found similar benefits in DCR, but not ORR, as reported by our study. It is possible, that cryotherapy and immunotherapy could synergize to prevent cancer cells from forming metastases, although further research is required to confirm this.

Additional large controlled studies investigating the efficacy of cryotherapy in NSCLC treatment are currently underway (NCT03290677, NCT04049474, NCT04339218, NCT04793815, NCT06000358). Meanwhile, other treatment modalities have also been examined for synergy with immunotherapy. The PEMBRO-RT (NCT02492568) and MDACC (NCT02444741) trials examined the safety and effectiveness of pembrolizumab, with or without radiotherapy. A pooled analysis of these two studies revealed an abscopal response rate of 41.7% in the pembrolizumab-and-radiotherapy group, compared to 19.7% with pembrolizumab monotherapy, as well as increased progression-free and overall survival [33].

We observed no significant complications during bronchoscopic cryotherapy procedures. Bronchoscopy offers a relatively safe and efficient way for cryotherapy for lung tumors and is frequently used for the treatment of endobronchial lesions. Various studies have identified bleeding and pneumothorax as the primary complications of endobronchial cryotherapy, with reported rates of 0.7–12% and 0.1–0.7%, respectively [8]. The main limitations of current bronchoscopic cryotherapy include the difficult positioning of the cryoprobe to fully encompass the lesion, especially compared to percutaneous techniques, and the lower cooling capability of flexible cryoprobes compared to rigid ones [34]. The development of robotic bronchoscopy, advanced imaging techniques, such as cone beam CT, and improved cryoprobe designs may help mitigate these disadvantages in the future.

The safety profile concerning irAEs observed in our study was mainly consistent with previous studies of pembrolizumab treatment for metastatic NSCLC [5,6]. There was no increase in the total number of irAEs after cryotherapy, compared to controls. Two of the most observed irAEs in our study—hyperthyroidism and hepatitis—have also been reported to be among the earliest to arise, with the median time to onset reported at 43 and 63 days, respectively [35].

5. Limitations

Our study has several limitations, primarily a small sample size and a short follow-up period, which may have impacted the significance of some findings. This also prevented a subgroup analysis regarding such important factors as PD-L1 expression, the type of systemic treatment, or histological cancer type. Additionally, the lack of completed clinical studies involving metastatic NSCLC patients treated with a combination of cryotherapy and immunotherapy precludes direct comparisons. Despite these limitations, we believe our findings provide reasonable evidence to justify further research in this field.

6. Conclusions

Our study demonstrated that combined bronchoscopic cryotherapy and immunotherapy with or without chemotherapy may decrease the rate of progressive disease in metastatic non-small cell lung cancer, while maintaining a satisfactory safety profile.

Author Contributions: Conceptualization, G.V. and M.Ž.; Data curation, G.V. and E.Ž.; Funding acquisition, G.V. and M.Ž.; Investigation G.V., M.Ž. and G.M.; Methodology, G.V., M.Ž., S.M. and D.V.; Supervision M.Ž., E.S. and A.M.; Writing—original draft, G.V. and M.Ž.; writing—review and editing, D.V., S.M. and L.P. All authors have read and agreed to the published version of the manuscript.

Funding: This research was funded by a grant from the Research Council of Lithuania (Grant number No. S-MIP-23-97).

Institutional Review Board Statement: The study was conducted in accordance with the Declaration of Helsinki, approved by the Kaunas Regional Biomedical Research Ethics Committee (Protocol Number BE-2-14, 18 January 2023), and registered in the United States National Institutes of Health trial registry (https://clinicaltrials.gov/) under identifier NCT06000358 on 21 August 2023.

Informed Consent Statement: Written informed consent has been obtained from all patients involved in this study.

Data Availability Statement: The data presented in this study are available on request from the corresponding author.

Conflicts of Interest: The authors declare no conflicts of interest.

References

1. Bray, F.; Laversanne, M.; Sung, H.; Ferlay, J.; Siegel, R.L.; Soerjomataram, I.; Jemal, A. Global Cancer Statistics 2022: GLOBOCAN Estimates of Incidence and Mortality Worldwide for 36 Cancers in 185 Countries. *CA Cancer J. Clin.* **2024**, *74*, 229–263. [CrossRef] [PubMed]
2. Araghi, M.; Fidler-Benaoudia, M.; Arnold, M.; Rutherford, M.; Bardot, A.; Ferlay, J.; Bucher, O.; De, P.; Engholm, G.; Gavin, A.; et al. International Differences in Lung Cancer Survival by Sex, Histological Type and Stage at Diagnosis: An ICBP SURVMARK-2 Study. *Thorax* **2022**, *77*, 378–390. [CrossRef] [PubMed]
3. Binnewies, M.; Roberts, E.W.; Kersten, K.; Chan, V.; Fearon, D.F.; Merad, M.; Coussens, L.M.; Gabrilovich, D.I.; Ostrand-Rosenberg, S.; Hedrick, C.C.; et al. Understanding the Tumor Immune Microenvironment (TIME) for Effective Therapy. *Nat. Med.* **2018**, *24*, 541–550. [CrossRef]
4. O'Donnell, J.S.; Teng, M.W.L.; Smyth, M.J. Cancer Immunoediting and Resistance to T Cell-Based Immunotherapy. *Nat. Rev. Clin. Oncol.* **2019**, *16*, 151–167. [CrossRef] [PubMed]
5. Reck, M.; Rodríguez-Abreu, D.; Robinson, A.G.; Hui, R.; Csőszi, T.; Fülöp, A.; Gottfried, M.; Peled, N.; Tafreshi, A.; Cuffe, S.; et al. Pembrolizumab versus Chemotherapy for PD-L1-Positive Non-Small-Cell Lung Cancer. *N. Engl. J. Med.* **2016**, *375*, 1823–1833. [CrossRef] [PubMed]
6. Gandhi, L.; Rodríguez-Abreu, D.; Gadgeel, S.; Esteban, E.; Felip, E.; De Angelis, F.; Domine, M.; Clingan, P.; Hochmair, M.J.; Powell, S.F.; et al. Pembrolizumab plus Chemotherapy in Metastatic Non-Small-Cell Lung Cancer. *N. Engl. J. Med.* **2018**, *378*, 2078–2092. [CrossRef] [PubMed]
7. Yang, B.; Wang, B.; Chen, Y.; Wan, N.; Xie, F.; Yang, N.; Lu, L.; Xiao, W.; Yuan, J.; Li, J.; et al. Effectiveness and Safety of Pembrolizumab for Patients with Advanced Non-Small Cell Lung Cancer in Real-World Studies and Randomized Controlled Trials: A Systematic Review and Meta-Analysis. *Front. Oncol.* **2023**, *13*, 1044327. [CrossRef]
8. DiBardino, D.M.; Lanfranco, A.R.; Haas, A.R. Bronchoscopic Cryotherapy. Clinical Applications of the Cryoprobe, Cryospray, and Cryoadhesion. *Ann. Am. Thorac. Soc.* **2016**, *13*, 1405–1415. [CrossRef]
9. Yakkala, C.; Chiang, C.L.-L.; Kandalaft, L.; Denys, A.; Duran, R. Cryoablation and Immunotherapy: An Enthralling Synergy to Confront the Tumors. *Front. Immunol.* **2019**, *10*, 2283. [CrossRef]
10. Katzman, D.; Wu, S.; Sterman, D.H. Immunological Aspects of Cryoablation of Non-Small Cell Lung Cancer: A Comprehensive Review. *J. Thorac. Oncol.* **2018**, *13*, 624–635. [CrossRef] [PubMed]
11. Baust, J.G.; Snyder, K.K.; Santucci, K.L.; Robilotto, A.T.; Van Buskirk, R.G.; Baust, J.M. Cryoablation: Physical and Molecular Basis with Putative Immunological Consequences. *Int. J. Hyperth.* **2019**, *36*, 10–16. [CrossRef] [PubMed]
12. Zhu, C.; Lin, S.; Liang, J.; Zhu, Y. PD-1 Blockade Enhances the Anti-Tumor Immune Response Induced by Cryoablation in a Murine Model of Renal Cell Carcinoma. *Cryobiology* **2019**, *87*, 86–90. [CrossRef]
13. Liu, Q.; Chen, X.; Qi, M.; Li, Y.; Chen, W.; Zhang, C.; Wang, J.; Han, Z.; Zhang, C. Combined Cryoablation and PD-1 Inhibitor Synergistically Enhance Antitumor Immune Responses in Lewis Lung Adenocarcinoma Mice via the PI3K/AKT/mTOR Pathway. *Biochim. Biophys. Acta Mol. Basis Dis.* **2024**, *1870*, 167262. [CrossRef] [PubMed]
14. Adam, L.C.; Raja, J.; Ludwig, J.M.; Adeniran, A.; Gettinger, S.N.; Kim, H.S. Cryotherapy for Nodal Metastasis in NSCLC with Acquired Resistance to Immunotherapy. *J. Immunother. Cancer* **2018**, *6*, 147. [CrossRef] [PubMed]

15. Nian, J.; Zhu, Y.; Fu, Q.; Yang, G.; Wang, X. Significant Response of Pulmonary Sarcomatoid Carcinoma with Obstructive Atelectasis to Treatment with the PD-1 Inhibitor Camrelizumab Combined with Transbronchial Cryoablation: A Case Report and Literature Review. *Front. Oncol.* **2022**, *12*, 1013047. [CrossRef] [PubMed]
16. Gu, C.; Wang, X.; Wang, K.; Xie, F.; Chen, L.; Ji, H.; Sun, J. Cryoablation Triggers Type I Interferon-Dependent Antitumor Immunity and Potentiates Immunotherapy Efficacy in Lung Cancer. *J. Immunother. Cancer* **2024**, *12*, e008386. [CrossRef] [PubMed]
17. Feng, J.; Guiyu, D.; Xiongwen, W. The Clinical Efficacy of Argon-Helium Knife Cryoablation Combined with Nivolumab in the Treatment of Advanced Non-Small Cell Lung Cancer. *Cryobiology* **2021**, *102*, 92–96. [CrossRef]
18. Oken, M.M.; Creech, R.H.; Tormey, D.C.; Horton, J.; Davis, T.E.; McFadden, E.T.; Carbone, P.P. Toxicity and Response Criteria of the Eastern Cooperative Oncology Group. *Am. J. Clin. Oncol.* **1982**, *5*, 649–655. [CrossRef]
19. Eisenhauer, E.A.; Therasse, P.; Bogaerts, J.; Schwartz, L.H.; Sargent, D.; Ford, R.; Dancey, J.; Arbuck, S.; Gwyther, S.; Mooney, M.; et al. New Response Evaluation Criteria in Solid Tumours: Revised RECIST Guideline (Version 1. *1). Eur. J. Cancer* **2009**, *45*, 228–247. [CrossRef] [PubMed]
20. U.S. Department of Health and Human Services. *National Institutes of Health Common Terminology Criteria for Adverse Events (CTCAE) Version 5.0*; U.S. Department of Health and Human Services: Washington, DC, USA, 2017.
21. Wen, J.; Duan, Y.; Zou, Y.; Nie, Z.; Feng, H.; Lugnani, F.; Baust, J.G. Cryoablation Induces Necrosis and Apoptosis in Lung Adenocarcinoma in Mice. *Technol. Cancer Res. Treat.* **2007**, *6*, 635–640. [CrossRef] [PubMed]
22. Liu, Q.; Zhang, C.; Chen, X.; Han, Z. Modern Cancer Therapy: Cryoablation Meets Immune Checkpoint Blockade. *Front. Oncol.* **2024**, *14*, 1323070. [CrossRef] [PubMed]
23. den Brok, M.H.M.G.M.; Sutmuller, R.P.M.; Nierkens, S.; Bennink, E.J.; Frielink, C.; Toonen, L.W.J.; Boerman, O.C.; Figdor, C.G.; Ruers, T.J.M.; Adema, G.J. Efficient Loading of Dendritic Cells Following Cryo and Radiofrequency Ablation in Combination with Immune Modulation Induces Anti-Tumour Immunity. *Br. J. Cancer* **2006**, *95*, 896–905. [CrossRef] [PubMed]
24. Sánchez-Paulete, A.R.; Teijeira, A.; Cueto, F.J.; Garasa, S.; Pérez-Gracia, J.L.; Sánchez-Arráez, A.; Sancho, D.; Melero, I. Antigen Cross-Presentation and T-Cell Cross-Priming in Cancer Immunology and Immunotherapy. *Ann. Oncol.* **2017**, *28*, xii44–xii55. [CrossRef]
25. Hasegawa, H.; Matsumoto, T. Mechanisms of Tolerance Induction by Dendritic Cells In Vivo. *Front. Immunol.* **2018**, *9*, 350. [CrossRef]
26. Yu, Z.-P.; Sun, X.-W.; He, Y.-P.; Gu, J.; Jin, Y. PD-1 Monoclonal Antibodies Enhance the Cryoablation-Induced Antitumor Immune Response: A Breast Cancer Murine Model Research. *Int. J. Hyperth.* **2023**, *40*, 2164625. [CrossRef] [PubMed]
27. Desilets, A.; Pinheiro, G.; Belkaid, W.; Salko, O.; Malo, J.; Zarour, E.; Jouquan, A.; Thibaudeau, A.J.; Nolin, M.A.; Stagg, J.; et al. CRYOVATE: A Pilot Study of Lung Cancer Cryoactivation in Combination With Immunotherapy in Advanced NSCLC. *JTO Clin. Res. Rep.* **2024**, *5*, 100737. [CrossRef]
28. Kolodziejski, L.S.; Dyczek, S.; Duda, K.; Góralczyk, J.; Wysocki, W.M.; Lobaziewicz, W. Cavitated Tumor as a Clinical Subentity in Squamous Cell Lung Cancer Patients. *Neoplasma* **2003**, *50*, 66–73.
29. Chen, C.; Fu, S.; Ni, Q.; Yiyang, W.; Pan, X.; Jing, J.; Zhao, H.; Rui, W. Cavity Formation Is a Prognostic Indicator for Pathologic Stage I Invasive Lung Adenocarcinoma of $\geq$3 Cm in Size. *Med. Sci. Monit.* **2019**, *25*, 9003–9011. [CrossRef] [PubMed]
30. Nguyen, N.C.; Abhishek, K.; Nyon, S.; Farghaly, H.R.S.; Osman, M.M.; Reimers, H.-J. Are There Radiographic, Metabolic, and Prognostic Differences Between Cavitary and Noncavitary Nonsmall Cell Lung Carcinoma? A Retrospective Fluorodeoxyglucose Positron Emission Tomography/Computed Tomography Study. *Ann. Thorac. Med.* **2016**, *11*, 49–54. [CrossRef] [PubMed]
31. Chaudhry, A.; Grechushkin, V.; Hoshmand, M.; Kim, C.W.; Pena, A.; Huston, B.; Chaya, Y.; Bilfinger, T.; Moore, W. Characteristic CT Findings After Percutaneous Cryoablation Treatment of Malignant Lung Nodules. *Medicine* **2015**, *94*, e1672. [CrossRef] [PubMed]
32. Sabel, M.S.; Su, G.; Griffith, K.A.; Chang, A.E. Rate of Freeze Alters the Immunologic Response after Cryoablation of Breast Cancer. *Ann. Surg. Oncol.* **2010**, *17*, 1187–1193. [CrossRef] [PubMed]
33. Theelen, W.S.M.E.; Chen, D.; Verma, V.; Hobbs, B.P.; Peulen, H.M.U.; Aerts, J.G.J.V.; Bahce, I.; Niemeijer, A.L.N.; Chang, J.Y.; de Groot, P.M.; et al. Pembrolizumab with or without Radiotherapy for Metastatic Non-Small-Cell Lung Cancer: A Pooled Analysis of Two Randomised Trials. *Lancet Respir. Med.* **2021**, *9*, 467–475. [CrossRef] [PubMed]
34. Velez, A.; DeMaio, A.; Sterman, D. Cryoablation and Immunity in Non-Small Cell Lung Cancer: A New Era of Cryo-Immunotherapy. *Front. Immunol.* **2023**, *14*, 1203539. [CrossRef] [PubMed]
35. Brahmer, J.R.; Long, G.V.; Hamid, O.; Garon, E.B.; Herbst, R.S.; Andre, T.; Armand, P.; Bajorin, D.; Bellmunt, J.; Burtness, B.; et al. Safety Profile of Pembrolizumab Monotherapy Based on an Aggregate Safety Evaluation of 8937 Patients. *Eur. J. Cancer* **2024**, *199*, 113530. [CrossRef]

diagnostics

MDPI

Article

Improving Outcomes of CT-Guided Malignant Lung Lesion Microwave Ablation by Tract Sealing Using Venous Blood Clot

Aurimas Mačionis [1,*], Gertrūda Maziliauskienė [1], Rūta Dubeikaitė [1], Donatas Vajauskas [1], Dalia Adukauskienė [2], Irena Nedzelskienė [3] and Marius Žemaitis [4]

[1] Department of Radiology, Medical Academy, Lithuanian University of Health Sciences, LT-44307 Kaunas, Lithuania; gertruda.maziliauskiene@gmail.com (G.M.); ruta.pacinskaite@stud.lsmu.lt (R.D.); donatas.vajauskas@kaunoklinikos.lt (D.V.)
[2] Department of Intensive Care, Medical Academy, Lithuanian University of Health Sciences, LT-44307 Kaunas, Lithuania; dalia.adukauskiene@kaunoklinikos.lt
[3] Department of Dental and Oral Diseases, Hospital of Lithuanian University of Health Sciences Kauno Klinikos, LT-50161 Kaunas, Lithuania; irena.nedzelskiene@lsmu.lt
[4] Department of Pulmonology, Medical Academy, Lithuanian University of Health Sciences, LT-44307 Kaunas, Lithuania; marius.zemaitis@kaunoklinikos.lt
* Correspondence: aurimas.macionis@kaunoklinikos.lt

Abstract: Background: Complications, particularly pneumothorax, are common following lung interventions and occasionally necessitate further examinations, extend hospital stays, increase treatment costs, and result in long-term health impairment or even death. A few lung intervention tract sealants have been explored to reduce procedure-related complications. **Objectives:** The primary objective of this prospective non-randomized study was to assess the complication rates and risk factors for computed tomography-guided lung microwave ablation (MWA) with autologous blood clot as a tract sealant. **Methods:** Twenty-one patients underwent a total of 26 MWA sessions for lung malignancy followed by injection of the patient's clotted venous blood into the ablation tract while retracting the coaxial needle. Ablation tract sealing was successful in all MWA sessions. **Results:** Pneumothorax was the only complication observed in five (19.2%) sessions, with one patient (3.8%) requiring chest tube insertion. The male sex was a statistically significant risk factor for pneumothorax (p = 0.042), and patients with lung emphysema had almost fivefold higher odds of developing pneumothorax (OR 4.8; 95% CI, 0.617–37.351; p = 0.281). **Conclusions:** This study concludes that pneumothorax is the primary complication following lung MWA, and the male sex is a risk factor. Ablation tract sealing with autologous venous blood is a straightforward and inexpensive technique that can reduce the incidence of procedure-related pneumothorax.

Keywords: lung cancer; lung microwave ablation; pneumothorax; tract sealing; autologous blood clot

1. Introduction

There is no denying that the cancer burden is globally increasing. Trachea, bronchus, and lung cancer is currently the most common type of cancer and the leading cause of cancer-related death worldwide, accounting for 2.3 million new cases and 2.0 million deaths in 2021 [1]. Smoking remains the major risk factor for trachea, bronchus, and lung cancer followed by airborne particulate pollution, second-hand smoking, occupational exposure (e.g., asbestos, silica), household air pollution from solid fuels, ionizing radiation, a low-fruit diet, etc. [1,2]. In addition, the lungs are among the most frequent sites for metastatic spread. It is estimated that up to 54% of cancers from different primary sites metastasize to the lungs, most commonly colorectal, breast, renal, and head and neck cancers [3]. An aging population, ongoing exposure to risk factors, and the growing use of imaging techniques and screening programs contribute to the rising number of newly identified primary or metastatic lung lesions.

At present, surgery is considered the treatment of choice for early-stage primary lung cancer and resectable oligometastatic pulmonary disease. Lung thermal ablation techniques (radiofrequency ablation (RFA), microwave ablation (MWA), and cryoablation) are alternative therapeutic approaches that allow direct destruction of tumor lesions by hyperthermal or hypothermal conditions [4]. These procedures are repeatable, minimally invasive, and tissue-preserving because only small incisions are needed to introduce one or a few ablation antennas or probes, and the ablation zone can be adjusted to spare the healthy parenchyma. Regardless of these benefits, thermal ablation is still mostly used in unresectable cases.

The selection of an ablative modality depends on many variables, including the size and location of the tumor, the number of targets, patient comorbidities, and operator experience [4,5]. MWA is a relatively new modality for the treatment of lung tumors. It has several advantages over other thermal ablation techniques, e.g., shorter setup and ablation times, lower sensitivity to the "thermal sink" phenomenon, and the possibility to ablate larger than 3 cm tumors when using several antennas [4]. MWA and RFA are more effective for local disease control than cryoablation [6]. Compared with surgery, MWA can be beneficial due to shorter hospital stays and lower overall medical costs for the treatment [7].

Complications vary among thermal ablation modalities; nonetheless, the safety in terms of major adverse events is comparable between MWA, RFA, and cryoablation [6]. Pneumothorax is the most frequent complication following MWA. Rates for pneumothorax and drainage vary greatly among studies due to the lack of universal patient follow-up protocols for detecting procedure-related complications, the variability in institutional guidelines and general practice methods for managing pneumothorax, and the diversity in study populations regarding potential risk factors. However, recent studies estimate that pneumothorax occurs in 27–52% and requires drainage in 10–24% of lung MWA sessions [8,9]. Other less commonly reported complications following lung MWA include pulmonary hemorrhage, pleural or pericardial effusion, thickening of pericardial layers, pneumonia, lung abscess, and arrhythmia [8–10].

Lung biopsy-related complications demand additional examination, prolong hospitalization, and, on average, increase biopsy cost by 4 times [11]. In recent decades, more attention has been drawn to reducing intervention-related adverse events. Several lung biopsy tract sealants have been explored and shown to decrease pneumothorax and/or chest tube insertion rates, such as autologous blood [12–15], normal saline [16,17], gelatine sponge [18,19], hemostat gelatine powder [20], hydrogel plugs [21–23], collagen foam [24], and fibrin glue [25]. To the best of our knowledge, no human studies have been published analyzing tract sealants for lung microwave ablation and only a couple for radiofrequency ablation: using gelatine sponge slurry with an iodinated contrast medium [26] and gelatine torpedoes soaked in an iodinated contrast medium [27].

Autologous blood clot as an MWA tract sealant is an easy-to-use technique requiring no additional expenses and should be investigated in more detail for reducing post-procedure pneumothorax rates.

2. Materials and Methods

2.1. Study Design

Primary aim: To evaluate the impact of tract sealing using autologous venous blood clot on the rate of pneumothorax following malignant lung lesion microwave ablation.

Secondary aim: To evaluate risk factors for pneumothorax following malignant lung lesion microwave ablation.

This prospective, non-randomized study was approved by the Kaunas Regional Biomedical Research Ethics Committee. Between November 2022 and February 2024, twenty-one patients met the inclusion criteria of this study and underwent MWA for malignant lung lesions.

Inclusion Criteria:

1. Patient Profile:
    - Patients diagnosed with a primary malignant or metastatic lung tumor.
    - Lesions are accessible for microwave ablation at the time of treatment.
    - Maximum diameter of the lesion $\leq$ 3 cm.
    - The intent of radical treatment.
2. Agreement on curative MWA treatment confirmed by a multidisciplinary team, including an interventional radiologist, radiation therapist, thoracic surgeon, oncologist, and pulmonologist.
3. Medical Suitability:
    - No contraindications for general anesthesia or sedation.
    - No severe coagulopathy or patients must be able and willing to stop antiplatelet medications before the procedure.
4. Consent:
    - Patient agreement to participate in this study provided via a signed informed consent form.

Clinical data and tumor- and procedure-related data were collected to analyze risk factors for pneumothorax and its related intervention. Clinical characteristics included age, sex, presence of lung emphysema, or bullae. The tumor characteristics assessed were tumor histology, the number of lesions, and the size and location of these lesions concerning the pleura. All data were collected during patient consultation prior to the MWA procedure from each patient, their medical records, and imaging studies. After the procedure, the interventional radiologist documented the size of the coaxial needle used, the number of pleural punctures and lesions ablated in the session, the distance of aerated lung transversed, and the duration of ablation. Data obtained from control CT scans included the development and severity of complications and were documented by the operating interventional radiologist alongside the management tactic of observation or chest tube insertion. Delayed post-procedure complications were assessed from the patients and their clinical and imaging records the day following MWA and during subsequent patient consultations.

2.2. Microwave Ablation Procedure

Patient preparation included the withdrawal of antiplatelet and anticoagulation medications followed by a fasting period of 8 h before the procedure. Patients underwent sedation or general anesthesia alongside the administration of local anesthetic. The decision on the type of anesthesia was based on the patient's age, functional status, comorbidities, and expected duration of the procedure.

All procedures were performed by a trained and experienced interventional radiologist under CT guidance using Revolution Ascend 64-slice CT scanner (GE Healthcare, Louisville, KY, USA). A low-dose CT scan protocol (tube voltage 100.0 kV, tube current 50.0–100.0 mA) with a 1.25 mm slice thickness was used for initial, intra-procedural, and follow-up imaging. Based on initial diagnostic imaging, the scanning field was adjusted to visualize the area of the lesion to further minimize radiation exposure. An initial CT scan of the area of interest was obtained to determine the safest and most convenient path for intervention as well as the positioning of the patient. The TATO2 system (Biomedical Srl, approved by 93/42/EEC directive, Florence, Italy) was used in all MWA sessions. The system operating frequency was 2.4–2.483 GHz with a maximum output power of 120 W.

All operations were performed using the coaxial needle technique. A 15 G (gauge) coaxial needle was used to introduce an ablation antenna. Antennas with a diameter of 17 G were used by applying a single puncture or overlapping techniques. The used ablative output power was 30 W.

The ablation procedure was considered successful if the post-ablation area completely encompassed all tumor borders by the end of the procedure (Figure 1).

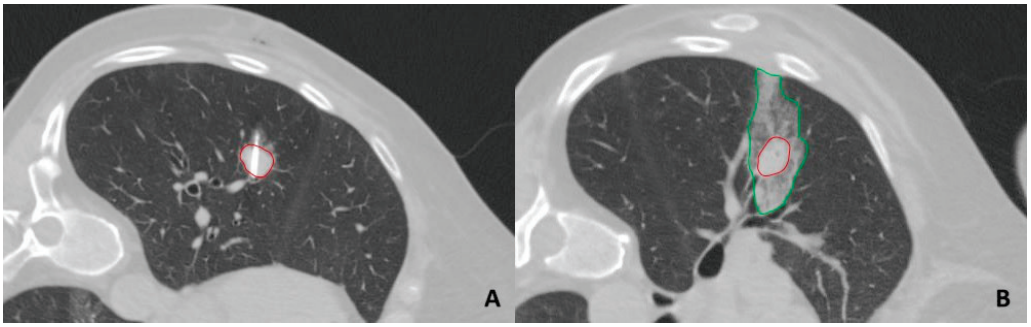

Figure 1. Lung tumor MWA. Image (**A**) shows a tumor transected by the ablation antenna. Image (**B**) shows the post-ablation zone of ground-glass opacity surrounding tumor borders. The red line indicates tumor borders, and the green line indicates ablation zone borders. MWA—microwave ablation.

2.3. Tract Sealing Using an Autologous Venous Blood Clot

Before the MWA procedure, each patient had 10–40 mL of their venous blood drawn into an anticoagulant-free syringe. The blood-filled syringe was kept plunger side down for a minimum of 40 min during the procedure. This allows the formed elements to separate from the plasma, facilitating the formation of a blood clot. The plasma was drained prior to tract sealing.

Upon completion of lesion ablation, the microwave antenna was immediately removed, and a syringe with clotted blood was attached to the coaxial needle. Clotted blood was injected while the coaxial needle was withdrawn by 0.5–1 cm at a time, allowing a few minutes between the steps for the clot to firmly set in the ablation tract. The sealing was repeated in the same manner until the coaxial needle was retracted into the chest wall. Typically, 5 to 20 mL of the patient's venous blood clot was utilized for sealing depending on the number and length of the intervention tracts.

The presence of parenchymal consolidation throughout the course of the ablation antenna up to the pleura was a desired finding consistent with successful ablation tract sealing (Figure 2).

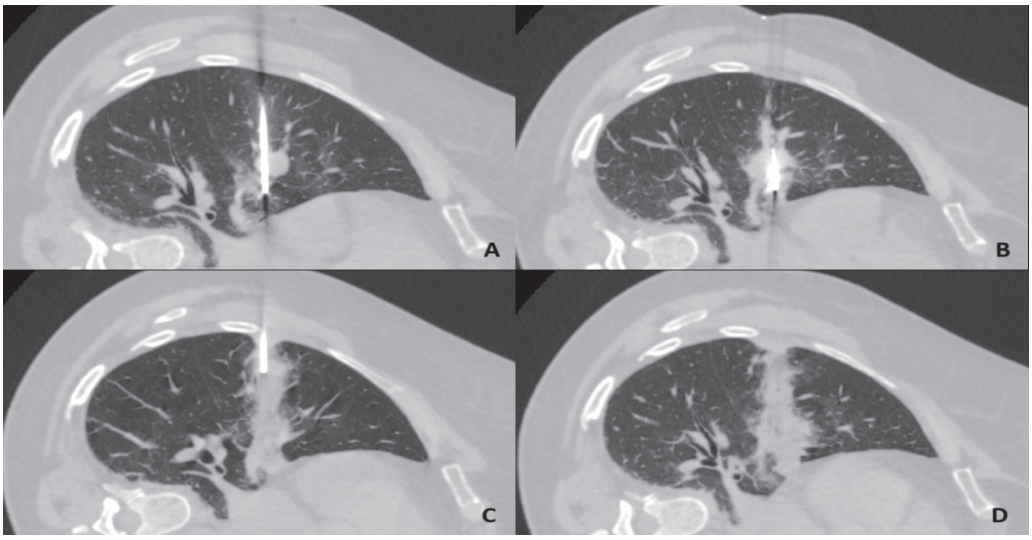

Figure 2. CT-guided lung microwave ablation procedure with tract sealing using clotted autologous blood. (**A**): Right lung middle lobe tumor penetrated by ablation antenna. (**B**): Ablation procedure with the formation of a consolidation zone. (**C**): Ablation tract sealing by injecting autologous blood clot while retracting the coaxial needle. (**D**): Fully sealed ablation tract—focal parenchymal consolidation is present through the entire distance of the transected lung. CT—computed tomography.

Immediately following completion of intervention tract sealing, a sterile patch was applied to the puncture site, and the patient was rolled over to a supine or lateral decubitus position on a puncture-dependent side. If adequate intervention site pressure was not achieved solely through patient positioning, a sandbag was placed at the puncture site to apply additional compression. During recovery, patients were advised to avoid coughing and to remain lying puncture-site down for a minimum of 4 h.

2.4. Assessment of Complications

Patient follow-up for MWA-related complications included a first control chest CT scan 10 min after placing the patient on a puncture-dependent side and a second one 24 h following MWA. If the first control scan was deemed abnormal, an additional CT scan was obtained in the following 10–15 min.

Pneumothorax was regarded as significant if it was large upon initial examination; it increased over time; or the patient had experienced breathing difficulty or chest pain on the ipsilateral side or had developed cyanosis, hypotension, or tachycardia. Only pneumothoraces deemed significant were treated with drainage. If a pneumothorax or hemorrhage was considered non-significant during the first control CT scan, it was assessed on an additional follow-up scan. No parenchymal or pleural hemorrhage increasing with time or requiring treatment was observed in this study population.

Pneumothorax was graded in accordance with the Cardiovascular and Interventional Radiological Society of Europe (CIRSE) criteria [28]:

- Grade 1—complication during the procedure that can be solved within the same session; no additional therapy, no post-procedure sequelae, no deviation from the normal post-therapeutic course.
- Grade 2—prolonged observation including overnight stay (as a deviation from the normal post-therapeutic course < 48 h); no additional post-procedure therapy, no post-procedure sequelae.
- Grade 3—additional post-procedure therapy or prolonged hospital stay (>48 h) required; no post-procedure sequelae.
- Grade 4—complication causing a permanent mild sequela (resuming work and independent living).
- Grade 5—complication causing a permanent severe sequela (requiring ongoing assistance in daily life).
- Grade 6—death.

Parenchymal hemorrhage along the sealed intervention tract and minimal post-procedural pleural effusion were not considered complications as these are likely findings consistent with tract embolization using clotted blood.

All individuals were monitored for at least 24 h after the MWA procedure. Those without significant complications on the second control CT scan were discharged on the same day.

2.5. Statistical Analysis

Statistical analysis of the data was performed using software packages for the storage and analysis of data, SPSS 29.0 (IBM, Armonk, NY, USA). The Mann–Whitney U test was used to compare the quantitative sizes of two independent samples. The interdependence of qualitative evidence was evaluated using the chi-square (χ^2) criteria. Depending on the sample size, exact (for a small-sized sample) and asymptomatic criteria were used. Logistic regression analysis was performed to determine the odds ratio predictive value. Differences between groups were considered significant when the level of significance was $p < 0.05$.

2.6. Control Group

In our center, we began using autologous blood clots as tract sealants for lung lesion biopsy. Noticing the decrease in post-procedure pneumothorax rates [12] and the tech-

nique's cost-effectiveness and simplicity, we have since implemented it for all lung MWA procedures at our institution. For the purpose of evaluating the effectiveness of autologous blood clot as a tract sealant, we refer to our patients who underwent lung lesion biopsy without tract sealing as the control group [12]. Patient follow-up for the assessment of biopsy-related complications slightly differed from MWA patients and included a control chest CT scan 10 min following patient placement on the biopsy-dependent side and a control chest X-ray 24 h post-procedure. If the control CT scan was deemed abnormal, an additional CT scan was obtained in the following 10–15 min. No significant hemorrhagic complications were observed among the biopsy patients. The criteria for dividing pneumothoraces into clinically significant and insignificant were the same in both studies and are described in detail above. Only significant pneumothoraces following biopsy were drained.

3. Results

Twenty-one patients (11 men and 10 women, mean age 67.3 ± 9.3 years; range 48–86 years) were enrolled in this study. A total of 26 MWA sessions were performed in which 30 lesions were ablated. All ablation sessions were successfully completed. Findings consistent with successful ablation tract sealing were observed on control CT scans in all MWA sessions. The histological characteristics of ablated lesions are included in Table 1. Three lesions were repeatedly ablated due to local recurrence observed on follow-up CT scans.

Table 1. Histological characteristics of the ablated lesions.

Characteristic	Number of Lesions (%)
Primary lung cancer	18 (60)
Adenocarcinoma (including adenocarcinoma in situ)	15 (50)
Squamous cell carcinoma	3 (10)
Metastatic lung lesions	12 (40)
Hemangioendothelioma	4 (13.3)
Intestinal adenocarcinoma	3 (10)
Hemangiopericytoma	2 (6.7)
Renal carcinoma	2 (6.7)
Melanoma	1 (3.3)
Repeatedly ablated tumors	3
Total	30

No progressive parenchymal or pleural hemorrhage requiring treatment was noted in this study population. Pneumothorax occurred in five MWA sessions (19.2%), of which one patient had an increasing pneumothorax requiring chest tube insertion (3.8%). The average maximum separation of visceral and parietal pleural surfaces in sessions with pneumothorax was 13.8 mm (range 6–36 mm). The drained patient had a chest tube inserted for three days until pneumothorax was no longer detected on the chest X-ray. No additional intervention was needed, and the patient was discharged four days after MWA with no procedure-related sequelae. Therefore, the complications were graded as Grade 1 or Grade 3 pneumothoraces (Table 2). No procedure-related deaths, events of pneumonia, lung abscess, empyema, pericardial effusion, or arrhythmia was recorded.

In a previous published study conducted in our center, 218 patients underwent lung lesion biopsy, of which for 113 patients, the biopsy tract was sealed using autologous venous blood clot and, for 105 patients, no tract sealing was performed [12]. Comparing the results of the lung lesion biopsy control group with the data from this study, we can observe a decrease in pneumothorax and chest tube insertion rates, though the results are not statistically significant (Table 3).

Table 2. Grading of pneumothorax severity according to the Cardiovascular and Interventional Radiological Society of Europe criteria [28].

Pneumothorax Grade	Number of Patients
Grade 1	4
Grade 2	0
Grade 3	1
Grade 4	0
Grade 5	0
Grade 6	0

Table 3. Comparison of complication rates of lung lesion biopsy without tract sealing versus lung microwave ablation with autologous blood clot as a tract sealant. MWA—microwave ablation.

Group \ Complication	Pneumothorax	*p*-Value	Chest Tube Insertion	*p*-Value
Biopsy without tract sealing	31.4% (33/105)	0.220	10.5% (11/105)	0.458
MWA with tract sealing	19.2% (5/26)		3.8% (1/26)	

The analysis of risk factors for pneumothorax following lung lesion MWA is demonstrated in Table 4. Patient- and procedure-related factors were analyzed with respect to the number of MWA sessions, while lesion-related factors were calculated with respect to the number of lesions treated. Among all investigated factors, only the male sex was found to be a statistically significant risk factor for pneumothorax ($p = 0.042$).

Table 4. Patient-, procedure-, and lesion-related factors for pneumothorax in patients treated with microwave ablation.

	Characteristics		Overall	Pneumothorax	No Pneumothorax	*p*-Value
	Number of Sessions		26	5	21	
Patient-related	Age (y)		66.0 ± 8.8	62.6 ± 5.0	66.8 ± 9.4	0.308
	Sex	Men	14	5 (100%)	9 (42.9%)	0.042
		Women	12	0 (0%)	12 (57.1%)	
	Lung emphysema, bullae	Yes	8	3 (60%)	5 (23.8%)	0.281
		No	18	2 (40%)	16 (76.2%)	
Procedure-related	Number of lesions ablated per session	1	22	4 (80%)	18 (85.7%)	1.000
		2	4	1 (20%)	3 (14.3%)	
	Number of pleural punctures	1	20	5 (100%)	15 (71.4%)	0.298
		2	6	0 (0%)	6 (28.6%)	
	Number of lesions		30	5	25	
Lesion-related	Contact with pleura	Yes	4	1 (20%)	3 (12%)	0.538
		No	26	4 (80%)	22 (88%)	
	Length of aerated lung traversed (mm)		41.4 ± 12.3	36.6 ± 15.3	42.4 ± 12.0	0.300
	Duration of ablation (min)		20.0 ± 10.2	18.4 ± 7.6	20.4 ± 10.8	0.829
	Lesion's maximum diameter (mm)		14.0 ± 6.6	11.4 ± 6.8	14.5 ± 6.6	0.327

Patients with lung emphysema had almost fivefold higher odds of developing pneumothorax (OR 4.8, 95% CI, 0.617–37.351; $p = 0.281$), and lesions in contact with the pleura had almost twice-higher odds of inducing pneumothorax (OR 1.833, 95% CI, 0.150–22.366; $p = 0.538$); however, these findings were not statistically significant. In this study, the only patient who required insertion of a chest tube had emphysema.

4. Discussion

Lung microwave ablation has been insufficiently studied so far as a treatment option for lung cancer. Studies comparing the safety and efficacy of thermal ablation methods with more conventional surgical and stereotactic radiotherapy treatment strategies are scarce. Based on existing publications, MWA seems to be safer in terms of clinically significant and life-threatening complications than surgery [10,29]. However, lung ablation procedures typically require CT guidance, and radiation exposure is a considerable factor in patient management. With the widespread implementation of low-dose CT for lung cancer screening, more attention is drawn to limiting radiation exposure during interventional procedures. Several studies have demonstrated a meaningful reduction in the radiation dose with non-inferior diagnostic accuracy and safety with the implementation of low- or ultra-low-dose CT protocols for lung biopsy [30,31]. To lower patient radiation exposure, we performed all the MWA procedures in this study using a low-dose CT protocol while limiting and adjusting the scanning field.

Pneumothorax is the most common adverse event of lung tumor MWA. Some argue that pneumothorax should not be considered a complication as long as it does not prolong hospitalization stay or require specific treatment [32]. However, according to the literature, up to a quarter of lung MWA patients require chest tube insertion due to increasing or clinically significant pneumothoraces. In this study, the rates of pneumothorax and chest tube insertion following tract sealing are lower compared with those in the most recent MWA studies of a larger sample size without tract sealing: 19.2% vs. 27.4–52% for pneumothorax and 3.8% vs. 10.5–23.5% for chest tube insertion [8,9]. To the best of our knowledge, this is the first human study investigating tract sealing following lung MWA. In a rabbit study, tract sealing with gelatine sponge particles reduced the pneumothorax rate from 56.5% to 25.0% ($p = 0.028$) and the aspiration rate from 26.1% to 8.3% ($p = 0.137$) [33].

Autologous blood has been shown to be beneficial for lung lesion biopsy. Topal U and Berkman Y [34] found that bleeding occurring in the intervention tract has a preventative effect on the development of pneumothorax. In support of this, in a different study conducted in our center, we observed that, among patients without lung biopsy tract sealing, those who had parenchymal hemorrhage surrounding the biopsy site were twice less likely to develop pneumothorax [12]. There are some variations in biopsy tract sealing techniques among researchers that use autologous blood. Clayton J et al. [14] and Graffy P et al. [15] used non-clotted blood and were able to significantly lower both the rate of pneumothorax and its related intervention. Malone L et al. [13] used fragmented blood clot and observed a reduction in pneumothorax from 35% to 26% ($p = 0.12$) and chest tube placement from 18% to 9% ($p = 0.048$). In our center, we were able to reduce pneumothorax rates from 31.4% to 21.2% ($p = 0.087$) and chest tube insertion rates from 10.5% to 7.1% ($p = 0.374$) by introducing autologous blood clots into the biopsy tracts [12]. Results of a recent meta-analysis of studies using intraparenchymal injection of autologous blood (both clotted and un-clotted) following lung biopsy have strongly confirmed a significant reduction in both the incidence of pneumothorax and chest tube placement [35]. Results of the subgroup analysis from the study indicate that the effectiveness of tract sealing is improved when clotted blood is used. In agreement with this idea, we continue to believe that clotted blood is more advantageous than non-clotted blood due to its higher density, which should prolong resorption time, thus further reducing the risk of early air leakage.

One would expect a pneumothorax to occur and require drainage more often for lung MWA patients compared with biopsy patients considering the typically larger-diameter needles used and the longer procedure duration for ablation. For instance, in our center, we use 15 G coaxial needles and 17 G ablation antennas for MWA and 16 G coaxial and 18 G biopsy needles for biopsy. Surprisingly, the rates of pneumothorax and chest tube insertion in our center were slightly lower for MWA patients compared with lung lesion biopsy patients with tract sealing: 19.2% vs. 21.2% and 3.8% vs. 7.1%, respectively [12]. These results can, in part, be attributed to the imbalance in the sizes of the study groups: 113 biopsy patients and 26 MWA sessions.

The results of the current study are non-inferior to the ones published by researchers investigating tract sealants for RFA. In Dassa M et al.'s study [26], pneumothorax occurred in 34%, and drainage was needed in 10% of the patients following RFA with tract sealing using gelatine sponge slurry. In Izaaryene J et al.'s study [27] investigating gelatine torpedoes soaked in an iodinated contrast medium as a sealant for RFA, pneumothorax occurred in 47%, and drainage was needed for 8% of the patients.

No meta-analysis of risk factors for pneumothorax following lung MWA can be found in the literature. However, researchers analyzing pneumothorax complicating RFA concluded that male sex, older age, no previous lung surgeries, an increased diameter of aerated lung crossed, and a greater number of tumors treated in a session are risk factors for ablation-related pneumothorax [36]. A few single-center studies established that the duration of the ablation procedure, the size of the ablated lesion, and the presence of invasion of the adjacent lung lobe were associated with an increased incidence of pneumothorax following MWA [37,38]. The male sex and the presence of emphysema were found to be predisposing factors for the insertion of a chest tube to manage pneumothorax [39]. Our results support these statements as we have established that the male sex was a significant risk factor for pneumothorax, and patients with emphysema have higher odds of developing pneumothorax. Due to the small number of patients requiring chest tube insertion, no risk factors for drainage can be evaluated in our study; however, the only patient who was drained was a man and had lung emphysema.

Despite the evident advantages of various tract-sealing materials in reducing pneumothorax rates, the autologous blood technique is exceptional due to the little to no expenses and time resources required for making a blood clot and sealing the tract. Additional steps needed to perform tract sealing are uncomplicated and, therefore, can be quickly mastered. Due to the natural origin of the substance used, no allergic or inflammatory responses should be activated.

There are some limitations to this study. Firstly, all lung tumor MWA sessions performed in our institution were followed by tract sealing. In order to illustrate the efficacy of tract sealing with autologous blood clot, we referred to our previously published data pertaining to lung lesion biopsy as a control group. We acknowledge differences in the procedural lengths, the materials used, and the sizes of the study groups that can influence the results. Secondly, a small MWA patient sample size may be responsible for some of the contradictory trends we observed, e.g., among sessions that resulted in pneumothorax patients being younger, their lesions being smaller, and the duration of ablation and the distance of traversed lung being shorter. Nonetheless, these trends were not statistically significant. Finally, there is a lack of research on this specific topic. The variety of sealants used and differences in MWA techniques, equipment (e.g., the diameter of the antenna and coaxial needle, and the duration of ablation), and the assessment of risk factors and procedure-related complications among institutions pose a challenge for analyzing and comparing our data with other published research.

Despite the need for further prospective control studies to determine the efficacy of this method in more detail and to provide decisive recommendations, we encourage the application of this methodology as routine practice for patients requiring lung biopsy or ablation.

5. Conclusions

Pneumothorax is the primary complication following lung MWA. This study identified the male sex as the sole risk factor for pneumothorax after lung MWA. Additionally, patients with lung emphysema and lesions adjacent to the pleura were more likely to experience pneumothorax following the ablation. Lung microwave ablation tract sealing using autologous venous blood clot is a quick, easily applied, and low-cost technique that can reduce the incidence of procedure-related pneumothorax. More detailed controlled trials with larger datasets are needed to accurately determine the role of clotted autologous venous blood in reducing complication rates following lung MWA.

Author Contributions: Conceptualization, A.M., M.Ž. and D.V.; methodology, A.M., D.V. and D.A.; data analysis, I.N., R.D. and G.M.; writing—original draft preparation, A.M., R.D. and G.M.; writing—review and editing, A.M., R.D., M.Ž., D.V. and D.A.; supervision, M.Ž. and D.V. All authors have read and agreed to the published version of the manuscript.

Funding: This research received no external funding.

Institutional Review Board Statement: This study was conducted according to the guidelines of the Declaration of Helsinki and approved by the Biomedical Research Ethics Committee of Kaunas Region (protocol number: 2022-BE-10-0015; date: 8 November 2022).

Informed Consent Statement: Informed consent was obtained from all the subjects involved in this study.

Data Availability Statement: The raw data supporting the conclusions of this article will be made available by the authors on request.

Conflicts of Interest: The authors declare no conflicts of interest.

References

1. Kuang, Z.; Wang, J.; Liu, K.; Wu, J.; Ge, Y.; Zhu, G.; Cao, L.; Ma, X.; Li, J. Global, Regional, and National Burden of Tracheal, Bronchus, and Lung Cancer and its Risk Factors from 1990 to 2021: Findings from the Global Burden of Disease Study 2021. *eClinicalMedicine* **2024**, *75*, 102804. [CrossRef] [PubMed]
2. Shankar, A.; Dubey, A.; Saini, D.; Singh, M.; Prasad, C.P.; Roy, S.; Bharati, S.J.; Rinki, M.; Singh, N.; Seth, T.; et al. Environmental and Occupational Determinants of Lung Cancer. *Transl. Lung Cancer Res.* **2019**, *8*, 31–49. [CrossRef] [PubMed]
3. Stella, G.M.; Kolling, S.; Benvenuti, S.; Bortolotto, C. Lung-Seeking Metastases. *Cancers* **2019**, *11*, 1010. [CrossRef]
4. Tafti, B.A.; Genshaft, S.; Suh, R.; Abtin, F. Lung Ablation: Indications and Techniques. *Semin. Interv. Radiol.* **2019**, *36*, 163–175. [CrossRef]
5. Murphy, M.; Wrobel, M.; Fisher, D.; Cahalane, A.M.; Fintelmann, F.J. Update on Image-Guided Thermal Lung Ablation: Society Guidelines, Therapeutic Alternatives, and Postablation Imaging Findings. *Am. J. Roentgenol.* **2022**, *219*, 471–485. [CrossRef]
6. Jiang, B.; Mcclure, M.; Chen, T.; Chen, S. Efficacy and safety of thermal ablation of lung malignancies: A Network meta-analysis. *Ann. Thorac. Med.* **2018**, *13*, 243–250.
7. Han, X.; Wei, Z.; Zhao, Z.; Yang, X.; Ye, X. Cost and effectiveness of microwave ablation versus video-assisted thoracoscopic surgical resection for ground-glass nodule lung adenocarcinoma. *Front. Oncol.* **2022**, *12*, 962630. [CrossRef]
8. Tan, C.; Ho, A.; Robinson, H.; Huang, L.; Ravindran, P.; Chan, D.L.; Alzahrani, N.; Morris, D.L. A Systematic Review of Microwave Ablation for Colorectal Pulmonary Metastases. *Anticancer Res.* **2023**, *43*, 2899–2907. [CrossRef]
9. Yang, X.; Jin, Y.; Lin, Z.; Li, X.; Huang, G.; Ni, Y.; Li, W.; Han, X.; Meng, M.; Chen, J.; et al. Microwave ablation for the treatment of peripheral ground–glass nodule-like lung cancer: Long-term results from a multi-center study. *J. Cancer Res. Ther.* **2023**, *19*, 1001–1010. [CrossRef]
10. Hu, H.; Zhai, B.; Liu, R.; Chi, J.C. Microwave Ablation Versus Wedge Resection for Stage I Non-small Cell Lung Cancer Adjacent to the Pericardium: Propensity Score Analyses of Long-term Outcomes. *Cardiovasc. Interv. Radiol.* **2021**, *44*, 237–246. [CrossRef]
11. Lokhandwala, T.; Bittoni, M.A.; Dann, R.A.; D'Souza, A.O.; Johnson, M.; Nagy, R.J.; Lanman, R.B.; Merritt, R.E.; Carbone, D.P. Costs of Diagnostic Assessment for Lung Cancer: A Medicare Claims Analysis. *Clin. Lung Cancer* **2017**, *18*, 27–34. [CrossRef] [PubMed]
12. Macionis, A.; Zemaitis, M.; Maziliauskiene, G.; Dubeikaite, R.; Vajauskas, D. Reduction of complication rate following CT-guided percutaneous transthoracic lung biopsy by sealing biopsy tract with patient's blood clot. In Proceedings of the ECR 2024 "Next Generation Radiology", Vienna, Austria, 28 February–3 March 2024; p. C-24651.
13. Malone, L.; Stanfill, R.; Wang, H.; Fahey, K.M.; Bertino, R.E. Effect of Intraparenchymal Blood Patch on Rates of Pneumothorax and Pneumothorax Requiring Chest Tube Placement After Percutaneous Lung Biopsy. *AJR Am. J. Roentgenol.* **2013**, *200*, 1238–1243. [CrossRef] [PubMed]
14. Clayton, J.D.; Elicker, B.M.; Ordovas, K.G.; Kohi, M.P.; Nguyen, J.; Naeger, D.M. Nonclotted Blood Patch Technique Reduces Pneumothorax and Chest Tube Placement Rates After Percutaneous Lung Biopsies. *J. Thorac. Imaging* **2016**, *31*, 243–246. [CrossRef]
15. Graffy, P.; Loomis, S.B.; Pickhardt, P.J.; Lubner, M.G.; Kitchin, D.R.; Lee, F.T.; Hinshaw, J.L. Pulmonary Intraparenchymal Blood Patching Decreases the Rate of Pneumothorax-Related Complications following Percutaneous CT–Guided Needle Biopsy. *J. Vasc. Interv. Radiol.* **2017**, *28*, 608–613. [CrossRef]
16. Billich, C.; Muche, R.; Brenner, G.; Schmidt, S.A.; Kruger, S.; Brambs, H.; Pauls, S. CT-guided lung biopsy: Incidence of pneumothorax after instillation of NaCl into the biopsy track. *Eur. Radiol.* **2008**, *18*, 1146–1152. [CrossRef]
17. Li, Y.; Du, Y.; Lou, T.Y.; Yang, H.F.; Yu, J.H.; Xu, X.X.; Zheng, H.J.; Li, B. Usefulness of normal saline for sealing the needle track after CT-guided lung biopsy. *Clin. Radiol.* **2015**, *70*, 1192–1197. [CrossRef]

18. Tran, A.A.; Brown, S.B.; Rosenberg, J.; Hovsepian, D.M. Tract Embolization With Gelatin Sponge Slurry for Prevention of Pneumothorax After Percutaneous Computed Tomography-Guided Lung Biopsy. *Cardiovasc. Interv. Radiol.* **2014**, *37*, 1546–1553. [CrossRef]
19. Renier, H.; Gerard, L.; Lamborelle, P.; Cousin, F. Efficacy of the tract embolization technique with gelatin sponge slurry to reduce pneumothorax and chest tube placement after percutaneous CT-guided lung biopsy. *Cardiovasc. Interv. Radiol.* **2020**, *43*, 597–603. [CrossRef]
20. Baadh, A.S.; Hoffmann, J.C.; Fadl, A.; Danda, D.; Bhat, V.R.; Georgiou, N.; Hon, M. Utilization of the track embolization technique to improve the safety of percutaneous lung biopsy and/or fiducial marker placement. *Clin. Imaging* **2016**, *40*, 1023–1028. [CrossRef]
21. Zaetta, J.M.; Licht, M.O.; Fisher, J.S.; Avelar, R.L. A Lung Biopsy Tract Plug for Reduction of Postbiopsy Pneumothorax and Other Complications: Results of a Prospective, Multicenter, Randomized, Controlled Clinical Study. *J. Vasc. Interv. Radiol.* **2010**, *21*, 1235–1243. [CrossRef]
22. Grage, R.A.; Naveed, M.A.; Keogh, S.; Wang, D. Efficacy of a Dehydrated Hydrogel Plug to Reduce Complications Associated With Computed Tomography–guided Percutaneous Transthoracic Needle Biopsy. *Thorac. Imaging* **2017**, *32*, 57–62. [CrossRef]
23. Ahrar, J.; Gupta, S.; Ensor, J.; Mahvash, A.; Sabir, S.; Steele, J.; McRae, S.; Avritscher, R.; Huang, S.Y.; Odisio, B.; et al. Efficacy of a Self-expanding Tract Sealant Device in the Reduction of Pneumothorax and Chest Tube Placement Rates After Percutaneous Lung Biopsy: A Matched Controlled Study Using Propensity Score Analysis. *Cardiovasc. Interv. Radiol.* **2017**, *40*, 270–276. [CrossRef] [PubMed]
24. Engeler, C.E.; Hunter, D.W.; Castaneda-Zuniga, W.; Tashjian, J.H.; Yedlicka, J.W.; Amplatz, K. Pneumothorax after lung biopsy: Prevention with transpleural placement of compressed collagen foam plugs. *Radiology* **1992**, *184*, 787–789. [CrossRef] [PubMed]
25. Petsas, T.; Siamblis, D.; Giannakenas, C.; Tepetes, K.; Dougenis, D.; Spiropoulos, K.; Fezoulis, I.; Dimopoulos, I. Fibrin glue for sealing the needle track in fine-needle percutaneous lung biopsy using a coaxial system: Part II--Clinical study. *Cardiovasc. Interv. Radiol.* **1995**, *18*, 378–382. [CrossRef]
26. Dassa, M.; Izaaryene, J.; Daidj, N.; Piana, G. Efficacy of Tract Embolization After Percutaneous Pulmonary Radiofrequency Ablation. *Cardiovasc. Interv. Radiol.* **2021**, *44*, 903–910. [CrossRef]
27. Izaaryene, J.; Mancini, J.; Louis, G.; Chaumoitre, K.; Bartoli, J.; Vidal, V.; Gaubert, J. Embolisation of pulmonary radio frequency pathway—A randomised trial. *Int. J. Hyperth.* **2017**, *33*, 814–819. [CrossRef]
28. Filippiadis, D.K.; Binkert, C.; Pellerin, O.; Hoffmann, R.T.; Krajina, A.; Pereira, P.L. Cirse Quality Assurance Document and Standards for Classification of Complications: The Cirse Classification System. *Cardiovasc. Interv. Radiol.* **2017**, *40*, 1141–1146. [CrossRef]
29. Yao, W.; Lu, M.; Fan, W.; Huang, J.; Gu, Y.; Gao, F.; Wang, Y.; Li, J.; Zhu, Z. Comparison between microwave ablation and lobectomy for stage I non-small cell lung cancer: A propensity score analysis. *Int. J. Hyperth.* **2018**, *34*, 1329–1336. [CrossRef]
30. Lee, H.N.; Lee, S.M.; Choe, J.; Lee, S.M.; Chae, E.J.; Do, K.; Seo, J.B. Diagnostic Performance of CT-Guided Percutaneous Transthoracic Core Needle Biopsy Using Low Tube Voltage (100 kVp): Comparison with Conventional Tube Voltage (120 kVp). *Acta Radiol.* **2017**, *59*, 425–433. [CrossRef]
31. Li, C.; Liu, B.; Meng, H.; Lv, W.; Jia, H. Efficacy and Radiation Exposure of Ultra-Low-Dose Chest CT at 100 kVp with Tin Filtration in CT-Guided Percutaneous Core Needle Biopsy for Small Pulmonary Lesions Using a Third-Generation Dual-Source CT Scanner. *J. Vasc. Interv. Radiol.* **2019**, *30*, 95–102. [CrossRef]
32. De Baere, T. Pneumothorax and Lung Thermal Ablation: Is It a Complication? Is It Only About Tract Sealing? *Cardiovasc. Interv. Radiol.* **2021**, *44*, 911–912. [CrossRef] [PubMed]
33. Peng, J.; Bie, Z.; Su, F.; Sun, J.; Li, X. Effects of tract embolization on pneumothorax rate after percutaneous pulmonary microwave ablation: A rabbit study. *Int. J. Hyperth.* **2023**, *40*, 2165728. [CrossRef]
34. Topal, U.; Berkman, Y.M. Effect of needle tract bleeding on occurrence of pneumothorax after transthoracic needle biopsy. *Eur. J. Radiol.* **2005**, *53*, 495–499. [CrossRef] [PubMed]
35. Li, T.; Zhang, Q.; Li, W.; Liu, Y. Autologous Blood Patch Intraparenchymal Injection Reduces the Incidence of Pneumothorax and the Need for Chest Tube Placement Following CT-Guided Lung Biopsy: A Systematic Review and Meta-analysis. *Eur. J. Med. Res.* **2024**, *29*, 108. [CrossRef] [PubMed]
36. Kennedy, S.A.; Milovanovic, L.; Dao, D.; Farrokhyar, F.; Midia, M. Risk Factors for Pneumothorax Complicating Radiofrequency Ablation for Lung Malignancy: A Systematic Review and Meta-Analysis. *J. Vasc. Interv. Radiol.* **2014**, *25*, 1671–1681. [CrossRef]
37. Zhao, H.; Steinke, K. Long-term outcome following microwave ablation of early-stage non-small cell lung cancer. *J. Med. Imaging Radiat. Oncol.* **2020**, *64*, 787–793. [CrossRef]

38. Xu, S.; Bie, Z.X.; Li, Y.M.; Li, B.; Guo, R.Q.; Li, X.G. Computed tomography-guided microwave ablation for the treatment of non-small cell lung cancer patients with and without adjacent lobe invasion: A comparative study. *Thorac. Cancer* **2021**, *12*, 2780–2788. [CrossRef]
39. Zheng, A.; Wang, X.; Yang, X.; Wang, W.; Huang, G.; Gai, Y.; Ye, X. Major Complications After Lung Microwave Ablation: A Single-Center Experience on 204 Sessions. *Ann. Thorac. Surg.* **2014**, *98*, 243–248. [CrossRef]

diagnostics

MDPI

Article

Effectiveness of Apparent Diffusion Coefficient Values in Predicting Pathologic Subtypes and Grade in Non-Small-Cell Lung Cancer

Hasibe Gokce Cinar [1], Kemal Bugra Memis [2], Muhammet Firat Oztepe [3], Erdem Fatihoglu [2], Sonay Aydin [2,*] and Mecit Kantarci [2]

[1] Department of Pediatric Radiology, Etlik City Hospital, 06170 Ankara, Turkey; hgecinar@yahoo.com
[2] Department of Radiology, Erzincan Binali Yildirim University, 24100 Erzincan, Turkey; kemalbugramemis@gmail.com (K.B.M.); erdemfatihoglu@erzincan.edu.tr (E.F.); abdulmecit.kantarci@erzincan.edu.tr (M.K.)
[3] Department of Radiology, Batman Training and Research Hospital, 72000 Batman, Turkey; firatoztepe92@gmail.com
* Correspondence: sonay.aydin@erzincan.edu.tr; Tel.: +90-506-625-91-55

Abstract: Background and Objective: The aim of this study is to evaluate the effectiveness of apparent diffusion coefficient (ADC) values in predicting pathologic subtypes and grade in non-small-cell lung cancer (NSCLC). Materials and Methods: From January 2018 to March 2020, 48 surgically diagnosed NSCLC cases were included in this study. To obtain ADC values, ADC maps were constructed, and a region of interest was put on the tumor. The values were measured three times from different places of the lesion, and the mean value of these measurements was recorded. All MRI scans were evaluated by two radiologists in consensus. Results: A total of 14 cases were squamous cell cancer, 32 cases were adenocarcinoma, and 2 cases were large cell carcinoma. The mean ADC values of adenocarcinoma, squamous cell carcinoma, and large cell cancer were $1.51 \pm 0.19 \times 10^{-3}$ mm^2/s, $1.32 \pm 0.15 \times 10^{-3}$ mm^2/s, and $1.39 \pm 0.25 \times 10^{-3}$ mm^2/s, respectively. There were 11 grade 1, 27 grade 2, and 10 grade 3 NSCLC cases. The mean ADC value was $1.44 \pm 0.14 \times 10^{-3}$ mm^2/s in grade 1 tumors, $1.25 \pm 0.10 \times 10^{-3}$ mm^2/s in grade 2 tumors, and $1.07 \pm 0.15 \times 10^{-3}$ mm^2/s in grade 3 tumors. The cut-off value to discriminate grade 2 from grade 1 tumors was $1.31 \pm 0.11 \times 10^{-3}$ mm^2/s (85% sensitivity, 75% specificity). The cut-off value to discriminate grade 3 from grade 2 tumors was $1.11 \pm 0.15 \times 10^{-3}$ mm^2/s (87% sensitivity, 69% specificity). Conclusions: ADC values can accurately predict NSCLC histopathologic subtypes and tumor grade.

Keywords: non-small-cell lung cancer; diffusion-weighted imaging; ADC value; tumor grade; squamous cell lung cancer; lung adenocarcinoma

1. Introduction

Lung cancer is the most prevalent form of malignant neoplasm and the primary cause of mortality. Based on the latest GLOBOCAN forecasts, there were over 2 million newly diagnosed cases worldwide in 2018. Lung cancer is the next most common type of cancer in males after prostate cancer, with approximately 1.3 million cases. It is the next most common type of cancer in women after breast cancer, with approximately 725,000 cases [1–3].

Lung cancer is classified into two main groups, small-cell lung cancer (SCLC) and non-small-cell lung cancer (NSCLC), based on the origin of the cells. NSCLC is undergoing further division [1]. According to the 2021 WHO classification, the most common forms of NSCLC are adenocarcinoma, squamous cell carcinoma (SCC), and neuroendocrine tumors, such as large cell neuroendocrine carcinoma (LCNEC) and carcinoid [4]. The most common

histological subtype of lung cancer is adenocarcinoma. SCC accounts for 20% of primary lung cancers and is the second most common subtype in the United States [5].

In thoracic radiology, the diagnosis of pulmonary lesions is typically made based on a detailed analysis of the morphological features of the lesion as visualized on computed tomography (CT) scans. Although certain specific features have been clearly defined to help distinguish between benign and malignant lesions, the use of CT alone as a standalone imaging method can sometimes lead to diagnostic difficulties and uncertainties. Additionally, various pathological conditions in which the normal lung structure is significantly damaged, such as in cases of lung fibrosis, further complicate the evaluation and accurate assessment of the lesion with CT imaging alone. These challenges show that CT imaging alone will not be sufficient for a comprehensive evaluation of pulmonary lesions, and additional imaging modalities will be needed [6].

Multiple therapeutic approaches exist for lung cancer, which differ according to the histological subtype of the tumor. Hence, accurately anticipating the pathological attributes of the tumor is essential in order to select the appropriate therapeutic approach. The literature suggests that the apparent diffusion coefficient (ADC) values obtained from diffusion-weighted magnetic resonance imaging (DWI) can be utilized to showcase the histological subtypes of lung malignancies [5].

Recent studies showed that the ADC may emerge as a candidate biomarker associated with histopathological cancer subtypes and the biological properties of tissues. However, DWI of the lung is problematic due to the biochemical and magnetic properties of lung tissue and the physiological movements caused by the heart and large vessels. These factors make it challenging to standardize ADC values, thus raising doubts about their reliability as a biomarker. With the continuous development of MRI technology, fast DWI methods for the lung have been developed. These advanced DWI methods have significantly minimized the artifacts caused by physiological movements within the lung, enhancing the potential of DWI to provide reliable diagnostic information [7,8].

The rapid growth of MRI procedures, such as echo-planar imaging sequences, multichannel coils, and parallel imaging, has made DWI a practical and efficient tool for detecting and identifying tumors [6,9]. DWI of the lung can be performed using two methods: breath hold scanning and free breath scanning. The breath hold imaging method is advantageous because it does not require a long time; images can be taken in a relatively short period of time. However, this method has some notable disadvantages. These include a decrease in the signal-to-noise ratio at high b values, which can compromise the quality of the images, and a low spatial resolution, which can affect the detail and accuracy of the images obtained. On the other hand, free breath imaging can be performed with either cardiac triggering or respiratory triggering to prevent movement artifacts caused by the patient's breathing. Cardiac triggering is effective in preventing pulsation artifacts that can occur due to the heart's motion, but this method typically takes a longer time to complete the imaging process [10]. Respiratory triggering, on the other hand, also plays a significant role in improving the quality of DWI by reducing artifacts that may occur due to respiratory movements, thus providing clearer and more accurate images [11,12]. The 2019 Japanese treatment guidelines recommend the use of MRI for diagnosing lung cancer [13]. DWI has demonstrated considerable promise in distinguishing between malignant and benign pulmonary lesions by using ADC for differential diagnosis in many organs, including the lung, breast, and prostate [9,14]. DWI and ADC mapping have been applied in lung cancer cases in recent years, including the definition of pathological subtypes, tumor grading, establishing the patient's treatment approach, and predicting treatment response [15].

MRI stands out with its better imaging of soft tissue, multiparametric features, and absence of ionizing radiation compared to CT and PET/CT. There is a connection between the functional and metabolic information of imaging methods and the biophysical properties of tissues. DWI identifies microscopic Brownian motions of water in biological tissues. It provides information about diffusion limitations in tissues, reflecting the properties of biological tissues [7,16]. A quantitative assessment of water molecule diffusion in bio-

logical tissues may be achieved by measuring ADC values. Malignant tumors exhibit a significantly lower ADC value compared to normal tissues or benign lesions [17]. In a meta-analysis, Wu et al. [18] showed that DWI can effectively distinguish between malignant and benign lung lesions. Moreover, research has shown that the use of functional DWI is superior to CT in evaluating the effectiveness of chemotherapy and/or radiation in lung tumors [19].

In lung cancer, ADC values have the potential to differentiate between benign and malignant lesions. Furthermore, they can differentiate between various histological subtypes of NSCLC. There are some studies that suggest that ADC values may be prognostic biomarkers correlating with tumor grades. Tumors with lower ADC values tend to have higher grades and more aggressive behavior and thus have a poor prognosis [20].

DWI, which is a non-invasive imaging method and ensures valuable knowledge about the tumor microenvironment, is promising in the management of lung cancer. Integrating ADC values with clinical practices could play a valuable role in guiding the diagnosis and management of lung cancer.

Recently, radiomics has emerged as a non-invasive method for extracting high-dimensional data from radiological images, supplementing the standard methods used in lung cancer diagnosis. This approach offers insights into the cellular and molecular properties of the tissue in addition to the visible characteristics of the tumors, providing a more comprehensive understanding. Radiomics features are valuable for distinguishing between different types of tumors, determining prognosis, and guiding treatment through objective and quantitative data [21].

While there is a substantial body of research exploring the importance of DWI in distinguishing between benign and malignant lung masses, there is a scarcity of studies addressing the diagnostic use of ADC values. The purpose of this study was to assess the diagnostic effectiveness of ADC values in distinguishing between different tumor grades and pathological subtypes in NSCLC.

2. Materials and Methods

The local ethical committee authorized the study protocol for evaluating the use of DWI in lung cancer patients (ethics committee no. Ebyü-kaek-2021-3-2543.32465.11). Because of this investigation's methodology, the informed consent requirement was waived.

2.1. Study Design and Population

In this retrospective cross-sectional investigation, we analyzed MRI scans to establish the correlation between ADC levels and histopathologic subtypes, as well as the tumor grade, in patients with NSCLC.

The criteria for inclusion were as follows: (1) easily accessible chest MRI scans in the medical records of our hospital, spanning from January 2018 to March 2020; (2) patients who had not received any prior treatment; (3) a complete chest MRI examination with DWI data and no missing MRI sequences; and (4) patients who were operated on in our hospital and whose pathology results were obtained after the MRI scan. (1) Patients receiving neoadjuvant chemoradiotherapy, (2) patients who underwent MRI examination but were not operated on in our hospital, (3) patients with a history of lung operation, (4) patients without DWI images in MRI examination, and (5) unusable chest MRI scans (with motion artifacts, etc.) were excluded.

2.2. MRI Protocol

All MRI examinations were conducted using a 1.5-Tesla MRI scanner (MAGNETOM Aera; Siemens Healthineers, Erlangen, Germany) equipped with two six-channel body phased-array coils positioned in the front. The MR images were generated using a coronal T1-weighted spin-echo sequence, an axial fat-saturated T2-weighted sequence, and coronal and axial T2-weighted fast spin-echo sequences. The axial plane was used for the DWI using a single-shot, echo-planar imaging procedure. The DWI series included the following

parameters: In a respiratory-triggered scan, the thickness of each slice was 6 mm. The TR/TE/flip angle values were in the range of 3000–4500/65/90. The b value was between 0 and 800 s/mm^2. The field of vision was 350 mm, and the matrix size was 128 × 128. The ADC maps were automatically created from each DW image using the MR system software (syngo® MR E11, Siemens Healthineers, Erlangen, Germany).

2.3. Measurements and Interpretation

The cross-sectional images were examined via PACS. Two radiologists, one with 9 years of expertise and the other with 11 years of experience, collaboratively evaluated all MRI images. The ADC maps were automatically created using the MR system software, and a region of interest (ROI) was positioned on the tumor to acquire ADC data. Values were calculated at three different points on the lesions. Calculations from cystic–necrotic parts were avoided, and the mean values of these measurements were recorded. A two-dimensional (2D) round ROI area was standardized to 1 cm^2. The obtained ADC values were compared according to both the tumor grade and histopathological subtypes of the NSCLC.

2.4. Statistical Analysis

IBM SPSS Statistics for Windows version 22.0 (IBM Corp., Armonk, NY, USA) was used for all statistical analyses. The normal distribution of the data was tested with the Kolmogorov–Smirnov test. Continuous parameters with normal distribution were stated as the mean ± standard deviation. Categorical data were stated as frequencies (n) and percentages (%). The mean ADC values of the numerical variables in the pathological subtypes and various tumor grade subgroups were compared using a one-way ANOVA test. The effectiveness and success of the diagnostic test were defined by an ROC curve analysis and shown as the positive/negative predictive value, sensitivity, and specificity. Predictive values were calculated using the Youden index. A two-tailed value of $p < 0.05$ was considered statistically significant.

3. Results

During our retrospective analysis, we reviewed chest MRI scans of 72 individuals that were conducted within the designated time frame. A total of 10 patients were eliminated from the research due to the unavailability of pathology data, while 12 patients were omitted because DWI pictures were not acquired. Two patients were eliminated because of inadequate imaging quality.

Totally, 48 pathologically diagnosed NSCLC cases after surgery were included in the study. Of these, 29 (60%) were male and 19 (40%) were female. The mean age was 66.12 ± 8.3 years (range: 47 to 88).

A total of 14 cases were squamous cell cancer, 32 cases were adenocarcinoma, and 2 cases were large cell carcinoma. Figure 1 shows the mean ADC values for NSCLC pathologic cell types. The mean ADC value of adenocarcinoma (1.51 ± 0.19 × 10^{-3} mm^2/s) was substantially greater than that of squamous cell (1.32 ± 0.15 × 10^{-3} mm^2/s) carcinoma ($p = 0.023$). The mean ADC value of large cell cancer was 1.39 ± 0.25 × 10^{-3} mm^2/s. No significant difference was found between squamous cell cancer and large cell cancer or between the mean ADC values for adenocarcinoma and large cell cancer ($p = 0.073$ and $p = 0.061$).

There were 11 grade 1, 27 grade 2, and 10 grade 3 NSCLC cases. Figure 2 shows the mean ADC values for tumor grades. The mean ADC value was 1.44 ± 0.14 × 10^{-3} mm^2/s in grade 1 tumors, 1.25 ± 0.10 × 10^{-3} mm^2/s in grade 2 tumors, and 1.07 ± 0.15 × 10^{-3} mm^2/s in grade 3 tumors. We found a significant negative correlation between tumor grade and ADC values ($p < 0.01$).

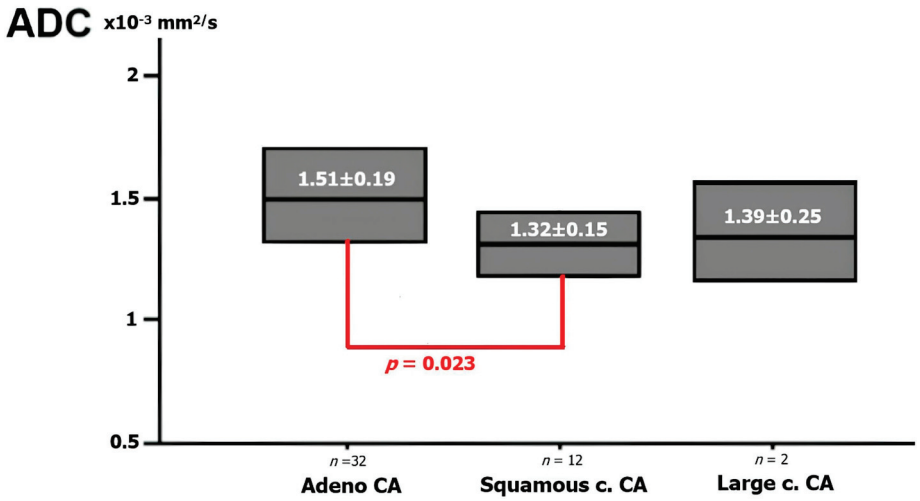

Figure 1. The ADC value for pathologic cell types of NSCLC. The graph shows the ADC values according to each NSCLC pathological subtype. There is a statistically significant difference between adenocarcinoma and SCC, but no significant difference was found between adenocarcinoma and LHH and between SCC and LHH.

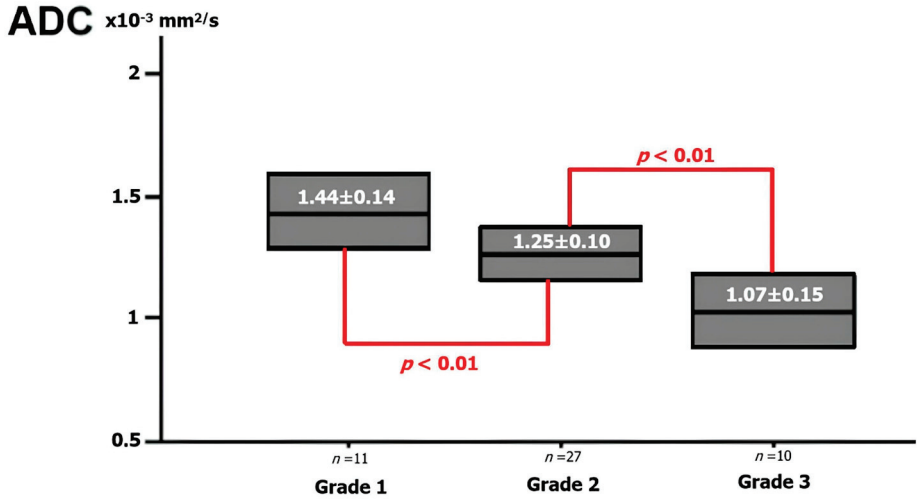

Figure 2. The ADC value for the pathologic grade of NSCLC. The graph shows ADC values according to each NSCLC pathological grade. There is a statistically significant difference between grade 1 and grade 2 and between grade 2 and grade 3 tumors.

Figures 3–5 show thorax MRI images of patients with tumors in the grade 1, 2, and 3 categories, respectively.

The cut-off value to discriminate grade 2 from 1 tumors was $1.31 \pm 0.11 \times 10^{-3}$ mm^2/s (85% sensitivity, 75% specificity). The cut-off value to discriminate grade 3 from 2 tumors was $1.11 \pm 0.15 \times 10^{-3}$ mm^2/s (87% sensitivity, 69% specificity).

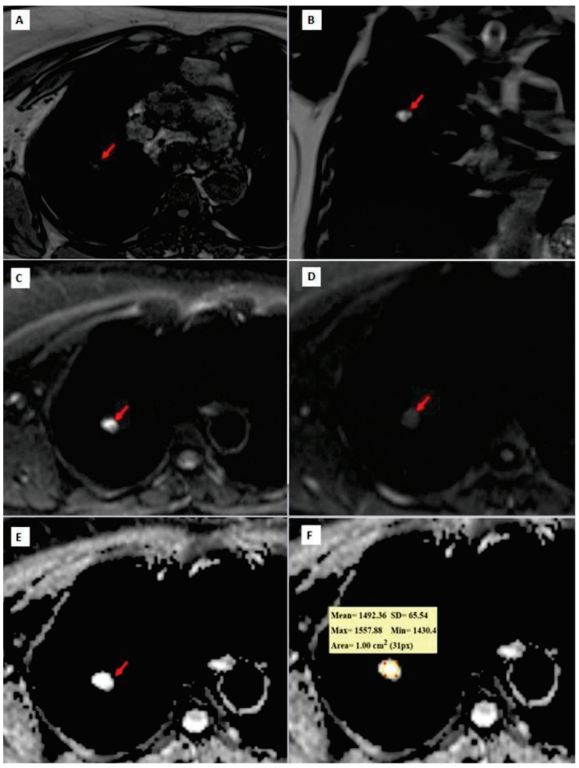

Figure 3. A 72-year-old patient diagnosed with grade 1 adenocarcinoma. (**A**) An axial T1W image showing a hypo-isointense nodule with lobulated contour at the right upper lobe (red arrow). (**B**) A coronal T2W MRI image showing a hyperintense right upper lobe lung nodule (red arrow); (**C**,**D**) b = 0 and b = 800 DW images are shown, respectively. In the b = 0 DW image, there is a hyperintense nodule in the upper lobe of the right lung. In the b = 800 DW images, it is seen that the nodule has lost its signal significantly. (**E**,**F**) In the ADC map, the mean ADC value is measured as 1492.36 $\times$ 10^{-6} mm^2/s within the lesion.

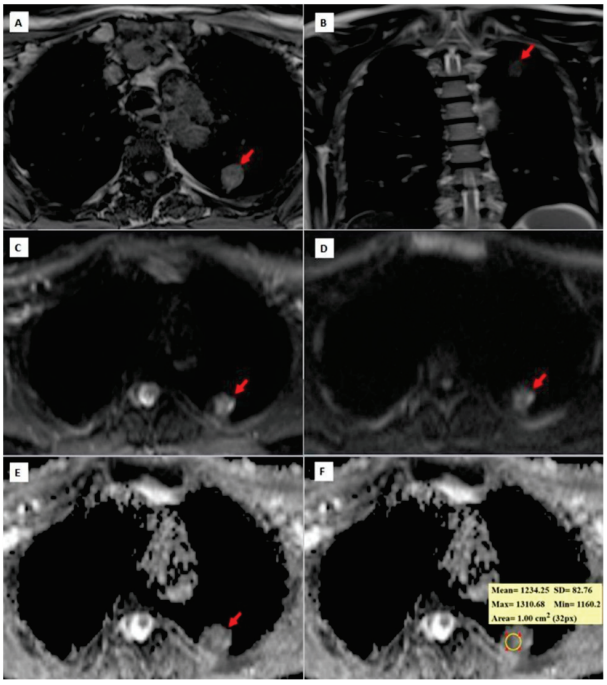

Figure 4. A 62-year-old patient diagnosed with grade 2 squamous cell carcinoma. (**A**) An axial T1W image showing an isointense, round-shaped lung nodule with a slightly spiculated extension towards

the pleura in the upper lobe of the left lung. (**B**) A coronal T2W MRI image showing an isointense left upper lobe lung nodule (red arrow); (**C**,**D**) b = 0 and b = 800 DW images, respectively. In the b = 0 DW images, the nodule has a heterogeneous internal structure and there is a more hyperintense area on the left side of the lesion. In the b = 800 DW images, it is seen that the signal of the lesion decreases slightly and the left side remains more hyperintense than the lesion. (**E**,**F**) ADC maps showing a hypointense nodule and a mean ADC value of 1234.25 $\times$ 10^{-6} mm^2/s. While placing the ROI for measurement on the ADC maps, the asymmetric signal area on the left side of the lesion was excluded in the DW images in order to prevent the DW parameters from being affected by non-tumor areas, such as necrosis, abscess, etc., within the tumor.

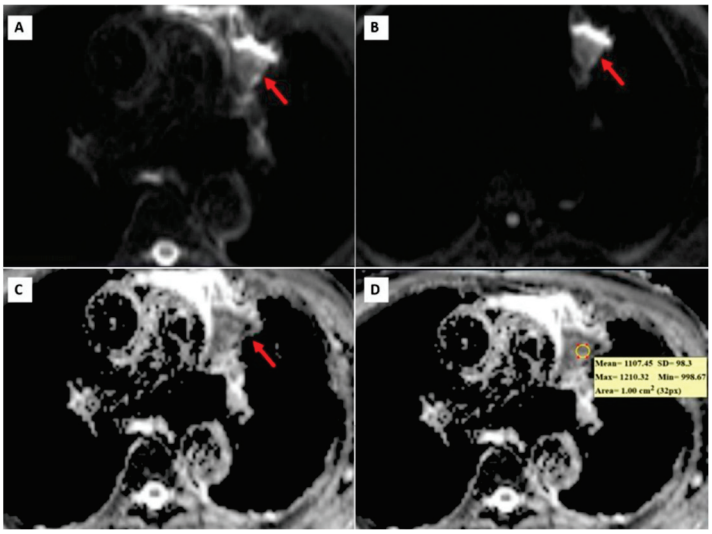

Figure 5. A 68-year-old patient with grade 3 squamous cell carcinoma. (**A**,**B**) b = 0 and b = 800 DW images, respectively. A heterogeneous left upper lobe lung mass (red arrows). (**C**,**D**). ADC maps showing a heterogeneous mass and a mean ADC value of 1107.45 $\times$ 10^{-6} mm^2/s.

4. Discussion

Lung cancer is one of the most important causes of cancer-related deaths worldwide, as stated in numerous studies and supported by statistical data [1]. The prognosis and treatment outcomes of lung cancer vary significantly depending on the histological subtypes and the stage at which the cancer is diagnosed. Therefore, early and accurate determination of these histological subtypes is of critical importance for effective treatment planning and management. Despite advances in imaging technologies and molecular diagnostic methods, there are still some challenges in the diagnosis and prognosis of lung cancer due to the heterogeneous structure and complex behavior of the tumor, which can vary greatly among patients.

Fluoro-2-deoxy-glucose positron emission tomography/computed tomography (FDG-PET/CT) is a widely used imaging technique in lung cancer staging and in distinguishing between benign and malignant nodules [22]. The maximum standardized uptake value (SUVmax) provided by FDG-PET/CT scans offers critical information about the aggressiveness of the tumor. However, there are instances where this method can yield false negative or false positive results, which pose a challenge to its reliability [17]. Additionally, the high radiation dose and significant cost associated with FDG-PET/CT scans constitute considerable limitations of this imaging method.

Recent studies showed that the ADC may emerge as a candidate biomarker associated with histopathological cancer subtypes and the biological properties of tissues. However, DWI of the lung is problematic due to the biochemical and magnetic properties of lung tissue and the physiological movements caused by the heart and large vessels. These factors make it challenging to standardize ADC values, thus raising doubts about its reliability as a biomarker. With the continuous development of MRI technology, fast DWI methods for

the lung have been developed. These advanced DWI images have significantly minimized the artifacts caused by physiological movements within the lung, enhancing the potential of DWI to provide reliable diagnostic information [7,8].

The rapid growth of MRI procedures, such as echo-planar imaging sequence, multi-channel coils, and parallel imaging, has made DWI a practical and efficient tool for detecting and identifying tumors [6,9]. DWI of the lung can be performed using two methods: breath hold scanning and free breath scanning. The breath hold imaging method is advantageous because it does not require a long time; images can be taken in a relatively short period. However, this method has some notable disadvantages. These include a decrease in the signal-to-noise ratio at high b values, which can compromise the quality of the images, and a low spatial resolution, which can affect the detail and accuracy of the images obtained. On the other hand, free breath imaging can be performed with either cardiac triggering or respiratory triggering to prevent movement artifacts caused by the patient's breathing. Cardiac triggering is effective in preventing pulsation artifacts that can occur due to the heart's motion, but this method typically takes a longer time to complete the imaging process [10]. Respiratory triggering, on the other hand, also plays a significant role in improving the quality of DWI by reducing artifacts that may occur due to respiratory movements, thus providing clearer and more accurate images [11,12]. The 2019 Japanese treatment guidelines recommended the use of MRI for diagnosing lung cancer [13]. DWI has demonstrated considerable promise in distinguishing between malignant and benign pulmonary lesions by using ADC for differential diagnosis in many organs, including the lung, breast, and prostate [9,14]. DWI and ADC mapping have been applied in lung cancer cases in recent years, including the definition of pathological subtypes, tumor grading, and establishing the patient's treatment approach and predicting treatment response [15].

DWI is performed with at least two b values. There is no standardized b value in the lung. Increasing the b value increases the sensitivity for detecting diffusion restriction, but this time, image distortion occurs. This affects the image quality more, especially in an organ such as the lung, which is prone to artifacts in MR imaging. In our study, we used two b values: 0 and 800 s/mm^2 [23].

In line with the findings of Usuda et al.'s study [19] involving 226 patients, our current investigation reveals that adenocarcinoma exhibits a much higher ADC value compared to squamous cell carcinoma or large cell carcinoma. Adenocarcinomas include a glandular architecture and produce mucin. This increases the extracellular space and water diffusion. Thus, adenocarcinomas tend to have higher ADC values [12]. In contrast, squamous cell carcinomas and large cell carcinomas have higher cellularity and denser stromal components with lower ADC values [17]. Unfortunately, according to the data collected by Shen et al. [6] in a meta-analysis, a correlation between the ADC values and histological types of lung carcinoma has been suggested; this suggests that ADC measurements may be helpful to distinguish the subtypes of NSCLC. Regrettably, the combined results indicate that there was a convergence of ADC values among the different histological categories of lung cancer. Consequently, ADC measurements were unable to discern between the subtypes of NSCLC. There are some factors, such as keratinization, stratification, and cellular atypias for the classification of lung cancer. These factors play a critical role in defining the histological category of the tumor as they provide detailed information about the cellular architecture and differentiation status of the cancer cells. Furthermore, necrosis, abscess, and other lesions can significantly affect ADC measurements. Abscess with necrosis has low ADC values because it blocks mobility due to its high cellularity and viscosity [24]. These factors can obscure the true diffusion characteristics of tumor tissue. During this study, we found that DWI scanning could reveal histological necrosis and mucinous regions in lung cancer that can affect the ADC values. For accurate ADC measurements, we avoid placing the ROI in these areas and instead perform it from three different points within each lesion. This helps us avoid misleading necrosis and mucinous regions on ADC values and provides a more reliable measurement of tumor diffusion

characteristics. Furthermore, similar to the literature, our investigation found a relationship between ADC values and pathological structures [6,19,25,26].

The pathological type and grade are prognostic factors for lung cancer that can be used in treatment [20]. The ADC value has been used for prognostic factors in some cancer types, including gliomas, prostate cancer, and breast cancer [27–29]. Wang et al. evaluate the effectiveness of fractional anisotropy and ADC values in distinguishing grade 2 and 3 brain gliomas. They reported that the cut-off value of the minimum ADC value was 0.895×10^{-3} mm^2/s and that the sensitivity and specificity were 81.0% and 89.1%, respectively [27]. In their study, Yan et al. investigated the relationship between ADC values in distinguishing low- and intermediate-risk prostate cancer and the Gleason score, which is a prognostic factor for prostate cancer; they reported that the invasiveness of prostate cancer was correlated with low ADC values, and the cut-off values for the discrimination of low- and intermediate-risk prostate cancer were 0.703×10^{-3} mm^2/s for the minimum ADC and 0.927×10^{-3} mm^2/s for the mean ADC, while the sensitivity and specificity were determined to be 85% and 85% for the minimum ADC and 89% and 86% for the mean ADC, respectively [28].

In our study, we investigate the relationship between the ADC value and the prognosis of lung cancer. Our findings indicate that there is a substantial drop in the mean ADC values as the grade of tumors increases in patients with NSCLC. Patients were categorized into grade 1, grade 2, or grade 3 depending on the grades of their tumors. The study conducted by Li et al. on the relationship between ADC values and tumor differentiation degree and pathological subtypes in lung cancer reported that the cut-off value of the mean ADC values in differentiating between well- and moderately-differentiated NSCLC and poorly differentiated NSCLC was 1059.5×10^{-6} mm^2/s, and the sensitivity and specificity were reported as 88% and 76%, respectively. There was a significant difference in the ADC values between small-cell carcinoma and other NSCLC subtypes, but there was no significant difference between SCC and adenocarcinoma [7]. In Kumar et al.'s study that investigated the effectiveness of DW imaging in distinguishing between malignant and benign pulmonary nodules, the mean ADC cut-off value was reported as 1209×10^{-6} mm^2/s, and the sensitivity and specificity values were reported as % 65.2 and % 87.5, respectively [23]. In the ADC histogram analysis conducted by Tsuchiya et al. [15], it is seen that the ADC values corresponding to the 50% percentile of grades 1, 2, and 3 in NSCLC are 1.37, 1.18, and 1.09, respectively. The existing literature contains research that provides evidence of a negative association between tumor grade and ADC levels, as seen in [20,30,31]. The finding that a decreased ADC value is correlated with an elevated pathological tumor grade in NSCLC provides compelling evidence that the ADC value has the potential to be utilized for prognosis evaluation.

This study has some limitations. Significantly, this study conducted a retrospective single-center investigation, which may limit the generalizability of the results. The sample size was relatively small, which could affect the robustness of the statistics. Further research with larger populations is needed to improve the statistical power of the findings. Moreover, we acquired the DWI using a 1.5-T MR scanner with two different b-values in our investigation. The use of a more potent magnetic field, such as a 3.0-T scanner, could potentially enhance the quality of the images and provide more detailed information. More external validation from multiple centers would help to determine the reproducibility and reliability of the results across different clinical settings. The retrospective nature of this study also introduces potential biases which could influence the findings. Additionally, there is a lack of integration of ADC values with other imaging modalities and molecular biomarkers that can affect the diagnostic accuracy in lung cancer.

5. Conclusions

ADC levels are highly helpful in predicting the tumor grade and histopathologic subtypes of NSCLC. The mean ADC value of adenocarcinoma ($1.51 \pm 0.19 \times 10^{-3}$ mm^2/s) was greater than that of squamous cell ($1.32 \pm 0.15 \times 10^{-3}$ mm^2/s) carcinoma ($p = 0.023$).

ADC levels are also helpful in predicting the tumor grade. The mean ADC value is $1.31 \pm 0.11 \times 10^{-3}$ mm^2/s for discriminating grade 2 from grade 1 tumors, and the mean ADC value is $1.11 \pm 0.15 \times 10^{-3}$ mm^2/s for discriminating grade 3 from grade 2 tumors. These values can provide information about the tumor cellularity and structure in addition to traditional histopathological methods. However, additional validation is required for the use of ADC values in clinical practice. Prospective studies are needed in larger populations in which ADC values are compared with other conventional methods to determine the effectiveness of ADC values in the discrimination and categorization of different types of lung lesions. Additionally, the integration of ADC values with other imaging and molecular biomarkers may increase diagnostic accuracy in lung cancer.

Author Contributions: Conceptualization, H.G.C., K.B.M. and E.F.; formal analysis, K.B.M., M.F.O., E.F. and M.K.; funding acquisition and investigation, H.G.C., K.B.M., M.F.O., E.F. and S.A.; methodology, H.G.C., K.B.M. and E.F.; project administration, H.G.C. and S.A.; resources, H.G.C. and K.B.M.; software, H.G.C.; supervision, S.A. and MK; validation, H.G.C., M.F.O., S.A. and M.K.; visualization, E.F.; writing—original draft, H.G.C., K.B.M., M.F.O., E.F. and S.A.; writing—review and editing, H.G.C., M.F.O., S.A. and M.K. All authors have read and agreed to the published version of the manuscript.

Funding: This research received no external funding.

Institutional Review Board Statement: This study was approved by the institutional ethics review board Erzincan Binali Yıldırım University, date: 25 March 2021, approval no: Ebyü-kaek-2021-3-2543.32465.11.

Informed Consent Statement: Informed consent requirement was waived due to this investigation's methodology.

Data Availability Statement: Patient data are not available to the public due to privacy and confidentiality issues.

Conflicts of Interest: The authors declare no conflicts of interest.

References

1. Chaitanya Thandra, K.; Barsouk, A.; Saginala, K.; Sukumar Aluru, J.; Barsouk, A. Epidemiology of Lung Cancer. *Współczesna Onkol.* **2021**, *25*, 45–52. [CrossRef] [PubMed]
2. *Global Cancer Observatory: Cancer Today*; International Agency for Research on Cancer: Lyon, France; Available online: https://gco.iarc.fr/today (accessed on 15 September 2020).
3. Sung, H.; Ferlay, J.; Siegel, R.L.; Laversanne, M.; Soerjomataram, I.; Jemal, A.; Bray, F. Global Cancer Statistics 2020: GLOBOCAN Estimates of Incidence and Mortality Worldwide for 36 Cancers in 185 Countries. *CA Cancer J. Clin.* **2021**, *71*, 209–249. [CrossRef]
4. Nicholson, A.G.; Tsao, M.S.; Beasley, M.B.; Borczuk, A.C.; Brambilla, E.; Cooper, W.A.; Dacic, S.; Jain, D.; Kerr, K.M.; Lantuejoul, S.; et al. The 2021 WHO Classification of Lung Tumors: Impact of Advances Since 2015. *J. Thorac. Oncol.* **2022**, *17*, 362–387. [CrossRef] [PubMed]
5. Barta, J.A.; Powell, C.A.; Wisnivesky, J.P. Global Epidemiology of Lung Cancer. *Ann. Glob. Health* **2019**, *85*, 8. [CrossRef]
6. Shen, G.; Jia, Z.; Deng, H. Apparent Diffusion Coefficient Values of Diffusion-Weighted Imaging for Distinguishing Focal Pulmonary Lesions and Characterizing the Subtype of Lung Cancer: A Meta-Analysis. *Eur. Radiol.* **2016**, *26*, 556–566. [CrossRef]
7. Li, G.; Huang, R.; Zhu, M.; Du, M.; Zhu, J.; Sun, Z.; Liu, K.; Li, Y. Native T1-Mapping and Diffusion-Weighted Imaging (DWI) Can Be Used to Identify Lung Cancer Pathological Types and Their Correlation with Ki-67 Expression. *J. Thorac. Dis.* **2022**, *14*, 443–454. [CrossRef] [PubMed]
8. Keogan, M.T.; Edelman, R.R. Technologic Advances in Abdominal MR Imaging. *Radiology* **2001**, *220*, 310–320. [CrossRef]
9. Rashed, M.M.; Nekooei, S.; Nouri, M.; Borji, N.; Khadembashi, A. Evaluation of DWI and ADC Sequences' Diagnostic Values in Benign and Malignant Pulmonary Lesions. *Turk. Thorac. J.* **2020**, *21*, 390–396. [CrossRef]
10. Razek, A.A.K.A. Diffusion Magnetic Resonance Imaging of Chest Tumors. *Cancer Imaging* **2012**, *12*, 452–463. [CrossRef]
11. Kartalis, N.; Loizou, L.; Edsborg, N.; Segersvärd, R.; Albiin, N. Optimising Diffusion-Weighted MR Imaging for Demonstrating Pancreatic Cancer: A Comparison of Respiratory-Triggered, Free-Breathing and Breath-Hold Techniques. *Eur. Radiol.* **2012**, *22*, 2186–2192. [CrossRef]
12. Chen, L.; Liu, M.; Bao, J.; Xia, Y.; Zhang, J.; Zhang, L.; Huang, X.; Wang, J. The Correlation between Apparent Diffusion Coefficient and Tumor Cellularity in Patients: A Meta-Analysis. *PLoS ONE* **2013**, *8*, e79008. [CrossRef]

13. Akamatsu, H.; Ninomiya, K.; Kenmotsu, H.; Morise, M.; Daga, H.; Goto, Y.; Kozuki, T.; Miura, S.; Sasaki, T.; Tamiya, A.; et al. The Japanese Lung Cancer Society Guideline for Non-Small Cell Lung Cancer, Stage IV. *Int. J. Clin. Oncol.* **2019**, *24*, 731–770. [CrossRef] [PubMed]
14. Santos, M.K.; Elias Júnior, J.; Mauad, F.M.; Muglia, V.F.; Trad, C.S. Ressonância Magnética Do Tórax: Aplicações Tradicionais e Novas, Com Ênfase Em Pneumologia. *J. Bras. Pneumol.* **2011**, *37*, 242–258. [CrossRef] [PubMed]
15. Tsuchiya, N.; Doai, M.; Usuda, K.; Uramoto, H.; Tonami, H. Non-Small Cell Lung Cancer: Whole-Lesion Histogram Analysis of the Apparent Diffusion Coefficient for Assessment of Tumor Grade, Lymphovascular Invasion and Pleural Invasion. *PLoS ONE* **2017**, *12*, e0172433. [CrossRef] [PubMed]
16. Le Bihan, D.; Breton, E.; Lallemand, D.; Aubin, M.L.; Vignaud, J.; Laval-Jeantet, M. Separation of Diffusion and Perfusion in Intravoxel Incoherent Motion MR Imaging. *Radiology* **1988**, *168*, 497–505. [CrossRef]
17. Usuda, K.; Iwai, S.; Yamagata, A.; Sekimura, A.; Motono, N.; Matoba, M.; Doai, M.; Yamada, S.; Ueda, Y.; Hirata, K.; et al. Relationships and Qualitative Evaluation between Diffusion-Weighted Imaging and Pathologic Findings of Resected Lung Cancers. *Cancers* **2020**, *12*, 1194. [CrossRef]
18. Wu, L.-M.; Xu, J.-R.; Hua, J.; Gu, H.-Y.; Chen, J.; Haacke, E.M.; Hu, J. Can Diffusion-Weighted Imaging Be Used as a Reliable Sequence in the Detection of Malignant Pulmonary Nodules and Masses? *Magn. Reson. Imaging* **2013**, *31*, 235–246. [CrossRef] [PubMed]
19. Usuda, K.; Iwai, S.; Funasaki, A.; Sekimura, A.; Motono, N.; Matoba, M.; Doai, M.; Yamada, S.; Ueda, Y.; Uramoto, H. Diffusion-Weighted Magnetic Resonance Imaging Is Useful for the Response Evaluation of Chemotherapy and/or Radiotherapy to Recurrent Lesions of Lung Cancer. *Transl. Oncol.* **2019**, *12*, 699–704. [CrossRef]
20. Razek, A.A.K.A.; Fathy, A.; Gawad, T.A. Correlation of Apparent Diffusion Coefficient Value With Prognostic Parameters of Lung Cancer. *J. Comput. Assist. Tomogr.* **2011**, *35*, 248–252. [CrossRef]
21. Pan, F.; Feng, L.; Liu, B.; Hu, Y.; Wang, Q. Application of Radiomics in Diagnosis and Treatment of Lung Cancer. *Front. Pharmacol.* **2023**, *14*, 1295511. [CrossRef]
22. Gould, M.K.; Maclean, C.C.; Kuschner, W.G.; Rydzak, C.E.; Owens, D.K. Accuracy of Positron Emission Tomography for Diagnosis of Pulmonary Nodules and Mass Lesions. *JAMA* **2001**, *285*, 914. [CrossRef] [PubMed]
23. Kumar, N.; Sharma, M.; Aggarwal, N.; Sharma, S.; Sarkar, M.; Singh, B.; Sharma, N. Role of Various DW MRI and DCE MRI Parameters as Predictors of Malignancy in Solid Pulmonary Lesions. *Can. Assoc. Radiol. J.* **2021**, *72*, 525–532. [CrossRef]
24. Ebisu, T.; Tanaka, C.; Umeda, M.; Kitamura, M.; Naruse, S.; Higuchi, T.; Ueda, S.; Sato, H. Discrimination of Brain Abscess from Necrotic or Cystic Tumors by Diffusion-Weighted Echo Planar Imaging. *Magn. Reson. Imaging* **1996**, *14*, 1113–1116. [CrossRef]
25. Usuda, K.; Sagawa, M.; Motono, N.; Ueno, M.; Tanaka, M.; Machida, Y.; Maeda, S.; Matoba, M.; Kuginuki, Y.; Taniguchi, M.; et al. Diagnostic Performance of Diffusion Weighted Imaging of Malignant and Benign Pulmonary Nodules and Masses: Comparison with Positron Emission Tomography. *Asian Pac. J. Cancer Prev.* **2014**, *15*, 4629–4635. [CrossRef] [PubMed]
26. Nasu, K.; Kuroki, Y.; Minami, M. Diffusion-Weighted Imaging Findings of Mucinous Carcinoma Arising in the Ano-Rectal Region: Comparison of Apparent Diffusion Coefficient with That of Tubular Adenocarcinoma. *Jpn. J. Radiol.* **2012**, *30*, 120–127. [CrossRef]
27. Wang, Q.; Zhang, J.; Xu, X.; Chen, X.; Xu, B. Diagnostic Performance of Apparent Diffusion Coefficient Parameters for Glioma Grading. *J. Neurooncol.* **2018**, *139*, 61–68. [CrossRef]
28. Yan, X.; Ma, K.; Zhu, L.; Pan, Y.; Wang, Y.; Shi, J.; Mai, X. The Value of Apparent Diffusion Coefficient Values in Predicting Gleason Grading of Low to Intermediate-Risk Prostate Cancer. *Insights Imaging* **2024**, *15*, 137. [CrossRef] [PubMed]
29. Aktas, E.; Uylar Seber, T.; Seber, T.; Burcek, N.V.; Akay, E.; Arslan, A.; Karagöz Eren, S.; Ozhan, N.; Yaltırık Bilgin, E.; Savran, B.; et al. The Relationship between Breast Cancer Subtypes, Prognostic Factors, and Apparent Diffusion Coefficient Histogram Analysis. *Curr. Med. Imaging Rev.* **2024**, *20*, e15734056271069. [CrossRef] [PubMed]
30. Weiss, E.; Ford, J.C.; Olsen, K.M.; Karki, K.; Saraiya, S.; Groves, R.; Hugo, G.D. Apparent Diffusion Coefficient (ADC) Change on Repeated Diffusion-Weighted Magnetic Resonance Imaging during Radiochemotherapy for Non-Small Cell Lung Cancer: A Pilot Study. *Lung Cancer* **2016**, *96*, 113–119. [CrossRef]
31. Jagoda, P.; Fleckenstein, J.; Sonnhoff, M.; Schneider, G.; Ruebe, C.; Buecker, A.; Stroeder, J. Diffusion-Weighted MRI Improves Response Assessment after Definitive Radiotherapy in Patients with NSCLC. *Cancer Imaging* **2021**, *21*, 15. [CrossRef]

diagnostics

MDPI

Article

Rare Driver Mutations in Advanced, Oncogene-Addicted Non-Small Cell Lung Cancer: A North Italian, Real-World, Registry Experience

Kalliopi Andrikou [1], Paola Ulivi [2,*], Elisabetta Petracci [3], Irene Azzali [3], Federica Bertolini [4], Giulia Alberti [5], Stefania Bettelli [6], Daniele Calistri [2], Elisa Chiadini [2], Laura Capelli [2], Paola Cravero [1], Giorgia Guaitoli [4], Francesca Zanelli [5], Marco Angelo Burgio [1], Maria Pagano [5], Alberto Verlicchi [1], Enrica Martinelli [4], Katia Di Emidio [4], Massimo Dominici [4], Carmine Pinto [5] and Angelo Delmonte [1]

[1] Medical Oncology, IRCCS Istituto Romagnolo per lo Studio dei Tumori "Dino Amadori" (IRST), 47014 Meldola, Italy; kalliopi.andrikou@irst.emr.it (K.A.); paola.cravero@irst.emr.it (P.C.); marco.burgio@irst.emr.it (M.A.B.); alberto.verlicchi@irst.emr.it (A.V.); angelo.delmonte@irst.emr.it (A.D.)
[2] Bioscience Laboratory, IRCCS Istituto Romagnolo per lo Studio dei Tumori "Dino Amadori" (IRST), 47014 Meldola, Italy; daniele.calistri@irst.emr.it (D.C.); elisa.chiadini@irst.emr.it (E.C.); laura.capelli@irst.emr.it (L.C.)
[3] Unit of Biostatistics and Clinical Trials, IRCCS Istituto Romagnolo per lo Studio dei Tumori (IRST) "Dino Amadori", 47014 Meldola, Italy; elisabetta.petracci@irst.emr.it (E.P.); irene.azzali@irst.emr.it (I.A.)
[4] Oncology Department, Modena University Hospital, 41125 Modena, Italy; bertolini.federica@policlinico.mo.it (F.B.); giorgia.guaitoli@unimore.it (G.G.); enrichelli14@gmail.com (E.M.); diemidio.katia@aou.mo.it (K.D.E.); massimo.dominici@unimore.it (M.D.)
[5] Medical Oncology, IRCCS Arcispedale Santa Maria Nuova, 42123 Reggio Emilia, Italy; giulia.alberti@ausl.re.it (G.A.); zanelli.francesca@ausl.re.it (F.Z.); maria.pagano@ausl.re.it (M.P.); carmine.pinto@ausl.re.it (C.P.)
[6] Biomolecular Pathology Unit, Azienda Ospedaliera Unica di Modena, 41125 Modena, Italy; bettelli.stefania@aou.mo.it
* Correspondence: paola.ulivi@irst.emr.it

Abstract: The real-world, retrospective, NEROnE registry investigated the impact of next-generation sequencing (NGS) in advanced non-small-cell lung cancer (NSCLC) patients (pts) at three oncology units in the north of Italy between January 2020 and December 2022. We focused on the clinical characterization and outcomes of NSCLC with rare molecular alterations: *EGFR* exon 20 insertion, non-activating *EGFR* mutations, *BRAF* V600E and non-V600, *ROS1* and *RET* rearrangements, *MET*, ErbB2, and *FGFR* mutations. Overall, these represented 6.4% (62/970) of the pts analysed with NGS in the daily practice. The most heavily represented rare alterations were ROS1 rearrangement (15 pts—24%) and MET exon 14 skipping mutation (11 pts—18%). No associations were found with the demographic and clinical features. Forty-nine pts received targeted therapies, of which 38.8% were first- and 9.8% were second-line. The remaining pts received chemotherapy and/or immunotherapy. In terms of the clinical outcomes, although not statistically significant, a tendency toward shorter OS was seen when therapies other than specific targeted therapies were used (HR: 1.84, 95% CI: 0.79–4.33, $p = 0.158$). The pts with co-mutations (19.4%) seemed to receive an advantage from the front-line chemotherapy-based regimen. Finally, an NLR score (a well-known inflammatory index) ≥ 4 seemed to be related to shorter OS among the pts treated with immunotherapy alone or in combination with chemotherapy (HR: 2.83, 95% CI: 1.08–7.40, $p = 0.033$). Prospective evaluations need to be performed to clarify whether these indexes may help to identify patients with oncogene-addicted NSCLC who could benefit from immunotherapy.

Keywords: NSCLC; oncogene addiction; inflammatory indexes

1. Introduction

Lung cancer is one of the most frequent types of cancer in developed countries, accounting, in the USA, for almost a quarter of cancer-related deaths and being the leading and second-leading cause of cancer in Europe for men and women, respectively [1]. Among lung cancers, non-small-cell lung cancer (NSCLC) represents more than 85% of all cases, with adenocarcinoma being the most heavily represented histological subtype [2]. Although they are still crucial, currently, histologic features in NSCLC are not enough to define the correct therapeutic strategy. In fact, the discovery of epidermal growth factor receptor (*EGFR*)-activating mutations and anaplastic lymphoma kinase (*ALK*) gene rearrangements and their specific treatments [3,4] has changed the therapeutic landscape, given their ability to modify outcomes for many patients with such alterations. Moreover, several retrospective multicentric evaluations have shown that the outcomes of patients with oncogene-addicted NSCLC are significantly improved when therapies are given according to the target [5,6]. Furthermore, data from Surveillance, Epidemiology, and End Results (SEER) have highlighted improvements in incidence-based mortality greater than in previous periods since 2013, in men, and since 2014, in women, considering that since 2013, the use of EGFR inhibitors has been approved as a first-line treatment for advanced NSCLC [7]. For these reasons it has become mandatory to define the molecular hallmarks of each NSCLC in order to use the most appropriate and active treatment from the beginning. At present, it is mandatory to define the molecular status of of ten oncogenes from the point of diagnosis, preferentially through simultaneous next-generation sequencing (NGS): mutations of *EGFR* (activation and insertion of exon 20), *KRAS*, *BRAF*, *MET*, *HER2*, and *FGFR* and rearrangements of *ALK*, *ROS1*, *RET*, and *NTRK* [8,9]. In fact, for all of these molecular alterations, in first or in further lines of treatment, a specific targeted treatment is available in routine practice or in the advanced stage of clinical development: osimertinib for EGFR-activating mutations [10]; amivantamab for the insertion of exon 20 of EGFR [11]; sotorasib and adagrasib for KRAS G12C mutations [12]; dabrafenib plus trametinib for BRAF V600 mutations [13]; capmatinib and tepotinib for MET skipping mutations [14]; trastuzumab and deruxtecan for HER2 mutation [15]; AZD4547 for FGFR alterations [16]; alectinib, brigatinib, and lorlatinib for ALK rearrangements [17]; crizotinib, entrectinib, and repotrectinib for ROS1 rearrangements [18]; selpercatinib for RET rearrangement [19]; and entrectinib and larotrectinib for NTRK rearrangement [20]. Finally, the expression of PD-L1 needs to be obtained by immunohistochemistry in order to clarify responsiveness to immunotherapy [21].

The NEROnE study is an observational, retrospective registry aiming to define the real-world impact of molecular testing on NSCLC characterization and outcomes for patients with at least one of the ten molecular targets for which a specific therapy is available, approved by national regulatory authorities or in clinical trials available in Italy in the period of observation. In the NEROnE study, data were obtained from the routine clinical practice of three oncologic units located in the Emilia Romagna Region in the north of Italy: the patients involved were molecularly defined by NGS analyses according to the local standard of diagnosis and cure. No supplementary molecular characterizations, other than those approved by the Italian regulatory authorities, were performed. In this paper, we focus on the rarest molecular subpopulations among the mandatory ten, describing their clinical features and outcomes according to the therapies approved in Italy for each subtype following the initial diagnosis.

2. Materials and Methods

2.1. Study Design and Population

NEROnE is a retrospective, real-world, observational registry of patients with advanced NSCLC carrying at least one driver mutation in 10 genes for which, at present, targeted therapies are available, approved by the government, or in clinical trials: EGFR exon 20 insertion, non-activating EGFR mutations, BRAF V600E and non-V600, ROS1, RET, and NTRK rearrangements, and MET, ErbB2, and FGFR mutations. All consecutive

patients tested with NGS as per clinical practice between January 2020 and December 2022, presenting driver mutations, and starting a first-line treatment at three centres in Northern Italy were included in this study. The three oncology units involved were: AUSL-IRCCS Arcispedale Santa Maria Nuova, in Reggio Emilia, and Modena University Hospital and IRCCS Istituto Romagnolo per lo Studio dei Tumori "Dino Amadori" (IRST), in Meldola (FC). Considering NGS procedures, samples from Modena and Reggio Emilia were analysed at Modena University Hospital Molecular Pathology Laboratory using Myriapod IL-56G, Cancer Panel DNA, Cancer Panel RNA, Oncomine DX Target Test Assay (Diatech Pharmacogenetics, Jesi, Italia), and Oncomine Focus (ThermoFisher Scientific, Waltham, MA, USA). Samples from IRST Meldola were studied at its Molecular Diagnostic Unit with Myriapod NGS cancer panel DNA and RNA, Oncomine Focus Assay, and Oncomine Comprehensive Assay v3, (Thermo Fisher Scientific, Waltham, MA, USA). In the present substudy, only those with molecular alterations with an incidence of less than 2.5% were considered, and defined as infrequent mutations. Clinical and laboratory information were obtained from medical chart review.

2.2. Immunoscores Definition

The white blood cell count and differential counts, evaluated at the baseline, were used to determine neutrophil-to-lymphocyte ratio (NLR) [22], platelet-to-lymphocyte ratio (PLR) [23], advanced lung cancer inflammation index (ALI) [24], and the systemic immune inflammatory (SII) index [25]. NLR was computed as the ratio of the absolute neutrophil count to the absolute lymphocyte count, PLR as the ratio of absolute platelet count to the absolute lymphocyte count, ALI as BMIxALB/NLR, where BMI = body mass index and ALB = serum albumin g/dL, and SII as platelet count $\times$ neutrophil count/lymphocyte count.

2.3. Statistical Analysis

Data were summarised by the median, first (IQ), and third (IIIQ) quartiles, by minimum and maximum values for continuous variables, and by means of absolute frequencies and percentages for categorical variables.

Comparisons between categorical variables were performed using the Pearson's χ^2 test of the Fisher exact test, as appropriate, whereas those between categorical and continuous variables were performed through the Wilcoxon signed-rank sum test or the Kruskal–Wallis test, as appropriate.

The inflammatory indexes were reported as log-transformed continuous variables and as categorical variables using the median as a cut-off value.

Progression-free survival (PFS) was defined as the time in months between the start of first-line treatment and the date of disease progression, death from any cause, or last follow-up, whichever occurred first. Overall survival (OS) was defined as the time in months between the start of first-line treatment and the date of death from any cause or last follow-up, whichever occurred first. These outcomes were analysed using the Kaplan–Meier method, the log-rank test for group comparisons, and the Cox proportional hazards model. Results were reported as median and in terms of hazard ratios (HRs) and corresponding 95% confidence intervals (CI)s. The median follow-up time was computed using the reverse Kaplan–Meier method.

All analyses were carried out with STATA 15.0 (College Station, TX, USA). Results were considered statistically significant if the two-sided *p*-values were <0.05.

3. Results

3.1. Molecular and Clinical Features

Nine-hundred seventy patients with a new diagnosis of NSCLC underwent NGS, and 501 patients with at least one druggable oncogene mutation were identified, representing the overall population of the NEROnE study. Among these 501 patients, 62 (12.4%) had rare driver mutations: nine (1.8%) showed *EGFR* exon 20 mutations, three (0.6%) showed non-activating *EGFR* mutations, five (1%) showed *BRAF* V600E mutations, three (0.6%)

showed *BRAF* non-V600 mutations, 15 (3%) showed *ROS1* and four (0.8%) showed *RET* rearrangements, 11 (2.2%) showed *MET* exon 14 skipping mutations, eight (1.6%) showed ErbB2 mutations, two (0.4%) showed *FGFR* mutations, and two (0.4%) showed other molecular alterations (Figure 1). No *NTRK* rearrangements were found. If we consider the total of 970 patients analysed with NGS, those with a rare mutation represent 6.4%.

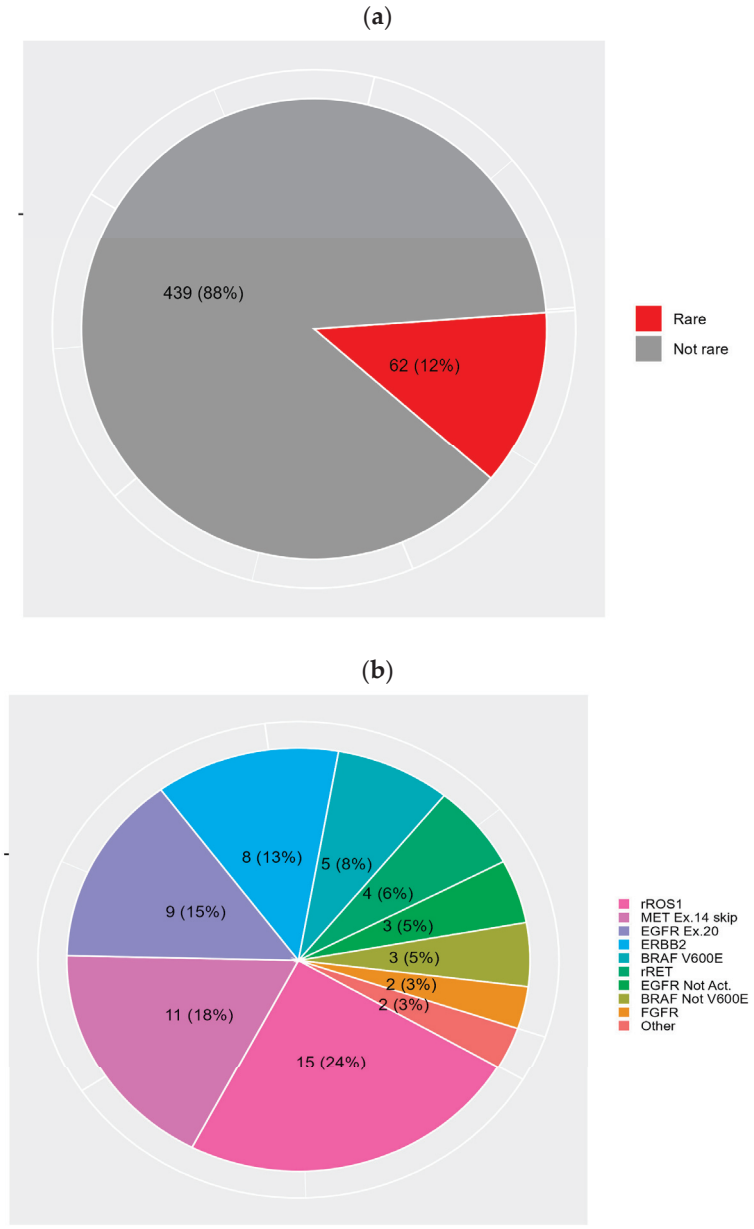

Figure 1. (**a**) Prevalence of rarest molecular alterations among the whole oncogene-addicted population of the NEROnE study: the red slice represents patients with the rarest mutations, accounting for 12% of the population; (**b**) prevalence distribution of the type of rare mutation considered in the present study.

The patients had a median age of 69.2 years (35.2–87.00); 27 (43.5%) were male and 35 (56.5%) were female; 23 (37.1%) were never-smokers, 28 (45.2%) were previous smokers, and 11 were current smokers (17.7%). Sixty (96.8%) patients had adenocarcinoma and two (3.2%) had squamous cell carcinoma; the expression of PD-L1 was <1% in eight (13.1%) patients, between 1 and 49% in 35 (57.4%), and ≥50% in 18 (29.5%); and the PD-L1 status was missing in one patient. The main patients characteristics are reported in Table 1.

Table 1. Baseline characteristics of patients with rare molecular alterations (*n* = 62).

	n	**%**
Sex		
M	27	(43.6)
F	35	(56.5)
Age at diagnosis (y)		
Median (IQ–IIIQ)	69.2 (65.0–76.2)	
Min–max	35.2–87.0	
<65	15	(24.2)
≥65	47	(75.8)
Smoking habit		
Never-smoker	23	(37.1)
Ex-smoker	28	(45.2)
Current smoker	11	(17.7)
ECOG PS		
0	19	(30.7)
1	30	(48.4)
2	10	(16.1)
3	2	(3.2)
4	1	(1.6)
BMI		
Median (IQ–IIIQ)	24 (22.0–28.0)	
Min–max	16–48	
<18.50	6	(9.7)
18.5–24.99	29	(46.8)
25.00–29.99	17	(27.4)
≥30.00	10	(16.1)
Histotype		
Adenocarcinoma	60	(96.8)
Squamous cell carcinoma	2	(3.2)
Type of treatment		
Target therapy	20	(32.3)
Chemo-immunotherapy	20	(32.3)
Immunotherapy	10	(16.1)
Chemotherapy	8	(12.9)
Clinical trial	4	(6.5)
PD-L1		
<1%	8	(13.1)
1–49%	35	(57.4)
≥50%	18	(29.5)
missing	1	
NLR		
Median (IQ–IIIQ)	4.0 (2.3–4.8)	
Min–max	0.6–25.2	
missing	13	
PLR		
Median (IQ–IIIQ)	194.4 (138.7–257.5)	
Min–max	23.1–779.6	
missing	12	
ALI		
Median (IQ–IIIQ)	24.6 (15.1–50.8)	
Min–max	3.5–56.7	
missing	41	
ALI		
<18	7	33.3
≥18	14	66.7
missing	41	
SII		
Median (IQ–IIIQ)	1095.2 (641.1–1842.1)	
Min–max	143.9–10,337.7	
missing	13	

Categorical variables are presented with absolute frequencies and percentages, while continuous variables are presented as median, first- and third-quartile, and minimum and maximum values. Percentages may not equal 100 due to rounding. IQ: first quartile; IIIQ: third quartile; BMI: body mass index; PD-L1: programmed death ligand 1; NLR: neutrophil-to-lymphocyte ratio; PLR: platelet-to-lymphocyte ratio; ALI: advanced lung cancer inflammation index; SII: systemic immune-inflammation index.

No associations were detected between the molecular features and specific clinical features, as shown in Table 2.

Table 2. Descriptive statistics of the demographic and clinical characteristics of the patients harbouring the most heavily represented rare molecular alterations.

	rROS1 (*n* = 15)		**MET Ex.14 Skip (*n* = 11)**		**EGFR Ex.20 (*n* = 9)**		**ERBB2 (*n* = 8)**	
	n	**%**	***n***	**%**	***n***	**%**	***n***	**%**
Sex								
M	7	(46.7)	6	(54.6)	1	(11.1)	2	(25.0)
F	8	(53.3)	5	(45.5)	8	(88.9)	6	(75.0)
Age at diagnosis (y)								
Median (IQ–IIIQ)	69.6 (55.3–76.2)		74.5 (69.0–78.5)		72.4 (63.2–76.3)		68.5 (63.3–69.2)	
Min–max	35.2–82.4		65.0–83.7		57.1–80.1		53.3–83.7	
<65	6	(40.0)	-		3	(33.3)	2	(25.0)
≥65	9	(60.0)	11	(100.0)	6	(66.7)	6	(75.0)
Smoking habit								
Never smoker	6	(40.0)	2	(18.2)	6	(66.7)	5	(62.5)
Ex-smoker	7	(46.7)	7	(63.6)	1	(11.1)	1	(12.5)
Current smoker	2	(13.3)	2	(18.2)	2	(22.2)	2	(25.0)
ECOG PS								
0	9	(60.0)	1	(9.1)	4	(44.4)	-	
1	4	(26.7)	8	(72.7)	4	(44.4)	5	(62.5)
2	1	(6.7)	2	(18.2)	1	(11.1)	2	(25.0)
3	-		-		-		1	(12.5)
4	1	(6.7)	-		-		-	
Histotype								
Adenocarcinoma	14	(93.3)	11	(100.0)	9	(100.0)	8	(100.0)
Squamous cell carcinoma	1	(6.7)	-		-		-	
Type of treatment								
Target therapy	13	(86.7)	1	(9.1)	-		-	
Chemo-immunotherapy	1	(6.7)	3	(27.3)	3	(33.3)	5	(52.5)
Immunotherapy	1	(6.7)	5	(45.5)	-		1	(12.5)
Chemotherapy	-		1	(9.1)	3	(33.3)	2	(25.0)
Clinical trial	-		1	(9.1)	3	(33.3)	-	
Presence of co-mutations								
No	10	(66.7)	10	(90.9)	9	(100.0)	6	(75.0)
Yes	5	(33.3)	1	(9.1)	-		2	(25.0)
PD-L1								
<1%	-		-		2	(22.2)	3	(37.5)
1–49%	10	(71.4)	5	(45.5)	4	(44.4)	5	(62.5)
≥50%	4	(28.6)	6	(54.6)	3	(33.3)	-	
Missing	1		-		-		-	
NLR								
Median (IQ–IIIQ)	2.4 (2.1–4.6)		4.2 (3.8–8.5)		2.2 (1.7–4.4)		4.4 (3.8–5.6)	
Min–max	0.6–15.4		2.1–12.7		0.8–6.7		1.9–9.4	
Missing	4		2		1		-	
PLR								
Median (IQ–IIIQ)	159.2 (108.6–234.2)		186.1 (151.7–240.9)		191.4 (130.3–235.4)		271.8 (170.4–321.7)	
Min–max	26.7–779.6		110.2–437.8		23.1–346.3		114.6–365.0	
Missing	4		2		1			

Table 2. *Cont.*

	rROS1 (*n* = 15)		MET Ex.14 Skip (*n* = 11)		EGFR Ex.20 (*n* = 9)		ERBB2 (*n* = 8)	
	n	**%**	***n***	**%**	***n***	**%**	***n***	**%**
ALI								
Median (IQ–IIIQ)	43.5 (4.4–57.6)		14.9 (14.8–14.9)		55.4 (25.2–57.4)		17.3 (12.7–22.0)	
Min–max	4.2–58.0		14.8–14.9		25.2–57.4		12.7–22.0	
Missing	8		9		6		6	
ALI								
<18	2	28.6	2	(100.0)	-		1	(50.0)
≥18	5	71.4	-		3	(100.0)	1	(50.0)
Missing	8		9		6		6	
SII								
Median (IQ–IIIQ)	656.3 (519.4–1598.5)		1360.9 (1109.6–2724.2)		707.9 (483.3–1045.5)		1490.4 (1127.1–2056.7)	
Min–max	143.9–10,337.7		282.1–5130.7		226.1–1842.1		555.9–3004.6	
Missing	4		2		1		-	

Categorical variables are presented with absolute frequencies and percentages, while continuous variables are presented as median, first- and third-quartile, and minimum and maximum values. Percentages may not equal 100 due to rounding. IQ: first quartile; IIIQ: third quartile; BMI: body mass index; PD-L1: programmed death ligand 1; NLR: neutrophil-to-lymphocyte ratio; PLR: platelet-to-lymphocyte ratio; ALI: advanced lung cancer inflammation index; SII: systemic immune-inflammation index; -: no result present.

3.2. Treatments and Clinical Outcomes

The median follow-up time was 25.1 months (95% CI, 18.4–30.2). All the patients received at least one line of treatment. Overall, the median progression-free survival (PFS) and median overall survival (OS) were 5.0 months (95% CI, 3.1–13.3) and 20.7 months (95% CI, 8.2—not reached (NR)), respectively. Twenty-four (38.8%) patients received targeted agents as first-line therapy (group 1), including crizotinib [13], afatinib [1], dabrafenib and trametinib [4], and capmatinib [2], and four patients were enrolled in clinical trials. Thirty-eight (61.2%) patients received non-targeted therapies (group 2): among them, 20 received chemo–immunotherapy, 10 received immunotherapy alone, five received platinum-based chemotherapy doublets, and three had single-agent chemotherapy.

The median duration of treatment in group 1 was 3.6 months (IQ-IIIQ: 1.6–15.8), and it was 4.3 months (IQ-IIIQ: 2.0–14.6) in group 2; the *p*-value = 0.851. The median OS rates at 12 and 24 months were 69% (95% CI, 42–85%) and 61% (95% CI, 34–80%) in group 1 and 49% (95% CI, 32–64%) and 39% (95% CI, 23–55%) in group 2. The median PFS rates at 12 and 24 months were 49% (95% CI, 27–68%) and 42% (95% CI, 20–63%) in group 1 and 33% (95% CI, 18–48%) and 23% (95% CI, 11–38%) in group 2. No statistically significant differences were observed between the treatment group with respect to the OS (*p*-value = 0.151) and PFS (*p*-value = 0.286) (Figure 2). Among the patients in group 2, the median OS rates were 23.4 months (95% CI: 7.2–not reached (NR)), 2 months (95% CI: 0.4–NR), and 6.3 months (95% CI: 0.2–14.1) for the patients treated with chemo–immunotherapy, with immunotherapy alone, and with chemotherapy alone, respectively. The corresponding estimates for PFS were 8.4 months (95% CI: 3.3–29.6), 2 months (95% CI: 0.4–16.4), and 2.6 (95% CI: 0.13–10.39), respectively.

Overall, 21 (33.9%) patients received a second line of therapy, of whom five were in group 1 and 16 were in group 2 (*p*-value = 0.534). Among the five patients in group 1, two (40%) received targeted therapies; among the 16 in group 2, six (37.5%) received targeted therapies or participated to clinical trials. This latter group represents the 9.8% of the population analysed.

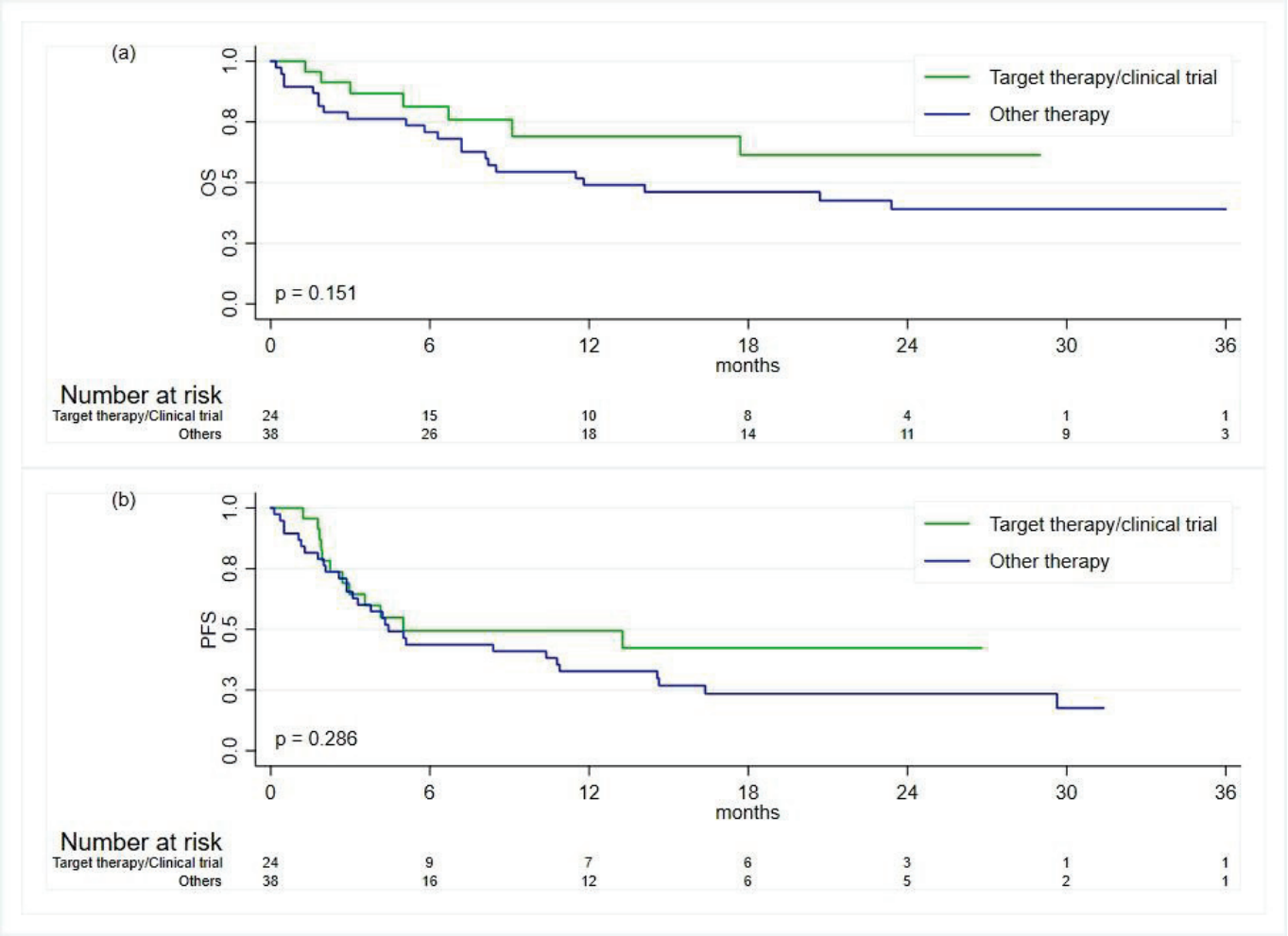

Figure 2. Kaplan–Meier curves for the comparison of the clinical outcomes between patients treated with targeted therapies or in clinical trials and patients treated with chemotherapy and/or immunotherapy: (**a**) overall survival (OS); (**b**) progression-free survival (PFS).

3.3. Patients with Co-Mutations

Twelve out of 62 patients (19.4%) presented with a co-mutation: five out of 62 (8%) presented a *ROS1* rearrangement synchronous with *EGFR* rare mutations (exon 20 insertion or inactivating mutation), a *KRAS* G12C mutation, or other non-target alterations; one out of 62 (1.6%) presented a *BRAF* V600E mutation with a PIK3CA mutation; one out of 62 (1.6%) presented a non-V600 *BRAF* mutation and a PIK3CA mutation; three out of 62 (4.8%) presented a *MET* exon 14 skipping mutation with *RET* rearrangement, with an erbB2 mutation, or with other non-target alterations; and one out of 62 (1.6%) presented with two synchronous mutations of *FGFR* genes. These patients showed similar characteristics to those with a single driver mutation, with no statistically significant differences (results not shown).

The patients with co-mutations had a median OS of 17.7 months (95% CI, 1.9–NR) versus 20.7 months (95% CI, 8.1–NR) for the patients with only one oncogene alteration, with *p*-value = 0.907. The corresponding medians for PFS were 4.1 months (95% CI, 1.8–10.9) and 5.1 months (95% CI, 3.1–14.6), with *p*-value = 0.191, respectively. Among the patients with co-mutations, five (41.7%) received first-line targeted therapies or participated in clinical trials, while seven (58.3%) received chemotherapy alone or combined with immunotherapy, with *p*-value = 0.815. The corresponding median durations of treatment were 2.2 months (IQ-IIIQ: 1.8–3.2) and 10.8 months (IQ-IIIQ: 2.9–29.6), with *p*-value = 0.123, respectively. The median OS for the patients with co-mutations and treated with targeted

therapies or in clinical trials was equal to 17.7 months (95% CI, 1.9–NR) and NR (95% CI, 0.5–NR) for those receiving other treatments, *p*-value = 0.459. The corresponding median PFSs were 2.2 months (1.8–NR) and 10.8 months (0.5–29.6), with *p*-value = 0.052.

3.4. Association with Inflammatory Indexes

Overall, on the univariate analysis, there was some evidence of a worse OS for patients with a baseline NLR index greater than or equal to 4 compared to patients with lower values (HR 2.3; 95% CI, 0.94–4.93, *p*-value = 0.069) (Table 3 and Figure 3). However, when adjusting for age at diagnosis and ECOG performance status (PS), the NLR was not found to be associated with OS (HR = 1.92, 95% CI, 0.82–4.45, *p*-value = 0.131).

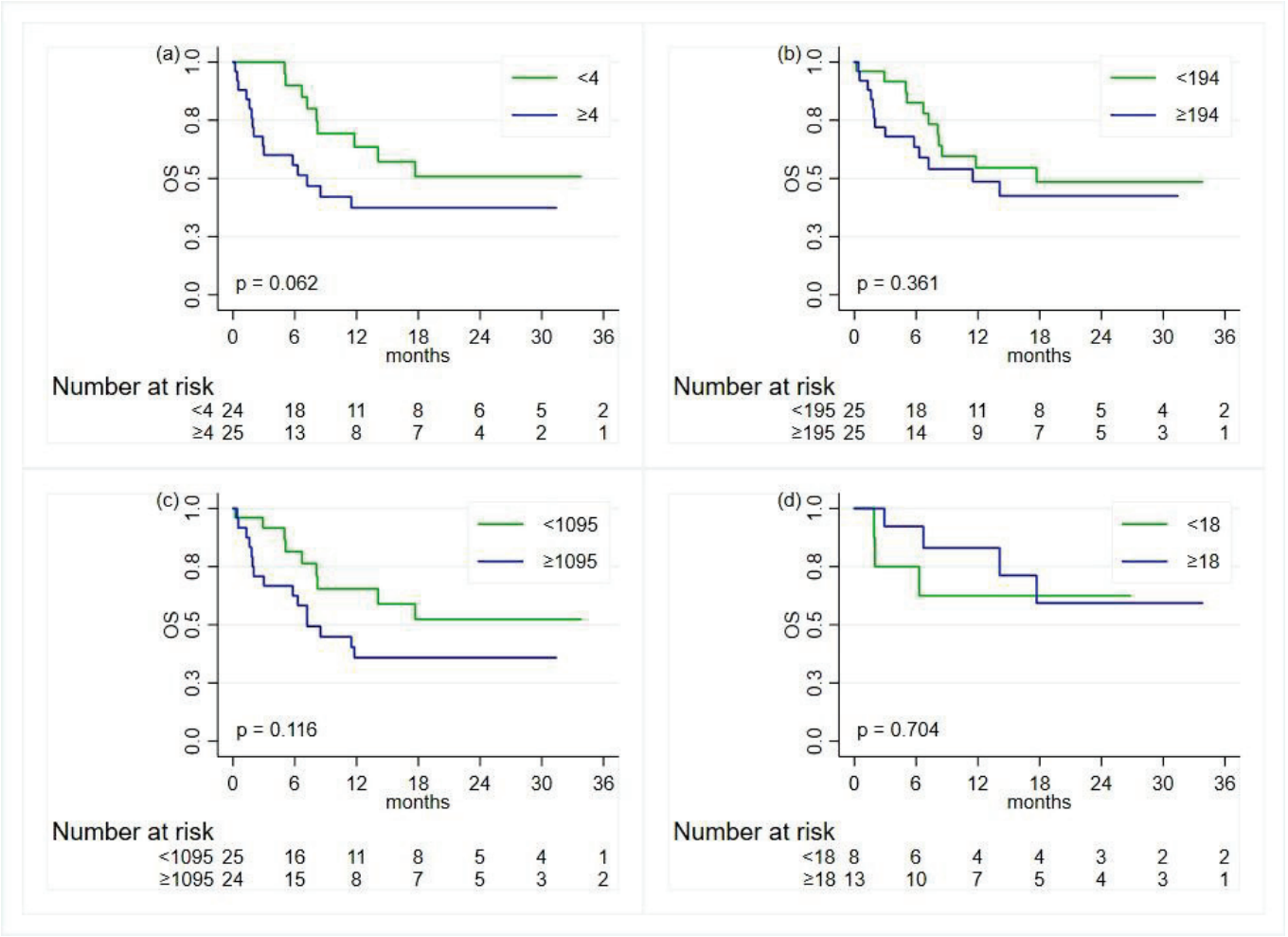

Figure 3. Kaplan–Meier curves for the comparison, in the overall population, of the overall survival (OS) between groups defined by the status of the inflammatory indexes—except for ALI, the cut-offs are based on the median value: (**a**) neutrophil-to-lymphocyte ratio; (**b**) platelet-to-lymphocyte ratio; (**c**) systemic immune-inflammation index; (**d**) advanced lung cancer inflammation index.

With regards to the PFS, no associations were found (Table 3 and Figure 4).

Table 3. Results from univariate analyses using the Cox model of the association between the inflammatory indexes and the overall survival (OS) and progression-free survival (PFS).

	OS			PFS		
	HR	**(95% CI)**	***p*-Value**	**HR**	**(95% CI)**	***p*-Value**
NLR						
<4.0	1.0			1.0		
≥4.0	2.16	(0.94–4.93)	0.069	1.42	(0.71–2.84)	0.327
Log-transformed NLR	1.37	(0.73–2.56)	0.324	1.17	(0.71–1.94)	0.539
PLR						
<194.4	1.0			1.0		
≥194.4	1.45	(0.65–3.25)	0.364	1.18	(0.59–2.37)	0.635
Log-transformed PLR	0.96	(0.52–1.76)	0.890	1.01	(0.62–1.64)	0.968
SII						
<1095.2	1.0			1.0		
≥1095.2	1.92	(0.84–4.38)	0.123	1.28	(0.63–2.57)	0.483
Log-transformed SII	1.17	(0.72–1.90)	0.532	1.06	(0.72–1.58)	0. 774
ALI						
<18	1.0			1.0		
≥18	0.75	(0.17–3.35)	0.705	0.46	(0.15–1.45)	0.188
Log-transformed ALI	0.89	(0.37–2.13)	0.797	0.83	(0.45–1.57)	0.581

HR: hazard ratio; CI: confidence interval; NLR: neutrophil-to-lymphocyte ratio; PLR: platelet-to-lymphocyte ratio; ALI: advanced lung cancer inflammation index; SII: systemic immune-inflammation index.

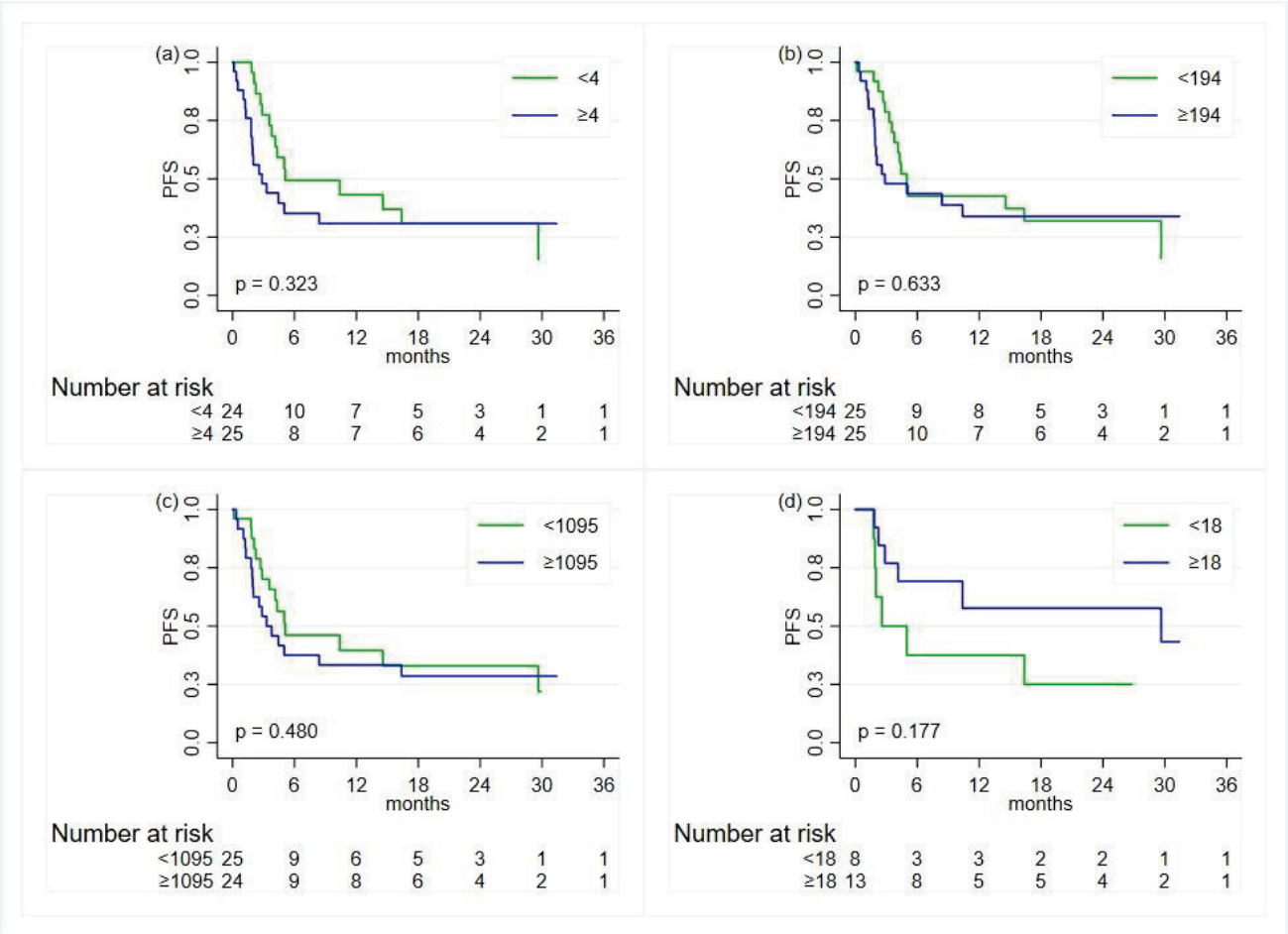

Figure 4. Kaplan–Meier curves for the comparison, in the overall population, of the progression-free survival (PFS) between groups defined by the status of the inflammatory indexes—except for the ALI, the cut-offs are based on the median value: (**a**) neutrophil-to-lymphocyte ratio; (**b**) platelet-to-lymphocyte ratio; (**c**) systemic immune-inflammation index; (**d**) advanced lung cancer inflammation index.

Looking at the association between the inflammatory indexes and the time-to-event outcomes within the groups of treatment, a statistically significant association with OS (HR 2.8, 95% CI, 1.08–7.40, *p*-value = 0.033) was observed for the NLR in the subgroup of patients treated with chemotherapy, immunotherapy, or their combination (Figure 5). Adjusting for age at diagnosis and ECOG PS, a HR of 2.63 (95% CI, 0.96–7.18, *p*-value = 0.060) was found.

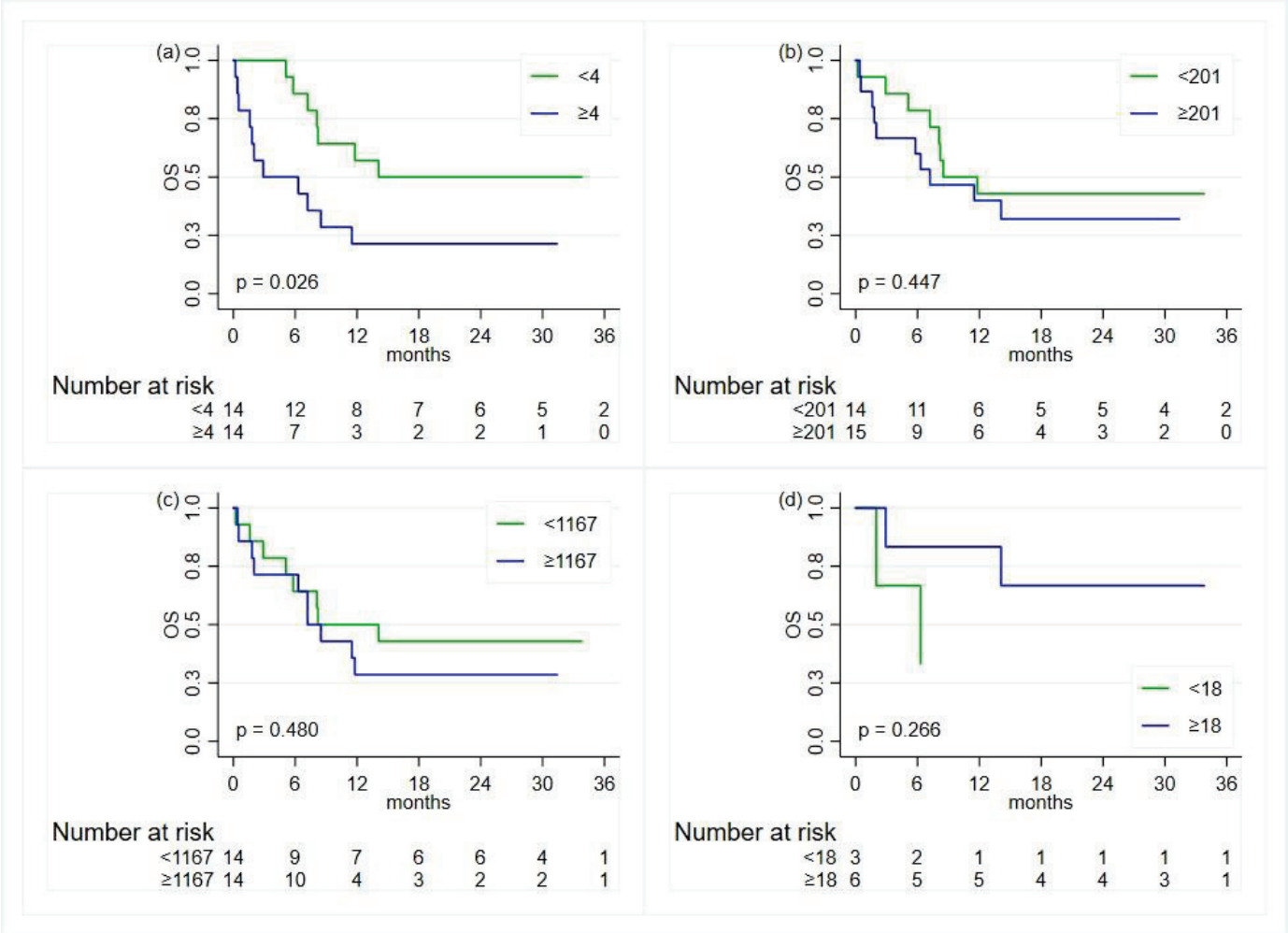

Figure 5. Kaplan–Meier curves for the comparison, in the population treated with chemotherapy and/or immunotherapy, of the overall survival (OS) between groups defined by the status of the inflammatory indexes—except for ALI, the cut-offs are based on the median value: (**a**) neutrophil-to-lymphocyte ratio; (**b**) platelet-to-lymphocyte ratio; (**c**) systemic immune-inflammation index; (**d**) advanced lung cancer inflammation index.

No other significant associations were observed with the OS. Concerning the PFS, there was some evidence of an association with the ALI index (HR 0.18, 95% CI, 0.03–1.09, *p*-value = 0.061) (Figure 6). However, in this subgroup, ALI data were available only for nine patients (six failures).

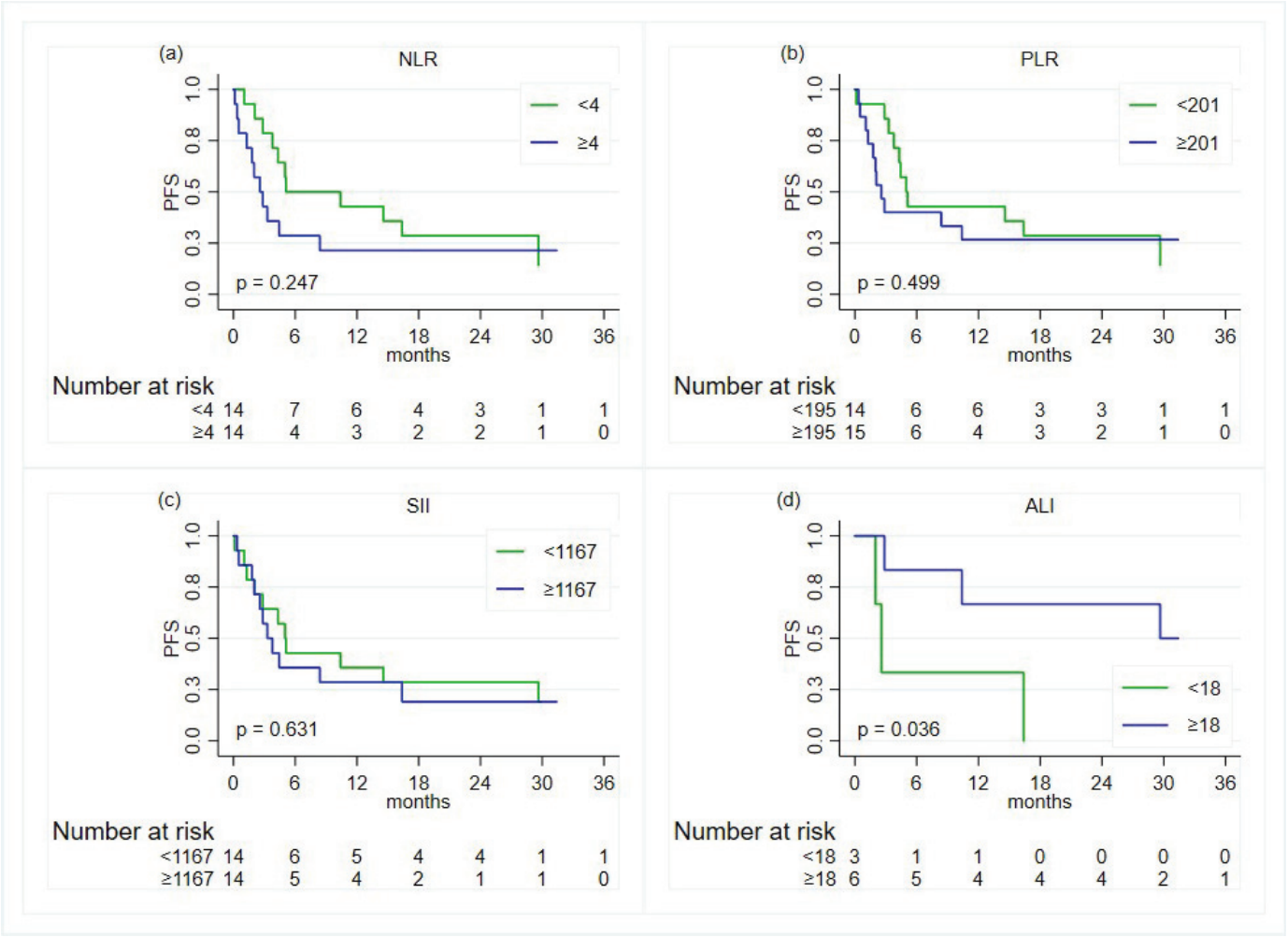

Figure 6. Kaplan–Meier curves for the comparison, in the population treated with chemotherapy and/or immunotherapy, of the progression-free survival (PFS) between groups defined by the status of the inflammatory indexes—except for ALI, the cut-offs are based on the median value: (**a**) neutrophil-to-lymphocyte ratio; (**b**) platelet-to-lymphocyte ratio; (**c**) systemic immune-inflammation index; (**d**) advanced lung cancer inflammation index.

Among the patients treated with target therapy or within a clinical trial, no associations were found.

4. Discussion

The data from the whole oncogene-addicted population of the NEROnE study, a real-world, retrospective data collection from three oncologic units in the north of Italy, were previously shown [26]. In the present work, we describe the patients with the rarest molecular, driver alterations among the pivotal ten analysed in the study. Considering that data for the activity of new drugs for NSCLC subpopulations arise from controlled clinical trials, real-world information is required in order to verify results from everyday clinical practice, especially for the less frequent alterations.

In our case series, cases of NSCLC with the rarest driver alterations encompassed6% of the overall population who underwent NGS. Each subgroup shows a prevalence lower than in the literature, where, in fact, *EGFR* exon 20 mutations represent2.5% of the analysed patients [27], *BRAF* mutations represent 3% [28], *RET* rearrangements represent 1–2% [29], *MET* exon 14 skipping mutations represent 2.7% [30], and *FGFR* mutations/rearrangements represent 0.1–3% [31]. Only the *ROS1*-rearranged and the erbB2-mutated patients had incidences similar to that of in the literature, of 2% and 1%, respectively [6,16]. The patients

with these alterations did not show associations with specific clinical features in our data. In the literature, although not all subgroups show well defined clinical features, it is possible to highlight some specificities: *EGFR* exon 20 mutants are more frequent in non-smoker patients [27], while the majority of BRAF-mutated patients are current or former smokers [28]; ROS1- and RET-rearranged patients are generally younger than 60 years and have limited smoking history [29–32]; and MET mutations are more frequent in older patients [30]. In our dataset, as in the literature, there are no clear correlations with PD-L1 expression [33].

From a therapeutic point of view, at present, in Italy, only a limited number of therapeutic options for these oncogene-addicted populations is available. First-line targeted therapies for BRAF-V600-mutated and ROS1-rearranged NSCLC and second-line therapies for the *EGFR* exon 20 mutation, *MET* exon 14 skipping mutation, and RET rearranged NSCLC are approved by regulatory autorities; treatments for erbB2 and FGFR are still under investigation. Only 48.6% of our patients had received targeted therapies or participated in dedicated clinical trials, of which 38.8% were first-line and 9.8% were second-line, respectively. Although there are no statistical differences in terms of OS and PFS between patients treated with targeted therapies and chemo-based regimens in the first line, there is a trend in terms of improvement in the median rates of OS and PFS at 12 and 24 months for those receiving targeted therapies. These results are consistent with the literature, in which a generic population with oncogene-addicted tumours had better outcomes when treated with specific drugs [5,6]. In our population, these results are not statistically significant, probably due to the small sample size and its heterogeneity, but also because not all patients can receive the most appropriate therapy as an initial option.

As in the historical data [34], in our study population, there was an incidence of NSCLC with co-mutations of 19.4%. We did not find any clinical or survival differences compared to the single-mutation population. However, the patients treated with targeted therapies as a first line had a shorter treatment period than those treated with a chemotherapy-based regimen, which, in addition, seems to obtain better OS and PFS.

Finally, we analysed the association between the previously validated inflammatory indexes [22–25] and outcomes after immunotherapy-based regimens for these oncogene-addicted-NSCLC patients. As is known from the literature [23], responses to immunotherapy seem to vary according to the NSCLC subtype, requiring potential tools for selecting patients who can respond in a better way. Among the indexes analysed, NLR showed some potential. This result suggests that these indexes may be tools for patient selection in these subpopulations. However, further, prospective evaluations in larger cohorts of patients should be performed in order to clarify their real role.

5. Conclusions

Our study focuses on subpopulations of oncogene-addicted NSCLCs with rare molecular alterations, as emerged in the retrospective, real-world-registry NERONE trial. We have shown that their incidence was lower than in the literature, with the exception of the ROS1 and erbB2 subgroups, with an incidence that was expected. The results in terms of the OS and PFS, although not statistically significant, show a tendency towards improved survival when specific targeted therapies are used from the beginning in the therapeutic strategy. Despite this, patients with co-mutations seem to receive an advantage from front-line chemotherapy-based regimens. Finally, the NLR score, a well-known inflammatory index, may have a relationship with the outcomes of immunotherapeutic-based strategies: in fact, when it is $\geq$4, it seems to be related to a worse OS in patients treated with immunotherapy alone or in combination with chemotherapy. This consideration seems to suggest that some patients with oncogene-addicted NSCLC may benefit from immunotherapy strategies. Given the limited number of patients and their molecular heterogeneity, these results are not conclusive and further prospective studies are warranted.

Author Contributions: Conceptualization, A.D. and K.A.; methodology, software, and formal analysis: E.P. and I.A.; investigation, all authors; resources, all authors; data curation, all authors; writing—original draft preparation, K.A., E.P. and A.D.; writing—review and editing, all authors. All authors have read and agreed to the published version of the manuscript.

Funding: This research received no external funding.

Institutional Review Board Statement: The study was approved by the Romagna Ethics Committee (CEROM), No. IRST162.15, n. 3591, Prot. 3481/2023 I.5/113, approved on 12 May 2023.

Informed Consent Statement: No informed consent was required, given the fact that we used aggregated and anonymous data.

Data Availability Statement: The data that support the findings will be available in www.zenodo.org at https://doi.org/10.5281/zenodo.11164367 following receipt of approval from Privacy Guarantor.

Conflicts of Interest: The authors declare no conflicts of interest.

References

1. Leiter, A.; Veluswamy, R.R.; Wisnivesky, J.P. The global burden of lung cancer: Current status and future trends. *Nat. Rev. Clin. Oncol.* **2023**, *20*, 624–639. [CrossRef] [PubMed]
2. Travis, W.D.; Brambilla, E.; Burke, A.P.; Marx, A.; Nicholson, A.G. WHO Classification of Tumours of the Lung, Pleura, Thymus and Heart (IARC, 2015); Schabath, M.B.; Cote, M.L. Cancer progress and priorities: Lung cancer. *Cancer Epidemiol. Biomark. Prev.* **2019**, *28*, 1563–1579.
3. Lynch, T.J.; Bell, D.W.; Sordella, R.; Gurubhagavatula, S.; Okimoto, R.A.; Brannigan, B.W.; Harris, P.L.; Haserlat, S.M.; Supko, J.G.; Haluska, F.G.; et al. Activating mutations in the epidermal growth factor receptor underlying responsiveness of non-small-cell lung cancer to gefi tinib. *N. Engl. J. Med.* **2004**, *350*, 2129–2139. [CrossRef] [PubMed]
4. Shaw, A.T.; Kim, D.W.; Nakagawa, K.; Seto, T.; Crinó, L.; Ahn, M.J.; De Pas, T.; Besse, B.; Solomon, B.J.; Blackhall, F.; et al. Crizotinib versus chemotherapy in advanced ALK-positive lung cancer. *N. Engl. J. Med.* **2013**, *368*, 2385–2394. [CrossRef] [PubMed]
5. Kris, M.G.; Johnson, B.E.; Berry, L.D.; Kwiatkowski, D.J.; Iafrate, A.J.; Wistuba, I.I.; Varella-Garcia, M.; Franklin, W.A.; Aronson, S.L.; Su, P.F.; et al. Using multiplexed assays of oncogenic drivers in lung cancers to select targeted drugs. *JAMA* **2014**, *311*, 1998–2006. [CrossRef] [PubMed]
6. Barlesi, F.; Mazieres, J.; Merlio, J.P.; Debieuvre, D.; Mosser, J.; Lena, H.; Ouafik, L.; Besse, B.; Rouquette, I.; Westeel, V.; et al. Routine molecular profiling of patients with advanced non-small-cell lung cancer: Results of a 1-year nationwide programme of the French Cooperative Thoracic Intergroup (IFCT). *Lancet* **2016**, *387*, 1415–1426. [CrossRef]
7. Howlader, N.; Forjaz, G.; Mooradian, M.J.; Meza, R.; Kong, C.Y.; Cronin, K.A.; Mariotto, A.B.; Lowy, D.R.; Feuer, E.J. The Effect of Advances in Lung-Cancer Treatment on Population Mortality. *N. Engl. J. Med.* **2020**, *383*, 640–649. [CrossRef] [PubMed]
8. Mosele, F.; Remon, J.; Mateo, J.; Westphalen, C.B.; Barlesi, F.; Lolkema, M.P.; Normanno, N.; Scarpa, A.; Robson, M.; Meric-Bernstam, F.; et al. Recommendations for the use of next-generation sequencing (NGS) for patients with metastatic cancers: A report from the ESMO Precision Medicine Working Group. *Ann. Oncol.* **2020**, *31*, 1491–1505. [CrossRef] [PubMed]
9. Chakravarty, D.; Johnson, A.; Sklar, J.; Lindeman, N.I.; Moore, K.; Ganesan, S.; Lovly, C.M.; Perlmutter, J.; Gray, S.W.; Hwang, J.; et al. Somatic Genomic Testing in Patients with Metastatic or Advanced Cancer: ASCO Provisional Clinical Opinion. *J. Clin. Oncol.* **2022**, *40*, 1231–1258. [CrossRef] [PubMed]
10. Mok, T.S.; Wu, Y.-L.; Ahn, M.-J.; Garassino, M.C.; Kim, H.R.; Ramalingam, S.S.; Shepherd, F.A.; He, Y.; Akamatsu, H.; Theelen, W.S.; et al. Osimertinib or Platinum-Pemetrexed in EGFR T790M-Positive Lung Cancer. *N. Engl. J. Med.* **2017**, *376*, 629–640. [CrossRef] [PubMed]
11. Park, K.; Haura, E.B.; Leighl, N.B.; Mitchell, P.; Shu, C.A.; Girard, N.; Viteri, S.; Han, J.Y.; Kim, S.W.; Lee, C.K.; et al. Amivantamab in EGFR Exon 20 Insertion-Mutated Non-Small-Cell Lung Cancer Progressing on Platinum Chemotherapy: Initial Results from the CHRYSALIS Phase I Study. *J. Clin. Oncol.* **2021**, *39*, 3391–3402. [CrossRef] [PubMed]
12. Luo, W.; Zhu, J.; Zhang, W.; Yu, A.; Zhou, W.; Xu, K. Efficacy and toxicity of drugs targeting $KRAS^{G12C}$ mutation in non-small cell lung cancer: A meta- analysis. *Expert Rev. Anticancer. Ther.* **2023**, *23*, 1295–1303. [CrossRef] [PubMed]
13. Sforza, V.; Palumbo, G.; Cascetta, P.; Carillio, G.; Manzo, A.; Montanino, A.; Sandomenico, C.; Costanzo, R.; Esposito, G.; Laudato, F.; et al. BRAF Inhibitors in Non-Small Cell Lung Cancer. *Cancers* **2022**, *14*, 4863. [CrossRef] [PubMed]
14. Chagas, G.C.L.; Rangel, A.R.; El Osta, B. MET alterations in advanced non-small cell lung cancer. *Curr. Probl. Cancer* **2024**, *12*, 101075. [CrossRef] [PubMed]
15. Smit, E.F.; Felip, E.; Uprety, D.; Nagasaka, M.; Nakagawa, K.; Paz-Ares Rodríguez, L.; Pacheco, J.M.; Li, B.T.; Planchard, D.; Baik, C.; et al. Trastuzumab deruxtecan in patients with metastatic non-small-cell lung cancer (DESTINY-Lung01): Primary results of the HER2-overexpressing cohorts from a single-arm, phase 2 trial. *Lancet Oncol.* **2024**, *25*, 439–454. [CrossRef] [PubMed]

16. Aggarwal, C.; Redman, M.W.; Lara, P.N., Jr.; Borghaei, H.; Hoffman, P.; Bradley, J.D.; Newman, A.J., III; Feldman, M.J.; Minichiello, K.; Miao, J.; et al. SWOG S1400D (NCT02965378), a Phase II Study of the Fibroblast Growth Factor Receptor Inhibitor AZD4547 in Previously Treated Patients with Fibroblast Growth Factor Pathway-Activated Stage IV Squamous Cell Lung Cancer (Lung-MAP Substudy). *J. Thorac. Oncol.* **2019**, *14*, 1847–1852. [CrossRef] [PubMed]
17. Delmonte, A.; Burgio, M.A.; Verlicchi, A.; Bronte, G.; Cravero, P.; Ulivi, P.; Martinelli, G.; Crinò, L. New generation anaplastic lymphoma kinase inhibitors. *Transl. Lung Cancer Res.* **2019**, *8* (Suppl. S3), S280–S289. [CrossRef] [PubMed]
18. Gálffy, G.; Morócz, É.; Korompay, R.; Hécz, R.; Bujdosó, R.; Puskás, R.; Lovas, T.; Gáspár, E.; Yahya, K.; Király, P.; et al. Targeted therapeutic options in early and metastatic NSCLC-overview. *Pathol. Oncol. Res.* **2024**, *30*, 1611715. [CrossRef]
19. Zhou, C.; Solomon, B.; Loong, H.H.; Park, K.; Pérol, M.; Arriola, E.; Novello, S.; Han, B.; Zhou, J.; Ardizzoni, A.; et al. First-Line Selpercatinib or Chemotherapy and Pembrolizumab in *RET* Fusion-Positive NSCLC. *N. Engl. J. Med.* **2023**, *389*, 1839–1850. [CrossRef]
20. Chen, J.; Xu, C.; Lv, J.; Lu, W.; Zhang, Y.; Wang, D.; Song, Y. Clinical characteristics and targeted therapy of different gene fusions in non-small cell lung cancer: A narrative review. *Transl. Lung Cancer Res.* **2023**, *12*, 895–908. [CrossRef] [PubMed]
21. Camidge, D.R.; Doebele, R.C.; Kerr, K.M. Comparing and contrasting predictive biomarkers for immunotherapy and targeted therapy of NSCLC. *Nat. Rev. Clin. Oncol.* **2019**, *16*, 341–355. [CrossRef] [PubMed]
22. Minami, S.; Ogata, Y.; Ihara, S.; Yamamoto, S.; Komuta, K. Neutrophil-to-Lymphocyte Ratio Predicts Overall Survival of Advanced Non-Small Cell Lung Cancer Harboring Mutant Epidermal Growth Factor Receptor. *World J. Oncol.* **2017**, *8*, 180–187. [CrossRef] [PubMed]
23. Chan, S.W.S.; Smith, E.; Aggarwal, R.; Balaratnam, K.; Chen, R.; Hueniken, K.; Fazelzad, R.; Weiss, J.; Jiang, S.; Shepherd, F.A.; et al. Systemic Inflammatory Markers of Survival in Epidermal Growth Factor-Mutated Non-Small-Cell Lung Cancer: Single-Institution Analysis, Systematic Review, and Meta-analysis. *Clin. Lung Cancer* **2021**, *22*, 390–407. [CrossRef] [PubMed]
24. Ozyurek, B.A.; Ozdemirel, T.S.; Ozden, S.B.; Erdoğan, Y.; Ozmen, O.; Kaplan, B.; Kaplan, T. Does advanced lung inflammation index (ALI) have prognostic significance in metastatic non-small cell lung cancer? *Clin. Respir. J.* **2018**, *12*, 2013–2019. [CrossRef] [PubMed]
25. Huang, W.; Luo, J.; Wen, J.; Jiang, M. The Relationship Between Systemic Immune Inflammatory Index and Prognosis of Patients with Non-Small Cell Lung Cancer: A Meta-Analysis and Systematic Review. *Front. Surg.* **2022**, *9*, 898304. [CrossRef] [PubMed]
26. Bertolini, F.; Alberti, G.; Petracci, E.; Bettelli, S.; Ulivi, P.; Cravero, P.; Guaitoli, G.; Zanelli, F.; Burgio, M.A.; Andrikou, K.; et al. Genomic profiling in advanced NSCLC in Italy: First results of NERoNE (NSCLC Emilia Romagna Next Generation Sequencing Evaluation) project. *J. Clin. Oncol.* **2023**, *41*, e21077. [CrossRef]
27. Oxnard, G.R.; Lo, P.C.; Nishino, M.; Dahlberg, S.E.; Lindeman, N.I.; Butaney, M.; Jackman, D.M.; Johnson, B.E.; Jänne, P.A. Natural history and molecular characteristics of lung cancers harbouring EGFR exon 20 insertions. *J. Thorac. Oncol.* **2013**, *8*, 179–184. [CrossRef] [PubMed]
28. Paik, P.K.; Arcila, M.E.; Fara, M.; Sima, C.S.; Miller, V.A.; Kris, M.G.; Ladanyi, M.; Riely, G.J. Clinical characteristics of patients with lung adenocarcinomas harboring BRAF mutations. *J. Clin. Oncol.* **2011**, *29*, 2046–2051. [CrossRef] [PubMed]
29. Drilon, A.; Hu, Z.I.; Lai, G.G.Y.; Tan, D.S.W. Targeting RET-driven cancers: Lessons from evolving preclinical and clinical landscapes. *Nat. Rev. Clin. Oncol.* **2018**, *15*, 151–167. [CrossRef] [PubMed]
30. Schrock, A.B.; Frampton, G.M.; Suh, J.; Chalmers, Z.R.; Rosenzweig, M.; Erlich, R.L.; Halmos, B.; Goldman, J.; Forde, P.; Leuenberger, K.; et al. Characterization of 298 Patients with Lung Cancer Harboring MET Exon 14 Skipping Alterations. *J. Thorac. Oncol.* **2016**, *11*, 1493–1502. [CrossRef]
31. Pacini, L.; Jenks, A.D.; Lima, N.C.; Huang, P.H. Targeting the Fibroblast Growth Factor Receptor (FGFR) Family in Lung Cancer. *Cells* **2021**, *10*, 1154. [CrossRef] [PubMed]
32. Davies, K.D.; Doebele, R.C. Molecular pathways: ROS1 fusion proteins in cancer. *Clin. Cancer Res.* **2013**, *19*, 4040–4045. [CrossRef] [PubMed]
33. Mushtaq, R.; Cortot, A.B.; Gautschi, O.; Mazieres, J.; Camidge, D.R. PD-1/PD-L1 inhibitor activity in patients with gene-rearrangement positive non-small cell lung cancer-an IMMUNOTARGET case series. *Transl. Lung Cancer Res.* **2022**, *11*, 2412–2417. [CrossRef] [PubMed]
34. Ulivi, P.; Urbini, M.; Petracci, E.; Canale, M.; Dubini, A.; Bartolini, D.; Calistri, D.; Cravero, P.; Fonzi, E.; Martinelli, G.; et al. Wide Next-Generation Sequencing Characterization of Young Adults Non-Small-Cell Lung Cancer Patients. *Cancers* **2022**, *14*, 2352. [CrossRef]

diagnostics

MDPI

Article

A Retrospective Analysis: Investigating Factors Linked to High Lung-RADS Scores in a Nonsmoking, Non-Family History Population

Chi-Shen Chen [1,2], Hsien-Chung Yu [1,2,3], Chun-Hao Yin [4,5], Jin-Shuen Chen [6], Yao-Shen Chen [6] and I-Shu Chen [1,7,8,*]

[1] Health Management Center, Kaohsiung Veterans General Hospital, Kaohsiung 813414, Taiwan; chirise0720@gmail.com or chirise@vghks.gov.tw (C.-S.C.); hcyu@vghks.gov.tw (H.-C.Y.)
[2] Department of Nursing, Mei-ho University, Pingtung 91202, Taiwan
[3] Division of Gastroenterology and Hepatology, Department of Internal Medicine, Kaohsiung Veterans General Hospital, Kaohsiung 813414, Taiwan
[4] Department of Medical Education and Research, Kaohsiung Veterans General Hospital, Kaohsiung 813414, Taiwan; chyin@vghks.gov.tw
[5] Institute of Health Care Management, National Sun Yat-sen University, Kaohsiung 80421, Taiwan
[6] Department of Administration, Kaohsiung Veterans General Hospital, Kaohsiung 813414, Taiwan; dgschen@vghks.gov.tw (J.-S.C.); yschen@vghks.gov.tw (Y.-S.C.)
[7] Division of General Surgery, Department of Surgery, Kaohsiung Veterans General Hospital, Kaohsiung 813414, Taiwan
[8] Department of Physical Therapy, Shu-Zen Junior College of Medicine and Management, Kaohsiung 82144, Taiwan
* Correspondence: ishu1295070@gmail.com; Tel.: +886-7-3422121 (ext. 3085)

Abstract: Low-dose computed tomography screening for lung cancer is currently targeted at heavy smokers or those with a family history of lung cancer. This study aimed to identify risk factors for lung cancer in individuals who do not meet the current lung cancer screening criteria as stipulated by the Taiwan Health Promotion Agency's low-dose computed tomography (LDCT) screening policy. A cohort analysis was conducted on 12,542 asymptomatic healthy subjects aged 20–80 years old who voluntarily underwent LDCT scans from January 2016 to December 2021. Logistic regression demonstrated that several factors, including age over 55 years, female gender, a body mass index (BMI) less than 23, a previous history of respiratory diseases such as tuberculosis or obstructive respiratory diseases (chronic obstructive pulmonary disease [COPD], asthma), and previous respiratory symptoms such as cough or dyspnea, were associated with high-risk lung radiology scores according to LDCT scans. These findings indicate that risk-based assessments using primary data and questionnaires to identify risk factors other than heavy smoking and a family history of lung cancer may improve the efficiency of lung cancer screening.

Keywords: lung cancer; LDCT screening; risk factors; high-risk group

1. Introduction

In recent years, lung cancer has become the leading cause of cancer-related death in both men and women worldwide. The National Lung Screening Trial (NLST) demonstrated that annual low-dose computed tomography (LDCT) screening can reduce lung cancer mortality by 20% compared to chest radiography in heavy smokers with a history of at least 30 pack-years [1]. Following the NLST, the Taiwan Health Promotion Agency formulated a policy to subsidize LDCT lung cancer screening for individuals at a high risk of lung cancer, including heavy smokers and individuals with a family history of lung cancer. On 1 July 2022, the Ministry of Health and Welfare launched the Lung Cancer Early Detection Program to provide biannual low-dose computed tomography (LDCT) lung screening for

high-risk groups. Taiwan is the first country to provide lung screening for heavy smokers and individuals with a family history of lung cancer. Those in the following groups at a high risk for lung cancer may apply for screening at any given hospital under the program: (1) Individuals with a family history of lung cancer, specifically, men aged between 50 and 74 years and women aged between 45 and 74 years whose parents, children, or siblings have been diagnosed as having lung cancer, and (2) individuals with a history of heavy smoking, specifically, individuals aged between 50 and 74 years with a smoking history of 30 or more pack-years who are willing to quit smoking or who have quit smoking within the past 15 years.

According to the National Lung Screening Trial (NLST) in the United States, it was found that individuals screened for lung cancer using low-dose CT had a 20% lower mortality rate compared to those screened using traditional X-rays. However, the study also found that 96.4% of the individuals with positive screening results had negative follow-up examinations. Therefore, developing a system for effectively managing and tracking positive screening results has become an important issue. In 2015, the American College of Radiology introduced a standardized, structured reporting system and corresponding management process for lung cancer screening, based on the successful concept of the Breast Imaging Reporting and Data System (BI-RADS) used in mammography screening. It is hoped that this system, called Lung-RADS, can effectively reduce the occurrence of false positive results.

While LDCT screening has been shown to be effective in reducing lung cancer mortality, not all individuals meet the criteria for LDCT screening as established by the Taiwan Health Promotion Agency. Accordingly, identifying risk factors for lung cancer is particularly important in individuals who may not be eligible for LDCT screening and may help identify individuals at high risk of developing lung cancer who may benefit from alternative screening strategies or preventative interventions.

The present study aimed to identify risk factors for lung cancer among individuals who do not meet the criteria for LDCT lung cancer screening in Taiwan. This may allow for the targeting of screening and preventative measures for individuals at a high risk of developing lung cancer.

2. Materials and Methods

This retrospective analysis included 12,542 asymptomatic healthy subjects who voluntarily underwent self-paid LDCT exams at the health check-up center of Kaohsiung Veterans General Hospital between January 2016 and December 2021. The study population comprised 6792 males and 4949 females aged 18–96 years, and excluded individuals who were heavy smokers or who had a family history of lung cancer.

Patients were classified into a high-risk group or low-risk group according to Lung-RADS score [2]. The high-risk group comprised cases with Lung-RADS scores of 3 and 4, with cases with a Lung-RADS score of 2 that had undergone follow-up examinations in thoracic medicine or thoracic surgery clinics within 6 months also assigned to the high-risk group. Cases with Lung-RADS scores of 1 and 2 who did not have follow-up examinations in thoracic medicine or thoracic surgery clinics within 6 months were assigned to the low-risk group.

Information, including gender, age, BMI, cigarette smoking habits, previous respiratory disease (including tuberculosis, asthma, and COPD), previous respiratory symptoms, cooking habits, and residential zone, was collected through a questionnaire. We then evaluated LDCT reports and clinical information from individuals in the high-risk and low-risk groups to verify whether the cases were diagnosed with lung cancer.

Statistical Analysis

Baseline demographics and clinical characteristics were summarized for the entire analytical population (gender, age, BMI, cigarette smoking habits, previous respiratory disease, previous respiratory symptoms, cooking habits, and residential zone), divided into the high-risk group or not, and they are appropriately expressed as mean ± standard deviation or number (percentage). The differences between these two groups were compared using independent Student's *t*-test for continuous and chi-squared test for categorical variables, respectively. In addition, significant determinants of the high-risk group were evaluated using univariate and multivariate logistic regression models. Multivariate logistic regression models were used to estimate adjusted odd ratios (ORs) with 95% confidence intervals (95% CIs).

All statistical analyses were performed using Statistical Analysis Software (SAS; version 9.4; SAS System for Windows) and SPSS (version 20; SPSS Inc., Chicago, IL, USA). A p-value < 0.05 was considered statistically significant.

3. Results

A summary of the baseline characteristics of the 12,542 individuals included in the present study is shown in Table 1. The high-risk group comprised 801 individuals, and the low-risk group comprised 11,741 individuals. The mean age of all the study participants was 53.0 ± 11.3 years, with a mean age of 56.7 ± 10.9 years in the high-risk group and 52.8 ± 11.2 years in the low-risk group. A statistically significant age difference was observed between the two groups (p < 0.001). A higher proportion of individuals in the high-risk group were over 55 years old (53%) compared to the low-risk group (42%; p < 0.001), with no significant difference in gender distribution observed between the two groups (p = 0.212). However, a higher proportion of individuals in the high-risk group were not overweight (BMI < 25, 68%) compared to individuals in the low-risk group (61%; p < 0.001). The proportion of individuals with previous chest symptoms (e.g., chest pain or tightness) did not significantly differ between the two groups (p = 0.218). Statistically significant differences in the prevalence of previous respiratory symptoms such as coughing (p = 0.001) and dyspnea or breathlessness when exercising (p = 0.001) were observed between the two groups. A higher proportion of individuals in the high-risk group reported previous respiratory symptoms than those in the low-risk group. A higher proportion of individuals in the high-risk group had underlying respiratory disease (e.g., asthma, tuberculosis, or obstructive pulmonary disease) compared to the low-risk group (p < 0.001). No significant difference in smoking habits was observed between the two groups (p = 0.218). However, a higher proportion of individuals in the high-risk group reported a high-risk cooking habit than the low-risk group (p < 0.001). No significant difference in residential location was observed between the two groups (p = 0.286).

The results of the logistic regression analysis are presented in Table 2. This logistic regression model identified several variables significantly associated with high-risk Lung-RADS scores in univariate and multivariate models. In the univariate model, age, sex, BMI, previous respiratory symptoms, underlying respiratory disease, and cooking habits were all significant predictors of high-risk Lung-RADS scores. Individuals over the age of 55 years had 1.61-fold higher odds of having high-risk Lung-RADS scores compared to individuals aged 55 years or younger. Females had 1.38-fold higher odds of having high-risk Lung-RADS scores compared to males. Similarly, individuals who were not overweight (BMI < 25) had 1.36-fold higher odds of having high-risk Lung-RADS scores compared to individuals who were overweight (BMI ≥ 25). Individuals with previous chest pain or tightness had 1.35-fold higher odds of having high-risk Lung-RADS scores than those without. Individuals with COPD or pulmonary tuberculosis were more likely to have high-risk Lung-RADS scores than individuals with COPD or pulmonary tuberculosis. Finally, individuals who engaged in high-risk cooking practices had 1.47-fold higher odds of having high-risk Lung-RADS scores than those who engaged in low-risk cooking practices.

Table 1. Characteristics at baseline.

	Total	**With High-Risk Group**	**Without High-Risk Group**	
Variables	**N = 12,542 (%)**	**N = 801 (%)**	**N = 11,741 (%)**	***p*-Value**
Age (mean ± SD), year	53.0 ± 11.3	56.7 ± 10.9	52.8 ± 11.2	<0.001
Age				<0.001
≤55	7234 (58)	374 (47)	6860 (58)	
>55	5308 (42)	427 (53)	4881 (42)	
Sex				<0.001
Male	7192 (57)	400 (50)	6792 (58)	
Female	5350 (43)	401 (50)	4949 (42)	
BMI				<0.001
Not overweight (<25)	7722 (62)	546 (68)	7176 (61)	
Overweight (25–29)	4820 (38)	255 (32)	4565 (39)	
Previous chest symptom *				0.212
Yes	2389 (19)	166 (21)	2223 (19)	
No	10,153 (81)	635 (79)	9518 (81)	
Previous respiratory symptom				0.001
Cough	2303 (18)	176 (22)	2127 (18)	
Dyspnea/breathless when exercising	1399 (11)	108 (14)	1291 (11)	
No	8840 (71)	517 (65)	8323 (71)	
Underlying chest disease				<0.001
Asthma	409 (3)	40 (5)	369 (3)	
Tuberculosis	157 (1)	27 (3)	130 (1)	
Obstructive pulmonary disease	204 (2)	18 (2)	186 (2)	
No	11,772 (94)	716 (89)	11,056 (94)	
Smoking habit				0.218
≥20 pack-year	10,532 (84)	685 (86)	9847 (84)	
No smoking Or <20 pack-year	2010 (16)	116 (15)	1894 (16)	
Residential location				0.286
Living in South Taiwan	9288 (74)	606 (76)	8682 (74)	
Not living in South Taiwan	3254 (26)	195 (24)	3059 (26)	
Cooking habit				<0.001
High-risk	1794 (14)	154 (19)	1640 (14)	
Low-risk	10,748 (86)	647 (81)	10,101 (86)	

* Significant chest symptom includes chest pain or chest tightness.

In the multivariate model, age, sex, BMI, and previous respiratory symptoms remained significant predictors of high-risk Lung-RADS scores. Individuals over the age of 55 years had 1.56-fold higher odds of having high-risk Lung-RADS scores compared to individuals who were aged 55 years or younger. Females had 1.30-fold higher odds of having high-risk Lung-RADS scores compared to males. Individuals who were underweight (BMI < 25) had 1.29-fold higher odds of having high-risk Lung-RADS scores compared to those who were overweight (BMI ≥ 25). Individuals with chest pain or tightness had 1.25-fold higher odds of having high-risk Lung-RADS scores than those without. These results indicate that age, sex, BMI, and previous respiratory symptoms are associated with high-risk Lung-RADS scores according to LDCT scans.

Of the 12,542 individuals, 55 had lung cancer, with 47 cases detected in the high-risk group and 8 in the low-risk group (Figure 1). The diagnosis of lung cancer was made through advanced biopsy or thoracic surgery within the last year. A statistically significant difference in the prevalence of lung cancer was observed between the two groups (Pearson's $chi^2 = 577.6555$, $Pr < 0.0001$). These findings indicate that individuals in the high-risk group based on radiographic abnormalities on LDCT may be more likely to develop lung cancer.

Table 2. Odds of being in high-risk group by RADS.

	Univariate		Multivariate	
Variables	**OR (95% CI)**	***p*-Value**	**aOR (95% CI)**	***p*-Value**
Age				
≤55	Ref		Ref	
>55	1.61 (1.39–1.85)	<0.001	1.56 (1.35–1.80)	<0.001
Sex				
Male	Ref		Ref	
Female	1.38 (1.19–1.59)	<0.001	1.30 (1.12–1.51)	0.001
BMI				
Not overweight (<25)	1.36 (1.17–1.59)	<0.001	1.29 (1.10–1.51)	0.002
Overweight (≥25)	Ref		Ref	
Previous respiratory symptom				
Yes	1.35 (1.16–1.56)	<0.001	1.25 (1.08–1.46)	0.004
No	Ref		Ref	
Underlying chest disease				
Obstructive pulmonary disease	1.54 (1.16–2.03)	0.003	1.48 (1.11–1.97)	0.007
Pulmonary tuberculosis	3.10 (2.03–4.70)	<0.001	2.72 (1.78–4.16)	<0.001
No	Ref		Ref	
Smoking habit				
No smoking Or <20 pack-year	Ref			
≥20 pack-year	0.88 (0.72–1.08)	0.218		
Residential location				
Living in South Taiwan	1.10 (0.93–1.29)	0.286		
Not living in South Taiwan	Ref			
Cooking habit				
High-risk	1.47 (1.22–1.76)	<0.001		
Low-risk	Ref			

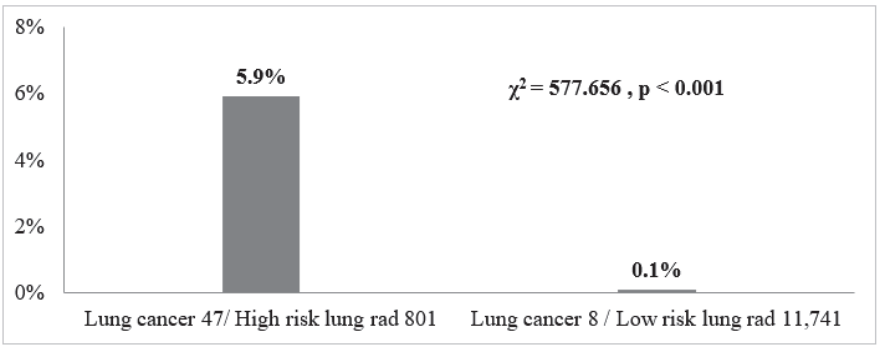

Figure 1. The density histogram depicts all individuals divided into two groups: one categorized as "high-risk of lung cancer by CT radiography" and the other as "low-risk of lung cancer by CT radiography." The histogram further records the proportions of cases within each group that have developed lung cancer.

The following factors were found to be associated with an increased Lung-RADS score (presented in Table 3): age over 55 years (2 points), female gender (1 point), not overweight BMI (1 point), previous respiratory symptoms (1 point), presence of obstructive pulmonary disease (2 points), and presence of pulmonary tuberculosis (4 points). The number of points assigned to each factor was determined by beta coefficients from the multivariate regression analysis. Individuals who are older, female, underweight, and have significant respiratory symptoms or underlying respiratory disease had higher scores, indicating a higher likelihood of developing lung cancer. The presence of pulmonary

tuberculosis was found to have the largest impact on the risk of lung cancer, with 4 points. The high-risk group comprised 86% and 94% of the individuals who scored more than 4 and 5 points, respectively. This result indicates individuals with a score of 5 or more according to questionnaire answers and basic information should undergo LDCT, as a high-risk Lung-RADS score is more likely (Figure 2).

Table 3. Points are estimated by beta coefficients from multivariate regression.

Variables	Points
Age > 55	2
Female	1
Underweight (<25)	1
Previous respiratory symptom	1
Obstructive pulmonary disease	2
Pulmonary tuberculosis	4

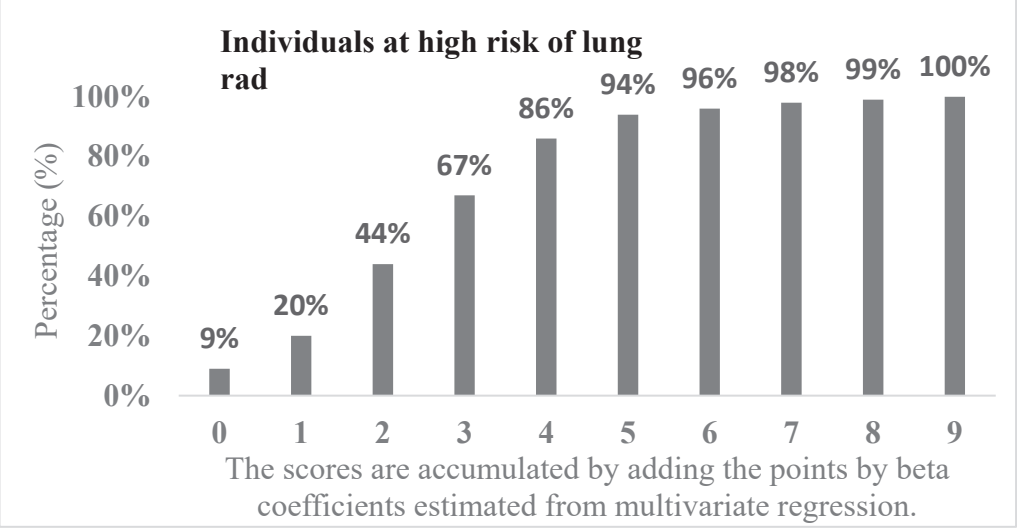

Figure 2. The density histogram describes how the scores are accumulated by adding points based on beta coefficients estimated from multivariate regression. The histogram further records the cumulative percentage of cases related to a high risk of lung cancer by CT radiography.

4. Discussion

In 2013, the United States Preventive Services Task Force recommended annual lung cancer screening with LDCT for smokers aged between 55 years and 80 years with at least 30 pack-years of smoking exposure who currently smoke or have quit smoking within the previous 15 years [3].

Age is closely associated with the incidence of lung cancer, with older individuals having higher rates of lung cancer than younger individuals. Further, histologic subtypes of lung cancer have differing age distributions [4]. The incidence and mortality of lung cancer increase with age, with the highest rates observed among individuals in their eighth and ninth decades of life. This is likely due to a combination of factors, including longer exposure to tobacco smoke and other environmental factors that increase the risk of lung cancer [5]. Overall, the results of these studies indicate that age is an important factor in the development and prognosis of lung cancer and that early detection and intervention may improve outcomes, particularly among older individuals at a higher risk of developing lung cancer.

Previous studies have suggested that women who smoke are at a higher risk of developing lung cancer than men who smoke, while other studies have found no significant

difference between genders. Studies conducted in 1993 and 1994 by Risch et al. found that women who smoke are at a higher risk of developing lung cancer than men who smoke, particularly for certain subtypes of lung cancer [6,7]. A study by Bain et al. in 2004 found that women have a higher risk of developing lung cancer than men with similar smoking histories, indicating that females may be more susceptible to lung cancer than males [8]. A further study found that female smokers are more likely to develop lung cancer than male smokers, suggesting that the increased risk may be related to gender-specific differences in biological or hormonal factors [9]. Zang and Wynder also found that women have a higher risk of developing lung cancer than men and suggested that this difference may be due to variations in smoking habits, hormonal factors, or other biological differences [10]. Taken together, these studies indicate that females who smoke are at a higher risk of developing lung cancer than male smokers and that biological or hormonal factors may contribute to this difference. However, more research is required to fully understand the reasons for the higher risk of developing lung cancer in females and to develop effective prevention strategies. A 2013 study by De Matteis et al. found no significant difference in the risk of developing lung cancer between male and female smokers after adjusting for smoking intensity and duration [11]. While there may be some evidence suggesting that women who smoke are at a higher risk of developing lung cancer than men who smoke, this evidence is inconsistent across studies.

A cohort study from China and the United States that used data from the UK Biobank to examine the associations of genetic risk, BMI trajectories, and the risk of non-small cell lung cancer (NSCLC) found that both genetic risk and BMI trajectories were independently associated with NSCLC risk and that the joint effects of genetic risk and BMI trajectories were stronger than their individual effects. They also found that BMI trajectories modified the effects of genetic risk on NSCLC risk and that the highest risk was observed among individuals with high genetic risk and increasing BMI trajectories [12].

A large-scale randomized controlled trial based on data from the National Lung Screening Trial (NLST) that evaluated the effectiveness of low-dose CT screening for lung cancer reported a difference in the association between BMI and lung cancer diagnosis according to ethnicity. Specifically, a higher BMI was associated with a lower risk of lung cancer diagnosis among non-Hispanic white participants but not among Black participants. The study also found that Black participants had a higher risk of lung cancer diagnosis than non-Hispanic white participants, even after adjusting for BMI and other factors [13].

A separate study used data from the HUNT study to examine the causal association between BMI and lung cancer incidence using observational and Mendelian randomization approaches and found that BMI was inversely associated with lung adenocarcinoma but not with other lung cancer types [14].

Previous studies have reported a strong association between COPD and the risk of developing lung cancer, with our results corroborating these previous findings. For example, a study of a nationally representative cohort of the US population with up to 22 years of follow-up found that moderate or severe obstructive lung disease was associated with an increased risk of incident lung cancer [15]. The coexistence of chronic obstructive pulmonary disease (COPD) and lung cancer is characterized by shared risk factors, including tobacco smoke exposure and genetic predispositions. Chronic inflammation, oxidative stress, epigenetic alterations, dysregulated cell signaling, and altered immune responses contribute to their comorbidity. Understanding these molecular mechanisms is crucial for developing effective therapeutic strategies and improving clinical outcomes [16]. The presence of comorbidities such as tuberculosis in COPD patients may also be related to the increased risk of lung cancer. It has been suggested that COPD patients with a history of tuberculosis, particularly never-smokers, may benefit from regular screening or evaluation for the development of lung cancer [17].

Participants with tuberculosis (TB) sequelae had a higher number of nodules and higher emphysema rates than those without TB sequelae. Additionally, the proportion of individuals with positive screening results was higher among participants with TB sequelae.

The authors concluded that TB within a particular population should be considered when interpreting lung cancer screening results [18].

A 2015 study by Kocher et al. investigated the presenting symptoms of patients with NSCLC and found that cough was present in 50–75% of patients with lung cancer and that a cough productive of large volumes of thin, mucoid secretions was seen in patients with mucinous adenocarcinoma [19].

Ying-Chin Ko et al. found that exposure to Chinese food cooking fumes was associated with an increased risk of lung cancer in nonsmoking women, highlighting the potential health risks associated with traditional cooking methods in Chinese cuisine [20]. Yingbo Xue et al. conducted a meta-analysis of eight studies and confirmed a significant association between cooking oil fume exposure and lung cancer risk in Chinese nonsmoking women [21]. The authors posited that this association may be due to the production of carcinogenic substances, such as PAHs, during high-temperature cooking. Yu et al. also found a dose–response relationship between cooking fume exposure and lung cancer risk in Chinese nonsmoking women, further supporting the potential health risks associated with cooking [22]. The results of these studies highlight the importance of understanding the potential health risks associated with cooking, particularly for Chinese nonsmoking women who may be at increased risk of developing lung cancer due to traditional cooking methods [23]. However, Bigert et al. found no statistically significant increase in the overall risk of developing lung cancer among individuals who regularly cook when accounting for smoking in men or women, with no association between exposure duration and risk of lung cancer [24].

Previous studies have indicated strong evidence linking outdoor air pollution, particularly PM 2.5 and NOx, with an increased risk of various types of cancer, including lung, bladder, and cardiovascular disease [25–27]. One study reported that there was no difference in the incidence of lung cancer between different regions of Taiwan. However, this study focused on the relationship between air pollution and lung cancer in nonsmokers throughout Taiwan rather than regional variations [28].

Owing to the retrospective nature of this study, it is imperative to acknowledge certain limitations inherent in it. The primary limitation lies in the reliance on the 2014 version of LUNG RAD (Radiology) for the interpretation and judgment of findings within the reports. Despite the availability of more recent versions, this study adheres to the standards and criteria established by healthcare professionals during the retrospective period. Consequently, the exclusion of newer versions of LUNG RAD may limit the generalizability of findings to the latest diagnostic advancements. This limitation underscores the importance of considering the evolving nature of medical standards and the potential impact on the interpretation of results.

Lung cancer is a major global health concern, and lung cancer screening effectively reduces mortality in high-risk populations. However, not all individuals may meet the criteria for LDCT screening as established by the Taiwan Health Promotion Agency. The present study identified potential risk factors for lung cancer among individuals who do not meet these criteria, including age, gender, and previous medical history. By considering these additional risk factors and symptoms related to the previous respiratory system, it may be possible to identify individuals at a high risk of developing lung cancer who may benefit from earlier diagnosis and treatment.

5. Conclusions

Although LDCT screening has been shown to be effective in improving lung cancer outcomes, further research is required to determine optimal screening intervals and protocols for specific populations. Long-term follow-up using LDCT may also provide valuable information regarding changes in lung health over time and the incidence of lung cancer in high-risk populations. By continuing to identify novel risk factors for lung cancer and refining screening strategies, it may be possible to further reduce the burden of lung cancer and improve patient outcomes.

Author Contributions: The authors confirm contributions to the paper as follows: Conception and design of the work: C.-S.C. and I.-S.C.; analysis and interpretation of the data: C.-H.Y. and J.-S.C.; the drafting of the paper: H.-C.Y. and C.-S.C.; data collection, revising it critically for intellectual content: C.-S.C., I.-S.C., H.-C.Y., C.-H.Y., J.-S.C. and Y.-S.C.; the final approval of the version to be published: C.-S.C., I.-S.C., H.-C.Y., C.-H.Y., J.-S.C. and Y.-S.C. All authors have read and agreed to the published version of the manuscript.

Funding: This study was supported by grants from Kaohsiung Veterans General Hospital, KSVGH24-CT3-05, Taiwan, R.O.C.

Institutional Review Board Statement: The study was conducted in accordance with the Declaration of Helsinki, and approved by The Kaohsiung Veterans General Hospital Institutional Review Board (protocol code 24-CT3-05(240207-2)) for studies involving humans.

Informed Consent Statement: The Kaohsiung Veterans General Hospital Institutional Review Board approved this study and waived the requirement for informed consent due to the retrospective nature of this study.

Data Availability Statement: All results are available from the Kaohsiung Veterans General Hospital. The database used for the study can be made available from the corresponding author under request if needed.

Conflicts of Interest: None of the authors have conflicts of interest to declare in relation to this work.

References

1. National Lung Screening Trial Research Team; Aberle, D.R.; Adams, A.M.; Berg, C.D.; Black, W.C.; Clapp, J.D.; Fagerstrom, R.M.; Gareen, I.F.; Gatsonis, C.; Marcus, P.M.; et al. Reduced lung-cancer mortality with low-dose computed tomographic screening. *N. Engl. J. Med.* **2011**, *365*, 395–409. [CrossRef] [PubMed]
2. American College of Radiology. Lung CT Screening Reporting & Data System (Lung-RADS®) 11 August 2014. Available online: https://www.acr.org/Clinical-Resources/Reporting-and-Data-Systems/Lung-Rads (accessed on 1 March 2024).
3. Potter, A.L.; Bajaj, S.S.; Yang, C.J. The 2021 USPSTF lung cancer screening guidelines: A new frontier. *Lancet Respir. Med.* **2021**, *9*, 689–691. [CrossRef] [PubMed]
4. Houston, K.A.; Henley, S.J.; Li, J.; White, M.C.; Richards, T.B. Patterns in lung cancer incidence rates and trends by histologic type in the United States, 2004–2009. *Lung Cancer* **2014**, *86*, 22–28. [CrossRef] [PubMed]
5. Barta, J.A.; Powell, C.A.; Wisnivesky, J.P. Global epidemiology of lung cancer. *Ann. Glob. Health* **2019**, *85*, 8. [CrossRef] [PubMed]
6. Risch, H.A.; Howe, G.R.; Jain, M.; Burch, J.D.; Holowaty, E.J.; Miller, A.B. Are female smokers at higher risk for lung cancer than male smokers? A case-control analysis by histologic type. *Am. J. Epidemiol.* **1993**, *138*, 281–293. [CrossRef] [PubMed]
7. Risch, H.A.; Howe, G.R.; Jain, M.; Burch, J.D.; Holowaty, E.J.; Miller, A.B. Lung cancer risk for female smokers. *Science* **1994**, *263*, 1206–1208. [CrossRef] [PubMed]
8. Bain, C.; Feskanich, D.; Speizer, F.E.; Thun, M.; Hertzmark, E.; Rosner, B.A.; Colditz, G.A. Lung cancer rates in men and women with comparable histories of smoking. *J. Natl. Cancer Inst.* **2004**, *96*, 826–834. [CrossRef] [PubMed]
9. Hovanec, J.; Siemiatycki, J.; Conway, D.I.; Olsson, A.; Stücker, I.; Guida, F.; Jöckel, K.H.; Pohlabeln, H.; Ahrens, W.; Brüske, I.; et al. Lung cancer and socioeconomic status in a pooled analysis of case-control studies. *PLoS ONE* **2018**, *13*, e0192999. [CrossRef] [PubMed]
10. Zang, E.A.; Wynder, E.L. Differences in lung cancer risk between men and women: Examination of the evidence. *J. Natl. Cancer Inst.* **1996**, *88*, 183–192. [CrossRef]
11. De Matteis, S.; Consonni, D.; Pesatori, A.C.; Bergen, A.W.; Bertazzi, P.A.; Caporaso, N.E.; Lubin, J.H.; Wacholder, S.; Landi, M.T. Are women who smoke at higher risk for lung cancer than men who smoke? *Am. J. Epidemiol.* **2013**, *177*, 601–612. [CrossRef]
12. You, D.; Wang, D.; Wu, Y.; Chen, X.; Shao, F.; Wei, Y.; Zhang, R.; Lange, T.; Ma, H.; Xu, H.; et al. Associations of genetic risk, BMI trajectories, and the risk of non-small cell lung cancer: A population-based cohort study. *BMC Med.* **2022**, *20*, 203. [CrossRef]
13. Zhao, J.; Barta, J.A.; McIntire, R.; Shusted, C.; Zeigler-Johnson, C.; Juon, H.S. Racial difference in BMI and lung cancer diagnosis: Analysis of the National Lung Screening Trial. *BMC Cancer* **2022**, *22*, 797. [CrossRef] [PubMed]
14. Jiang, L.; Sun, Y.Q.; Brumpton, B.M.; Langhammer, A.; Chen, Y.; Mai, X.M. Body mass index and incidence of lung cancer in the HUNT study: Using observational and Mendelian randomization approaches. *BMC Cancer* **2022**, *22*, 1152. [CrossRef]
15. Mannino, D.M.; Aguayo, S.M.; Petty, T.L.; Redd, S.C. Low lung function and incident lung cancer in the United States: Data from the First National Health and Nutrition Examination Survey follow-up. *Arch. Intern. Med.* **2003**, *163*, 1475–1480. [CrossRef] [PubMed]
16. Forder, A.; Zhuang, R.; Souza, V.G.P.; Brockley, L.J.; Pewarchuk, M.E.; Telkar, N.; Stewart, G.L.; Benard, K.; Marshall, E.A.; Reis, P.P.; et al. Mechanisms Contributing to the Comorbidity of COPD and Lung Cancer. *Int. J. Mol. Sci.* **2023**, *24*, 2859. [CrossRef]
17. Park, H.Y.; Kang, D.; Shin, S.H.; Choi, H.; Jang, S.H.; Lee, C.H.; Cho, J. Pulmonary tuberculosis and the incidence of lung cancer among patients with chronic obstructive pulmonary disease. *Ann. Am. Thorac. Soc.* **2022**, *19*, 640–648. [CrossRef]

18. Kim, H.; Kim, H.Y.; Goo, J.M.; Kim, Y. Lung cancer CT screening and lung-RADS in a tuberculosis-endemic country: The Korean lung cancer screening project (K-LUCAS). *Radiology* **2020**, *296*, 181–188. [CrossRef]
19. Kocher, F.; Hilbe, W.; Seeber, A.; Pircher, A.; Schmid, T.; Greil, R.; Auberger, J.; Nevinny-Stickel, M.; Sterlacci, W.; Tzankov, A.; et al. Longitudinal analysis of 2293 NSCLC patients: A comprehensive study from the TYROL registry. *Lung Cancer* **2015**, *87*, 193–200. [CrossRef] [PubMed]
20. Chen, T.Y.; Fang, Y.H.; Chen, H.L.; Chang, C.H.; Huang, H.; Chen, Y.S.; Hsiung, C.A. Impact of cooking oil fume exposure and fume extractor use on lung cancer risk in non-smoking Han Chinese women. *Sci. Rep.* **2020**, *10*, 6774. [CrossRef]
21. Xue, Y.; Jiang, Y.; Jin, S.; Li, Y. Association between cooking oil fume exposure and lung cancer among Chinese nonsmoking women: A meta-analysis. *OncoTargets Ther.* **2016**, *9*, 2987–2992. [CrossRef]
22. Yu, I.T.; Chiu, Y.L.; Au, J.S.; Wong, T.W.; Tang, J.L. Dose-response relationship between cooking fumes exposures and lung cancer among Chinese nonsmoking women. *Cancer Res.* **2006**, *66*, 4961–4967. [CrossRef] [PubMed]
23. Ko, Y.C.; Cheng, L.S.; Lee, C.H.; Huang, J.J.; Huang, M.S.; Kao, E.L.; Wang, H.Z.; Lin, H.J. Chinese food cooking and lung cancer in women nonsmokers. *Am. J. Epidemiol.* **2000**, *151*, 140–147. [CrossRef] [PubMed]
24. Bigert, C.; Gustavsson, P.; Straif, K.; Pesch, B.; Brüning, T.; Kendzia, B.; Schüz, J.; Stücker, I.; Guida, F.; Brüske, I.; et al. Lung cancer risk among cooks when accounting for tobacco smoking: A pooled analysis of case-control studies from Europe, Canada, New Zealand, and China. *J. Occup. Environ. Med.* **2015**, *57*, 202–209. [CrossRef] [PubMed]
25. Swanton, C.; Hill, W.; Lim, E.; Lee, C.; Weeden, C.E.; Augustine, M.; Chen, K.; Kuan, F.C.; Marongiu, F.; Rodrigues, F.; et al. LBA1 Mechanism of action and an actionable inflammatory axis for air pollution induced non-small cell lung cancer: Towards molecular cancer prevention. *Ann. Oncol.* **2022**, *33*, S1413. [CrossRef]
26. Liu, X.; Mubarik, S.; Wang, F. Lung cancer death attributable to long-term ambient particulate matter (PM(2.5)) exposure in East Asian countries during 1990–2019. *Front. Med.* **2021**, *8*, 742076. [CrossRef] [PubMed]
27. Turner, M.C.; Andersen, Z.J.; Baccarelli, A.; Diver, W.R.; Gapstur, S.M.; Pope, C.A., III; Prada, D.; Samet, J.; Thurston, G.; Cohen, A. Outdoor air pollution and cancer: An overview of the current evidence and public health recommendations. *CA Cancer J. Clin.* **2020**, *70*, 460–479. [CrossRef]
28. Tseng, C.H.; Tsuang, B.J.; Chiang, C.J.; Ku, K.C.; Tseng, J.S.; Yang, T.Y.; Hsu, K.H.; Chen, K.C.; Yu, S.L.; Lee, W.C.; et al. The relationship between air pollution and lung cancer in nonsmokers in Taiwan. *J. Thorac. Oncol.* **2019**, *14*, 784–792. [CrossRef]

diagnostics

MDPI

Article

Usefulness of Saline Sealing in Preventing Pneumothorax after CT-Guided Biopsies of the Lung

Andrei Roman [1,2], Andreea Brozba [1,*], Alexandru Necula [1], Delia Doris Muntean [1,3], Paul Kubelac [1,4], Zsolt Fekete [1,5], Ciprian Tomuleasa [1,6], Csaba Csutak [1,3], Diana Feier [1,3], Roxana Pintican [1,3] and Catalin Vlad [1,7]

[1] Faculty of Medicine, "Iuliu Hatieganu" University of Medicine and Pharmacy, 400347 Cluj-Napoca, Romania; andrei.roman678@gmail.com (A.R.); alexnecula10@gmail.com (A.N.); paulkubelac@gmail.com (P.K.); drfekete@gmail.com (Z.F.); ciprian.tomuleasa@gmail.com (C.T.); csutakcsaba@yahoo.com (C.C.); diana.feier@gmail.com (D.F.); roxana.pintican@gmail.com (R.P.); catalinvlad@yahoo.it (C.V.)
[2] Department of Radiology, Oncology Institute "Prof. Dr. Ion Chiricuta", 400015 Cluj-Napoca, Romania
[3] Department of Radiology, Cluj County Emergency Hospital, 400347 Cluj-Napoca, Romania
[4] Department of Oncology, Oncology Institute "Prof. Dr. Ion Chiricuta", 400015 Cluj-Napoca, Romania
[5] Department of Radiotherapy, Oncology Institute "Prof. Dr. Ion Chiricuta", 400015 Cluj-Napoca, Romania
[6] Department of Hematology, Oncology Institute "Prof. Dr. Ion Chiricuta", 400015 Cluj-Napoca, Romania
[7] Department of Surgery, Oncology Institute "Prof. Dr. Ion Chiricuta", 400015 Cluj-Napoca, Romania
* Correspondence: andreeabrozba@gmail.com; Tel.: +40-758782848

Abstract: This study aimed to assess the effectiveness of saline sealing in reducing the incidence of pneumothorax after a CT-guided lung biopsy. This was a retrospective case-control study of patients who underwent CT-guided biopsies for lung tumors using 18 G semiautomatic core needles in conjunction with 17 G coaxial needles. The patients were divided into two consecutive groups: a historical Group A (n = 111), who did not receive saline sealing, and Group B (n = 87), who received saline sealing. In Group B, NaCl 0.9% was injected through the coaxial needle upon its removal. The incidence of pneumothorax and chest tube insertion was compared between the two groups. Multivariate logistic regression was performed to verify the contribution of other pneumothorax risk factors. The study included 198 patients, with 111 in Group A and 87 in Group B. There was a significantly (p = 0.02) higher pneumothorax rate in Group A (35.1%, n = 39) compared to Group B (20.7%, n = 18). The difference regarding chest tube insertion was not significant (p = 0.1), despite a tendency towards more insertions in Group A (5.4%, n = 6), compared to Group B (1.1%, n = 1). Among the risk factors for pneumothorax, only the presence of emphysema (OR = 3.5, p = 0.0007) and belonging to Group A (OR = 2.2, p = 0.02) were significant. Saline sealing of the needle tract after a CT-guided lung biopsy can significantly reduce the incidence of pneumothorax. This technique is safe, readily available, and inexpensive, and should be considered as a routine preventive measure during this procedure.

Keywords: saline sealing; CT-guided lung biopsy; pneumothorax prevention

1. Introduction

Lung cancer is the most frequent type of cancer among men and the second most diagnosed cancer on the globe with 2,206,771 new cases in 2020 [1]. It is responsible for 18% of all cancer mortality with 1,796,144 deaths attributed to it in 2020, which makes it the leading cause of cancer-related deaths [1]. In the wake of new lung cancer screening strategies, the discovery of an increasing number of early-stage lung tumors can be expected [2,3]. According to the European Society of Medical Oncology guidelines, an attempt to obtain a pathological sample should be made for any suspicious lung nodule prior to surgery or stereotactic radiation therapy if the patient's clinical condition and the nodule's size or location allows it [4]. For advanced disease, where a surgical sample is unlikely to be

obtained, the demand for adequate biopsy material needed to enable accurate molecular profiling has become imperative due to the availability of numerous targeted therapies [5]. Computed tomography-guided lung biopsy is an essential technique for characterizing pulmonary nodules.

Although fine needle aspiration can be used for the biopsy of lung tumors, accurate histopathological and molecular analysis is favored by larger tissue samples that can be obtained through core needle biopsy, especially in the absence of a cytopathologist on the site to ensure the adequacy of the sample [6–10]. The thicker needles that are used for core biopsies are, however, associated with a higher complication rate [11–14]. According to a recent meta-analysis, the overall complication rate for a CT-guided core lung biopsy is 38.8%, of which pneumothorax is the most frequent, occurring in 25.3% of cases, 5.6% requiring the insertion of a chest tube [15,16].

Various techniques have been attempted for reducing the risk of pneumothorax and chest tube insertion. These include maneuvers such as rapid roll-over, deep expiration and breath-hold, the injection of various sealant materials such as autologous clotted or non-clotted blood, collagen, haemocoagulase, or hydrogel plugs [17–24]. Saline sealing of the needle tract is another method that has been shown to be useful in reducing the rate of periprocedural pneumothorax [25–28].

Saline sealing is performed in conjunction with the coaxial biopsy technique by injecting NaCl 0.9% through the coaxial needle as it is removed at the end of the procedure. Saline solution has the advantage of causing no adverse reactions, being readily available and inexpensive. However, this technique has been described in fewer reports compared to the other pneumothorax prevention methods and evidence for its effectiveness is still limited.

Our study aimed to assess the effectiveness of the saline sealing technique in preventing pneumothorax using as a control group a consecutive series of patients on whom no specific pneumothorax prevention method was employed.

2. Materials and Methods

2.1. Patients

This was a retrospective case-control study and was approved by the institutional ethics committee of the Oncology Institute "Prof. Dr. Ion Chiricuta" with the approval protocol number 89/16.03/2021. Patients that underwent CT-guided biopsies of lung tumors were split into two groups. Group A, considered as the control group, consisted of a series of consecutive patients (August 2017–October 2020) who underwent biopsies without any sealing technique. Group B consisted of a series of consecutive patients (November 2020–January 2023) that underwent biopsies followed by saline sealing. Exclusion criteria for both groups were as follows: (a) the needle did not cross the aerated lung; (b) a hemorrhage was visible along the needle tract prior to its removal; (c) the procedure was aborted before the biopsy was taken; (d) the pneumothorax occurred prior to the removal of the coaxial needle; (e) a missing follow-up radiograph.

2.2. Procedure

The patients were referred for percutaneous biopsy by oncologists, pneumologists and thoracic surgeons after bronchoscopy was deemed to be either inconclusive or unfeasible due to the location of the tumor. If the tumor was in extensive contact with the chest wall, or more accessible metastases, such as cervical lymph nodes, hepatic or superficial lytic bone metastases were present, an ultrasound guided biopsy was performed. Informed consent was received from all patients prior to the procedure, including procedure-related complications and the administration of saline solution for Group B. Anticoagulant and antiplatelet therapy was ceased according to the Consensus Guidelines for Periprocedural Management of Coagulation Status and Hemostasis Risk in Percutaneous Image-guided Interventions and the coagulation status was verified on the day of the procedure [29]. The procedures were performed by a single radiologist using a 64 slice Optima 660 (GE Medical

Systems, Chicago, IL, USA) CT scanner or a 64 slice Somatom Confidence (Siemens, Munich, Germany) CT scanner. An unenhanced low-dose (120 KV; 60 mA) planning CT scan of the thorax was performed prior to the biopsy and the shortest and safest puncture path was chosen, avoiding fissures and significant blood vessels. When possible, a prone position of the patient was preferred, as well as a perpendicular angle between the pleura and the needle. No sedation medication was used. The patient was instructed to maintain regular breathing and not to talk or cough during the procedure. The puncture site was disinfected and covered in sterile drapes, followed by local anesthesia using 1% Lidocaine. A 17 G coaxial needle was inserted in a stepwise manner towards the margin of the tumor using ultra-low-dose (120 kV; 20 mA) single- or triple-slice scans for guidance. The radiologist was present in the CT room during the entire procedure, the scans being started using a footswitch. No breathing commands were issued during the procedure. For tumors located in the lower lobes that were highly mobile during respiration, the scans were synchronized with the respiratory phase by observing the patient's respiratory motion. The needle position was stabilized using gauzes soaked in povidone iodine. A semiautomatic, 18 G biopsy cutting needle (VELOX 2, Medax Medical Devices, Poggio Rusco, Italy) was inserted through the coaxial needle, obtaining 1–5 tissue samples that were stored in formalin solution. In patients belonging to Group A, the coaxial needle was removed after tissue sampling without any further action. In patients belonging to Group B, 3–5 mL of saline solution (NaCl 0.9%) was gradually injected through the coaxial needle during its removal at the end of the biopsy (Figure 1). The presence of pneumothorax and further complications were verified on a single-slice CT scan immediately following the procedure and at 2 h on a chest X-ray. If no pneumothorax was present and the patients were asymptomatic, they were released on the following day. If a small, asymptomatic pneumothorax occurred, patients received a second X-ray 2 h later and were released the following day if the pneumothorax remained relatively unchanged. A chest tube was inserted if the pneumothorax was progressing rapidly or was symptomatic by a surgeon who was blinded regarding the usage of saline sealing. The tube was removed 1–4 days later, after air leakage ceased completely.

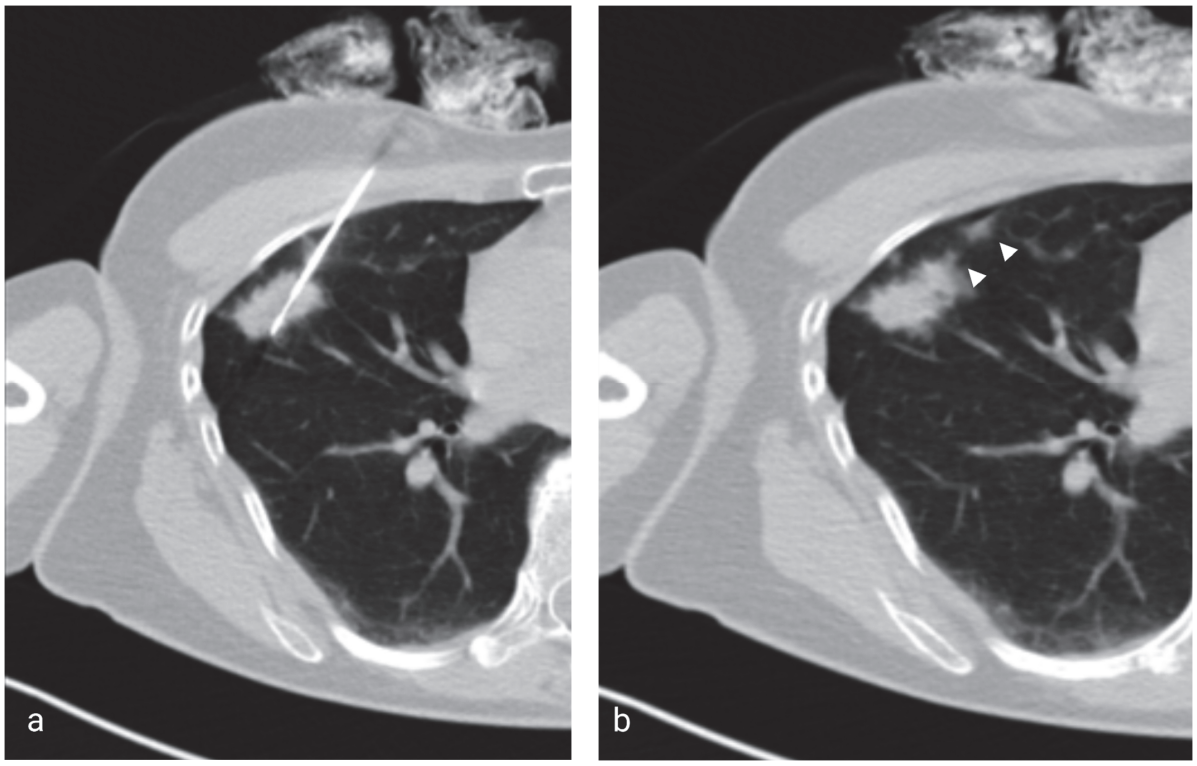

Figure 1. (**a**) Axial low-dose CT showing the 17G coaxial needle and the 18G biopsy needle within a right middle lobe mass. (**b**) Image taken immediately after the injection of saline solution and removal of the coaxial needle showing the hyperattenuating needle tract (arrowheads).

2.3. Study Design

CT and X-ray images were retrospectively reviewed. Based on the CT images and the patient's medical record, gender, age, tumor size, location, biopsy tract length, and the histopathological result were noted. The presence of emphysema was registered according to the Fleischner Society criteria [30]. The presence of a pneumothorax and its size were recorded based on the X-ray where it appeared largest. The insertion of a chest tube was recorded from the patient's file.

The statistical analysis was performed using a GraphPad Prism 9.1.2 (GraphPad Software, Inc., San Diego, CA, USA). Data normality was verified using the Shapiro–Wilk test. The data were considered to be normally distributed for a p value > 0.05. To compare the two groups, a Fisher exact test was used for categorical variables and a Mann–Whitney test for continuous variables, not normally distributed. Multiple logistic regression was used in order to analyze the pneumothorax risk factors (gender, age, belonging to Group A, emphysema, tumor location, tumor size, biopsy tract length) and odds ratios were calculated. A p value < 0.05 was considered statistically significant.

3. Results

A total of 198 patients were included in the study, of whom 111 belonged to Group A and 87 belonged to Group B. The overall success rate was 97.4% (n = 193), with 2.6% (n = 5) inconclusive biopsies due to necrosis. The most prevalent type of cancer identified was adenocarcinoma, accounting for nearly 50% of all histopathological findings. Metastatic lung tumors were the second most common outcome, representing over 20% of all results (Table 1).

Table 1. Histopathological results.

Histopathological Result	Number of Histopathological Results (%)
NSCLC	
Adenocarcinoma	96 (48.48%)
Squamous cell carcinoma	15 (7.58%)
NSCLC-NOS	12 (6.06%)
Neuroendocrine neoplasms	
SCLC	2 (1.01%)
Neuroendocrine tumor-NOS	11 (5.56%)
Metastases	40 (20.20%)
Benign (fibrosis, inflammation)	11 (5.56%)
Necrosis	5 (2.53%)
Other tumors	
Mesenchymal tumors specific to the lung (Pulmonary hamartoma)	2 (1.01%)
Malignant fibrous histiocytoma	1 (0.51%)
Inflammatory myofibroblastic tumor	1 (0.51%)
Hematolymphoid tumors (Large B-cell lymphoma)	2 (1.01%)

NSCLC—Non-Small Cell Lung Cancer. NOS—Not Otherwise Specified. SCLC—Small Cell Lung Cancer.

There were no significant differences between the two groups regarding age, number of tissue samples taken, the presence of emphysema, tumor location and biopsy tract length. Moderate centrilobular emphysema was present in three patients belonging to Group A and in two patients belonging to Group B. All other patients where emphysema was present had either a trace or mild centrilobular or paraseptal emphysema. In Group A (37.8%, n = 42), there was a significantly lower (p = 0.03) proportion of female patients, compared to Group B (54.1%, n = 47). The average nodule size was significantly larger (p = 0.04) in Group A (32.7 $\pm$ 16.4), compared to Group B (29.2 $\pm$ 17.5) (Table 2).

Table 2. Clinical characteristics of patients.

Variable	Group A	Group B	*p*
N	111	87	
Age (years)			
Mean ± SD	63.7 ± 8.9	63.4 ± 9.0	0.8
Range	30–80	34–82	
Normal distribution	No	No	
Gender			
Men	69 (62.2%)	40 (45.9%)	0.03
Women	42 (37.8%)	47 (54.1%)	
Biopsy fragments			
Mean ± SD	2.1 ± 0.9	2.1 ± 0.7	0.5
Range	1–5	1–3	
Normal distribution	No	No	
Emphysema			
Yes	31 (27.9%)	31 (35.6%)	0.2
No	80 (72.1%)	56 (64.4%)	
Nodule size (mm)			
Mean ± SD	32.7 ± 16.4	29.2 ± 17.5	0.04
Range	9–87	8–110	
Normal distribution	No	No	
Nodule location			
Right lower lobe	38	15	
Right middle lobe	3	2	
Right upper lobe	28	35	
Left lower lobe	16	14	
Left upper lobe	26	21	
Biopsy tract length (mm)			
Mean ± SD	17.7 ± 10.4	19.2 ± 10.1	0.2
Range	2–54	4–43	
Normal distribution	No	No	
Pneumothorax			
Yes	39 (35.1%)	18 (20.7%)	0.02
No	72 (64.9%)	69 (79.3%)	
Pneumothorax size (mm)			
Mean ± SD	14.9 ± 16.1	13.3 ± 15.6	0.6
Range	2–61	3–56	
Normal distribution	No	No	
Chest tube insertion			
Yes	6 (5.4%)	1 (1.1%)	0.1
No	105 (94.6%)	86 (98.9%)	

Group A—control group. Group B—treatment group. N—number of patients included in the study. SD—standard deviation.

Group A (35.1%, n = 39) had a significantly higher (p = 0.02) pneumothorax rate compared to Group B (20.7%, n = 18) (Figure 2). If pneumothorax was present, its thickness was not significantly different (p = 0.6) between the two groups. The insertion of a chest tube was required in 5.4% (n = 6) of patients belonging to Group A and in 1.1% (n = 1) of patients belonging to Group B (Figure 3); however, the difference was not statistically significant (p = 0.1).

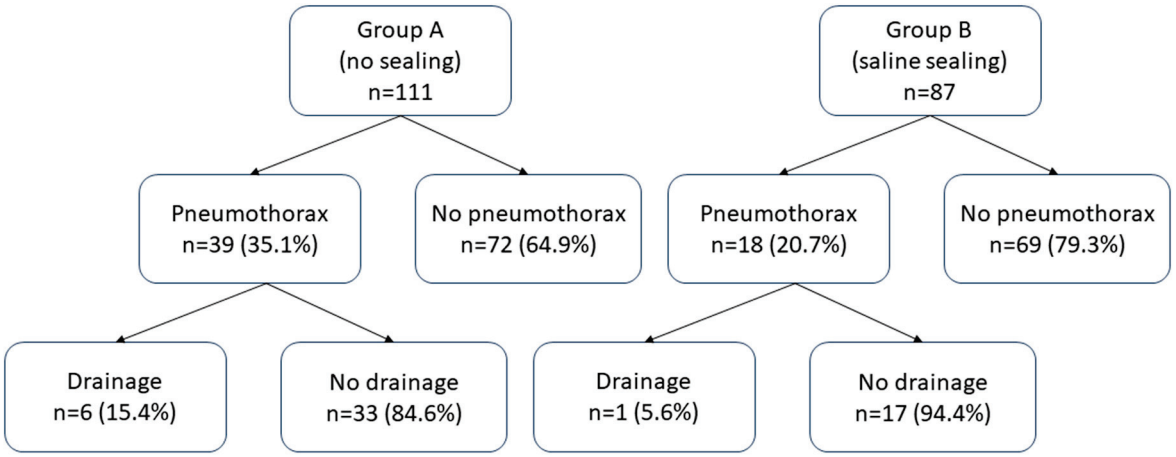

Figure 2. Proportions of pneumothorax and drainage insertion among the two groups.

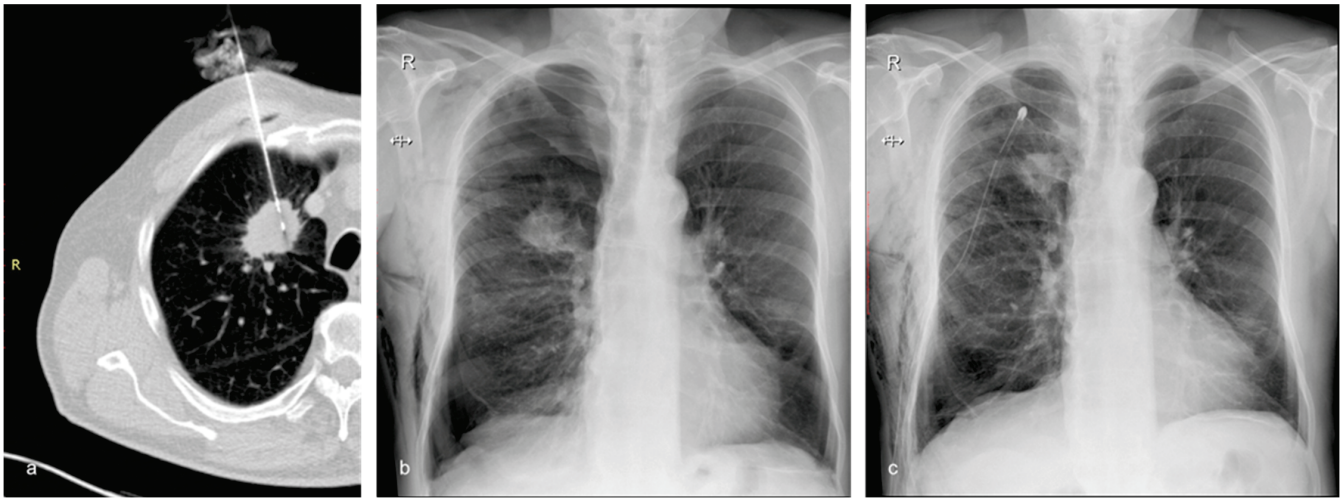

Figure 3. A 72-year-old man with emphysema and a tumor in the right upper lobe belonging to Group B (the treatment group). The nodule was confirmed to be adenocarcinoma by the histopathological examination. (**a**) Axial CT showing the 17G coaxial needle and the 18G biopsy needle within the lung mass. (**b**) Chest X-ray performed 2 h after the biopsy showing moderate post-procedural pneumothorax and subcutaneous emphysema. The patient complained of right chest pain and dyspnea. It was decided to insert a chest tube to prevent further expansion of the pneumothorax and to alleviate the symptoms. (**c**) Chest X-ray of the same patient following the insertion of the chest drain.

Multiple logistic regression showed that emphysema (OR = 3.5, p = 0.0007) and belonging to Group A (OR = 2.2, p = 0.02) represented a significant independent risk factor for pneumothorax. Gender, age, tumor location, tumor size and biopsy tract length had no significant influence on the occurrence of pneumothorax (Table 3). Multiple logistic regression could not be performed for the analysis of a chest tube insertion due to the limited number of events.

Other complications besides pneumothorax were small hemothorax (1.01%, n = 2), severe, but self-limiting hemoptysis (1.01%, n = 2), a large reactive pleural effusion (0.51%, n = 1), and a necrotic tumor infection with sepsis (0.51%, n = 1). Mild intra- or periprocedural hemoptysis was not recorded in the patient's file. No deaths occurred consecutive to the biopsies.

Table 3. Multiple logistic regression evaluating pneumothorax risk factors.

Variable	OR	95% CI	*p* Value
Gender (female)	0.52	0.24–1.07	0.08
Age	1.00	0.96–1.04	0.7
Group A	2.26	1.10–4.80	0.02
Emphysema	3.50	1.71–7.33	0.0007
Location (RLL)	Reference		
Location (LLL)	1.56	0.57–4.28	0.3
Location (ML)	1.18	0.12–9.14	0.8
Location (LUL)	0.43	0.15–1.16	0.1
Location (RUL)	0.61	0.24–1.48	0.2
Nodule size	0.99	0.97–1.01	0.4
Biopsy tract length	1.00	0.97–1.03	0.7

OR—Odds Ratio. CI—Confidence Interval. RLL—Right Lower Lobe. LLL—Left Upper Lobe. ML—Middle Lobe. LUL—Left Upper Lobe. RUL—Right Upper Lobe.

4. Discussion

This study shows that the saline sealing technique significantly diminishes pneumothorax risk after CT-guided biopsies, with a tendency towards reducing the chest tube insertion rate. In the analyzed patient group, the only other independent factor significantly influencing the pneumothorax rate was the presence of emphysema.

Pneumothorax is the most common complication associated with CT-guided biopsies of the lung occurring in 25.3% of patients. Despite the fact that most instances of pneumothorax are asymptomatic and self-limiting, in approximately 5.6% of cases drainage is needed [15]. In order to reduce the morbidity and costs associated with pneumothorax, various preventive methods have been proposed.

One group of these is related to patient positioning or respiratory maneuvers such as positioning the patient biopsy side down during the procedure, rapid or slow roll-over to puncture the site down after the biopsy, or breath hold on needle extraction [24,31]. The studies that compared the benefit of rapid roll-over vs. slow or no roll-over to puncture the side down after the lung biopsy showed no significant reduction in pneumothorax incidence; however, the rate of drainage catheter placement due to pneumothorax was significantly lower in the treatment group with an overall incidence of 1.9% compared to 5.2% in the control group [18,24,32]. Drumm et al. assessed the effectiveness of positioning the patient with the puncture side down during and immediately after the CT-guided lung biopsy and showed that the pneumothorax rate was significantly reduced compared to a supine or prone position (10.6% compared to 27.2%), but that no substantial difference in chest drain insertion was reported [31]. Another study evaluated the benefits of breath-hold after forced expiration before extracting the needle, demonstrating a statistically significant reduction in the pneumothorax rate (8.2% compared to 15.8%), but no significant reduction in the number of patients requiring a drainage catheter [33]. Although altering the patient's position seems promising, adjusting and maintaining a certain attitude may be difficult for a postoperative patient to achieve.

The other group of preventive measures consists of injecting a sealing substance along the needle tract such as a saline solution, clotted or non-clotted autologous blood, and heterologous plugs consisting of collagen foam, fibrin glue, hydrogel plug or gelatin powder [17–19,21–23]. The sealing techniques are based on the observation that a pneumothorax occurs through the parenchymal and pleural defect that remains after the removal of the needle. Filling that defect and the nearby alveoli using a sealant is presumed to stop the airflow towards the pleural space. A multitude of reports regarding the efficiency of the blood patch technique and of various heterologous plugs exist; however, these techniques have some downsides. Although inexpensive, and theoretically devoid of side-effects, the blood patch technique can be time-consuming in patients with difficult venous access, or with inadequate cannulation, thus prolonging the discomfort of the procedure [34].

Heterologous plugs can be expensive, their preparation can be time-consuming, and some of them have been shown to cause a granulomatous inflammatory reaction [35,36].

Six research articles included in the meta-analysis by Huo et al. using autologous blood patches showed an overall reduction in the risk of pneumothorax (27.9% compared to 40.1% in the control group) and of a chest drain insertion (4.8% compared to 11.1%) [18]. Lang et al. used a technique in which the clotted blood was separated and the supernatant was injected into the track and at the level of the biopsied nodule, and the solid clot elements were deployed at the periphery [17]. In a retrospective analysis performed by Perl and colleagues, intraparenchymal blood patching reduced the incidence of pneumothorax for nodules located in the lower lobes, closer to the pleura (<2 cm) or deeper inside the lung (>4 cm) and when four or more samples were taken [22]. Zlevor et al. studied the effects of blood patching as a preventive measure as well as a therapeutic method for pneumothorax to avoid a chest tube placement and reported a success rate of 83.4% [21].

The most obvious theoretical disadvantages of saline sealing compared to other sealing techniques are the rapid resorption and diffusion of saline solution in the lung parenchyma and the fact that it may be more easily pushed out from the needle tract by the pulmonary pressure due to its low viscosity. Possibly due to these assumptions, the efficacy of saline sealing has been less extensively investigated. However, the saline sealing technique has the advantage of being both inexpensive and easily applied, without having any side-effects, and its effectiveness has been shown to hold promise based on the few existing reports (Table 4).

Table 4. Articles published on saline sealing.

Study	Method	N	Incidence of PTX	*p*	Chest Drainage	*p*
Billich 2008 [25]	NaCl 0.9%	140	34% vs. 8%	<0.001	11.4% vs. 1.4%	0.01
Li 2015 [26]	NaCl 0.9%	322	26.1% vs. 6.2%	<0.001	5.6% vs. 0.6%	0.01
Khorochkov 2018 [27]	NaCl 0.9% and rapid patient roll-over	278	25% vs. 20%	0.22	10% vs. 3.9%	0.03
Babu 2020 [28]	NaCl 0.9%	200	46% vs. 32%	<0.05	7% vs. 1%	<0.05
The present study	NaCl 0.9%	198	35.1% vs. 20.7%	0.02	5.4% vs. 1.1%	0.1

The British Thoracic Society (BTS) recommends complication rates equal to or below 20.5% for pneumothorax and 3.1% for pneumothorax requiring chest drainage [37]. With a pneumothorax rate of 35.1% and a chest tube insertion rate of 5.4%, Group A did not comply with the BTS quality requirements. By applying the saline sealing technique, the pneumothorax and chest tube insertion rates dropped to 20.7% (just above BTS standards) and 1.1% (within BTS standards), respectively. In our study, the decrease in the frequency of pneumothorax was statistically significant, and comparable to the frequency reported by Babu et al., but less important compared to the decrease reported by Billich et al. and Li et al. [25,26,28]. All previous studies reported a significant decrease in the rate of drainage insertion. A decrease was also noticeable in our study; however, the difference was not statistically significant, likely due to the relatively low number of patients and of chest tube insertions in the control group. It is worth mentioning that all the above-mentioned studies had higher chest tube insertion rates in the control groups, which suggests possible differences regarding patient selection, technique, or the threshold for inserting a chest tube, the latter being the most likely explanation, as their pneumothorax rates were lower than in our study with the exception of Babu et al. (Table 4).

In contrast with the study of Billich et al., patients with tumors in direct contact with the chest wall were excluded as air leakage from the lungs is highly unlikely in this context [25]. Unlike in the previously mentioned papers, patients who had visible hemorrhage along the needle tract prior to its removal were excluded, as this has been shown to be associated with a lesser pneumothorax rate [38,39].

After correcting for other known pneumothorax risk factors using multiple logistic regression, besides the presence of emphysema (OR = 3.5), only the saline sealing technique (OR = 1/2.26 = 0.44) showed a statistical significance. The results were equivalent or favorable compared to the results published in the meta-analysis by Huo et al. for the positional and breathing techniques (OR = 0.48–0.69) as well as for the blood patch technique (OR = 0.57) and the heterologous plug technique (OR = 0.47) [18]. It must be mentioned that some of the studies included in the above-mentioned meta-analysis are older than 30 years, and also include fluoroscopic guidance. In addition, most biopsies were performed using 19 G coaxial needles and 20–22 G biopsy needles, which makes an accurate comparison difficult.

There are a few limitations to the present study, including its retrospective nature, the single center approach, and the relatively low number of patients. There was a difference between the groups regarding gender and tumor size, with significantly more female patients and slightly smaller tumors (29.2 mm vs. 32.7 mm) in the saline sealing group, but neither of these factors showed a significant influence on the occurrence of pneumothorax at multiple logistic regression. Nevertheless, a smaller tumor size has been shown to be a risk factor for pneumothorax and may have influenced the results [14]. Another source of bias could be the operator's experience, as the biopsies belonging to Group A were all performed prior to those in Group B, despite the fact that the overall technique remained identical. The lack of standardization regarding the quantity of saline that was injected could be another confounding factor for this study. It is possible that injecting a larger quantity of saline solution would further reduce the risk of pneumothorax, without any significant side-effects.

5. Conclusions

Besides the presence of emphysema, the only independent factor influencing the occurrence of pneumothorax was the application of the saline sealing technique. Our study shows that using saline solution to seal the needle tract after a percutaneous pulmonary biopsy significantly reduces the pneumothorax rate and shows a tendency towards a reduction in the drainage insertion rate. Further randomized controlled trials could prove useful in determining the most appropriate needle tract sealing technique.

Author Contributions: Conceptualization, A.R. and A.B.; Data curation, A.R., A.B. and A.N.; Formal analysis, A.R. and A.B.; Investigation, A.R., A.B., A.N., D.D.M., P.K., Z.F., C.T. and C.V.; Methodology, A.R. and A.B.; Project administration, A.R.; Resources, A.R., D.D.M., P.K., Z.F., C.T. and C.V.; Supervision, A.R.; Validation, A.R.; Visualization, A.B.; Writing—original draft, A.R., A.B. and A.N.; Writing—review and editing, C.C., D.F. and R.P. All authors have read and agreed to the published version of the manuscript.

Funding: This research received no external funding.

Institutional Review Board Statement: The study was conducted in accordance with the Declaration of Helsinki and approved by the Institutional Review Board (or Ethics Committee) of THE ONCOLOGY INSTITUTE "PROF. DR. ION CHIRICUTA" (protocol code 89/16.03.2021).

Informed Consent Statement: Informed consent was obtained from all subjects involved in the study.

Data Availability Statement: The data presented in this study are available on request from the corresponding author. The data are not publicly available due to institutional policy.

Conflicts of Interest: The authors declare no conflict of interest.

References

1. Sung, H.; Ferlay, J.; Siegel, R.L.; Laversanne, M.; Soerjomataram, I.; Jemal, A.; Bray, F. Global Cancer Statistics 2020: GLOBOCAN Estimates of Incidence and Mortality Worldwide for 36 Cancers in 185 Countries. *CA Cancer J. Clin.* **2021**, *71*, 209–249. [CrossRef]
2. Wu, F.-Z.; Huang, Y.-L.; Wu, C.C.; Tang, E.-K.; Chen, C.-S.; Mar, G.-Y.; Yen, Y.; Wu, M.-T. Assessment of Selection Criteria for Low-Dose Lung Screening CT Among Asian Ethnic Groups in Taiwan: From Mass Screening to Specific Risk-Based Screening for Non-Smoker Lung Cancer. *Clin. Lung Cancer* **2016**, *17*, e45–e56. [CrossRef] [PubMed]

3. Wolf, A.M.D.; Oeffinger, K.C.; Shih, T.Y.-C.; Walter, L.C.; Church, T.R.; Fontham, E.T.H.; Elkin, E.B.; Etzioni, R.D.; Guerra, C.E.; Perkins, R.B.; et al. Screening for lung cancer: 2023 guideline update from the American Cancer Society. *CA Cancer J. Clin.* **2023**. [CrossRef] [PubMed]
4. Vansteenkiste, J.; Crinò, L.; Dooms, C.; Douillard, J.Y.; Faivre-Finn, C.; Lim, E.; Rocco, G.; Senan, S.; Van Schil, P.; Veronesi, G.; et al. 2nd ESMO Consensus Conference on Lung Cancer: Early-stage non-small-cell lung cancer consensus on diagnosis, treatment and follow-up. *Ann. Oncol.* **2014**, *25*, 1462–1474. [CrossRef] [PubMed]
5. Russo, U.; Sabatino, V.; Nizzoli, R.; Tiseo, M.; Cappabianca, S.; Reginelli, A.; Carrafiello, G.; Brunese, L.; De Filippo, M. Transthoracic computed tomography-guided lung biopsy in the new era of personalized medicine. *Future Oncol.* **2019**, *15*, 1125–1134. [CrossRef] [PubMed]
6. Sangha, B.S.; Hague, C.J.; Jessup, J.; O'Connor, R.; Mayo, J.R. Transthoracic Computed Tomography-Guided Lung Nodule Biopsy: Comparison of Core Needle and Fine Needle Aspiration Techniques. *Can. Assoc. Radiol. J.* **2016**, *67*, 284–289. [CrossRef]
7. Ocak, S.; Duplaquet, F.; Jamart, J.; Pirard, L.; Weynand, B.; Delos, M.; Eucher, P.; Rondelet, B.; Dupont, M.; Delaunois, L.; et al. Diagnostic Accuracy and Safety of CT-Guided Percutaneous Transthoracic Needle Biopsies: 14-Gauge versus 22-Gauge Needles. *J. Vasc. Interv. Radiol.* **2016**, *27*, 674–681. [CrossRef]
8. Li, Y.; Yang, F.; Huang, Y.Y.; Cao, W. Comparison between computed tomography-guided core and fine needle lung biopsy: A meta-analysis. *Medicine* **2022**, *101*, e29016. [CrossRef]
9. Schneider, F.; Smith, M.A.; Lane, M.C.; Pantanowitz, L.; Dacic, S.; Ohori, N.P. Adequacy of core needle biopsy specimens and fine-needle aspirates for molecular testing of lung adenocarcinomas. *Am. J. Clin. Pathol.* **2015**, *143*, 193–200, quiz 306. [CrossRef]
10. Yoon, S.H.; Lee, S.M.; Park, C.H.; Lee, J.H.; Kim, H.; Chae, K.J.; Jin, K.N.; Lee, K.H.; Kim, J.I.; Hong, J.H.; et al. 2020 Clinical Practice Guideline for Percutaneous Transthoracic Needle Biopsy of Pulmonary Lesions: A Consensus Statement and Recommendations of the Korean Society of Thoracic Radiology. *Korean J. Radiol.* **2021**, *22*, 263–280. [CrossRef]
11. Geraghty, P.R.; Kee, S.T.; McFarlane, G.; Razavi, M.K.; Sze, D.Y.; Dake, M.D. CT-guided Transthoracic Needle Aspiration Biopsy of Pulmonary Nodules: Needle Size and Pneumothorax Rate. *Radiology* **2003**, *229*, 475–481. [CrossRef] [PubMed]
12. Kim, J.; Chee, C.G.; Cho, J.; Kim, Y.; Yoon, M.A. Diagnostic accuracy and complication rate of image-guided percutaneous transthoracic needle lung biopsy for subsolid pulmonary nodules: A systematic review and meta-analysis. *Br. J. Radiol.* **2021**, *94*, 20210065. [CrossRef] [PubMed]
13. Capalbo, E.; Peli, M.; Lovisatti, M.; Cosentino, M.; Mariani, P.; Berti, E.; Cariati, M. Trans-thoracic biopsy of lung lesions: FNAB or CNB? Our experience and review of the literature. *Radiol. Med.* **2014**, *119*, 572–594. [CrossRef] [PubMed]
14. Huo, Y.R.; Chan, M.V.; Habib, A.R.; Lui, I.; Ridley, L. Pneumothorax rates in CT-Guided lung biopsies: A comprehensive systematic review and meta-analysis of risk factors. *Br. J. Radiol.* **2020**, *93*, 20190866. [CrossRef] [PubMed]
15. Heerink, W.; de Bock, G.; de Jonge, G.; Groen, H.; Vliegenthart, R.; Oudkerk, M. Complication rates of CT-guided transthoracic lung biopsy: Meta-analysis. *Eur. Radiol.* **2017**, *27*, 138–148. [CrossRef] [PubMed]
16. Tsai, I.C.; Tsai, W.L.; Chen, M.C.; Chang, G.C.; Tzeng, W.S.; Chan, S.W.; Chen, C.C. CT-guided core biopsy of lung lesions: A primer. *AJR. Am. J. Roentgenol.* **2009**, *193*, 1228–1235. [CrossRef] [PubMed]
17. Lang, E.K.; Ghavami, R.; Schreiner, V.C.; Archibald, S.; Ramirez, J. Autologous blood clot seal to prevent pneumothorax at CT-guided lung biopsy. *Radiology* **2000**, *216*, 93–96. [CrossRef]
18. Huo, Y.R.; Chan, M.V.; Habib, A.R.; Lui, I.; Ridley, L. Post-Biopsy Manoeuvres to Reduce Pneumothorax Incidence in CT-Guided Transthoracic Lung Biopsies: A Systematic Review and Meta-analysis. *Cardiovasc. Interv. Radiol.* **2019**, *42*, 1062–1072. [CrossRef]
19. Salama, N.M.; Tabashy, R.H.; Mahmoud, I.H.; Rahman, A.E.R.M.A.E.; Mohamed, D.N.E.; Kassas, H.E. Does Gelfoam slurry embolization post-pulmonary biopsy reduce risk of pneumothorax? A prospective randomized control study. *Egypt. J. Radiol. Nucl. Med.* **2023**, *54*, 4. [CrossRef]
20. Zhou, S.Q.; Luo, F.; Gu, M.; Lu, X.J.; Xu, Y.; Wu, R.N.; Xiong, J.; Ran, X. Biopsy-tract haemocoagulase injection reduces major complications after CT-guided percutaneous transthoracic lung biopsy. *Clin. Radiol.* **2022**, *77*, e673–e679. [CrossRef]
21. Zlevor, A.M.; Mauch, S.C.; Knott, E.A.; Pickhardt, P.J.; Mankowski Gettle, L.; Mao, L.; Meyer, C.A.; Hartung, M.P.; Kim, D.H.; Lubner, M.G.; et al. Percutaneous Lung Biopsy with Pleural and Parenchymal Blood Patching: Results and Complications from 1112 Core Biopsies. *J. Vasc. Interv. Radiol.* **2021**, *32*, 1319–1327. [CrossRef] [PubMed]
22. Perl, R.M.; Risse, E.; Hetzel, J.; Bösmüller, H.; Kloth, C.; Fritz, J.; Horger, M. The effect of intraparenchymal blood patching on the rate of pneumothorax in patients undergoing percutaneous CT-guided core biopsy of the lung. *Eur. J. Radiol.* **2019**, *116*, 14–20. [CrossRef] [PubMed]
23. Maybody, M.; Muallem, N.; Brown, K.T.; Moskowitz, C.S.; Hsu, M.; Zenobi, C.L.; Jihad, M.; Getrajdman, G.I.; Sofocleous, C.T.; Erinjeri, J.P.; et al. Autologous Blood Patch Injection versus Hydrogel Plug in CT-guided Lung Biopsy: A Prospective Randomized Trial. *Radiology* **2019**, *290*, 547–554. [CrossRef] [PubMed]
24. Kim, J.I.; Park, C.M.; Lee, S.M.; Goo, J.M. Rapid needle-out patient-rollover approach after cone beam CT-guided lung biopsy: Effect on pneumothorax rate in 1191 consecutive patients. *Eur. Radiol.* **2015**, *25*, 1845–1853. [CrossRef] [PubMed]
25. Billich, C.; Muche, R.; Brenner, G.; Schmidt, S.A.; Kruger, S.; Brambs, H.J.; Pauls, S. CT-guided lung biopsy: Incidence of pneumothorax after instillation of NaCl into the biopsy track. *Eur. Radiol.* **2008**, *18*, 1146–1152. [CrossRef]
26. Li, Y.; Du, Y.; Luo, T.Y.; Yang, H.F.; Yu, J.H.; Xu, X.X.; Zheng, H.J.; Li, B. Usefulness of normal saline for sealing the needle track after CT-guided lung biopsy. *Clin. Radiol.* **2015**, *70*, 1192–1197. [CrossRef]

27. Khorochkov, E.; Garvin, G.J.; Potoczny, S.; Kozak, R.I. Injection of Saline Into the Biopsy Tract and Rapid Patient Rollover Decreases Pneumothorax Size Following Computed Tomography-Guided Transthoracic Needle Biopsy. *Can. Assoc. Radiol. J.* **2018**, *69*, 489–492. [CrossRef]
28. Babu, S.B.; Srinivasan, S.; Chung, R.; Chawla, A.; Tan, H.K.; Lohan, R. Tract sealing with normal saline after percutaneous transthoracic lung biopsies. *J. Med. Imaging Radiat. Oncol.* **2020**, *64*, 211–214. [CrossRef]
29. Patel, I.J.; Davidson, J.C.; Nikolic, B.; Salazar, G.M.; Schwartzberg, M.S.; Walker, T.G.; Saad, W.A. Consensus guidelines for periprocedural management of coagulation status and hemostasis risk in percutaneous image-guided interventions. *J. Vasc. Interv. Radiol.* **2012**, *23*, 727–736. [CrossRef]
30. Lynch, D.A.; Austin, J.H.; Hogg, J.C.; Grenier, P.A.; Kauczor, H.U.; Bankier, A.A.; Barr, R.G.; Colby, T.V.; Galvin, J.R.; Gevenois, P.A.; et al. CT-Definable Subtypes of Chronic Obstructive Pulmonary Disease: A Statement of the Fleischner Society. *Radiology* **2015**, *277*, 192–205. [CrossRef]
31. Drumm, O.; Joyce, E.A.; de Blacam, C.; Gleeson, T.; Kavanagh, J.; McCarthy, E.; McDermott, R.; Beddy, P. CT-guided Lung Biopsy: Effect of Biopsy-side Down Position on Pneumothorax and Chest Tube Placement. *Radiology* **2019**, *292*, 190–196. [CrossRef] [PubMed]
32. O'Neill, A.C.; McCarthy, C.; Ridge, C.A.; Mitchell, P.; Hanrahan, E.; Butler, M.; Keane, M.P.; Dodd, J.D. Rapid needle-out patient-rollover time after percutaneous CT-guided transthoracic biopsy of lung nodules: Effect on pneumothorax rate. *Radiology* **2012**, *262*, 314–319. [CrossRef] [PubMed]
33. Min, L.; Xu, X.; Song, Y.; Issahar, B.D.; Wu, J.; Zhang, L.; Huang, Q.; Chen, M. Breath-hold after forced expiration before removal of the biopsy needle decreased the rate of pneumothorax in CT-guided transthoracic lung biopsy. *Eur. J. Radiol.* **2013**, *82*, 187–190. [CrossRef] [PubMed]
34. Clayton, J.D.; Elicker, B.M.; Ordovas, K.G.; Kohi, M.P.; Nguyen, J.; Naeger, D.M. Nonclotted Blood Patch Technique Reduces Pneumothorax and Chest Tube Placement Rates after Percutaneous Lung Biopsies. *J. Thorac. Imaging* **2016**, *31*, 243–246. [CrossRef] [PubMed]
35. Skupin, A.; Gomez, F.; Husain, M.; Skupin, C.; Bigman, O. Complications of transthoracic needle biopsy decreased with isobutyl 2-cyanoacrylate: A pilot study. *Ann. Thorac. Surg.* **1987**, *43*, 406–408. [CrossRef] [PubMed]
36. Turgut, B.; Duran, F.M.; Bakdık, S.; Arslan, S.; Tekin, A.F.; Esme, H. Effectiveness of autologous blood injection in reducing the rate of pneumothorax after percutaneous lung core needle biopsy. *Diagn. Interv. Radiol.* **2020**, *26*, 470–475. [CrossRef] [PubMed]
37. Manhire, A. Guidelines for radiologically guided lung biopsy. *Thorax* **2003**, *58*, 920–936. [CrossRef]
38. De Filippo, M.; Saba, L.; Silva, M.; Zagaria, R.; Concari, G.; Nizzoli, R.; Bozzetti, C.; Tiseo, M.; Ardizzoni, A.; Lipia, S.; et al. CT-guided biopsy of pulmonary nodules: Is pulmonary hemorrhage a complication or an advantage? *Diagn. Interv. Radiol.* **2014**, *20*, 421–425. [CrossRef]
39. Soylu, E.; Ozturk, K.; Gokalp, G.; Topal, U. Effect of Needle-Tract Bleeding on Pneumothorax and Chest Tube Placement Following CT Guided Core Needle Lung Biopsy. *J. Belg. Soc. Radiol.* **2019**, *103*, 21. [CrossRef]

diagnostics

MDPI

Article

Predictive Value of Clinicopathological Factors to Guide Post-Operative Radiotherapy in Completely Resected pN2-Stage III Non-Small Cell Lung Cancer

Ju-Chun Chien [1,2], Yu-Chang Hu [1], Yi-Ju Tsai [3], Yu-Ting Chien [4], I-Jung Feng [5,*] and Yow-Ling Shiue [2,5,*]

[1] Department of Radiation Oncology, Kaohsiung Veterans General Hospital, Kaohsiung 81362, Taiwan
[2] Institute of Biomedical Sciences, National Sun Yat-sen University, Kaohsiung 80424, Taiwan
[3] Department of Medical Education and Research, Kaohsiung Veterans General Hospital, Kaohsiung 81362, Taiwan
[4] School of Post Baccalaureate Chinese Medicine, China Medical University, Taichung 404333, Taiwan
[5] Institute of Precision Medicine, National Sun Yat-sen University, Kaohsiung 80424, Taiwan
* Correspondence: ijfeng@g-mail.nsysu.edu.tw (I.-J.F.); shirley@imst.nsysu.edu.tw (Y.-L.S.); Tel.: +886-7-525-2000 (ext. 7252) (I.-J.F.); +886-7-525-2000 (ext. 5818) (Y.-L.S.)

Abstract: Introduction: With the evolution of radiotherapy techniques and a better understanding of clinicopathological factors, we aimed to evaluate the treatment effect of post-operative radiotherapy (PORT) and associated predictive factors in patients with completely resected pN2 stage III non-small cell lung cancer (R0 pN2-stage III NSCLC). **Material and Method:** The cancer registration database of a single medical center was searched for R0 pN2-stage III NSCLC. Clinicopathological factors and information about post-operative therapies, including PORT and adjuvant systemic treatment, were retrospectively collected and analyzed. The Kaplan-Meier method and a Cox regression model were applied for time-to-event analysis, with disease-free survival (DFS) being the primary outcome. **Results:** From 2010 to 2021, 82 R0 pN2-stage III NSCLC patients were evaluated, with 70.1% of tumors harboring epidermal growth factor receptor mutations (EGFR mut.). PORT was performed in 73.2% of cases, and the median dose was 54 Gy. After a median follow-up of 42 months, the 3-year DFS and overall survival (OS) rates were 40.6% and 77.3%, respectively. Distant metastasis (DM) was the main failure pattern. In the overall cohort, DFS was improved with PORT (3-year DFS: 44.9% vs. 29.8%; HR: 0.552, $p = 0.045$). Positive predictive factors for PORT benefit, including EGFR mut., negative extranodal extension, positive lymphovascular invasion, 1–3 positive lymph nodes, and a positive-to-dissected lymph node ratio $\leq$0.22, were recognized. OS improvement was also observed in subgroups with less lymph node burden. **Conclusions:** For R0 pN2-stage III NSCLC, PORT prolongs DFS and OS in selected patients. Further studies on predictive factors and the development of nomograms guiding the application of PORT are highly warranted, aiming to enhance the personalization of lung cancer treatment.

Keywords: non-small cell lung cancer; post-operative radiotherapy; predicting factors

1. Introduction

Lung cancer is the leading cause of cancer mortality and is ranked second in incidence among malignancies worldwide [1]. Based on histology, it is categorized into non-small cell lung cancer (NSCLC) and small cell lung cancer, with the former accounting for 81% of all lung cancer diagnoses. For localized early-stage NSCLC, radical surgery is the backbone of cancer treatment. The addition of adjuvant therapy is considered if a margin-negative (R0) resection is not achieved or if pathologically proven advanced disease is observed. Systemic treatment options, such as platinum-based chemotherapy (CT), epidermal growth factor receptor tyrosine kinase inhibitors (EGFR-TKIs), or immune checkpoint inhibitors (ICIs), are increasingly used post-operatively given their well-established disease-free survival

(DFS) benefit [2–4]. On the other hand, the role of post-operative radiotherapy (PORT) in NSCLC remains under debate.

Previous review articles have suggested that the effectiveness of PORT in R0 NSCLC was underestimated due to diminished benefits and relatively high radiation toxicity with the inclusion of patients with early-stage disease and the application of old radiotherapy techniques in early studies [5,6]. Therefore, recent studies have focused on patients with mediastinal lymph node involvement (pN2-stage III) and have applied modern radiotherapy techniques. In two recent large randomized control studies, the EORTC 22055/Lung ART trial and the PORT-C trial, both revealed no disease-free survival difference with the addition of PORT to R0 pN2-stage III NSCLC, despite a decreased mediastinal relapse [7,8]. The Lung ART trial reported high radiation toxicity with 16 cases in the PORT group dying from cardiopulmonary disease, compared to 2 in the control group [7]. This might be attributed to the fact that 89% of PORT was performed using the relatively outdated 3D conformal radiotherapy technique. On the other hand, radiotherapy was administered using intensity-modulated radiation therapy (IMRT) to 89.3% of cases in the PORT-C trial, and the study was conducted in East Asia, where epidermal growth factor receptor mutations (EGFR muts.) are more common in NSCLC [8–10]. A high protocol violation rate might influence the results of intention-to-treat analysis in the PORT-C trial, while superior DFS with PORT was observed in per-protocol analysis (HR: 0.75, $p = 0.05$) and in an exploratory analysis with stratification based on the number of dissected lymph nodes (DLNs) and positive lymph nodes (PLNs) (HR: 0.75, $p = 0.04$) [8].

Traditionally, radiotherapy was considered a localized treatment modality. By eradicating cancer cells within the mediastinal field, PORT might decrease locoregional recurrence and should prevent subsequent distal failure and cancer death. However, in the two large randomized control trials, distal metastasis was the main failure pattern in both the PORT and control groups, indicating that a poor prognostic factor might not necessarily be a good predictive factor for PORT if it leads to excessive distal failure risk [7,8]. Surgical margin status is a well-recognized parameter used to evaluate local recurrence risk. Nevertheless, only approximately 30% of the recruited cases in the Lung ART trial met the criteria for R0 resection in accordance with the International Association for the Study of Lung Cancer (IASLC), where not only the integrity of all margins, but also a predefined systematic nodal dissection, the absence of extranodal extension (ENE) of the positive node removed separately and of the highest mediastinal basin, and negativity of the highest mediastinal node removed are required, limiting its clinical applicability [7,11].

According to the latest National Comprehensive Cancer Network (NCCN) guideline, PORT is listed as an optional treatment for R0 pN2-stage III NSCLC with high-risk factors, such as ENE, multi-station involvement, inadequate dissected lymph nodes, and those not completing adjuvant systemic therapy. However, there was limited supporting evidence for the influence of these factors on the PORT effect. Considering the poor clinical application of the IASLC criteria for margin status and the lack of evidence to guide PORT beyond pN2-stage III NSCLC, we aimed to evaluate the predictive value of clinicopathological factors and to provide further guidance for the decision to administer PORT.

2. Materials and Methods

2.1. Study Cohort and Data Collection

The cancer registry database of a medical center, including all NSCLC cases diagnosed in the facility, was retrospectively screened for pathologically proven pN2-stage III NSCLC patients, staged according to the 7th or 8th editions of the American Joint Committee on Cancer (AJCC) staging manual. Patients should have received definite surgery with procedures, such as lobectomy, segmentectomy, or wedge resection, along with lymph node dissection or sampling. Complete surgical resection, defined as no tumor involvement of the resection margins and no positive cytology of pleural or pericardial effusion, was required. Patients who received neo-adjuvant treatment of any type prior to definite surgery and those with a positive surgical margin, lymph node involvement in the contralateral

or supraclavicular regions (N3), known distant metastasis (M1), or history of previous malignancies were excluded. The flow diagram of case inclusion is presented in Figure 1.

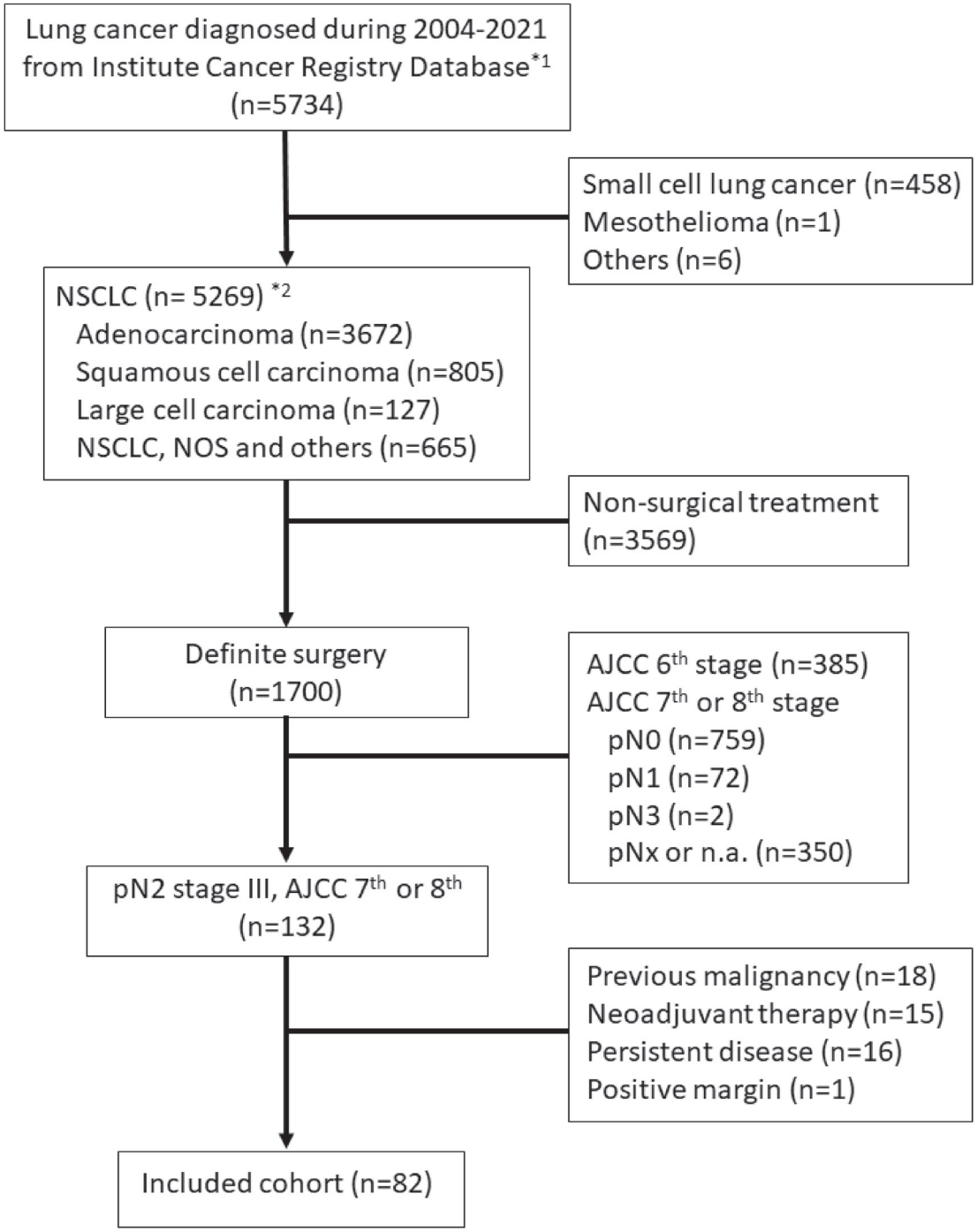

Figure 1. Flow diagram for case inclusion in the study cohort. *1 The Institute Cancer Registry Database contains all malignant disease records diagnosed in the facility, dating back from 2004 to 2021, the time of the data request. *2 Non-small cell lung cancer was classified according to the definition of the World Health Organization (WHO)/International Association for the Study of Lung Cancer (IASLC), and patients were identified from the database using the ICD-O-3 code. Abbreviations: NSCLC, non-small cell lung cancer; NOS, not otherwise specified; AJCC, American Joint Committee on Cancer, Cancer staging manual.

Baseline characteristics, treatment course, and histopathological factors, including but not limited to EGFR mut. status, ENE, PLNs, DLNs, and positive-to-dissected lymph node ratio (PD ratio), which was defined as the value of positive lymph node number divided by dissected lymph node number, were recorded. Recurrent and survival data were retrospectively collected from medical charts, hospital cancer registry records, and the National Death Registry. The study was approved by the institutional review board of our facility.

2.2. Definition of Endpoints

The primary endpoint was disease-free survival (DFS), defined as survival without evidence of disease. The coding of recurrence or metastasis was mainly based on medical records. For events not specified in the medical chart, an experienced radiation oncologist with expertise in thoracic malignancy, who was not aware of the study hypothesis and allocation at the time, was consulted. Lesions located in the mediastinum or around the hilum of the ipsilateral lung were coded as locoregional recurrence (LRR), while thoracic lesions beyond the above-mentioned area or extra-thoracic lesions were coded as distant metastases (DMs). Regarding cause of death, a death reported from the National Death Registry without a specific cause of death was coded as a non-cancer death, representing an event in overall survival (OS) but censored in disease-specific survival (DSS) analysis. All endpoints were evaluated in time-to-event analysis, starting from the date of definite surgery.

2.3. Statistical Analysis

The software Statistical Product and Service Solutions Statistics (SPSS statistics, 22nd) was used for data analysis. The distribution of the use of PORT based on baseline characteristics was compared using the Pearson's chi-square test for possible imbalance. DFS, LRR, DM, and survival outcomes were analyzed using the Kaplan-Meier method. The Cox regression model was used to recognize possible prognostic factors. Factors achieving a p-value less than 0.1 in univariate analysis were kept for multivariate tests. A p-value less than 0.05 was considered statistically significant.

To evaluate the treatment effect of PORT in each subgroup, hazard ratios (HRs) were calculated using the Cox regression model with stratification according to clinicopathological factors. The HRs were adjusted for prognostic factors and factors with an uneven distribution in multivariate analysis to prevent possible bias.

3. Results

From 2010 to 2021, 82 consecutive patients with R0 pN2-stage III NSCLC were identified, and 89.0% were diagnosed with adenocarcinoma. Fifty-five (67.1%) patients had ^{18}F-FDG PET/CT exams for pre-operative staging workup. After surgery, only one patient received an adjuvant EGFR-TKI, and 73.2% of the cases completed at least 4 courses of platinum-based chemotherapy.

Regarding radiotherapy, 60 patients underwent PORT, among which 84.5% received volumetric modulated arc therapy (VMAT). The patients were immobilized with a thermoplastic cast or wing board with free breathing since the respiratory motion was less significant in the PORT treatment field, namely, the mediastinal lymph node basins. Most patients (71.7%) received 50–54 Gy in 25–30 fractions, and boostirradiation to 58–60 Gy was given for some patients with ENE. The dose constraints and the mean value of planned dosimetry parameters were V20 < 30% (mean: 19.7%) and V30 < 20% (mean: 13.8%) for the bilateral lung, respectively, with a mean heart dose <20 Gy (mean: 11.2 Gy). The distribution of PORT according to baseline characteristics is presented in Table 1. A statistically non-significant trend of imbalance was observed with a greater portion of patients completing 4 cycles of platinum-based chemotherapy or presenting with lymphovascular invasion (LVSI) receiving PORT.

Table 1. Baseline Characteristics and Distribution of Post-operative Radiotherapy.

Subgroup		*n*	Port	No Port	*p* *1
Overall		82	73.2%	26.8%	
Age	≤60 y/o	41	75.6%	24.4%	0.618
	>60 y/o	41	70.7%	29.3%	
Sex	Male	34	70.6%	29.4%	0.657
	Female	48	75.0%	25.0%	
Laterality	Right lung	45	71.1%	28.9%	0.642
	Left lung	37	75.7%	24.3%	
Pre-OP tumor marker *2	Elevated	30	66.7%	33.3%	0.459
	w.n.l.	44	75%	25%	
	n.a.	8	87.5%	12.5%	
pT classification *3	pT1–2	68	75%	25%	0.410
	pT3–4	14	64.3%	35.7%	
Histology	Adeno.	73	71.2%	28.8%	0.327
	SCC	4	75%	25%	
	Others	5	100%	0%	
Grade	Grade 2	50	70%	30%	0.418
	Grade 3	32	78.1%	21.9%	
DLNs	≤20	57	75.4%	24.6%	0.484
	>20	25	68%	32%	
PLNs	1–3	45	66.7%	33.3%	0.143
	≥4	37	81.1%	18.9%	
PD ratio *4	≤0.22	48	68.8%	31.2%	0.283
	>0.22	34	79.4%	20.6%	
ENE	Present	25	68.0%	32.0%	0.736
	Absent	54	75.9%	24.1%	
	n.a.	3	66.7%	33.3%	
LVSI	Present	39	82.1%	17.9%	0.084
	Absent	43	65.1%	34.9%	
PNI	Present	5	80%	20%	0.722
	Absent	77	72.7%	27.3%	
EGFR mut.	Present	47	68.1%	31.9%	0.525
	Absent	20	80%	20%	
	n.a.	15	73.3%	26.7%	
Completion of CT *5	Yes	60	78.3%	21.7%	0.081
	No	22	59.1%	40.9%	

*1 The *p*-value of the 2-tailed Pearson's chi-square test. *2 Elevated tumor marker was defined as serum CEA ≥ 5 ng/mL or SCC ≥ 1.5 ng/mL before surgery. *3 All pT classifications were adjusted and recorded according to AJCC 8th edition. *4 PD ratio was the value of the positive lymph node number divided by the dissected lymph node number. *5 Patients receiving at least 4 cycles of platinum-based chemotherapy were recorded as completed CT. Abbreviations: PORT, post-operative radiotherapy; y/o, year-old; Pre-OP, pre-operative; w.n.l., within normal limitation; n.a., not available; Adeno., adenocarcinoma; SCC, squamous cell carcinoma; DLNs, dissected lymph nodes; PLNs, positive lymph nodes; PD ratio, positive to dissected lymph node ratio; ENE, extranodal extension; LVSI, lymph-vascular space invasion; PNI, peri-neural invasion; EGFR mut., epidermal growth factor receptor mutant; CT, chemotherapy.

3.1. Treatment Outcomes and Prognostic Factors

After a median follow-up of 42 months (IQR: 29–62 months), 11 locoregional recurrences, 53 distant metastases, and 34 mortality were recorded. The overall 3-year DFS was 40.6% (95% CI: 29.6–51.6%; median: 22 months). The 3-year LRR and DM risks were 13.7% (95% CI: 5.7–21.7%) and 57.9% (95% CI: 46.7–69.1%), respectively. The 3-year DSS was 80.7% (95% CI: 71.1–90.3%), and the 3-year OS was 77.3% (95% CI: 67.3–87.3%).

In terms of prognostic factors, elevated pre-operative tumor markers and not receiving PORT were associated with a worse DFS in multivariate analysis (Table 2). On the other hand, PORT might reduce LRR (HR: 0.092, $p < 0.001$, 95% CI: 0.024–0.351), and a PD ratio >0.22 increased the risk of DM (HR: 1.846, $p = 0.027$, 95% CI: 1.072–3.179; Table 2). No significant prognostic factor for DSS or OS was found in our cohort.

Table 2. Prognostic Value of Clinicopathological Factors.

		Distant Metastasis Univariate		Disease-Free Survival Univariate		Multivariate *5	
Factors		**HR**	***p***	**HR**	***p*** *5	**HR**	***p***
Pre-OP tumor marker *1	Elevated	1.532	0.150	1.698	0.063	1.823	0.039
pT classification *2	pT3–4	0.526	0.140	0.643	0.250		
DLNs	>20	0.901	0.735	0.865	0.624		
PLNs	≥4	1.574	0.102	1.359	0.251		
PD ratio *3	≤0.22	1.846	0.027	1.630	0.068	1.646	0.080
ENE	+	1.418	0.224	1.299	0.347		
LVSI	+	1.361	0.272	1.269	0.386		
PNI	+	1.484	0.452	1.803	0.261		
EGFR mut.	+	1.058	0.862	1.157	0.650		
Completion of CT *4	+	0.695	0.227	0.736	0.292		
PORT	+	0.697	0.221	0.541	0.030	0.552	0.045

*1 Elevated tumor marker was defined as serum CEA ≥ 5 ng/mL or SCC ≥ 1.5 ng/mL before surgery. *2 All pT classifications were adjusted and recorded according to AJCC 8th edition. *3 PD ratio was the value of the positive lymph node number divided by the dissected lymph node number. *4 Patients receiving at least 4 cycles of platinum-based chemotherapy were recorded as completed CT. *5 Factors with *p*-value < 0.1 in the univariate analysis were kept for multivariate analysis. Abbreviations: Pre-OP, pre-operative; DLNs, dissected lymph nodes; PLNs, positive lymph nodes; PD ratio, positive to dissected lymph node ratio; ENE, extranodal extension; LVSI, lymph-vascular space invasion; PNI, peri-neural invasion; EGFR mut., epidermal growth factor receptor mutant; CT, chemotherapy; PORT, post-operative radiotherapy; HR, hazard ratio.

3.2. Disease-Free Survival Benefit of PORT and Predicting Factors

When stratified by PORT, the 3-year DFS was 44.9% vs. 29.8% (95% CI: 32.0–57.8% vs. 9.8–49.8%; median: 27.0 vs. 17.0 months), and the 3-year OS was 76.3% vs. 80.1% (95% CI: 64.5–88.1% vs. 52.5–97.7%; median: 79.0 vs. 54.0 months) for those with vs. without PORT, respectively. Since the DFS benefit of PORT was observed in our cohort but not in many previous studies, we conducted a subgroup analysis to evaluate possible predictive factors. The effect of PORT on DFS is presented in Figure 2 using HRs adjusted for prognostic factors, including pre-operative tumor markers and the PD ratio. The benefit of PORT was more evident for pT1–2 tumors, 1–3 PLNs, a PD ratio ≤0.22, absence of ENE, presenting with LVSI, and EGFR mutation compared to their counterparts. Although the difference between pT classification was likely caused by the contrasting case numbers, other factors were considered possible predictive factors for PORT in R0 pN2-stage III NSCLC patients.

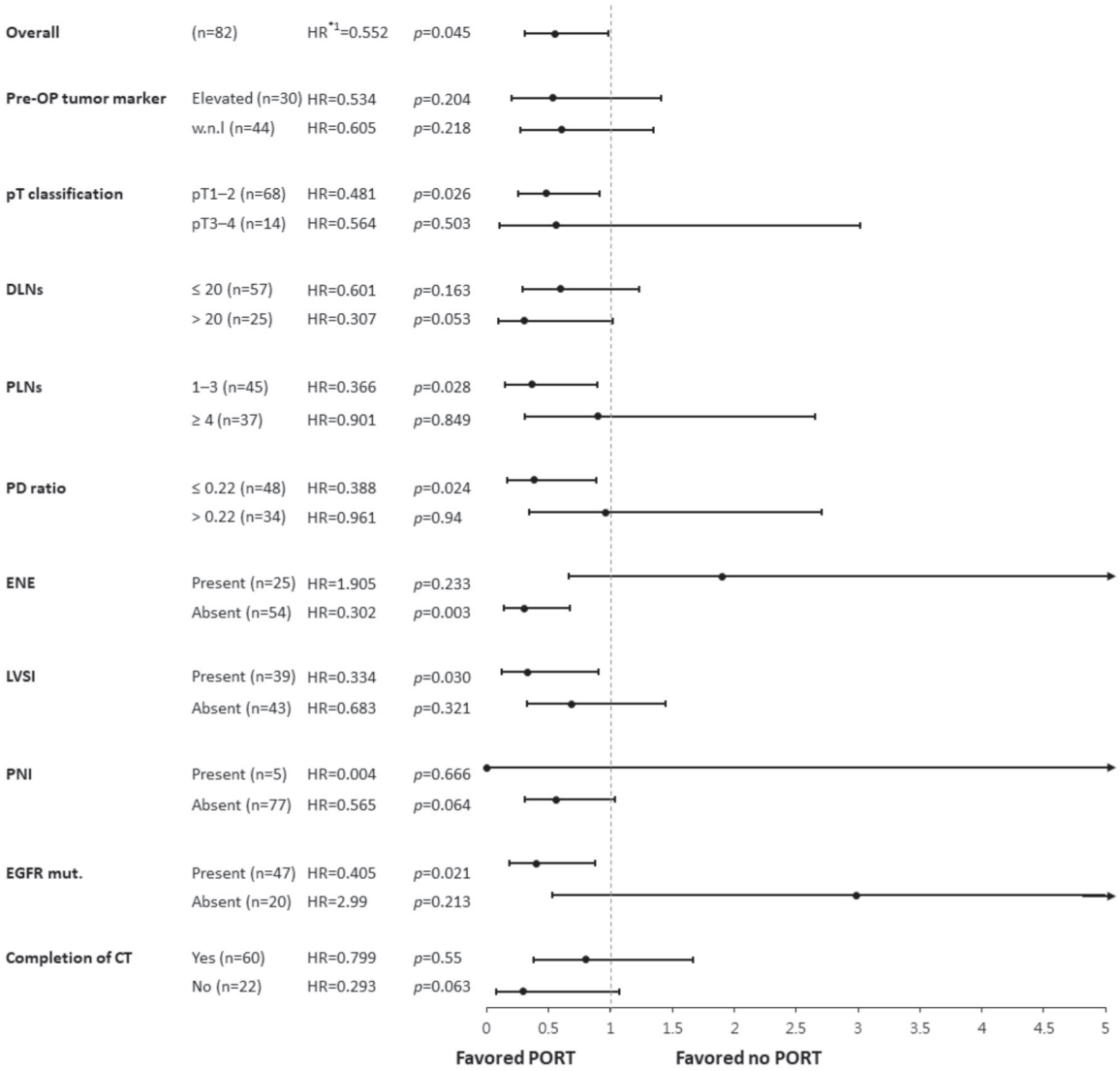

Figure 2. Forest plot of the post-operative radiotherapy effect on disease-free survival among subgroups. *1 The hazard ratios (HRs) displayed above, stratified by clinicopathological factors, were adjusted for pre-OP tumor markers and PD ratio using a Cox regression model. The forest plot was then constructed using the software Comprehensive Meta-Analysis (CMA). Abbreviations: Pre-OP, pre-operative; DLNs, dissected lymph nodes; PLNs, positive lymph nodes; PD ratio, positive to dissected lymph node ratio; ENE, extranodal extension; LVSI, lymph-vascular space invasion; PNI, peri-neural invasion; EGFR mut., epidermal growth factor receptor mutant; CT, chemotherapy; PORT, post-operative radiotherapy; HR, hazard ratio.

3.3. Possible Survival Benefits from PORT in Subgroups

Although no DSS or OS improvement was noted with PORT in the overall cohort, significant superior survival was observed in several subgroups. A better DSS was found in the subgroup of patients with 1–3 PLNs receiving PORT. Improved OS was noticed in the 1–3 PLNs and PD ratio $\leq$0.22 subgroups with PORT, while a similar trend was observed in patients without ENE (Figure 3). These results were compatible with the DFS analysis, indicating that the DFS benefit of PORT might translate into better DSS and OS in specific subgroups. Unexpectedly, the DSS and OS benefit of PORT was also found in those not completing 4 cycles of platinum-based chemotherapy (Figure 3).

A. Disease-specific Survival*1

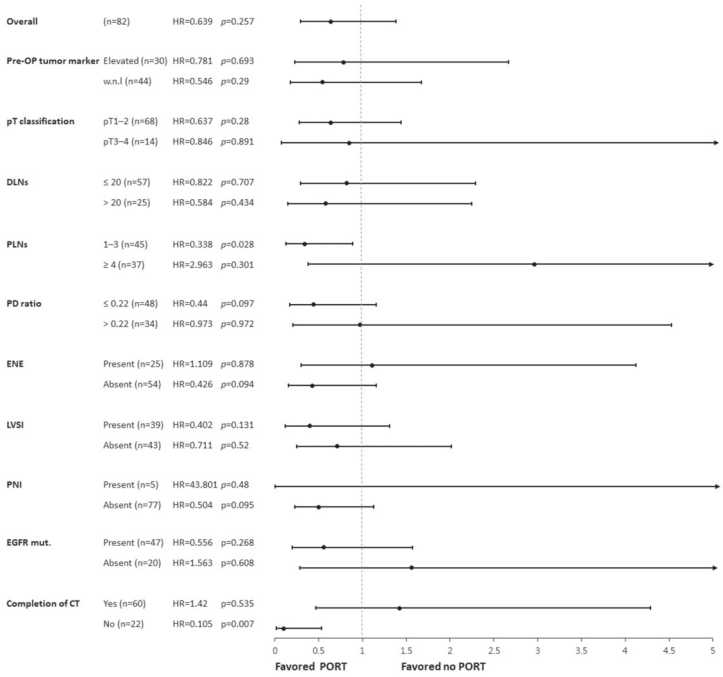

B. Overall Survival*1

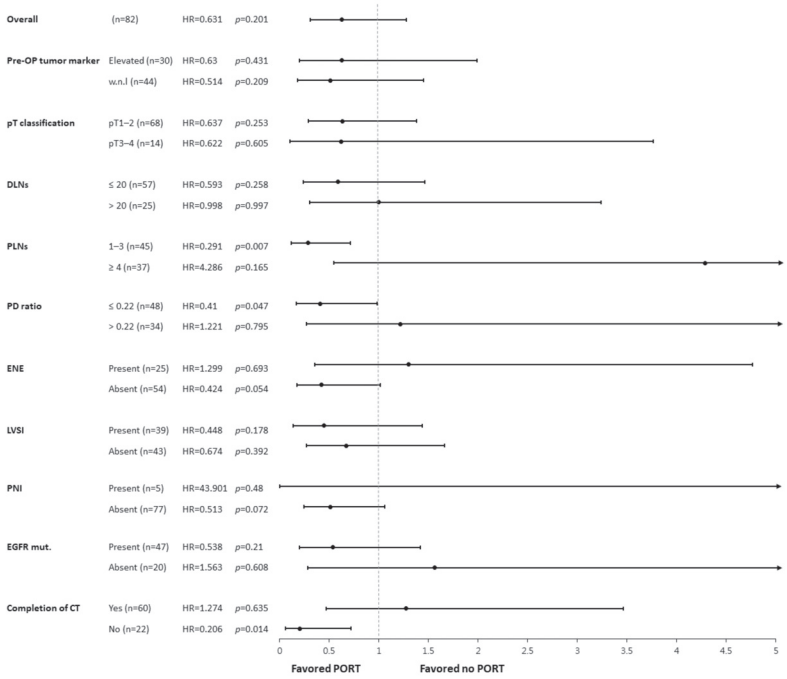

Figure 3. Forest plot of the post-operative radiotherapy effect on DSS and OS among subgroups. *1 The hazard ratios (HRs) displayed above were not corrected in the Cox regression model, except for stratification according to the listed clinicopathological factors. The forest plot was then constructed using the software Comprehensive Meta-Analysis (CMA). Abbreviations: DSS, disease-specific survival; OS, overall survival; Pre-OP, pre-operative; DLNs, dissected lymph nodes; PLNs, positive lymph nodes; PD ratio, positive to dissected lymph node ratio; ENE, extranodal extension; LVSI, lymph-vascular space invasion; PNI, peri-neural invasion; EGFR mut., epidermal growth factor receptor mutant; CT, chemotherapy; PORT, post-operative radiotherapy; HR, hazard ratio.

4. Discussion

In this retrospective cohort study carried out in an area with a high incidence of EGFR mutation-positive NSCLC and using a modern radiotherapy technique, PORT was associated with an improved DFS rate in patients with R0 pN2-stage III NSCLC. The DFS benefit was more profound in subgroups with fewer PLNs, a lower PD ratio, the absence of ENE, and the presence of LVSI and EGFR mutation. The potential translation of the DFS improvement into superior DSS and OS was also observed in those with low lymph node burden.

Using the study cohort developed from a single medical center database, we have achieved treatment outcomes compatible with those of recent clinical trials. In our analysis, the 3-year DFS was 44.9% with PORT and 29.8% without. Similarly, the PORT-C trial reported a 3-year DFS rate of 41% vs. 33% and 43% vs. 31% for the intention-to-treat and per-protocol analysis, respectively [8]. A slightly higher distant metastasis risk was observed, probably given that 26.8% of patients included in the study did not complete CT and the limited use of adjuvant EGFR-TKIs or ICIs in our cohort. Despite the relatively low DFS compared to that of the Lung-ART trial, the PORT-C trial and our cohort both yielded favorable 3-year OS rates of 80% and 77.3%, respectively [7,8]. The discrepancy was hypothesized to be linked to the higher incidence of EGFR-addicted tumors in the PORT-C trial in China as these tumors are associated with patients of a younger age, non-smokers, and those with a good response to EGFR-TKIs [10].

The EGFR mutation has been a well-known prognostic factor for superior progression-free and overall survival in NSCLC, even without EGFR-TKIs [12,13]. It is more commonly detected in adenocarcinomas of the lung in Asian, female, and non-smoking populations [14,15]. The presence of an EGFR mutation was considered a positive predictive factor for PORT in our study. The driver gene mutations were also associated with the PORT effect in a cohort study conducted in China, focusing on pN2 NSCLC with uncertain resection margins. An overall survival improvement from PORT was only observed in those with a positive driver gene mutation [16]. This might reflect the optimistic result for PORT in the PORT-C trial when compared to the Lung-ART trial. Research on the cross-reactivity between an EGFR mutation and PORT is limited, and the mechanism is not known. Hypotheses, such as less systemic hypoxia-induced radioresistance in non-smokers with EGFR mutations or an interaction within the PI3K/AKT/mTOR signaling pathway, which is shared by EGFR downstream activation and radiotherapy cytotoxicity, might warrant further research [17].

Several other potential predictive factors for PORT were identified in our cohort. The DFS benefit was more pronounced for factors primarily associated with a favorable prognosis, and an indistinct trend for lower distant metastasis (DM) risk was observed (Table 2). Traditionally, radiotherapy is recognized as a local treatment modality that eradicates cancer cells within the irradiated field. As distant metastasis is the main failure pattern, very high-risk pN2-stage III NSCLC patients deemed to have malignant cells beyond the mediastinum would experience limited benefits from PORT. A positive extranodal extension of the involved lymph node is one of the suggested indications for PORT in the NCCN guideline. However, the presence of a PORT benefit was only observed in the ENE-negative subgroup, not the ENE-positive subgroup, in our cohort. The same phenomenon that PORT paradoxically led to improved OS in resected pN2 NSCLC patients with a negative ENE status but not with a positive ENE status was also reported by Moretti et al. They speculated that a positive ENE status may indicate a higher risk for clinically occult distant metastasis at the time of surgery [18]. This might be supported by the association of ENE with poor distant recurrence-free survival (HR: 3.42, $p < 0.001$), and the link was even stronger than the prediction of locoregional recurrence-free survival (HR: 2.21, $p = 0.004$) [19]. On the other hand, the presence of LVSI has a more significant impact on nodal recurrence risk (5-year cumulative incidence of nodal recurrence: 22.5% vs. 8.7%, $p < 0.001$, RR: 2.6) than on distant metastasis (30.4% vs. 14.9%, $p = 0.004$, RR: 2.0) [20] and would, thus, be linked to the DFS benefit of PORT.

While the prognostic value of PLNs and the PD ratio has been well-recognized and verified in pN2 NSCLC patients receiving PORT [21], controversy exists regarding the use of lymph node burden as a predictive factor for PORT. In serial analyses based on the Surveillance, Epidemiology, and End Results (SEER) database, Wu et al. included all resected stage III NSCLC patients and reported a significant OS improvement with PORT in the stage IIIA/pN2 and PD ratio > 1/3 subgroups [22]. Urban et al. and Wang et al., focusing on resected pN1–2 and pN2-stage IIIA NSCLC, suggested a more profound PORT survival benefit with a PD ratio >50% or PLNs > 3, respectively [23,24]. In another study evaluating a similar cohort to ours and using a more sophisticated definition of PORT, Lee et al. proposed that a PD ratio of 0.6–0.8 was the optimal indicator of PORT benefit for pN2 NSCLC patients [25]. Nonetheless, the lack of information regarding surgical margin status and radiotherapy details in the SEER database should be considered when interpreting these results. It would be useful if the analysis of PLNs and the PD ratio from recent two large randomized control trials was available. Other clinicopathological factors, including the lymph node counts of only N2 nodes, the number of stations involved, or stratification with DLNs, might warrant further evaluation for the true influence of lymph node burden [26–28].

The DSS and OS advantages of PORT were observed for subgroups with DFS improvements. This might ensure the safety of modern radiotherapy with manageable toxicity and an overall gain from PORT. For subgroups with a PD ratio $\leq$0.22, a superior OS was found without DSS benefit. The difference might be attributed to the fact that 6 out of the 34 mortality events were coded as non-cancer deaths with no pre-specified cause of death provided in the National Death Registration.

The findings of this study should be considered in light of some limitations. The retrospective cohort study design might cause selection bias, such as the non-significant trend of a baseline imbalance regarding LVSI and chemotherapy completion observed in our cohort. Considering LVSI as a poor prognostic factor, patients with positive LVSI were more likely to receive PORT. Nevertheless, a superior disease-free survival was still observed in the intensively treated PORT subgroup, and the PORT benefit was also evident in the LVSI-positive subgroup. On the other hand, patients not completing chemotherapy and those without PORT were more likely to have an Eastern Cooperative Oncology Group (ECOG) performance score of 1, rather than 0. This might cause an overestimation of the PORT benefit. Further prospective studies are essential to eliminate the impact of these confounding factors. The study cohort was developed from an EGFR mutant-NSCLC pandemic area with restricted use of adjuvant EGFR-TKIs and ICIs. These findings should be carefully evaluated in other geographic areas and in the context of the use of modern systemic therapy.

5. Conclusions

Among R0 pN2-stage III NSCLC patients, PORT prolongs DFS and OS in selected subgroups. Patients with an EGFR mutation, the presence of LVSI, a negative ENE of an involved node, and less lymph node burden derive greater benefits from PORT. Patients who meet the criteria mentioned above should be offered the option of PORT through a shared decision-making model, given its clear benefit in locoregional control and the potential for improved survival when modern radiotherapy techniques are applied. Further research and the development of nomograms guiding the application of PORT are highly warranted, aiming to enhance the personalization of lung cancer treatment.

Author Contributions: J.-C.C. and I.-J.F. conceptualized the study; J.-C.C., Y.-C.H., I.-J.F. and Y.-L.S. developed the methods and study cohort; Y.-J.T. and Y.-T.C. collected the cohort data; J.-C.C., Y.-J.T. and Y.-T.C. prepared the original draft. All authors critically revised the manuscript. All authors have read and agreed to the published version of the manuscript.

Funding: This research received no external funding.

Institutional Review Board Statement: The study protocol was approved by the institutional review board of Kaohsiung Veterans General Hospital (IRB No. KSVGH22-CT9-13).

Informed Consent Statement: Not applicable.

Data Availability Statement: Data are not publicly available.

Acknowledgments: Thanks to Wu Fu-Zong, a research-oriented attending physician from the Research Department of Kaohsiung Veterans General Hospital, for his assistance during the research process.

Conflicts of Interest: The authors declare no conflict of interest.

Abbreviations

NSCLC	non-small cell lung cancer
PORT	post-operative radiotherapy
EGFR mut.	epidermal growth factor receptor mutation
ENE	extranodal extension
PLNs	number of positive lymph nodes
DLNs	number of dissected lymph nodes
PD ratio	Positive-to-dissected lymph node ratio

References

1. Oliver, A.L. Lung Cancer: Epidemiology and Screening. *Surg. Clin. N. Am.* **2022**, *102*, 335–344. [CrossRef] [PubMed]
2. Pignon, J.P.; Tribodet, H.; Scagliotti, G.V.; Douillard, J.Y.; Shepherd, F.A.; Stephens, R.J.; Dunant, A.; Torri, V.; Rosell, R.; Seymour, L.; et al. Lung adjuvant cisplatin evaluation: A pooled analysis by the LACE Collaborative Group. *J. Clin. Oncol.* **2008**, *26*, 3552–3559. [CrossRef] [PubMed]
3. Wu, Y.L.; Tsuboi, M.; He, J.; John, T.; Grohe, C.; Majem, M.; Goldman, J.W.; Laktionov, K.; Kim, S.W.; Kato, T.; et al. Osimertinib in Resected EGFR-Mutated Non-Small-Cell Lung Cancer. *N. Engl. J. Med.* **2020**, *383*, 1711–1723. [CrossRef]
4. Felip, E.; Altorki, N.; Zhou, C.; Csőszi, T.; Vynnychenko, I.; Goloborodko, O.; Luft, A.; Akopov, A.; Martinez-Marti, A.; Kenmotsu, H.; et al. Adjuvant atezolizumab after adjuvant chemotherapy in resected stage IB–IIIA non-small-cell lung cancer (IMpower010): A randomised, multicentre, open-label, phase 3 trial. *Lancet* **2021**, *398*, 1344–1357. [CrossRef]
5. Burdett, S.; Rydzewska, L.; Tierney, J.; Fisher, D.; Parmar, M.K.; Arriagada, R.; Pignon, J.P.; Le Pechoux, C.; Group, P.M.-a.T. Postoperative radiotherapy for non-small cell lung cancer. *Cochrane Database Syst. Rev.* **2016**, *10*, CD002142. [CrossRef] [PubMed]
6. Billiet, C.; Peeters, S.; Decaluwe, H.; Vansteenkiste, J.; Mebis, J.; Ruysscher, D. Postoperative radiotherapy for lung cancer: Is it worth the controversy? *Cancer Treat. Rev.* **2016**, *51*, 10–18. [CrossRef]
7. Le Pechoux, C.; Pourel, N.; Barlesi, F.; Lerouge, D.; Antoni, D.; Lamezec, B.; Nestle, U.; Boisselier, P.; Dansin, E.; Paumier, A.; et al. Postoperative radiotherapy versus no postoperative radiotherapy in patients with completely resected non-small-cell lung cancer and proven mediastinal N2 involvement (Lung ART): An open-label, randomised, phase 3 trial. *Lancet Oncol.* **2022**, *23*, 104–114. [CrossRef]
8. Hui, Z.; Men, Y.; Hu, C.; Kang, J.; Sun, X.; Bi, N.; Zhou, Z.; Liang, J.; Lv, J.; Feng, Q.; et al. Effect of Postoperative Radiotherapy for Patients With pIIIA-N2 Non-Small Cell Lung Cancer After Complete Resection and Adjuvant Chemotherapy: The Phase 3 PORT-C Randomized Clinical Trial. *JAMA Oncol.* **2021**, *7*, 1178–1185. [CrossRef]
9. Zhou, W.; Christiani, D.C. East meets West: Ethnic differences in epidemiology and clinical behaviors of lung cancer between East Asians and Caucasians. *Chin. J. Cancer* **2011**, *30*, 287–292. [CrossRef]
10. Levy, A.; Mercier, O.; Le Pechoux, C. Indications and Parameters Around Postoperative Radiation Therapy for Lung Cancer. *J. Clin. Oncol.* **2022**, *40*, 556–566. [CrossRef]
11. Rami-Porta, R.; Wittekind, C.; Goldstraw, P. Complete Resection in Lung Cancer Surgery: From Definition to Validation and Beyond. *J. Thorac. Oncol.* **2020**, *15*, 1815–1818. [CrossRef] [PubMed]
12. Eberhard, D.A.; Johnson, B.E.; Amler, L.C.; Goddard, A.D.; Heldens, S.L.; Herbst, R.S.; Ince, W.L.; Janne, P.A.; Januario, T.; Johnson, D.H.; et al. Mutations in the epidermal growth factor receptor and in KRAS are predictive and prognostic indicators in patients with non-small-cell lung cancer treated with chemotherapy alone and in combination with erlotinib. *J. Clin. Oncol.* **2005**, *23*, 5900–5909. [CrossRef] [PubMed]
13. Bell, D.W.; Lynch, T.J.; Haserlat, S.M.; Harris, P.L.; Okimoto, R.A.; Brannigan, B.W.; Sgroi, D.C.; Muir, B.; Riemenschneider, M.J.; Iacona, R.B.; et al. Epidermal growth factor receptor mutations and gene amplification in non-small-cell lung cancer: Molecular analysis of the IDEAL/INTACT gefitinib trials. *J. Clin. Oncol.* **2005**, *23*, 8081–8092. [CrossRef] [PubMed]
14. Melosky, B.; Kambartel, K.; Hantschel, M.; Bennetts, M.; Nickens, D.J.; Brinkmann, J.; Kayser, A.; Moran, M.; Cappuzzo, F. Worldwide Prevalence of Epidermal Growth Factor Receptor Mutations in Non-Small Cell Lung Cancer: A Meta-Analysis. *Mol. Diagn. Ther.* **2022**, *26*, 7–18. [CrossRef] [PubMed]

15. Zhang, Y.L.; Yuan, J.Q.; Wang, K.F.; Fu, X.H.; Han, X.R.; Threapleton, D.; Yang, Z.Y.; Mao, C.; Tang, J.L. The prevalence of EGFR mutation in patients with non-small cell lung cancer: A systematic review and meta-analysis. *Oncotarget* **2016**, *7*, 78985–78993. [CrossRef] [PubMed]
16. Deng, Q.; Wang, H.; Xiu, W.; Tian, X.; Gong, Y. Uncertain resection of highest mediastinal lymph node positive among pN2 non-small cell lung cancer patients: Survival analysis of postoperative radiotherapy and driver gene mutations. *Jpn. J. Radiol.* **2023**, *41*, 551–560. [CrossRef]
17. Mardanshahi, A.; Gharibkandi, N.A.; Vaseghi, S.; Abedi, S.M.; Molavipordanjani, S. The PI3K/AKT/mTOR signaling pathway inhibitors enhance radiosensitivity in cancer cell lines. *Mol. Biol. Rep.* **2021**, *48*, 1–14. [CrossRef]
18. Moretti, L.; Yu, D.S.; Chen, H.; Carbone, D.P.; Johnson, D.H.; Keedy, V.L.; Putnam, J.B., Jr.; Sandler, A.B.; Shyr, Y.; Lu, B. Prognostic factors for resected non-small cell lung cancer with pN2 status: Implications for use of postoperative radiotherapy. *Oncologist* **2009**, *14*, 1106–1115. [CrossRef]
19. Liu, W.; Shao, Y.; Guan, B.; Hao, J.; Cheng, X.; Ji, K.; Wang, K. Extracapsular extension is a powerful prognostic factor in stage IIA-IIIA non-small cell lung cancer patients with completely resection. *Int. J. Clin. Exp. Pathol.* **2015**, *8*, 11268–11277.
20. Sung, S.Y.; Kwak, Y.K.; Lee, S.W.; Jo, I.Y.; Park, J.K.; Kim, K.S.; Lee, K.Y.; Kim, Y.S. Lymphovascular Invasion Increases the Risk of Nodal and Distant Recurrence in Node-Negative Stage I-IIA Non-Small-Cell Lung Cancer. *Oncology* **2018**, *95*, 156–162. [CrossRef]
21. Deng, W.; Xu, T.; Xu, Y.; Wang, Y.; Liu, X.; Zhao, Y.; Yang, P.; Liao, Z. Survival Patterns for Patients with Resected N2 Non-Small Cell Lung Cancer and Postoperative Radiotherapy: A Prognostic Scoring Model and Heat Map Approach. *J. Thorac. Oncol.* **2018**, *13*, 1968–1974. [CrossRef] [PubMed]
22. Wu, K.; Peng, W.; Shuai, Z.; Peng, X.; Liu, H.; Zhang, S. The impact of postoperative radiotherapy on the survival of patients with stage III non-small cell lung cancer: A CONSORT-compliant analysis using the SEER database. *Medicine* **2023**, *102*, e34015. [CrossRef] [PubMed]
23. Urban, D.; Bar, J.; Solomon, B.; Ball, D. Lymph node ratio may predict the benefit of postoperative radiotherapy in non-small-cell lung cancer. *J. Thorac. Oncol.* **2013**, *8*, 940–946. [CrossRef] [PubMed]
24. Wang, S.; Ma, Z.; Yang, X.; Wang, Y.; Xu, Y.; Xia, W.; Chen, R.; Qiu, M.; Jiang, F.; Yin, R.; et al. Choice of postoperative radiation for stage IIIA pathologic N2 non-small cell lung cancer: Impact of metastatic lymph node number. *Radiat. Oncol.* **2017**, *12*, 207. [CrossRef] [PubMed]
25. Lee, S.; Noh, O.K. Optimal positive lymph node ratio showing the benefit of postoperative radiotherapy in pathologic N2 non-small cell lung cancer: An exploratory study using the Surveillance, Epidemiology, and End Results data. *Radiat. Oncol. J.* **2022**, *40*, 37–44. [CrossRef] [PubMed]
26. Yoo, C.; Yoon, S.; Lee, D.H.; Park, S.I.; Kim, D.K.; Kim, Y.H.; Kim, H.R.; Choi, S.H.; Kim, W.S.; Choi, C.M.; et al. Prognostic Significance of the Number of Metastatic pN2 Lymph Nodes in Stage IIIA-N2 Non-Small-Cell Lung Cancer After Curative Resection. *Clin. Lung Cancer* **2015**, *16*, e203–e212. [CrossRef] [PubMed]
27. Yuan, C.; Tao, X.; Zheng, D.; Pan, Y.; Ye, T.; Hu, H.; Xiang, J.; Zhang, Y.; Chen, H.; Sun, Y. The lymph node status and histologic subtypes influenced the effect of postoperative radiotherapy on patients with N2 positive IIIA non-small cell lung cancer. *J. Surg. Oncol.* **2019**, *119*, 379–387. [CrossRef] [PubMed]
28. Jin, J.; Xu, Y.; Hu, X.; Chen, M.; Fang, M.; Hang, Q.; Chen, M. Postoperative radiotherapy option based on mediastinal lymph node reclassification for patients with pN2 non-small-cell lung cancer. *Curr. Oncol.* **2020**, *27*, e283–e293. [CrossRef]

diagnostics

MDPI

Article

Comparison of the Outcomes between Systematic Lymph Node Dissection and Lobe-Specific Lymph Node Dissection for Stage I Non-small Cell Lung Cancer

Ching-Chun Huang [1,2], En-Kuei Tang [1,2,*], Chih-Wen Shu [3,4], Yi-Ping Chou [2,5], Yih-Gang Goan [1,2,6] and Yen-Chiang Tseng [1,2,7,*]

1 Division of Thoracic Surgery, Department of Surgery, Kaohsiung Veterans General Hospital, Kaohsiung 813, Taiwan
2 School of Medicine, National Yang Ming Chiao Tung University, Taipei 112, Taiwan
3 Institute of BioPharmaceutical Sciences, National Sun Yat-Sen University, Kaohsiung 804, Taiwan
4 Department of Biomedical Science and Environmental Biology, Kaohsiung Medical University, Kaohsiung 807, Taiwan
5 Division of Trauma, Department of Emergency, Kaohsiung Veterans General Hospital, Kaohsiung 813, Taiwan
6 Department of Surgery, Kaohsiung Veterans General Hospital Pingtung Branch, Pingtung 900, Taiwan
7 Institute of Clinical Medicine, National Yang Ming Chiao Tung University, Taipei 112, Taiwan
* Correspondence: ektang@vghks.gov.tw (E.-K.T.); yctseng@vghks.gov.tw (Y.-C.T.)

Abstract: Background: This study compares the surgical and long-term outcomes, including disease-free survival (DFS), overall survival (OS), and cancer-specific survival (CSS), between lobe-specific lymph node dissection (L-SND) and systematic lymph node dissection (SND) among patients with stage I non-small cell lung cancer (NSCLC).Methods: In this retrospective study, 107 patients diagnosed with clinical stage I NSCLC undergoing video-assisted thoracic surgery lobectomy (exclusion of the right middle lobe) from January 2011 to December 2018 were enrolled. The patients were assigned to the L-SND (n = 28) and SND (n = 79) groups according to the procedure performed on them. Demographics, perioperative data, and surgical and long-term oncological outcomes were collected and compared between the L-SND and SND groups. Results: The mean follow-duration was 60.6 months. The demographic data and surgical outcomes and long-term oncological outcomes were not significantly different between the two groups. The 5-year OS of the L-SND and SND groups was 82% and 84%, respectively. The 5-year DFS of the L-SND and SND groups was 70% and 65%, respectively. The 5-year CSS of the L-SND and SND groups was 80% and 86%, respectively. All the surgical and long-term outcomes were not statistically different between the two groups. Conclusion: L-SND showed comparable surgical and oncologic outcomes with SND for clinical stage I NSCLC. L-SND could be a treatment choice for stage I NSCLC.

Keywords: L-SND; NSCLC

1. Introduction

As the prevalence of non-smoking-related lung cancer has gradually increased in Asian countries, a low-dose computed tomography (LDCT) screening program has been implemented, bringing about a decrease in lung cancer mortality rates and a shift in the stage distribution toward earlier stages [1]. In Asia, LDCT has further increased the incidents of persistent subsolid nodules [2]. A high rate of persistent subsolid nodules is associated with lung adenocarcinoma [3]. Therefore, the application of thoracoscopic lung sparing surgery is more extensive. How to consider the patient's prognosis and reduce the scope of surgical resection and complications has become a major clinical factor. For the staging of lung cancer, mediastinoscopy was used to evaluate mediastinal

lymph node (LN) metastasis in the past, and it was gradually replaced recently by whole-body positron emission tomography (PET), since it allows less-invasive and non-operative examinations [4].

For patients diagnosed with early-stage non-small cell lung cancer (NSCLC),the standard treatment is lobectomy accompanied by systematic lymph node dissection (SND) [5]. In recent decades, several studies showed that lobe-specific lymph node dissection (L-SND) had no influence on overall survival (OS) or disease-free survival (DFS) and could reduce the risk for perioperative complications [6,7]. Additionally, several publications reported that systematic lymph node dissection was associated with greater blood loss, longer operative time, chylothorax, recurrent nerve palsy, and greater chest tube drainage, in contrast to lymph node sampling [6,8–10]. Otherwise, the lymph node mapping and lymphatic drainage rout of mediastinum were established [11–13]. In tumors located in the upper lobe, the lymph nodes commonly spread to the upper mediastinum, whereas those located in the lower lobe spread to the lower mediastinum. Skip metastasis was still observed, but rarely.

Since video-assisted thoracic surgery (VATS) was introduced, it has been adopted as a treatment for lung cancer. VATS has also been reported to reach similar long-term outcomes in early-stage lung cancer with fewer complications [14–17]. With the abovementioned perspectives, we hypothesized that lobectomy with L-SND by VATS could be taken into consideration for those patients with early-stage NSCLC. In our clinical experience, patients always ask if thoracoscopic surgery is available or not, and they are concerned with the length of wound or chest drainage. We hope to conduct less damage during the surgery, expecting to lessen the post-operative discomfort. Thus, the present study focused on the comparison of the surgical and long-term outcomes, including DFS, OS, and cancer-specific survival (CSS), between L-SND and SND among patients with stage I NSCLC.

2. Materials and Methods

Data of clinical stage I NSCLC patients who underwent a lobectomy from January 2011 to December 2018 were collected from the database of Kaohsiung Veteran General Hospital. The exclusion criteria were as follows: patients who received wedge excision or segmentectomy; patients who received right middle lobe lobectomy; patients with secondary lung cancer; and those who were lost to follow-up (Figure 1). The reason we excluded patients that underwent RML lobectomy is that there was no specific lymphatic spread pattern [18]. Altogether, 107 patients were enrolled in our study.

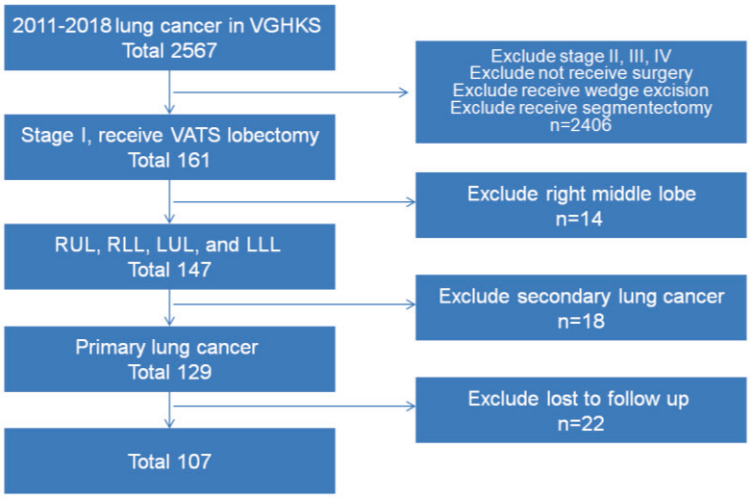

Figure 1. Patient selection. Inclusive and exclusive criteria.

All patients' data on demographics, operative course, clinical and pathologic staging, and postoperative follow-up were recorded. Preoperatively, each patient was staged with a

chest and brain CT, whole-body bone scan, abdominal sonography, and whole-body PET. The mediastinal lymph nodes were defined clinically negative if they were <10 mm onthe chest CT and were not hypermetabolic on the PET scan. Mediastinoscopy was not routinely used in our study. All patients underwent complete resection with negative tumor margins by VATS. The specimens were reviewed by a specialist from the pathology department.

The mediastinal lymph nodes were categorized into upper zone (stations 2–4 on the right, and stations 5 and 6 on the left) and lower zone (stations 7–9) lymph nodes [19]. The margin of station 2 (Figure 2) is the upper paratracheal nodes. Their upper border is the apex of the right lung and pleural space, and the lower border is the intersection of the caudal margin of the innominate vein with the trachea. The upper border of the mediastinum is in the midline.

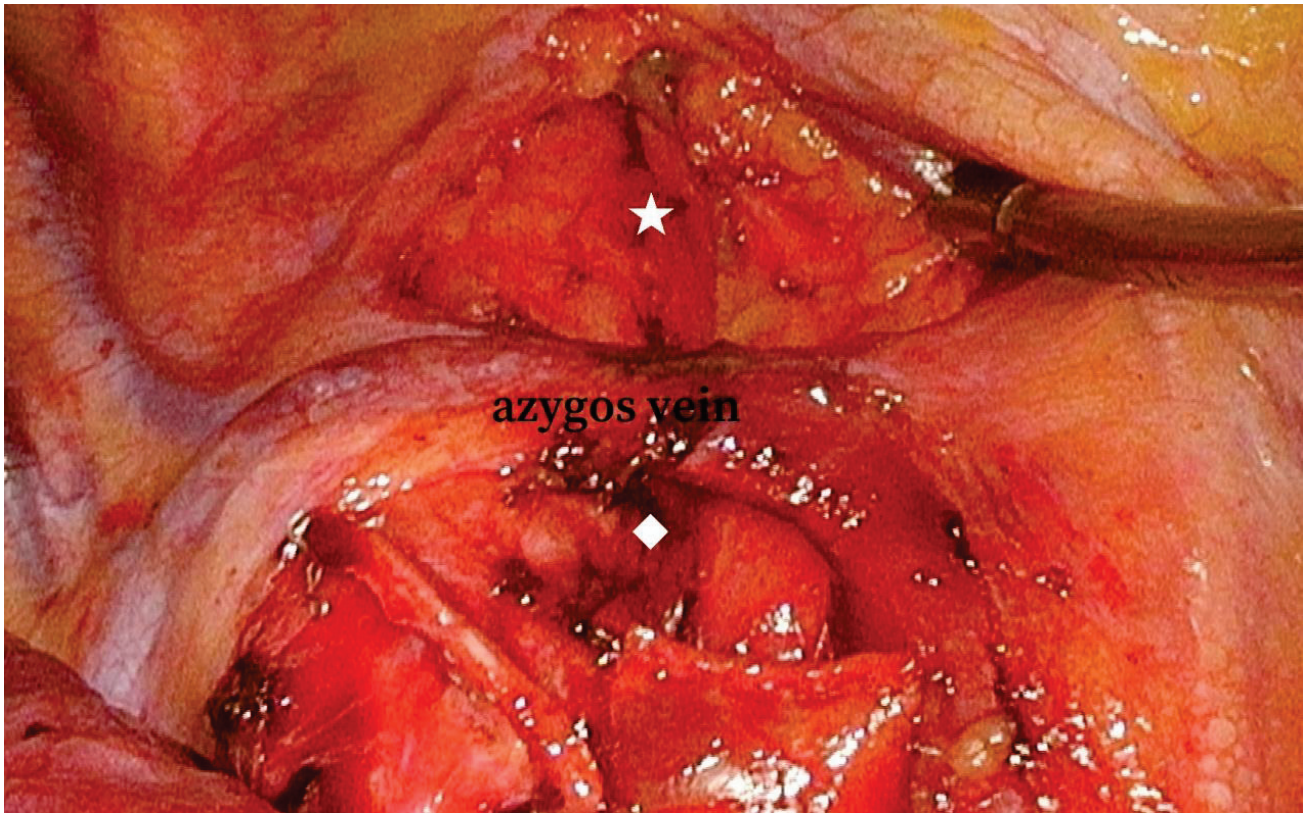

Figure 2. Lymph node stations 2 to 4. Asterisk: station 2; diamond: station 4; station 3 was between station 2 and 4 and the midline of the spine.

Station 3 is the prevascular and retrotracheal nodes, which are located from the apex of the chest to the level of the carina. The anterior border of station 3 is the posterior aspect of the sternum, and the posterior border is the anterior border of the superior vena cava. Station 4, the right lower paratracheal nodes, is within the intersection of the caudal margin of the innominate vein with the trachea and lower border of azygos vein. The margin of station 5 (Figure 3) is between the lower border of the aortic arch and the upper rim of the left main pulmonary artery, while station 6 is within a line tangential to the upper border of the aortic arch and the lower border of the aortic arch.

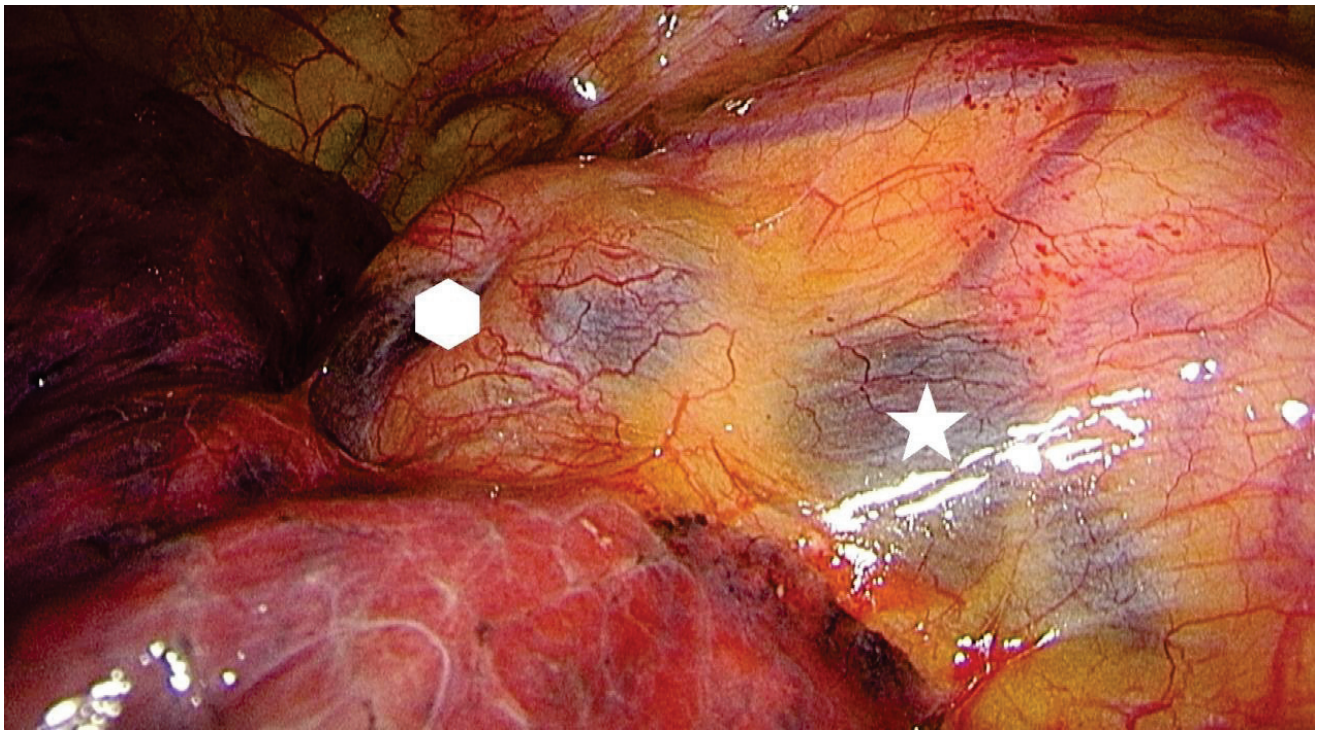

Figure 3. Lymph node station 5 and 6. Hexagon: station 5; asterisk: station 6.

Subcarinal nodes are defined as station 7 (Figure 4), which is located from the carina of the trachea to the upper border of the lower lobe bronchus.

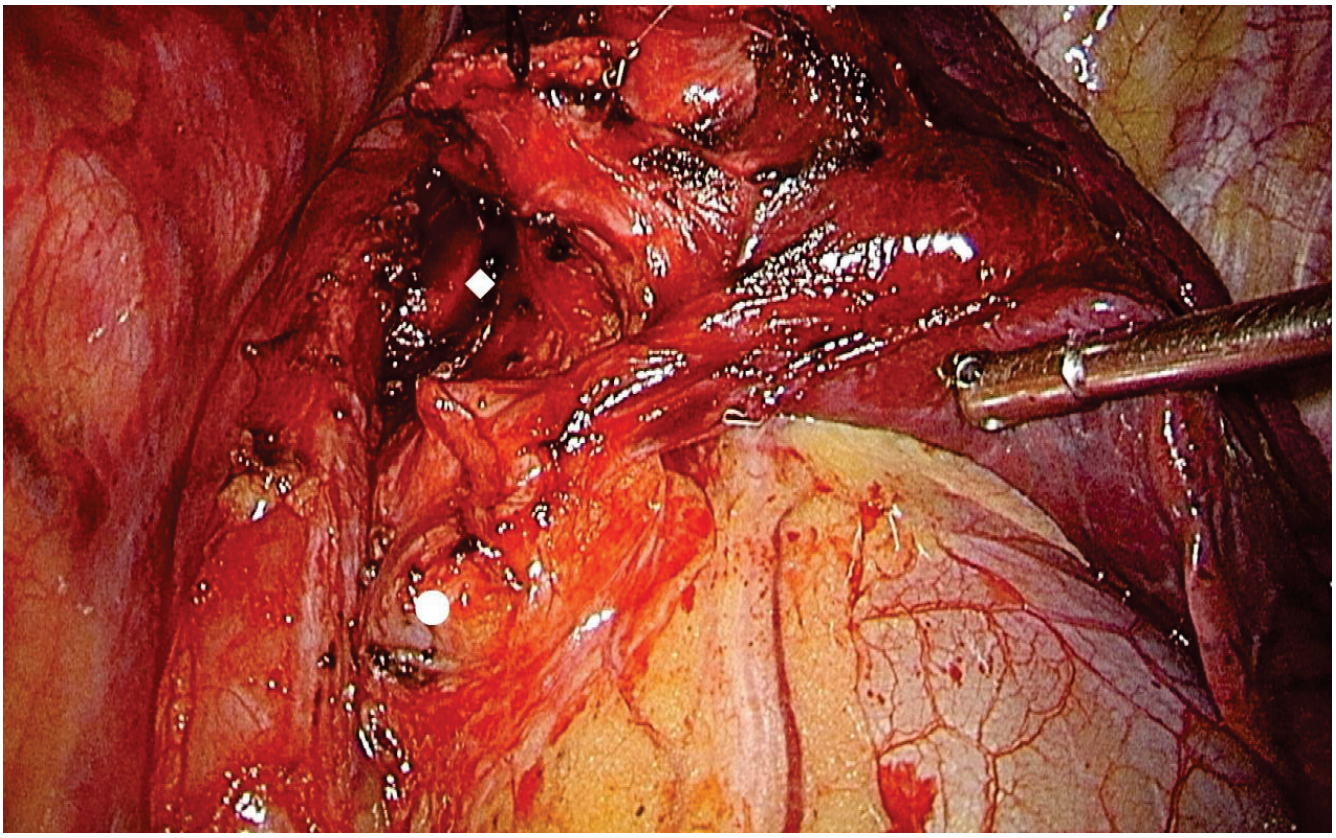

Figure 4. Lymph node station 7 and 8. Diamond: station 7; round: station 8.

Beneath station 7 is station 8, whose lower border is the diaphragm. Station 9 (Figure 5) is defined bilaterally from the inferior pulmonary vein to the diaphragm.

Figure 5. Lymph node station 9. Asterisk: station 9.

Our patients with upper-lobe tumors received upper-zone lymph node dissection (LND), and those with lower-lobe tumors received lower-zone LND. These patients were assigned to the L-SND group, also referred to as group 1. Patients receiving both upper and lower zone LNDs, on the other hand, were assigned to the SND group, also referred to as group 2.

The criteria of selecting the L-SND group was a tumor less than 30mm, no enlarged lymph nodes detected by a preoperative chest CT or those not hypermetabolic on a PET scan, and no obvious lymphadenopathy in the non-related station of the tumor during the operation. If patients did not undergo a PET scan and lymphadenopathy was observed by a chest CT, a perioperative frozen section was performed. Patients with benign frozen reports of mediastinal LNs were categorized to the L-SND group, while the others were categorized to the SND group. All patients categorized to the L-SND group received the lymph node dissection of related stations. Detailed procedures and anatomical landmarks of lymph node dissection were as follows. In the right upper mediastinal zone (stations 2 and 4), all fat tissue with LNs between the phrenic nerve, vagus nerve, right innominate artery, and right main bronchus were removed, exposing the superior vena cava, trachea, anterolateral aspect of the ascending aorta, right tracheobronchial angle, azygos vein, and right main bronchus. In the aortopulmonary zone (stations 5 and 6), all fat tissues with LNs between the phrenic and vagus nerves were removed down to the left main pulmonary artery (PA), including the subaortic space. It should be noted that we did not divide the ligamentum arteriosum, but we did identify the left recurrent laryngeal nerve along the ligament. In the subcarinal zone (station 7), all the subcarinal tissue was removed, ex-posing the right and left main bronchi and posterior pericardium. In the lower mediastinal zone, station 8 and 9 nodes were removed by clearing all LNs around the inferior pulmonary vein, esophagus,

and pulmonary ligament [20]. If patients were initially selected for the L-SND group but hardly underwent lymph node dissection, they would shift to the SND group.

Statistical Analysis

The clinical characteristics of patients with L-SND and SND were compared using the independent sample *t*-test, chi-square test, and Kaplan–Meier test. The independent sample *t*-test was used to calculate the age, pre-operative (pre-OP) tumor size, surgical time, admission duration, intensive care unit (ICU) duration, and forced expiratory volume in 1 s (FEV1)/forced vital capacity (FVC). The chi-square test was applied for analyzing data on sex, smoking history, histological findings, tumor location, adjuvant chemotherapy, clinical stage, differentiated type or not, underlying disease, and pathologic N (pN) stage. The Kaplan–Meier method was used to analyze DFS, OS, and CSS. Admission duration was defined as the duration from the day the patient underwent the surgery to the day of discharge. DFS was defined as the time interval from the patient receiving surgery to the first diagnosis of locoregional or distant disease recurrence or until the last follow-up. For the calculation of DFS, patients who died without recurrence or who were known to have no recurrence at the date of the last follow-up were censored. Patients who died of unnatural causes were excluded from the OS analysis, but they were included in the CSS analysis.

Locoregional recurrence was defined as the presence of any recurrent disease within the ipsilateral hemithorax or mediastinum. All other sites of recurrence were referred to as distant metastases. The length of OS was defined as the interval between the date of surgical intervention and death due to any cause or the last follow-up. To avoid calculating survival from a small number of observations, the data for DFS and OS curves were censored at 60 months for patients without recurrence or mortality. The IBM SPSS statistics version 20 was used for all statistical analyses. A two-tailed *p*-value of 0.05 was considered significant.

3. Results

3.1. The Study Cohort

The study cohort comprised 107 patients with clinical stage I NSCLC who received VATS lobectomy. In total, 28 and 79patients were assigned to the L-SND and SND groups, respectively. Totally, 72.9% of patients received a PET scan preoperatively. A total of 71.4% patients in group 1 and 73.4% in group 2 received a PET scan individually. There were no statistical differences in the baseline characteristics (Table 1), such as age, sex, smoking history, tumor histology, location, and size, adjuvant chemotherapy, clinical stage, differentiated type or not, pathological stage, underlying disease, and FEV1/FVC ratio between the two groups. There was a datum of FEV1/FVC lost.

Table 1. Patients' baseline characteristics.

Variables	L-SND (*n* = 28)	SND (*n* = 79)	*p*-Value
Age	61.3 ± 13.2	62.5 ± 8.4	0.643
Sex			
Male	15 (53.6%)	27 (34.2%)	0.071
Female	13 (46.4%)	52 (65.1%)	
Smoking history			
No	19 (67.9%)	58 (73.4%)	0.574
Yes	9 (32.1%)	21 (26.6%)	
Histology			
ADC	27 (96.4%)	74 (93.6%)	0.364
SCC	0	4 (5.1)	
Others	1 (3.6%)	1 (1.3%)	

Table 1. *Cont.*

Variables	L-SND (n = 28)	SND (n = 79)	p-Value
Tumor location			
Right upper	7 (25%)	30 (38.0%)	0.134
Right lower	10 (35.7%)	12 (15.2%)	
Left upper	6 (21.4%)	22 (27.8%)	
Left lower	5 (17.9%)	15 (19.0%)	
Tumor size	30.0 ± 9.4	29.8 ± 8.7	0.438
Adjuvant CTx			
No	9 (32.1%)	34 (43.0%)	0.312
yes	19 (67.9%)	45 (57.0%)	
Clinical stage			
IA	10 (35.7%)	29 (36.7%)	0.925
IB	18 (64.3%)	50 (63.3%)	
Differentiate			
Well	1 (3.6%)	6 (7.6%)	0.737
Moderately	22 (78.6%)	61 (77.2%)	
Poorly	5 (17.8%)	12 (15.2%)	
pN stage			
pN0	16 (57.1%)	55 (69.6%)	0.154
pN1	8 (28.6%)	10 (12.7%)	
pN2	4 (14.3%)	14 (17.7%)	
Type 2 DM			
No	22 (78.6%)	67 (84.8%)	0.448
Yes	6 (21.4%)	12 (15.2%)	
HTN			
No	21 (75%)	48 (60.8%)	0.176
Yes	7 (25%)	31 (39.2%)	
CAD			
No	26 (92.9%)	75 (94.9%)	0.681
Yes	2 (7.1%)	4 (5.1%)	
Old CVA			
No	27 (96.4%)	75 (94.9%)	0.748
Yes	1 (3.6%)	4 (5.1%)	
FEV1/FVC (%) [a]	81.26 ± 6.73	82.37 ± 7.09	0.886

Data are presented as number (%), or mean ± standard deviation. [a] Unknown for 1 patient. L-SND, lobe-specific lymph node dissection; SND, systematic lymph node dissection; ADC, adenocarcinoma; SCC, squamous cell carcinoma; CTx, chemotherapy; DM, diabetes mellitus; HTN, hypertension; CAD, coronary artery disease; CVA, cerebrovascular accident; FEV1, forced expiratory volume in 1 s; FVC, forced vital capacity.

3.2. Surgical Outcome

No patient had conversion to thoracostomy from VATS. Two patients developed postoperative complications. One had a hemothorax after the surgery, suspecting surgical wound hemorrhage in group 2. The symptoms were relieved after blood transfusion and drainage by using a chest tube. The other patient had postoperative chylothorax and persistent air leakage in group 1. The patient recovered after conservative management but had prolonged hospitalization of up to 37 days. All the patients did not undergo a second operation. Altogether, one patient's data on surgical time along with 11 patients' data on ICU durationwere lost. There were no statistical differences in surgical time, admission duration, and ICU duration (Table 2).

Table 2. Surgical outcomes.

Variables	L-SND (n = 28)	SND (n = 79)	p-Value
Surgical time (min) [a]	240 ± 56.7	244 ± 77.2	0.363
Admission duration (days)	8.14 ± 6.35	6.87 ± 2.61	0.312
ICU duration (days) [b]	1.04 ± 0.20	1.06 ± 0.23	0.597

[a] Unknown for1 patient. [b] Unknown for 11 patients. ICU, intensive care unit.

3.3. Survival Outcomes

The mean follow-up duration was 60.6 months. The 5-year OS rate was 80%, while the mean DFS rate was 74%. There were no statistical differences in OS (p = 0.566) (Figure 6), DFS (p = 0.497) (Figure 7), and CSS (p = 0.813) (Figure 8) between the two groups.

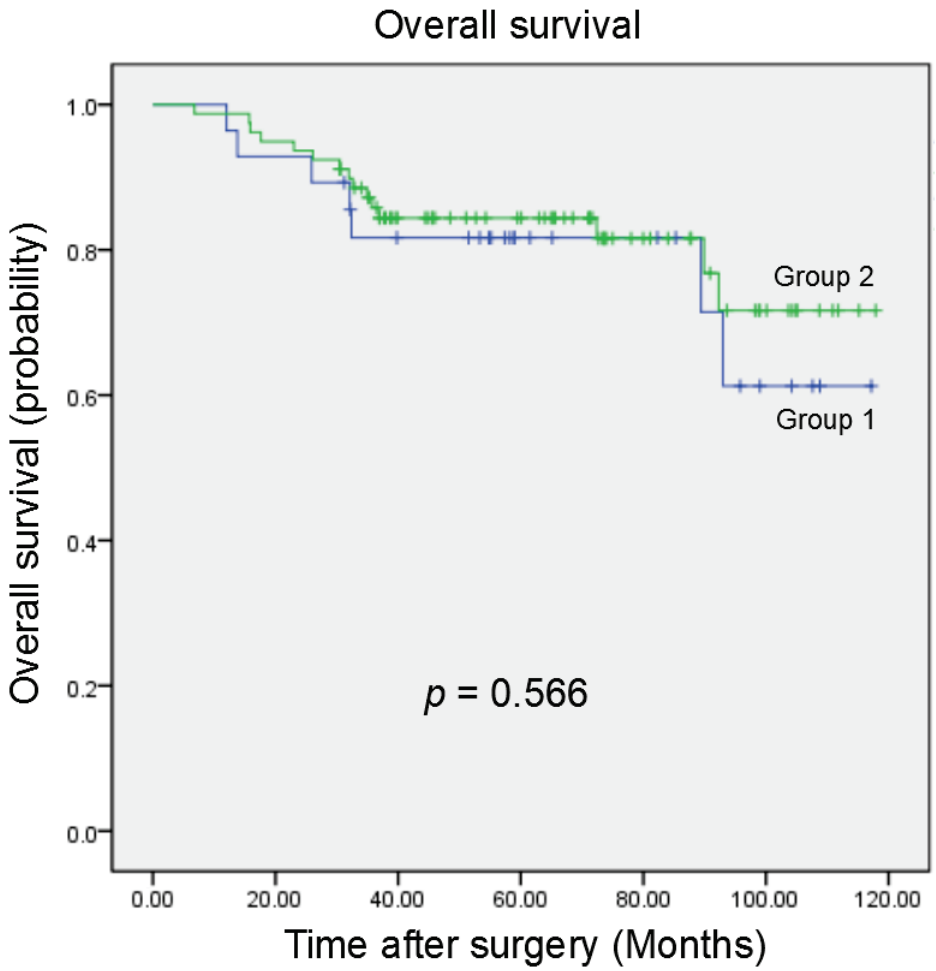

Figure 6. Survival outcomes: The Kaplan–Meier estimation showed no statistical difference in the OS (overall survival) rate between the lobe-specific lymph node dissection (L-SND) and systematic lymph node dissection (SND) groups.

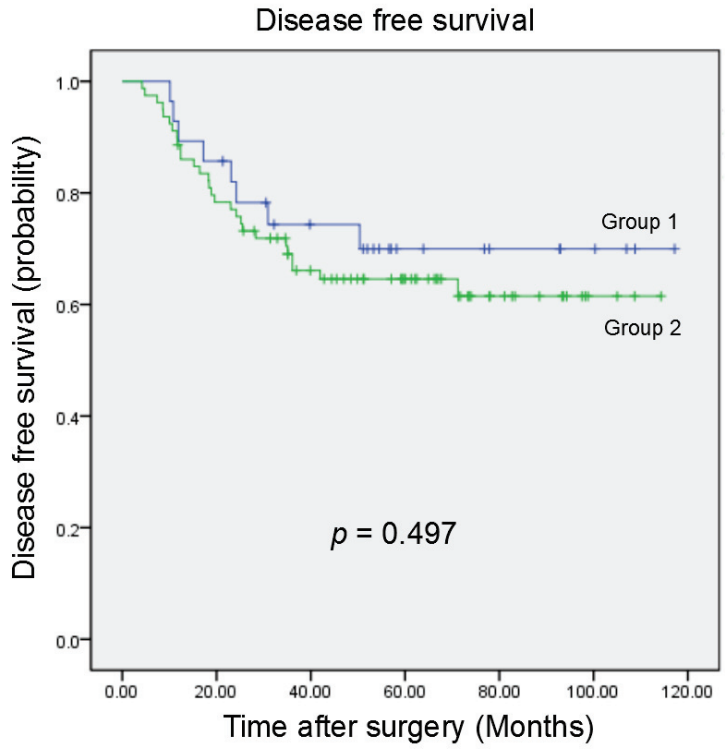

Figure 7. Survival outcomes: The Kaplan–Meier estimation showed no statistical difference in the disease-free survival (DFS) rate between the lobe-specific lymph node dissection (L-SND) and SND groups.

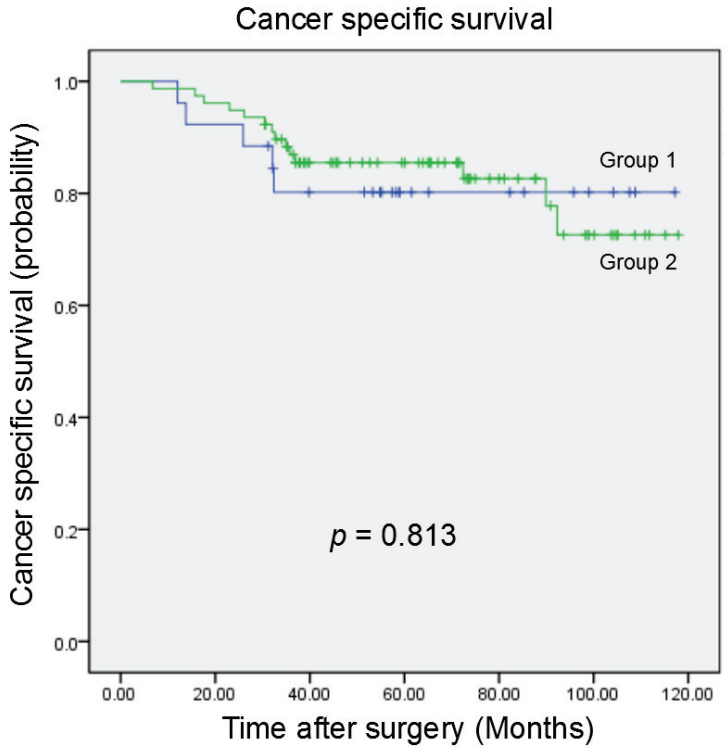

Figure 8. Survival outcomes: The Kaplan–Meier estimation showed no statistical difference in the cancer-specific survival (CSS) rate between the lobe-specific lymph node dissection (L-SND) and SND groups.

The 5- and 10-year OS rates of the L-SND group were 82% and 63%, respectively, whereas those of the SND group were 84% and 71%, respectively. The 5- and 10-year DFS rates of the L-SND group were 70% and 70%, whereas those of the SND group were 65% and 62%, respectively. The CSS rates of the L-SND group were 80% and 80%, whereas those of the SND group were 86% and 73%, respectively.

4. Discussion

Since the 1990s, it has been reported in several studies that the L-SND of NSCLC has had similar outcomes with and lesser morbidity rates than SND [14,21,22]. Okada and colleagues [14] concluded that the selective mediastinal LND of stage I NSCLC was an alternative to curative surgery, and no difference in the 5-year DFS (L-SND: 74.6%; SND: 73.4%) and OS (L-SND: 81.9%; SND: 79.7%) rates was noted. However, surgical procedures such as VATS or a thoracostomy were not mentioned and discussed. In this case, the complication rate and admission duration might be left for further research.

In a previous retrospective study, Ishiguro and colleagues [22] showed that there was no difference between complete mediastinal LND and selective dissection. They included the patients with clinical stages I to III, and the operations varied from lobectomy to lobectomy with adjacent organ resection. The complexity of the study has resulted in worse survival outcomes, as compared to our study. The previous study's 5-year OS rates were 76% and 71.9% for the L-SND and SND groups, respectively, whereas, in our study, these were 82% and 84%, respectively. Hishida and colleagues [14] performed a multi-institutional retrospective study with a propensity score analysis, in which they compared the outcomes between L-SND and SND among patients with stage I and II NSCLCs. The OS rate was not significantly different between the two groups (L-SND: 81.5%; SND: 75.9%), but there was a lack of peri-operative analysis, such as the surgical time.

Scott and colleagues [23] performed a secondary analysis of data from the American College of Surgeons Oncology Group Z0030 randomized clinical trial that compared VATS with an open lobectomy for lung cancer. Although bilobectomy, lobectomy, and segmentectomy are included in the procedures, the VATS group demonstrated a shortened operative time and hospital length of stay. The rates of at least one complication and chest tube drainage for <7 days were confirmed lower in the VATS group. Lee and colleagues[10] conducted a retrospective review of a prospective database under a propensity score-matched analysis comparing the long-term outcomes of NSCLC treated by VATS with those bythoracotomy. During the 36 months of mean follow-up, the OS and DFS rates were not different statistically. The 5-year OS rates were 74.9% and 76.6% in VATS and thoracostomy groups, respectively ($p = 0.767$). They reported a decreased 5-year DFS rate in the VATS group, but this was not statistically significant ($p = 0.552$). Overall, VATS was chosen as the surgical procedure in our study because it could lessen the complications and retain similar survival.

Lobectomy with LND was performed as the surgical procedure in our study, and lobectomy mainly occupied the surgical time. Scott and colleagues' secondary analysis [23] showed that the operative time of lobectomy via thoracostomy was longer than that of VATS (mean, 117.5 min for VATS vs. 171.5 min for thoracostomy; $p < 0.001$). To reduce the bias, we performed VATS for all patients in our studies, which accounted for no statistically significant difference between the two groups. In addition, only two patients had postoperative complications. Therefore, we took the ICU and admission durations as our surgical outcomes.

Chylothoraxis an annoying complication in pulmonary resection, occurring postoperatively. It occurs owing to injury of the thoracic duct and is highly related to aggressive mediastinal lymph node dissection [24]. The incident is about 0.7% to 2.5%. Conservative treatment through chest tube drainage and by maintaining the patient's nutritional balanceis the first choice. Severely, a second surgery is necessary if the chest drainage is greater than 1000mL per day or if there is continued drainage for more than 14 days.

Both management would postpone the admission period about 7 days or more. We initially put our efforts into analyzing the duration of the chest tube remaining, but the data collection and analysis were challenging. We thus replaced the chest tube duration with admission duration because the patients were usually discharged the next day when the chest tube was removed. In this study, we aimed to discover that the patients undergoing L-SND could shorten the admission period because the less-mediastinal lymph nodes were dissected. However, the admission duration in the L-SND group seemed to be longer in our study. We speculate that this might have resulted from the fact that only one case developed a complication. It turns out that no statistical difference was observed between the two groups.

Nodal upstaging has been observed in NSCLC, which is defined as the presence of unsuspected pathologic hilar (pN1) or mediastinal (pN2) disease detected during the final histopathologic evaluation of surgical specimens. These patients initially have clinical N0 diseases [25]. According to the Cancer and Leukemia Group B prospective clinical trial (CALGB 9761) [26], by excluding other malignant disease and benign processes, only 71.6% of patients with clinical stage I NSCLC disease retained that stage and diagnosis after complete surgical staging. A total of 14% of patients upgraded to stage II disease, while 13.5% upgraded to stage III. For evaluating the risk factors of inaccuracy in N staging, relevant research has been conducted. Al-Sarraf and colleagues [27] concluded that inaccurate nodal staging was common in patients with a history of tuberculosis, rheumatoid arthritis, and diabetes mellitus, bringing about the false detection by PET scan. The PET detection of primary NSCLC and its associated lymph nodal involvement is solely based on the metabolic uptake of 2-[18F] fluoro-2-deoxy-D-glucose (FDG) by tumors that are influenced by the inflammatory process, causing the inaccurate staging. Boffa and colleagues [28] also underlined that positron emission tomography did not improve staging accuracy. A retrospective study by Park and colleagues [29] reported that nodal upstaging measured by PET was 14.3%. In our studies, the total number of people with pN1 disease was 18 (16.8%), whereas the number with pN2 was 18 (16.8%), which are similar to the early cohort, and there was no statistical difference in the two groups. Hence, in this study, L-SND was proven to be not inferior to the standard SND.

Compared to thoracotomy, VATS has been accepted in the last decades. It is beneficial in decreasing pain, in less serious wounds, in shortening the length of postoperative stay, and in increasing the compliance to adjuvant chemotherapy [23]. Although the issues of incomplete lymph node dissection or less lymph nodes samples were mentioned [30,31], it was revised recently. Samayoa and colleagues even concluded that the number of LNs removed was correlated with an improved survival [32]. D'Amico and colleagues compared 199 patients from the NCCN NSCLC Database undergoing VATS with 189 patients undergoing thoracostomy and found similar numbers of N1 + N2 stations resected [33]. However, the complication rates as well as the oncologic outcomes were not mentioned. Kneuertz and colleagues collected patients with stage I-IIIa NSCLC who had undergone lobectomy that was robotic-assisted, VATS, or the open approach at a single center [34]. The total lymph node count and upstaging rate were similar in the three groups. Kneuertz and colleagues also analyzed the oncologic outcomes, the median follow-up period of which was 44.8 months. The stage-specific survival rates were similar in the three groups, and the 5-year OS of stage Ib was 70% in their studies. There is no denying that all surgical approaches of LN dissection are feasible in the surgery of lung cancer. Stephens and colleagues specifically established a cohort to make a comparison between thoracotomy and VATS groups in clinical stage I NSCLC [35]. The VATS group showed less perioperative morbidity, but the two groups shared similar results in regional lymphadenectomy, nodal upstaging, OS, and DFS. Denlinger and colleagues' studies discovered there was a slight trend toward more total nodes dissected in the late group as opposed to the early group [31]. Furthermore, they found no survival advantage in complete mediastinal lymph node dissection, compared to the systemic lymph node sampling in patients who underwent the surgery. Additionally, there was no survival difference between the two groups. This result,

as a matter of fact, matches the American College of Surgeons Oncology Group Z0030 trial. Licht and colleagues [36] compared VATS with thoracotomy in patients receiving lobectomy for clinical stage I NSCLC. They concluded that nodal upstaging occurred significantly higher after thoracotomy. Selective reporting bias, which should and could have been avoided in the use of complete national data, is considered the main reason; nevertheless, the multivariate survival analysis remained no statistical difference in the two groups. Lichtand colleagues [36] investigated 11,513 patients from the Society of Thoracic Surgeons database undergoing anatomical pulmonary resections in clinical stage T1N0M0 or T2N0M0 lung cancer. They concluded that upstaging from N0 to N1 was more frequently observed in the thoracotomy group; however, upstaging from N0 to N2 was similar between both approaches. This finding contradicts numerous studies that have reported that open and VATS approaches result in a similar number of lymph nodes and lymph node stations being evaluated. The VATS approach was therefore chosen as the standard operation in our study, showing that lobectomy with lymph node dissection via VATS is not inferior to traditional thoracotomy. In fact, it resulted in a shorter admission period and less perioperative complications.

Regarding the long-term outcomes, the mean follow-up duration in our study was 60.6 months, which was longer than those of previous studies; however, the 5-year OS and DFS rates in our study were similar to previous studies. We extended the survival test to up to 10 years and found no statistically significant difference. We also analyzed CSS to emphasize that the survival rate was similar between the two groups. For the issue of lymph node upstaging, our upstaging rate was similar to previous research, and there was no statistical difference of the pN stage in the two groups. In summary, the VATS lobectomy with L-SND is feasible for stage I NSCLC.

The present study has several limitations. First, we did not perform a randomized controlled trial. Second, there is a selection bias owing to the retrospective study design as well as the patient selection of the L-SND group. Third, the case number in the two groups was of great discrepancy. Fourth, we used a PET or CT scan for evaluating the clinical nodal stage, leading to the upstaging. Our upstaging rate was higher than previous research, and we thought it might be caused by the small sample size. Finally, there were no uniform criteria for selecting L-SND or SND. During surgery, lymph nodes that were found to be enlarged up to 1 cm, even if there was no uptake in the staging PET scan, still required removal. These cases were converted to SND from L-SND during the surgery. Our further plan is to keep collecting cases and consulting expertise for formulating the criteria of choosing L-SND or SND. A secondary analysis from other randomized controlled trial could also be a choice for a similar topic before the establishment of criteria. Once the selection criteria are established, the randomized control trial can be run and applied.

5. Conclusions

A VATS lobectomy with L-SND is feasible for clinical stage I NSCLC owing to the similar surgical and long-term outcomes with SND. For those patients with lymph node uptake seen on PET scans or a more advanced stage, the standard operation by lobectomy with SND is recommended.

Author Contributions: Conceptualization, E.-K.T.; Methodology, C.-W.S.; Resources, Y.-P.C. and Y.-G.G.; Writing–original draft, C.-C.H.; Writing–review & editing, Y.-C.T. All authors have read and agreed to the published version of the manuscript.

Funding: This research received no external funding.

Institutional Review Board Statement: Ethical review and approval were waived for this study due to our data were retrospectively collected from the lung cancer data base of Kaohsiung Veterans General Hospital.

Informed Consent Statement: Not applicable.

Data Availability Statement: The data presented in this study are available on request from the corresponding author.

Conflicts of Interest: The authors declare no conflict of interest.

References

1. Hung, Y.-C.; Tang, E.-K.; Wu, Y.-J.; Chang, C.-J.; Wu, F.-Z. Impact of low-dose computed tomography for lung cancer screening on lung cancer surgical volume: The urgent need in health workforce education and training. *Medicine* **2021**, *100*, e26901. [CrossRef] [PubMed]
2. Ricciardi, S.; Booton, R.; Petersen, R.H.; Infante, M.; Scarci, M.; Veronesi, G.; Cardillo, G. Managing of screening-detected sub-solid nodules—A European perspective. *Transl. Lung Cancer Res.* **2021**, *10*, 2368–2377. [CrossRef] [PubMed]
3. Henschke, C.I.; Yankelevitz, D.F.; Mirtcheva, R.; McGuinness, G.; McCauley, D.; Miettinen, O.S.; ELCAP Group. CT Screening for Lung Cancer: Frequency and significance of part-solid and nonsolid nodules. *AJR Am. J. Roentgenol.* **2002**, *178*, 1053–1057. [CrossRef] [PubMed]
4. Gao, S.J.; Kim, A.W.; Puchalski, J.T.; Bramley, K.; Detterbeck, F.C.; Boffa, D.J.; Decker, R.H. Indications for invasive mediastinal staging in patients with early non-small cell lung cancer staged with PET-CT. *Lung Cancer* **2017**, *109*, 36–41. [CrossRef]
5. Ettinger, D.S.; Wood, D.E.; Aisner, D.L.; Akerley, W.; Bauman, J.R.; Bharat, A.; Bruno, D.S.; Chang, J.Y.; Chirieac, L.R.; D'Amico, T.A.; et al. Non–Small Cell Lung Cancer, Version 3.2022, NCCN Clinical Practice Guidelines in Oncology. *J. Natl. Compr. Cancer Netw.* **2022**, *20*, 497–530. [CrossRef] [PubMed]
6. Izbicki, J.R.; Thetter, O.; Habekost, M.; Karg, O.; Passlick, B.; Kubuschok, B.; Busch, C.; Haeussinger, K.; Knoefel, W.T.; Pantel, P.; et al. Radical systematic lymphadenectomy in non-small cell lung cancer: A prospective controlled randomized clinical trial. *Br. J. Surg.* **1994**, *81*, 229–235. [CrossRef]
7. Izbicki, J.R.; Passlick, B.; Pantel, K.; Pichlmeier, U.; Hosch, S.B.; Karg, O.; Thetter, O. Effectiveness of radical systematic mediastinal lymphadenectomy in patients with resectable non-small cell lung cancer: Results of a prospective randomized trial. *Ann. Surg.* **1998**, *227*, 138–144. [CrossRef]
8. Shapiro, M.; Kadakia, S.; Lim, J.; Breglio, A.; Wisnivesky, J.P.; Kaufman, A.; Lee, D.-S.; Flores, R.M. Lobe-Specific Mediastinal Nodal Dissection Is Sufficient during Lobectomy by Video-Assisted Thoracic Surgery or Thoracotomy for Early-Stage Lung Cancer. *Chest* **2013**, *144*, 1615–1621. [CrossRef]
9. Sugi, K.; Nawata, K.; Fujita, N.; Ueda, K.; Tanaka, T.; Matsuoka, T.; Kaneda, Y.; Esato, K. Systematic Lymph Node Dissection for Clinically Diagnosed Peripheral Non-Small-Cell Lung Cancer Less Than 2 cm in Diameter. *World J. Surg.* **1998**, *22*, 290–295. [CrossRef]
10. Allen, M.S.; Darling, G.E.; Pechet, T.T.; Mitchell, J.D.; Herndon, J.E., II; Landreneau, R.J.; Inculet, R.I.; Jones, D.R.; Meyers, B.F.; Harpole, D.H.; et al. ACOSOG Z0030 Study Group Morbidity and mortality of major pulmonary resections in patients with early-stage lung cancer: Initial results of the randomized, prospective ACOSOG Z0030 trial. *Ann. Thorac. Surg.* **2006**, *81*, 1013–1019. [CrossRef]
11. Mountain, C.F.; Dresler, C.M. Regional Lymph Node Classification for Lung Cancer Staging. *Chest* **1997**, *111*, 1718–1723. [CrossRef] [PubMed]
12. Shimada, Y.; Saji, H.; Kakihana, M.; Honda, H.; Usuda, J.; Kajiwara, N.; Ohira, T.; Ikeda, N. Retrospective Analysis of Nodal Spread Patterns According to Tumor Location in Pathological N2 Non-small Cell Lung Cancer. *World J. Surg.* **2012**, *36*, 2865–2871. [CrossRef] [PubMed]
13. Riquet, M.; Rivera, C.; Pricopi, C.; Arame, A.; Mordant, P.; Foucault, C.; Dujon, A.; Le Pimpec-Barthes, F. Is the lymphatic drainage of lung cancer lobe-specific? A surgical appraisal. *Eur. J. Cardio-Thoracic Surg.* **2015**, *47*, 543–549. [CrossRef] [PubMed]
14. Hishida, T.; Miyaoka, E.; Yokoi, K.; Tsuboi, M.; Asamura, H.; Kiura, K.; Takahashi, K.; Dosaka-Akita, H.; Kobayashi, H.; Date, H.; et al. Lobe-Specific Nodal Dissection for Clinical Stage I and II NSCLC: Japanese Multi-Institutional Retrospective Study Using a Propensity Score Analysis. *J. Thorac. Oncol.* **2016**, *11*, 1529–1537. [CrossRef] [PubMed]
15. Lee, P.C.; Nasar, A.; Port, J.L.; Paul, S.; Stiles, B.; Chiu, Y.-L.; Andrews, W.G.; Altorki, N.K. Long-Term Survival After Lobectomy for Non-Small Cell Lung Cancer by Video-Assisted Thoracic Surgery versus Thoracotomy. *Ann. Thorac. Surg.* **2013**, *96*, 951–961. [CrossRef]
16. Yamamoto, K.; Ohsumi, A.; Kojima, F.; Imanishi, N.; Matsuoka, K.; Ueda, M.; Miyamoto, Y. Long-Term Survival After Video-Assisted Thoracic Surgery Lobectomy for Primary Lung Cancer. *Ann. Thorac. Surg.* **2010**, *89*, 353–359. [CrossRef]
17. Cattaneo, S.M.; Park, B.J.; Wilton, A.S.; Seshan, V.E.; Bains, M.S.; Downey, R.J.; Flores, R.M.; Rizk, N.; Rusch, V.W. Use of Video-Assisted Thoracic Surgery for Lobectomy in the Elderly Results in Fewer Complications. *Ann. Thorac. Surg.* **2008**, *85*, 231–236. [CrossRef]
18. Asamura, H.; Nakayama, H.; Kondo, H.; Tsuchiya, R.; Naruke, T. Lobe-specific extent of systematic lymph node dissection for non–small cell lung carcinomas according to a retrospective study of metastasis and prognosis. *J. Thorac. Cardiovasc. Surg.* **1999**, *117*, 1102–1111. [CrossRef]
19. Kim, J.H.; Van Beek, E.J.; Murchison, J.T.; Marin, A.; Mirsadraee, S. The International Association for the Study of Lung Cancer Lymph Node Map: A Radiologic Atlas and Review. *Tuberc. Respir. Dis.* **2015**, *78*, 180–189. [CrossRef]

20. Haruki, T.; Takagi, Y.; Kubouchi, Y.; Kidokoro, Y.; Nakanishi, A.; Nozaka, Y.; Oshima, Y.; Matsui, S.; Nakamura, H. Comparison between robot-assisted thoracoscopic surgery and video-assisted thoracoscopic surgery for mediastinal and hilar lymph node dissection in lung cancer surgery. *Interact. Cardiovasc. Thorac. Surg.* **2021**, *33*, 409–417. [CrossRef]
21. Okada, M.; Sakamoto, T.; Yuki, T.; Mimura, T.; Miyoshi, K.; Tsubota, N. Selective Mediastinal Lymphadenectomy for Clinico-Surgical Stage I Non–Small Cell Lung Cancer. *Ann. Thorac. Surg.* **2006**, *81*, 1028–1032. [CrossRef] [PubMed]
22. Ishiguro, F.; Matsuo, K.; Fukui, T.; Mori, S.; Hatooka, S.; Mitsudomi, T. Effect of selective lymph node dissection based on patterns of lobe-specific lymph node metastases on patient outcome in patients with resectable non–small cell lung cancer: A large-scale retrospective cohort study applying a propensity score. *J. Thorac. Cardiovasc. Surg.* **2010**, *139*, 1001–1006. [CrossRef] [PubMed]
23. Scott, W.J.; Allen, M.S.; Darling, G.; Meyers, B.; Decker, P.A.; Putnam, J.B.; Mckenna, R.W.; Landrenau, R.J.; Jones, D.R.; Inculet, R.I.; et al. Video-assisted thoracic surgery versus open lobectomy for lung cancer: A secondary analysis of data from the American College of Surgeons Oncology Group Z0030 randomized clinical trial. *J. Thorac. Cardiovasc. Surg.* **2010**, *139*, 976–983. [CrossRef]
24. Ziarnik, E.; Grogan, E.L. Postlobectomy Early Complications. *Thorac. Surg. Clin.* **2015**, *25*, 355–364. [CrossRef] [PubMed]
25. Toker, A.; Özyurtkan, M.O.; Kaba, E. Nodal upstaging: Effects of instrumentation and three-dimensional view in clinical stage I lung cancer. *J. Vis. Surg.* **2017**, *3*, 76. [CrossRef]
26. D'Cunha, J.; Herndon, J.E.; Herzan, D.L.; Patterson, G.A.; Kohman, L.J.; Harpole, D.H.; Kernstine, K.H.; Kern, J.; Green, M.R.; Maddaus, M.A.; et al. Poor correspondence between clinical and pathologic staging in stage 1 non-small cell lung cancer: Results from CALGB 9761, a prospective trial. *Lung Cancer* **2005**, *48*, 241–246. [CrossRef]
27. Al-Sarraf, N.; Aziz, R.; Doddakula, K.; Gately, K.; Wilson, L.; McGovern, E.; Young, V. Factors causing inaccurate staging of mediastinal nodal involvement in non-small cell lung cancer patients staged by positron emission tomography. *Interact. Cardiovasc. Thorac. Surg.* **2007**, *6*, 350–353. [CrossRef]
28. Boffa, D.J.; Kosinski, A.S.; Paul, S.; Mitchell, J.D.; Onaitis, M. Lymph Node Evaluation by Open or Video-Assisted Approaches in 11,500 Anatomic Lung Cancer Resections. *Ann. Thorac. Surg.* **2012**, *94*, 347–353. [CrossRef]
29. Park, H.K.; Jeon, K.; Koh, W.-J.; Suh, G.Y.; Kim, H.; Kwon, O.J.; Chung, M.P.; Lee, K.S.; Shim, Y.M.; Han, J.; et al. Occult nodal metastasis in patients with non-small cell lung cancer at clinical stage IA by PET/CT. *Respirology* **2010**, *15*, 1179–1184. [CrossRef]
30. Okada, M.; Sakamoto, T.; Yuki, T.; Mimura, T.; Miyoshi, K.; Tsubota, N. Hybrid surgical approach of video-assisted minithoracotomy for lung cancer: Significance of direct visualization on quality of surgery. *Chest* **2005**, *128*, 2696–2701. [CrossRef]
31. Denlinger, C.E.; Fernandez, F.; Meyers, B.F.; Pratt, W.; Zoole, J.B.; Patterson, G.A.; Krupnick, A.S.; Kreisel, D.; Crabtree, T. Lymph Node Evaluation in Video-Assisted Thoracoscopic Lobectomy versus Lobectomy by Thoracotomy. *Ann. Thorac. Surg.* **2010**, *89*, 1730–1736. [CrossRef] [PubMed]
32. Samayoa, A.; Pezzi, T.A.; Pezzi, C.M.; Gay, E.G.; Asai, M.; Kulkarni, N.; Carp, N.; Chun, S.; Putnam, J.B. Rationale for a Minimum Number of Lymph Nodes Removed with Non-Small Cell Lung Cancer Resection: Correlating the Number of Nodes Removed with Survival in 98,970 Patients. *Ann. Surg. Oncol.* **2016**, *23*, 1005–1011. [CrossRef] [PubMed]
33. D'Amico, T.A.; Niland, J.; Mamet, R.; Zornosa, C.; Dexter, E.U.; Onaitis, M.W. Efficacy of Mediastinal Lymph Node Dissection during Lobectomy for Lung Cancer by Thoracoscopy and Thoracotomy. *Ann. Thorac. Surg.* **2011**, *92*, 226–231; discussion 231–232. [CrossRef]
34. Kneuertz, P.J.; D'Souza, D.M.; Richardson, M.; Abdel-Rasoul, M.; Moffatt-Bruce, S.D.; Merritt, R.E. Long-Term Oncologic Outcomes After Robotic Lobectomy for Early-stage Non–Small-cell Lung Cancer versus Video-assisted Thoracoscopic and Open Thoracotomy Approach. *Clin. Lung Cancer* **2020**, *21*, 214–224.e2. [CrossRef]
35. Stephens, N.; Rice, D.; Correa, A.; Hoffstetter, W.; Mehran, R.; Roth, J.; Walsh, G.; Vaporciyan, A.; Swisher, S. Thoracoscopic lobectomy is associated with improved short-term and equivalent oncological outcomes compared with open lobectomy for clinical Stage I non-small-cell lung cancer: A propensity-matched analysis of 963 cases. *Eur. J. Cardio-Thorac. Surg.* **2014**, *46*, 607–613. [CrossRef] [PubMed]
36. Licht, P.B.; Jørgensen, O.D.; Ladegaard, L.; Jakobsen, E. A National Study of Nodal Upstaging After Thoracoscopic versus Open Lobectomy for Clinical Stage I Lung Cancer. *Ann. Thorac. Surg.* **2013**, *96*, 943–950. [CrossRef]

diagnostics

MDPI

Review

Managing Persistent Subsolid Nodules in Lung Cancer: Education, Decision Making, and Impact of Interval Growth Patterns

Yung-Chi Liu [1,2,3], Chia-Hao Liang [4], Yun-Ju Wu [5,6], Chi-Shen Chen [7], En-Kuei Tang [8] and Fu-Zong Wu [5,9,10,11,*]

1 Department of Radiology, Xiamen Chang Gung Hospital, Xiamen 361028, China; gigiliu1974@hotmail.com
2 Department of Imaging Technology Division, Xiamen Chang Gung Hospital, Xiamen 361028, China
3 Department of Healthcare Administration Department, Xiamen Chang Gung Hospital, Xiamen 361028, China
4 Department of Biomedical Imaging and Radiological Sciences, National Yang-Ming University, Taipei 112304, Taiwan; herrick@herricane-med.com.tw
5 Department of Radiology, Kaohsiung Veterans General Hospital, Kaohsiung 81362, Taiwan; yjwu@vghks.gov.tw
6 Department of Software Engineering and Management, National Kaohsiung Normal University, Kaohsiung 80201, Taiwan
7 Physical Examination Center, Kaohsiung Veterans General Hospital, Kaohsiung 81362, Taiwan; chirise@vghks.gov.tw
8 Department of Surgery, Kaohsiung Veterans General Hospital, Kaohsiung 813414, Taiwan; ektang@vghks.gov.tw
9 School of Medicine, College of Medicine, National Sun Yat-Sen University, Kaohsiung 80424, Taiwan
10 Faculty of Medicine, School of Medicine, National Yang Ming Chiao Tung University, Taipei 112, Taiwan
11 Institute of Education, National Sun Yat-Sen University, Kaohsiung 804241, Taiwan
* Correspondence: cmvwu1029@gmail.com; Tel.: +886-7-3422121-76256

Abstract: With the popularization of lung cancer screening, many persistent subsolid nodules (SSNs) have been identified clinically, especially in Asian non-smokers. However, many studies have found that SSNs exhibit heterogeneous growth trends during long-term follow ups. This article adopted a narrative approach to extensively review the available literature on the topic to explore the definitions, rationale, and clinical application of different interval growths of subsolid pulmonary nodule management and follow-up strategies. The development of SSN growth thresholds with different growth patterns could support clinical decision making with follow-up guidelines to reduce over- and delayed diagnoses. In conclusion, using different SSN growth thresholds could optimize the follow-up management and clinical decision making of SSNs in lung cancer screening programs. This could further reduce the lung cancer mortality rate and potential harm from overdiagnosis and over management.

Keywords: subsolid nodules; interval growth; overdiagnosis; lung cancer

1. Introduction

With the popularization and application of low-dose computed tomography (LDCT) screening for lung cancer worldwide, a high prevalence of early lung adenocarcinoma spectra manifesting as subsolid nodules (SSNs) have been identified, especially in Asian countries [1–5]. The American National Lung Screening Trial, a clinical randomized trial, has verified that compared to the chest radiograph screening group, an LDCT lung screening in high-risk smoking groups can reduce the lung cancer mortality by 20%, and improve the all-cause mortality by 6.7% [6]. A recent systematic review and meta-analysis has demonstrated that the current evidence supports a significant reduction in lung cancer-related mortality with the utilization of LDCT for lung cancer screening in high-risk populations with heavy smoking exposure [7]. However, there is limited evidence regarding the optimal screening frequency and interval period. Randomized trials are still ongoing for LDCT

lung cancer screening in non-smokers. However, several cohort studies have observed that the implementation of lung cancer screening in Asian non-smoking groups can gradually reduce lung cancer mortality with each passing year [8,9]. Unfortunately, relevant studies have also found that with an increase in the volume of LDCT lung cancer screening, the rate of overdiagnosis will also increase [3,10,11]. Most lung cancers in Asian non-smokers are lung adenocarcinoma spectrum lesions manifesting as SSNs. Therefore, an efficient evaluation of these SSNs with heterogeneous growth trends will become a major clinical issue in lung cancer screening programs for Asian non-smoking populations [12]. SSNs can be categorized as pure ground-glass nodules (pGGNs) or part-solid nodules (PSNs) according to the guidelines of the Fleischner Society for the management of SSNs [13,14]. Furthermore, in the context of a lung cancer screening setting, Lung-RADS offers appropriate guideline for managing SSNs [15]. According to previous literature reviews, as high as 90% of persistent pulmonary SSNs are early lung adenocarcinoma spectrum lesions after 3–6 months of follow up [16,17]. In the context of the subsolid nodules definition, persistent SSNs generally mean that there is no significant resolution or disappearance of the nodule observed within a three-month follow-up period [18]. Persistent SSNs presenting as lung cancer are often lung adenocarcinoma spectrum lesions, including atypical adenomatous hyperplasia, adenocarcinoma in situ, minimally invasive or invasive adenocarcinomas according to the histopathologic classification of adenocarcinoma of the lung, as reported by the International Association for the Study of Lung Cancer [19]. According to the 2021 WHO Classification of Lung Tumors, atypical adenomatous hyperplasia and adenocarcinoma in situ lesions are classified as precursor glandular lesions [20].

Previous studies have demonstrated that SSNs $\leq$ 3 cm in size have heterogeneous growth patterns, although most of these nodules have an indolent growth pattern [21–23]. A recent systematic review and meta-analysis has addressed that the pooled growth rate was 22% for SSNs and 26% for pGGNs using the definitions of SSN growth as follows: 2 mm or more increase in the longest diameter [24]. Furthermore, several studies have found that nodules, which remained stable in size for 2 or more years, have a very low incidence of growth (approximately 5%) on further surveillance [25–27]. However, the identification of SSNs that may grow faster and affect the clinical prognosis has become an important clinical problem [28]. Furthermore, the excessive use of medical and surgical interventions for slow-growing early lung adenocarcinomas and associated GGNs can lead to overdiagnosis in cancer screening programs, resulting in an unnecessary strain on healthcare resources [10]. Therefore, this review discusses the clinical impact of the different interval growth rates of SSNs and how to utilize this assessment for personalized pulmonary nodule follow-up and management recommendations. The definitions, study rationales, and clinical applications of the three different nodular growth patterns are discussed in the literature review, as shown in Figure 1.

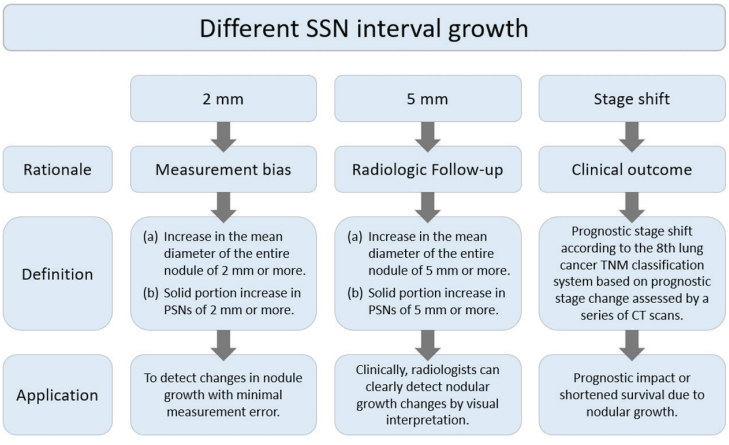

Figure 1. Rationale, definition, and clinical applications of different SSN interval growths in terms of 2 mm, 5 mm, and stage-shift interval growth. Definition: (a) Nodule's mean diameter increases by

≥2 mm or ≥5 mm based on the threshold; (b) Solid portion in PSNs grows by ≥2 mm or ≥5 mm per the threshold. CT, computed tomography; PSN, part-solid nodule; and SSN, subsolid nodules.

2. Relevant Sections

2.1. SSNs Interval Growth with an Increase of ≥2 mm

Many studies have investigated the natural growth course and relevant risk factors of SSNs based on the definition of growth of ≥2 mm in lung nodules by their longest diameter [21,22,25,26,29–36]. According to previous studies addressing the interval change in SSN measurement of <2 mm subjected to measurement bias, an increase of ≥2 mm in size was considered significant in the definition of SSN interval growth (Figure 2) [26,37]. In addition, different acquisition parameters and kernel reconstruction could introduce measurement bias in assessing nodule interval growth [38]. However, the nodule growth definition based on the 2 mm growth threshold does not allow further assessment of trends in the natural growth course of SSNs that may affect clinical outcomes or survival. The clinical management of pulmonary SSNs in lung cancer screening is often a dilemma in clinical decision making. While Lung-RADS guidelines offer clear recommendations for tracking and managing subsolid nodules, real-world scenarios may involve delays in diagnosis due to patient anxiety and concerns regarding nodule growth. Pulmonologists may also have concerns about potential medical litigation resulting from delays in diagnosis. On one end of the scale, the over management of small pGGNs (usually defined as a nodular diameter of less than 10 mm) meeting the 2 mm growth threshold may lead to increased overdiagnosis. The other end of the scale uses a follow-up strategy to monitor the subsolid pulmonary nodules. The delay in diagnosis and its impact on survival prognosis have considerable clinical implications for patients. According to a recent systematic review and meta-analysis clarifying the risk factors for SSN growth based on the definition of a nodule growing > 2 mm in diameter, male sex, history of lung cancer, a nodule size > 10 mm, nodule consistency, and age > 65 years were independent risk factors for SSN growth during the follow-up period of 24.2–112 months [39]. For pGGNs growth prediction, eight clinical or radiologic features, including male sex, smoking history, nodule size > 10 mm, larger nodule size, air bronchogram, higher mean CT attenuation, well-defined border, and lobulated margin, were independent risk factors. In the era of widespread lung cancer screening and to prevent overdiagnosis or delays in diagnosis and management, the implementation of risk-based follow-up guidelines for subsolid nodules (SSNs) or ground-glass nodules (GGNs) can assist in clinical decision-making and follow-up strategies. However, future research is needed to clarify the prediction of the growth threshold that affects the clinical prognosis or morbidity in patients with SSNs.

2.2. SSNs Interval Growth with an Increase of ≥5 mm

According to a previous literature review, some studies have defined nodule growth based on a growth threshold of ≥5 mm [21]. The main research rationale was that the growth threshold of 5 mm was the obvious or substantial SSNs interval growth during the follow-up period of CT scans through a visual assessment by radiologists or clinical physicians (Figure 3). Based on the nodule growth threshold of 5 mm, clinicians and radiologists can easily evaluate and compare the growth changes of nodules visually before and after the CT; defining an interval growth threshold of 5 mm is clinically feasible for clinical practice in the real-world setting. Tang et al. investigated the natural course of SSN in terms of substantial SSN growth based on the definition of an obvious increase of ≥5 mm in SSNs or solid portion in PSN from the baseline CT scan to detect substantial interval growth during interval CT scans [21]. Tang et al. demonstrated that the PSN group had a significantly higher growth rate than the GGN group in terms of substantial SSN growth. PSN group had an estimated 67.3% growth rate during the 5-year follow up. GGN group had an estimated 10.6% growth rate during the follow up.

The mean growth time for GGNs to reach a growth threshold of 5 mm was 9.426 years, whereas the PSN group had a mean growth time of 3.960 years to reach the threshold. Compared with a growth threshold of 2 mm, a growth threshold of 5 mm is more suitable for time-series clinical or radiologic evaluation of interval growth in SSNs. For example, one 3 mm GGN grows to 6 mm after 6 years, and such a GGN lesion meets the growth threshold of only 2 mm. A 6 mm GGN is very likely to be a pre-cancerous lesion or carcinoma in situ according to the pathological classification of the lung adenocarcinoma spectrum (Figure 4) [40]. However, if we just reach the growth threshold of 2 mm to make clinical decisions with surgical intervention, it may lead to overdiagnosis. Therefore, the use of a growth threshold of 5 mm for evaluation will increase the feasibility of clinical decision making and management of SSNs and reduce overtreatment and overdiagnosis in real-world lung cancer screening programs [41,42]. However, few studies have used this growth threshold (5 mm) to evaluate the SSNs growth rate. In the future, larger studies are needed with longer follow ups to verify the actual clinical benefit of the growth threshold of 5 mm in clinical nodule management and decision making.

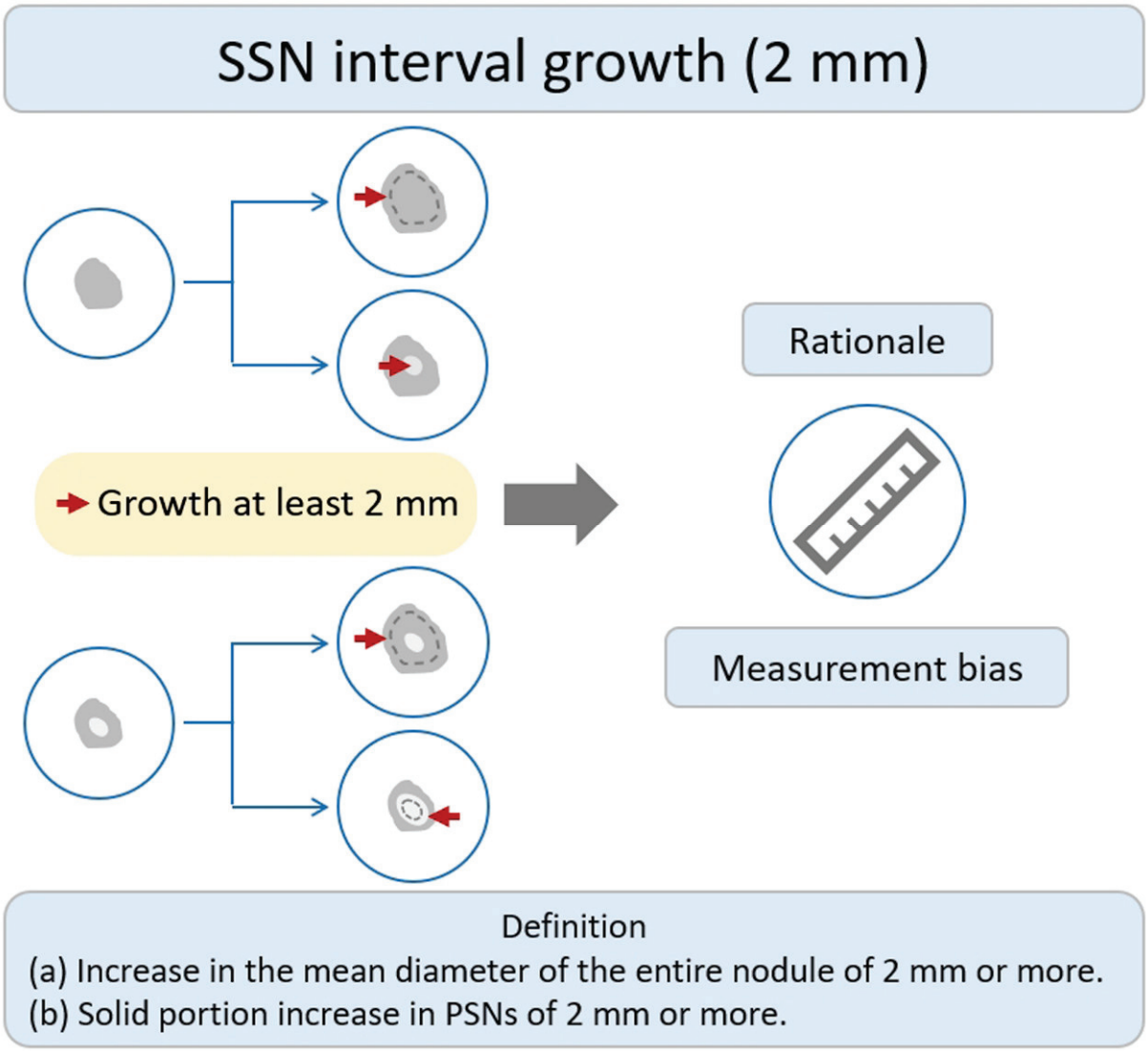

Figure 2. Definition, theoretical rationale, and clinical values based on interval growth threshold of 2 mm in SSN. The definition of growth (a & b) has been explained above. PSN, part-solid nodule; SSN, subsolid nodule.

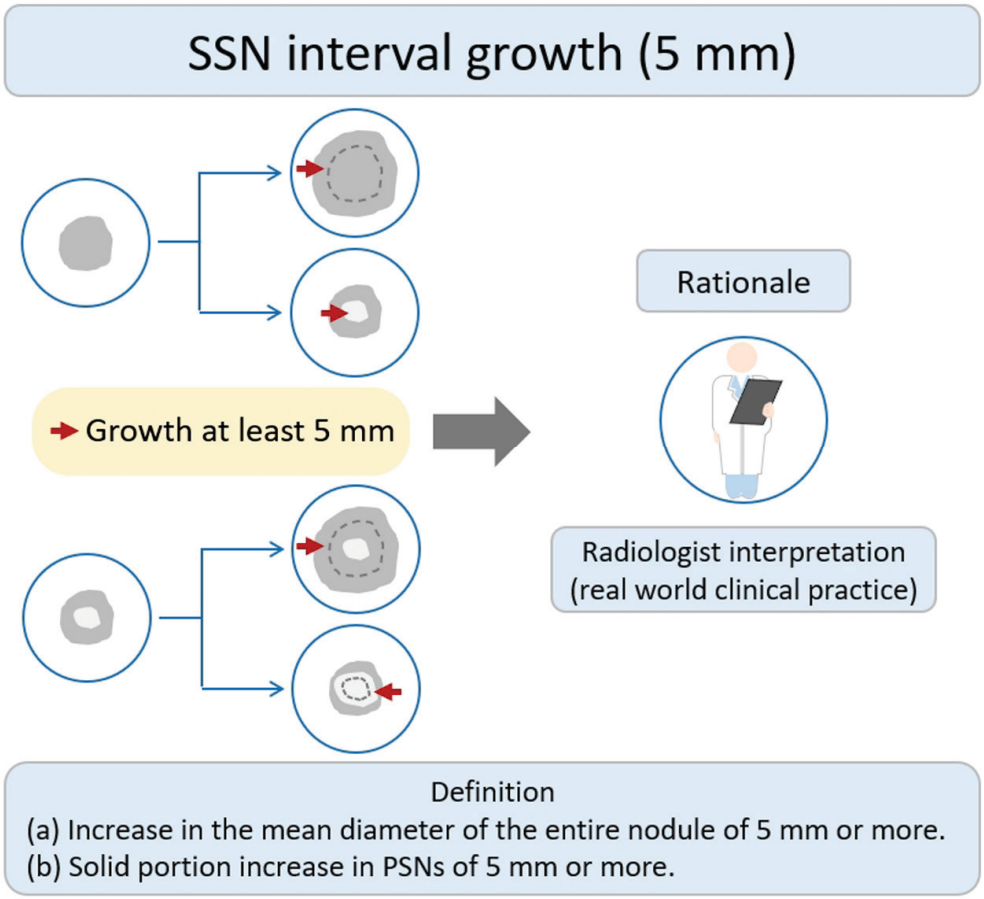

Figure 3. Definition, theoretical rationale, and clinical value based on interval growth threshold of 5 mm in SSN. The definition of growth (a & b) has been explained above. PSN, part-solid nodule; SSN, subsolid nodule.

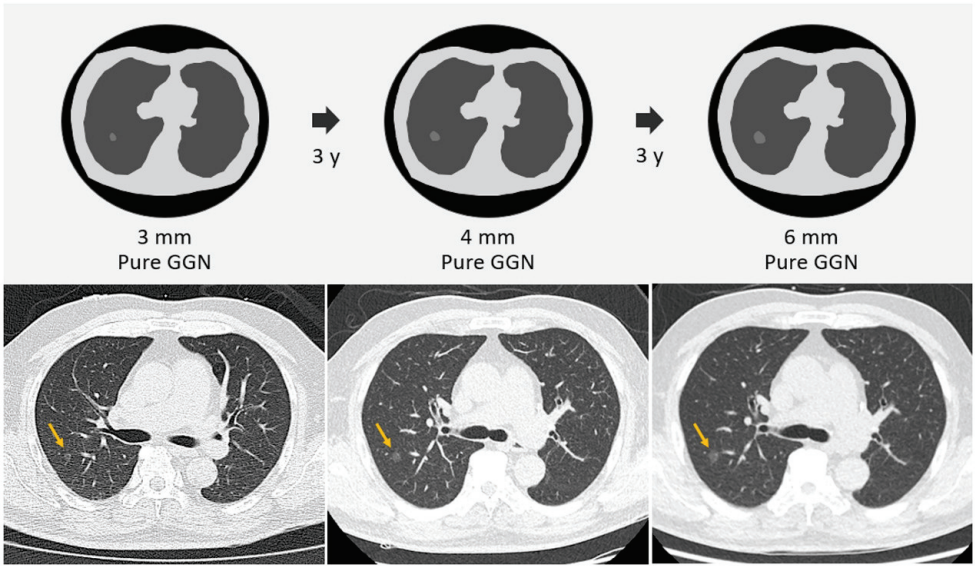

Figure 4. Example of one GGN 3 mm in a 50-year-old man in the right lower lobe. The first CT scan revealed a 3 mm GGN in the right upper lung (yellow arrows). After 3 years of follow up, the GGN had increased to 4 mm; however, it may be due to measurement errors with clinical follow-up strategies. After 3 years of tracking, the GGN had further increased to 6 mm, which meets the 2 mm threshold of interval growth. According to the pathological classification of lung adenocarcinoma spectrum, this lesion is most

likely adenocarcinoma in situ. Therefore, if surgery is performed according to this growth threshold of 2 mm, the possibility of overdiagnosis and over management for indolent lung cancer will be greatly increased. Finally, the pathology report also confirmed the diagnosis of adenocarcinoma in situ. CT, computed tomography; GGN, ground-glass nodule.

2.3. SSNs Interval Growth with Clinical Stage Shift

Stage-shift growth in this study refers to the change in the prognostic stage based on the 8th lung cancer TNM classification system described in the previous relevant studies, assessed through CT scans [43]. It primarily reflects the transition between different stages (e.g., from II to III or 0 to I) and is influenced by the AJCC 8th edition of TNM staging, which considers the impact of interval growth progression on lung cancer survival prognosis. The clinical stage shift as the nodule growth threshold can be used as an important clinically personalized lung cancer prognostic indicator. Clinically, if the interval growth of nodules reaches this threshold, it may lead to a worse prognosis in patients with SSNs. The study rationale for this research lies in using the growth threshold of stage shift to identify the interval growth of SSNs and its correlation with prognostic clinical outcomes, as shown in Figure 5. Therefore, surgical interventions or clinical treatment strategies should be implemented promptly to avoid delayed diagnosis and management. Several studies have investigated the natural course of SSNs based on the definition of stage-shift interval growth from a baseline CT scan to detect stage-shift growth during interval CT scans [21,27]. Tang et al. demonstrated that the PSN group had a significantly higher growth rate than the GGN group in terms of stage-shift growth. PSN group had an estimated 24.2% growth rate within the 5-year follow-up period. GGN group had an estimated 0% growth rate during the follow up [21].

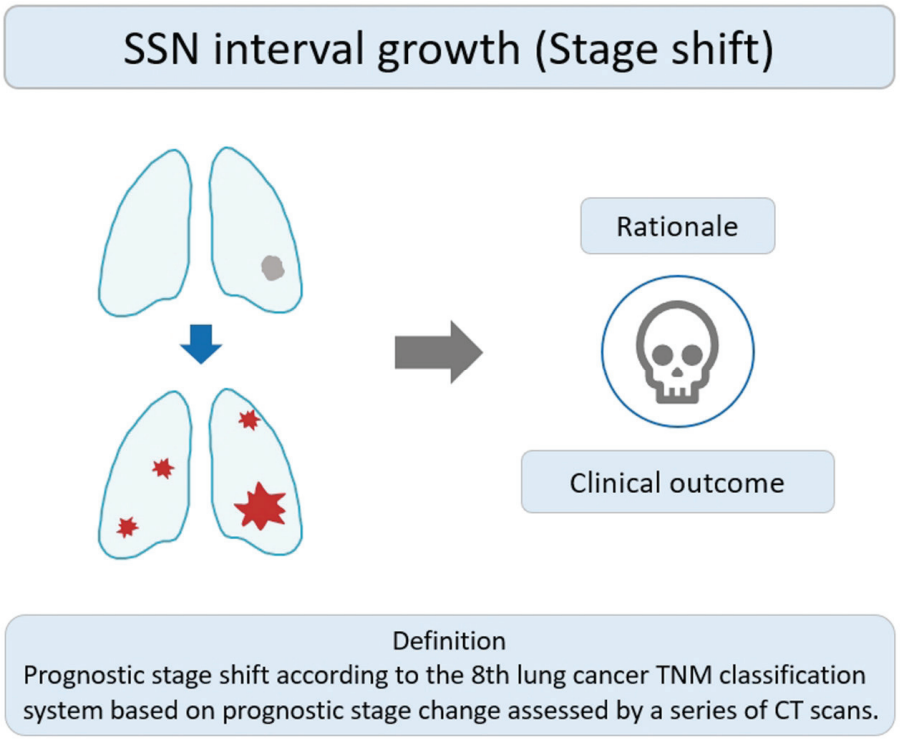

Figure 5. Definition, theoretical rationale, and clinical values based on interval growth threshold of stage shift in SSN. The visual illustration entails a single lung nodule's evolution (gray color) into advanced lung cancer. Concurrently, numerous lung nodules (red color) emerge, indicating metastases and prompting a shift in the disease stage. CT, computed tomography; SSN, subsolid nodule.

The mean growth time for GGNs to reach the growth threshold of the stage shift was 12.168 years, whereas the PSN group had a mean growth time of 7.198 years to reach the threshold point. Based on the interval growth threshold of stage shift in SSNs, clinicians and radiologists can identify high-risk SSNs based on initial CT parameters or clinical risk factors. By assessing the CT imaging characteristics and clinical profiles, they can predict further prognostic growth of these nodules. This information helps in determining the appropriate management strategy for patients with SSNs in order to identify any potential progression to invasive lung cancer associated prognostic outcome or stage-shift change. We also observed that certain clinical scenarios are particularly prone to rapidly worsening prognoses in patients presented with atypical peri-fissure SSNs [44]. Since atypical peri-fissure SSNs may be regarded as atypical peri-fissure nodules clinically, it is considered clinically benign without close follow up. However, since the lesion is close to the pleura surface or inter-fissure space, it is more likely to spread or metastasize along the inter-fissure space clinically [45,46]. Therefore, atypical peri-fissure SSNs should be tracked or dealt with more aggressively. Previous studies also have pointed out that if the subsolid nodule is close to the pleural surface or between pulmonary fissures, early lung cancer manifesting as SSNs could invade the inter-fissure space to form lung or pleural metastases/seeding (Figure 6) [21]. Compared to the growth threshold of 2 mm or 5 mm in SSNs, the clinical or radiologic risk features related to the growth threshold of stage shift represent the indicators that affect the prognosis of early lung adenocarcinoma. However, due to the emerging evidence-based medicine in SSN growth patterns, we have a better understanding of the growth history of SSNs, and have also pointed out that SSNs can be managed through active surveillance of follow-up strategies [24]. Currently, owing to the relevant medical evidence in SSN growth, a nodule growth threshold of 2 mm is often used as the basis for clinical decision making [24,39,42]. Moreover, it may be unacceptable in medical ethical issues to result in a poor prognosis of lung cancer due to a delayed diagnosis. Therefore, most relevant studies exploring the natural course of SSNs affecting the prognosis of growth adopt a retrospective research design for analysis. In the future, a comparison of the impact of different SSN growth patterns on clinical prognosis needs to be carried out through a more standardized image quantification method so as not to affect the patient's prognosis or survival outcome. Clinicians or radiologists can better understand the clinical or radiologic high-risk factors that may affect the prognosis of lung cancer to guide individualized surgical decision plans or active surveillance plans for SSN management [13].

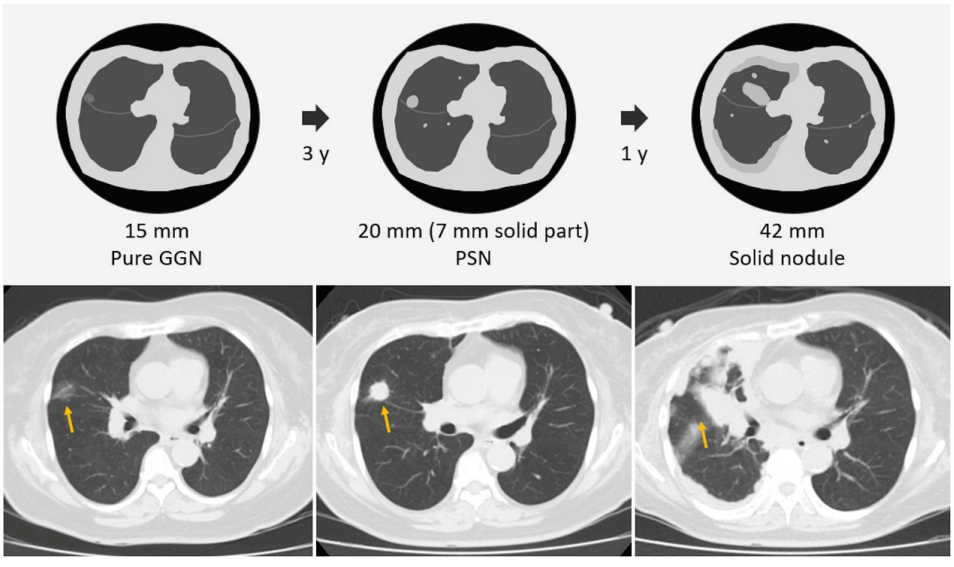

Figure 6. Example of one GGN 15 mm in a 65-year-old woman in the right middle lobe (yellow arrows). The first CT scan revealed a 15 mm GGN in the right upper lung. After 3 years of follow-up,

the GGN had increased to 20 mm PSN with solid part measuring 7 mm. After 1 year of tracking, the PSN had increased to 42 mm (solid nodule) with inter-fissure invasion and pleural nodular seeding. Bilateral lung metastases also confirmed the stage shift in terms of SSN growth. Delayed diagnosis and treatment will seriously affect the survival and prognosis of such patients. Finally, the pathology report also confirmed the diagnosis of advanced invasive adenocarcinoma with lung and pleural metastases. CT, computed tomography; GGN, ground-glass nodule; PSN, part-solid nodule; and SSN, subsolid nodule.

2.4. SSNs Interval Growth with Volumetric Assessment

Previous studies have used volumetric measurements to assess the interval growth change in SSNs [47–53]. Generally, the nodular volume can be measured in two ways. One is to measure the longest nodular diameter to calculate the volume. The other method involves segmenting and delineating the nodules to calculate the volume [54].

The main research rationale was that the European position statement recommended lung cancer screening follow up based on semi-automatically measured volume or volume-doubling time assessment of solid nodules (Figure 7) [55]. Several studies have reported the interval growth of pulmonary SSNs as a growth threshold of 20–30% volumetric increase for growth evaluation [47–52]. Previous studies have demonstrated that diameter-based assessments may overestimate the actual growth, as compared to growth assessments based on volume-based measurements [54]. In addition, both human and phantom studies have demonstrated that manual diameter measurements for nodule assessment are susceptible to errors influenced by nodule margin characteristics [56]. These characteristics can lead to either overestimation or underestimation of the true nodule size when measured manually [57]. Therefore, the volumetric assessment of SSN growth is clinically more sensitive than the nodule diameter measurement [48,58]. Therefore, it will be possible to avoid the delay of the disease or the rapid growth of nodules that affect the prognosis. However, if a volumetric growth assessment is used for small SSNs or GGNs < 5 mm, attention must be given to the problem of overdiagnosis or overtreatment due to the relatively high sensitivity in SSN growth thresholds based on volumetric measurements. Additionally, there are still some difficulties in the clinical practice of volumetric SSN measurements. Recently, an artificial intelligence (AI) analysis software has been used to measure volumetric parameters in a fully automatic or semi-automatic manner. However, clinical workflow integration and personalized pulmonary SSNs follow-up management platforms still need to be integrated with picture archiving and communication systems (PACS) and AI software in the future to practice more efficiently in the real world.

2.5. SSNs Interval Growth with Radiomic Assessment

Previous studies have demonstrated that radiomic assessment has achieved a good diagnostic performance in SSN interval growth pattern [59–62]. Gao et al. showed that the combined clinical and radiomic model showed good performance with an area under the curve (AUC) of 0.801 in predicting the 2 mm growth threshold of GGNs [59]. Furthermore, Sun et al. demonstrated that the radiomics model outperformed conventional radiographic parameters in GGN interval growth prediction [60]. Limited studies have also demonstrated radiomic features associated with SSN nodules with a high growth rate or shorter volume doubling time (VDT), especially margin-related radiomic features with higher volume-based doubling times in lung adenocarcinoma lesions manifesting as SSNs [61,62].

However, there are some limitations in radiomic-based research on the growth rate of longitudinal follow up of pulmonary nodules, such as the inconsistency of scanning protocols or vendors, which will affect the stability or robustness of radiomic features in interval growth prediction [63,64]. Moreover, delta-radiomics is a promising quantitative method that can assess serial changes through longitudinal CT imaging analysis, which could provide a potential growth tendency to guide high-and low-risk SSNs management [65]. Delta-

radiomic-based imaging biomarkers have recently emerged as promising non-invasive tools for allowing a comprehensive evaluation of the tumor habitant microenvironment and the temporal interval changes of spatial heterogeneity in lung adenocarcinoma spectrum lesions [66–68]. Currently, radiomics approaches for SSN interval growth are primarily limited to research settings and have not yet gained widespread adoption in clinical practice. In the future, a combination of radiomics analysis software and PACS reporting platforms can optimize the efficiency and accuracy of radiomics analysis workflow in longitudinal SSNs series follow up.

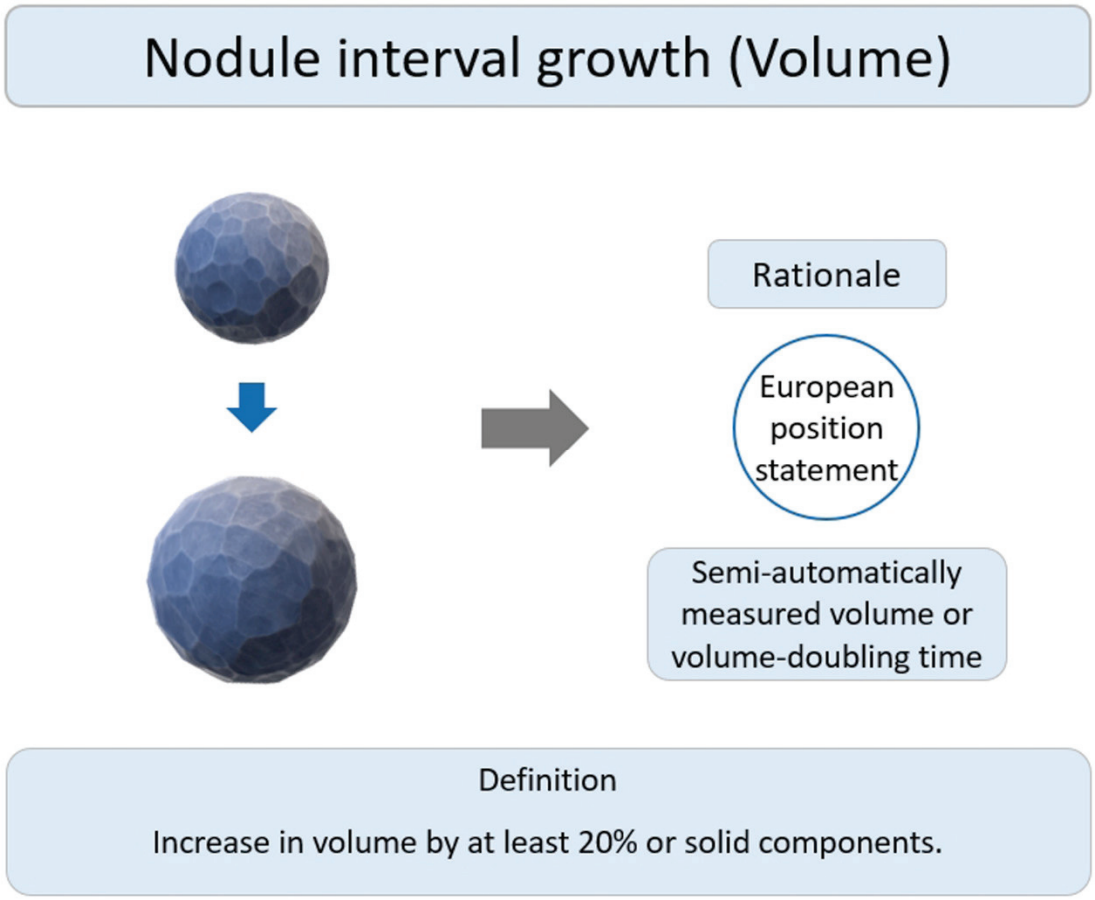

Figure 7. Definition, theoretical rationale, and clinical value based on interval growth threshold of volumetric assessment in subsolid nodules.

2.6. Summative Umbrella and Narrative Review Approach for SSN Growth

We conducted an umbrella review from inception until 31 January 2023, with the following "OR" or "AND" search strategies (key words lists: subsolid nodule; ground-glass nodule; part-solid nodule growth; natural course; natural history; computed tomography) to review the relevant systemic reviews/meta-analyses/narrative reviews to address the current evidence and future direction on this issue about natural growth of SSNs. We also manually searched the relevant reference lists of eligible articles, narrative reviews, and editorials in this research field. Among them, four published reviews are included in this summative umbrella/narrative review (a summary review of these studies is shown in Table 1).

Table 1. Characteristics and key findings of the included systematic reviews/meta-analyses and narrative reviews (summative umbrella review).

1st Author, Year	Type	Enrolled Studies	Sample Size	Purpose	Main Findings	Limitations
Chen Gao, 2020 [59]	Systematic review	*n* = 10	850	Association between quantitative features of initial CT imaging and interval natural growth of SSNs to explore the potential risk factors.	CT attenuation in predicting the natural growth of SSNs.	1. Small sample size. 2. Regarding the variable inclusion criteria among studies. 3. Length of follow up varied.
Zhedong Zhang, 2022 [41]	Narrative review	N/A	N/A	Briefly describe and review the differential diagnosis, growth patterns and rates, genetic characteristics, and factors that influence the growth of persistent SSNs.	Predicting and quantitatively evaluating the growth of GGNs based on clinical and imaging feature data can provide a reference for the formulation of clinical diagnosis and treatment strategies for GGNs.	Liquid biopsy, multi-omics, and delta-radiomics prediction model development for further research direction.
Linyu Wu, 2022 [24]	Systematic review and meta-analysis	*n* = 16	2898 (available SSNs)	To estimate the incidence of interval growth after long-term follow up and identify the predictors of interval growth in SSNs on chest CT.	The pooled incidence of SSN growth was 22%, with a 26% incidence for pure GGNs.	The heterogeneity of SSNs in the included studies was high.
Xin Liang, 2022 [39]	Systematic review and meta-analysis	*n* = 19	2444 (3012 SSNs)	To identify clinical and CT risk features correlated with SSN interval growth.	Male sex, history of lung cancer, nodule size > 10 mm, nodule consistency, and age > 65 y were identified as independent risk factors for SSN growth.	1. The patients in the included studies were not completely homogenous. 2. Most of the features had no multivariate analysis.

CT, computed tomography; SSNs, subsolid nodules; GGNs, ground-glass nodules; and N/A: not applicable.

3. Discussion

3.1. Overdiagnosis

The purpose of this article is to examine and establish the relationship between SSNs and various interval growth patterns in terms of three aspects: measurement bias, radiologic follow up, and clinical prognosis. Therefore, we know that using a threshold of 2 mm or 20–30% volume increase is a more sensitive way to evaluate the nodule growth, and it is clinically suitable for evaluating larger SSNs to avoid the delay in diagnosis. If a 2 mm growth threshold is used to track small GGNs, it may be overly sensitive and may overestimate the growth of nodules, resulting in overdiagnosis and overtreatment. Establishing an SSN different interval growth prediction model based on clinical, radiologic, and radiomic risk features could guide clinically active surveillance of these SSNs and determine the optimal surgical timing in personalized lung cancer screening programs. Overdiagnosis is an inevitable byproduct of lung cancer screening, especially in non-smoking Asian populations [69,70]. Owing to the widespread application of LDCT for lung cancer screening in Asian countries, the incidental discovery of persistent SSNs with a high prevalence rate in Asian non-smokers also presents an important dilemma in clinical management and decision making [10]. Screening high-risk populations for lung cancer is a crucial step towards efficient and effective screening, ensuring that resources are focused on those who are most likely to benefit from early detection and intervention [12].

There is a notable knowledge gap in the medical field and a clinical challenge in accurately assessing individual lung cancer risk stratification among non-smokers in Asia, particularly women. Currently, there is controversy surrounding the eligibility criteria for lung cancer screening in the non-smoker population. Therefore, the widespread acceptance of self-paid lung cancer screening examinations in Asian countries may lead to ineffective

screening programs and overdiagnosis/treatment [8,11]. The original purpose of screening is to find the clinically significant high-risk populations at the top of the iceberg [69,71]. However, if screening is not performed for high-risk groups, more preclinical or indolent-growing early stage lung cancer lesions in the form of persistent SSNs can occur, similar to the numerous asymptomatic or indolent-growing lung cancer lesions or precursor lesions under the iceberg phenomenon (Figure 8). We can solve the dilemma encountered in lung cancer screening programs in Asian non-smoking populations only by assessing the growth trend of SSNs through the SSN growth prediction model that can affect the clinical prognosis. Heterogeneous growth behavior of these SSNs (from indolent to rapid growth) may lead to delayed diagnosis or overdiagnosis if standardized nodule follow up or over management is neglected at the pre-cancerous stage. Combining multi-omics models to identify high-risk SSNs on the iceberg for early surgical intervention and active monitoring (wait-and-see policy) for a large number of low-risk indolent SSNs under the iceberg could optimize the overall quality of lung cancer screening [41]. Therefore, using different growth thresholds to evaluate the growth pattern of natural SSNs may be more effective in distinguishing clinically high-risk SSN lesions from subclinical indolent or stable SSN lesions. It is believed that through the development of personalized prediction models for different growth trends in SSNs, the SSNs management with follow-up strategies could be optimized to maintain a balance between the pros and cons in lung cancer screening programs. Overdiagnosis is inevitable in the screening process, similar to the tip of the iceberg [69,71,72]. However, through the evaluation of individualized nodule growth risk factors, initial size of SSNs, different growth patterns of SSNs, multidisciplinary teamwork, and patient education with a shared decision-making plan to maintain the two ends of the balance effect in lung cancer screening, the advantages and disadvantages of lung cancer screening can be realized in real-world practice (Figure 9).

The iceberg phenomenon is common in lung cancer screening programs. Screening for high-risk groups may help to identify more clinically significant lung cancers. However, targeting low-risk groups may find many subclinical or indolent lung cancers under icebergs. The use of different growth trend assessments can optimize individual subsolid nodule tracking and treatment strategies to reduce the occurrence of overdiagnosis and delayed diagnosis. SSNs, subsolid nodules.

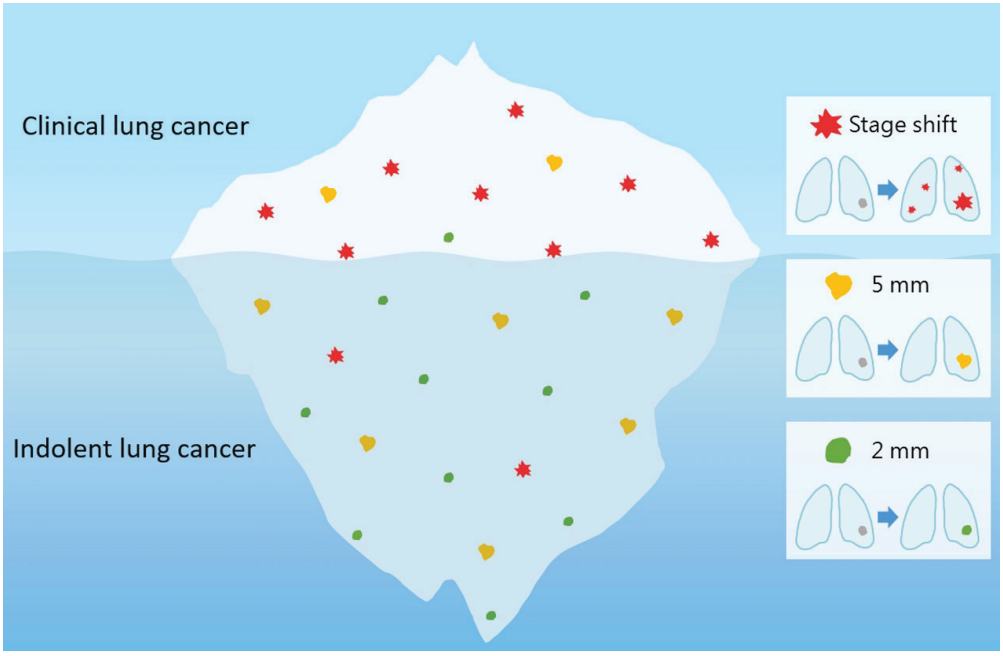

Figure 8. Iceberg phenomenon in interval growth of SSNs in lung cancer screening.

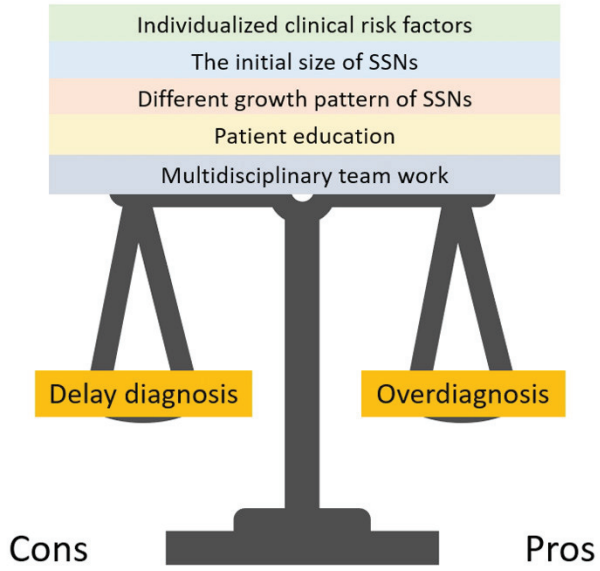

Figure 9. Five clinical strategies to help optimize common dilemmas in lung cancer screening: overdiagnosis and delayed diagnosis.

At present, relevant studies have shown that CT guided biopsy is a safe and effective method for determining preoperative diagnosis of SSNs of suspected lung adenocarcinoma [73]. In a recent study conducted by Kiranantawat et al., the biopsy procedure demonstrated a high technical success rate of 94.7% [74]. The study also reported a 100% positive predictive value (PPV) for malignancy, indicating accurate identification of cancerous nodules. Additionally, the study observed a low rate of complications associated with the biopsy procedure. However, many previous studies have shown that active surveillance of persistent SSNs can effectively monitor the interval growth and avoid problems such as overdiagnosis and over management caused by excessive surgical or biopsy procedure [75,76]. Therefore, we suggest that active surveillance of SSNs based on follow-up guidelines will be the most efficient strategies than tissue sampling through CT-guided biopsy. It is recommended to biopsy solid nodules (originating from SSNs) that have developed to 2–3 cm in diameter or SSNs that have progressed to include a solid component measuring 2–3 cm in diameter, which will have more clinical significance. Due to the clinical possibility of metastasizing to mediastinal lymph nodes or distal metastasis in this clinical setting, a complete preoperative evaluation including CT-guided biopsy and positron emission tomography can better understand the comprehensive lung cancer staging status of patients and to determine the benign and malignant lesions. CT-guided biopsy can be performed in specific situations, such as determining the benign or malignant lesions or further comprehensively evaluating lung cancer staging with pathologic invasiveness degree.

3.2. Succinct Summary According to Summative Umbrella and Narrative Review

In this summative umbrella/narrative review, two were systemic reviews and meta-analyses, one study addressed only the systemic review, and one narrative review addressed the issue of SSN growth from the perspectives of experts in this field [24,39,41,42]. In this comprehensive review, most of these articles discussed the potential risk factors for the interval growth of SSNs. Some articles discussed the prevalence and differences in SSN growth in terms of nodular subtype during the follow-up period, and the issue addressing the nodule growth rate of SSNs that have been stable after a long-term follow up of 5 years [39]. In a systematic review by Gao et al., the authors concluded that CT attenuation may be useful in predicting the risk of SSNs growth [42]. However, this review also mentioned that the nodular diameter had a limited role in predicting the SSN interval growth. Due to heterogeneity among articles and differences in study design, the

systematic review by Gao et al. did not perform pooling data analysis for further meta-analysis evaluation [42]. A meta-analysis by Wu et al. found that the pooled incidence of SSN growth rate was 22% based on a meta-analysis of 2898 SSNs among 16 enrolled studies [39]. In the subgroup analysis in terms of GGN growth, the pooled incidence of SSN growth rate was 26%. Moreover, the pooled incidence of SSN growth rate was only 5% after 2–5 years of stability, according to the subgroup meta-analysis results. The authors concluded that a long-term follow up with active surveillance of these SSNs was essential for SSN management.

However, the initial SSN size was found to predict the nodule interval growth in this study by Wu et al. but was not found in another systemic review by Cao et al. [24,42]. Sources of variability in the main findings may arise from differences in the initial nodular size from the enrolled studies. In the future, the use of personalized multivariate parameters to predict nodule interval growth may be more clinically beneficial for the growth prediction in the management of SSNs with different growth behaviors. A recent meta-analysis and systemic review by Liang et al. demonstrated that male sex, history of lung cancer, nodule size > 10 mm, nodule consistency, and age > 65 years were independent risk factors for predicting SSN growth [39]. Previous studies also demonstrated that the follow-up duration was significantly associated with SSN interval growth [21,32]. However, the study participants enrolled in this meta-analysis were not based on homogeneous populations and the presence of heterogeneity in the study design, which could limit the study outcome with external validity. A recent narrative review by Zhang et al. addressed the current evidence regarding clinical information with CT radiological features to predict SSN growth [41]. The results of the literature review showed that the interval growth threshold and patterns of SSNs were not standardized among the studies, and the related literature were diverse from Asian countries. Therefore, we can infer that this is related to the higher prevalence of subsolid nodules in the Asian population. In the future, it may be necessary to further standardize the interval growth threshold in SSNs and compare more Eastern and Western data for verification. Furthermore, future research should focus on how to use multi-omics combined with longitudinal delta-radiomics data or combined with tumor microenvironment habitant analysis to determine the heterogeneous growth pattern of these SSNs in their natural long-term follow-up course.

3.3. Future Direction

From the results of the current umbrella literature review, we know that the clinical risk factors (such as smoking, age, or family history of lung cancer) and conventional imaging characteristics (initial nodule size and nodule type) may play an important role in predicting the growth rate of SSNs. However, from this meta-analysis, we also found a high heterogeneity in the research design among different enrolled studies, such as follow-up period, nodule type, and initial nodular size. The relevant meta-analysis results showed a high degree of heterogeneity. Future study design should be directed towards standardization of study design, such as follow-up time, consistency of initial nodule size, and nodule type, to reduce the research bias. In addition, through the consistency of research design and imaging scan parameters, radiomics can be used to quantitatively analyze the delta-radiomics of SSNs at different time points, and combined with clinical, genetic, and tumor microenvironment parameters to construct a robust multiomics-based prediction model for SSN interval growth in the field of precise medicine.

4. Conclusions

This literature review addressing the different interval growths in SSNs with its clinical application, comprehensively discusses the definition, design rationale, and current applications of different SSN growth patterns and potential limitations. Summative umbrella reviews have also demonstrated current evidence regarding the natural growth of SSNs based on clinical and conventional CT characteristics. The summative umbrella review in this article also discussed the future research directions on the growth of SSNs. In the

future, personalized SSN management guidelines can be further optimized by integrating multi-omics and the impact of different growth patterns on the clinical prognosis. This literature review could allow clinicians and radiologists to understand how to optimize the common dilemma in the process of planning lung cancer screening through different personalized SSN growth trend prediction models to minimize over- and delayed diagnoses, and maximize screening benefits.

Author Contributions: F.-Z.W. conceptualized the study; Y.-J.W., Y.-C.L., C.-H.L. and F.-Z.W. developed the methods and planned the samples; Y.-C.L., Y.-J.W. and F.-Z.W. prepared and measured the samples; and Y.-J.W., C.-S.C., E.-K.T. and F.-Z.W. prepared the original draft. All authors critically revised the manuscript. All authors have read and agreed to the published version of the manuscript.

Funding: This study was supported by grants from the Kaohsiung Veterans General Hospital, KSVGH112-109, KSVGH111-D02-3, Taiwan, R.O.C., MOST 109-2314-B-075B-006, and MOST 110-2314-B-075B-008.

Institutional Review Board Statement: Not applicable.

Informed Consent Statement: Not applicable.

Data Availability Statement: The data are not publicly available.

Conflicts of Interest: The authors declare no conflict of interest.

Abbreviations

VDT	volume doubling time
PACS	picture archiving and communication system
SSNs	subsolid nodules
AUC	area under the curve
GGNs	ground-glass nodules
PSNs	part-solid nodules
AI	artificial intelligence
LDCT	low-dose computed tomography

References

1. Hsu, H.-T.; Tang, E.-K.; Wu, M.-T.; Wu, C.C.; Liang, C.-H.; Chen, C.-S.; Mar, G.-Y.; Lai, R.-S.; Wang, J.-C.; Wu, C.-L.; et al. Modified Lung-RADS Improves Performance of Screening LDCT in a Population with High Prevalence of Non–smoking-related Lung Cancer. *Acad. Radiol.* **2018**, *25*, 1240–1251. [CrossRef]
2. Lee, J.; Kim, Y.; Kim, H.Y.; Goo, J.M.; Lim, J.; Lee, C.-T.; Jang, S.H.; Lee, W.-C.; Lee, C.W.; Choi, K.S.; et al. Feasibility of implementing a national lung cancer screening program: Interim results from the Korean Lung Cancer Screening Project (K-LUCAS). *Transl. Lung Cancer Res.* **2021**, *10*, 723–736. [CrossRef]
3. Wang, M.; Lin, S.; He, N.; Yang, C.; Zhang, R.; Liu, X.; Suo, C.; Lin, T.; Chen, H.; Xu, W. The Introduction of Low-Dose CT Imaging and Lung Cancer Overdiagnosis in Chinese Women. *Chest* **2023**, *163*, 239–250. [CrossRef]
4. Wu, F.Z.; Huang, Y.L.; Wu, C.C.; Tang, E.K.; Chen, C.S.; Mar, G.Y.; Yen, Y.; Wu, M.T. Assessment of Selection Criteria for Low-Dose Lung Screening CT among Asian Ethnic Groups in Taiwan: From Mass Screening to Specific Risk-Based Screening for Non-Smoker Lung Cancer. *Clin. Lung Cancer* **2016**, *17*, e45–e56. [CrossRef]
5. Lin, K.F.; Wu, H.F.; Huang, W.C.; Tang, P.L.; Wu, M.T.; Wu, F.Z. Propensity score analysis of lung cancer risk in a population with high prevalence of non-smoking related lung cancer. *BMC Pulm. Med.* **2017**, *17*, 120. [CrossRef]
6. National Lung Screening Trial Research Team. Reduced Lung-Cancer Mortality with Low-Dose Computed Tomographic Screening. *N. Engl. J. Med.* **2011**, *365*, 395–409. [CrossRef]
7. Bonney, A.; Malouf, R.; Marchal, C.; Manners, D.; Fong, K.M.; Marshall, H.M.; Irving, L.B.; Manser, R. Low-dose computed tomography (LDCT) screening for lung cancer—Related mortality. *Cochrane Database Syst. Rev.* **2021**, *8*, CD013829. [CrossRef]
8. Wu, F.Z.; Huang, Y.L.; Wu, Y.J.; Tang, E.K.; Wu, M.T.; Chen, C.S.; Lin, Y.P. Prognostic effect of implementation of the mass low-dose computed tomography lung cancer screening program: A hospital-based cohort study. *Eur. J. Cancer Prev.* **2020**, *29*, 445–451. [CrossRef]
9. Nawa, T.; Nakagawa, T.; Mizoue, T.; Kusano, S.; Chonan, T.; Fukai, S.; Endo, K. Long-term prognosis of patients with lung cancer detected on low-dose chest computed tomography screening. *Lung Cancer* **2012**, *75*, 197–202. [CrossRef]
10. Gao, W.; Wen, C.P.; Wu, A.; Welch, H.G. Association of Computed Tomographic Screening Promotion with Lung Cancer Overdiagnosis among Asian Women. *JAMA Intern. Med.* **2022**, *182*, 283–290. [CrossRef]

11. Hung, Y.C.; Tang, E.K.; Wu, Y.J.; Chang, C.J.; Wu, F.Z. Impact of low-dose computed tomography for lung cancer screening on lung cancer surgical volume: The urgent need in health workforce education and training. *Medicine* **2021**, *100*, e26901. [CrossRef]
12. Wu, F.-Z.; Chang, Y.-C. Toward More Effective Lung Cancer Risk Stratification to Empower Screening Programs for the Asian Nonsmoking Population. *J. Am. Coll. Radiol.* **2023**, *20*, 156–161. [CrossRef]
13. MacMahon, H.; Naidich, D.P.; Goo, J.M.; Lee, K.S.; Leung, A.N.C.; Mayo, J.R.; Mehta, A.C.; Ohno, Y.; Powell, C.A.; Prokop, M.; et al. Guidelines for Management of Incidental Pulmonary Nodules Detected on CT Images: From the Fleischner Society 2017. *Radiology* **2017**, *284*, 228–243. [CrossRef]
14. Hansell, D.M.; Bankier, A.A.; MacMahon, H.; McLoud, T.C.; Müller, N.L.; Remy, J. Fleischner Society: Glossary of Terms for Thoracic Imaging. *Radiology* **2008**, *246*, 697–722. [CrossRef]
15. Martin, M.D.; Kanne, J.P.; Broderick, L.S.; Kazerooni, E.A.; Meyer, C.A. Lung-RADS: Pushing the Limits. *RadioGraphics* **2017**, *37*, 1975–1993. [CrossRef] [PubMed]
16. Ye, T.; Deng, L.; Xiang, J.; Zhang, Y.; Hu, H.; Sun, Y.; Li, Y.; Shen, L.; Wang, S.; Xie, L.; et al. Predictors of Pathologic Tumor Invasion and Prognosis for Ground Glass Opacity Featured Lung Adenocarcinoma. *Ann. Thorac. Surg.* **2018**, *106*, 1682–1690. [CrossRef]
17. Kim, Y.W.; Kwon, B.S.; Lim, S.Y.; Lee, Y.J.; Park, J.S.; Cho, Y.-J.; Yoon, H.I.; Lee, K.W.; Lee, J.H.; Chung, J.-H.; et al. Lung cancer probability and clinical outcomes of baseline and new subsolid nodules detected on low-dose CT screening. *Thorax* **2021**, *76*, 980. [CrossRef]
18. Borghesi, A.; Michelini, S.; Golemi, S.; Scrimieri, A.; Maroldi, R. What's New on Quantitative CT Analysis as a Tool to Predict Growth in Persistent Pulmonary Subsolid Nodules? A Literature Review. *Diagnostics* **2020**, *10*, 55. [CrossRef]
19. Travis, W.D.; Brambilla, E.; Noguchi, M.; Nicholson, A.G.; Geisinger, K.R.; Yatabe, Y.; Beer, D.G.; Powell, C.A.; Riely, G.J.; Van Schil, P.E.; et al. International association for the study of lung cancer/american thoracic society/european respiratory society international multidisciplinary classification of lung adenocarcinoma. *J. Thorac. Oncol.* **2011**, *6*, 244–285. [CrossRef]
20. Nicholson, A.G.; Tsao, M.S.; Beasley, M.B.; Borczuk, A.C.; Brambilla, E.; Cooper, W.A.; Dacic, S.; Jain, D.; Kerr, K.M.; Lantuejoul, S.; et al. The 2021 WHO Classification of Lung Tumors: Impact of Advances Since 2015. *J. Thorac. Oncol.* **2022**, *17*, 362–387. [CrossRef]
21. Tang, E.-K.; Chen, C.-S.; Wu, C.C.; Wu, M.-T.; Yang, T.-L.; Liang, H.-L.; Hsu, H.-T.; Wu, F.-Z. Natural History of Persistent Pulmonary Subsolid Nodules: Long-Term Observation of Different Interval Growth. *Heart Lung Circ.* **2019**, *28*, 1747–1754. [CrossRef]
22. Kakinuma, R.; Noguchi, M.; Ashizawa, K.; Kuriyama, K.; Maeshima, A.M.; Koizumi, N.; Kondo, T.; Matsuguma, H.; Nitta, N.; Ohmatsu, H.; et al. Natural History of Pulmonary Subsolid Nodules: A Prospective Multicenter Study. *J. Thorac. Oncol.* **2016**, *11*, 1012–1028. [CrossRef] [PubMed]
23. Pérez-Morales, J.; Lu, H.; Mu, W.; Tunali, I.; Kutuk, T.; Eschrich, S.A.; Balagurunathan, Y.; Gillies, R.J.; Schabath, M.B. Volume doubling time and radiomic features predict tumor behavior of screen-detected lung cancers. *Cancer Biomark* **2022**, *33*, 489–501. [CrossRef] [PubMed]
24. Wu, L.; Gao, C.; Kong, N.; Lou, X.; Xu, M. The long-term course of subsolid nodules and predictors of interval growth on chest CT: A systematic review and meta-analysis. *Eur. Radiol.* **2022**, *33*, 2075–2088. [CrossRef]
25. Lee, H.W.; Jin, K.N.; Lee, J.K.; Kim, D.K.; Chung, H.S.; Heo, E.Y.; Choi, S.H. Long-Term Follow-Up of Ground-Glass Nodules After 5 Years of Stability. *J. Thorac. Oncol.* **2019**, *14*, 1370–1377. [CrossRef]
26. Hiramatsu, M.; Inagaki, T.; Inagaki, T.; Matsui, Y.; Satoh, Y.; Okumura, S.; Ishikawa, Y.; Miyaoka, E.; Nakagawa, K. Pulmonary ground-glass opacity (GGO) lesions-large size and a history of lung cancer are risk factors for growth. *J. Thorac. Oncol.* **2008**, *3*, 1245–1250. [CrossRef]
27. Lee, J.H.; Lim, W.H.; Hong, J.H.; Nam, J.G.; Hwang, E.J.; Kim, H.; Goo, J.M.; Park, C.M. Growth and Clinical Impact of 6-mm or Larger Subsolid Nodules after 5 Years of Stability at Chest CT. *Radiology* **2020**, *295*, 448–455. [CrossRef]
28. Wu, Y.J.; Tseng, J.H.; Liang, C.H.; Tang, E.K.; Wu, F.Z. The fate of subsolid nodule: Predictable or unpredictable? *J. Thorac. Dis.* **2020**, *12*, 1118–1120. [CrossRef]
29. Silva, M.; Sverzellati, N.; Manna, C.; Negrini, G.; Marchianò, A.; Zompatori, M.; Rossi, C.; Pastorino, U. Long-term surveillance of ground-glass nodules: Evidence from the MILD trial. *J. Thorac. Oncol.* **2012**, *7*, 1541–1546. [CrossRef]
30. Chang, B.; Hwang, J.H.; Choi, Y.H.; Chung, M.P.; Kim, H.; Kwon, O.J.; Lee, H.Y.; Lee, K.S.; Shim, Y.M.; Han, J.; et al. Natural history of pure ground-glass opacity lung nodules detected by low-dose CT scan. *Chest* **2013**, *143*, 172–178. [CrossRef]
31. Matsuguma, H.; Mori, K.; Nakahara, R.; Suzuki, H.; Kasai, T.; Kamiyama, Y.; Igarashi, S.; Kodama, T.; Yokoi, K. Characteristics of subsolid pulmonary nodules showing growth during follow-up with CT scanning. *Chest* **2013**, *143*, 436–443. [CrossRef]
32. Lee, S.W.; Leem, C.S.; Kim, T.J.; Lee, K.W.; Chung, J.H.; Jheon, S.; Lee, J.H.; Lee, C.T. The long-term course of ground-glass opacities detected on thin-section computed tomography. *Respir. Med.* **2013**, *107*, 904–910. [CrossRef]
33. Kobayashi, Y.; Fukui, T.; Ito, S.; Usami, N.; Hatooka, S.; Yatabe, Y.; Mitsudomi, T. How long should small lung lesions of ground-glass opacity be followed? *J. Thorac. Oncol.* **2013**, *8*, 309–314. [CrossRef]
34. Eguchi, T.; Kondo, R.; Kawakami, S.; Matsushita, M.; Yoshizawa, A.; Hara, D.; Matsuoka, S.; Takeda, T.; Miura, K.; Agatsuma, H.; et al. Computed tomography attenuation predicts the growth of pure ground-glass nodules. *Lung Cancer* **2014**, *84*, 242–247. [CrossRef]

35. Kobayashi, Y.; Sakao, Y.; Deshpande, G.A.; Fukui, T.; Mizuno, T.; Kuroda, H.; Sakakura, N.; Usami, N.; Yatabe, Y.; Mitsudomi, T. The association between baseline clinical-radiological characteristics and growth of pulmonary nodules with ground-glass opacity. *Lung Cancer* **2014**, *83*, 61–66. [CrossRef]
36. Qiu, Y.; Mao, F.; Zhang, H.; Shen-Tu, Y. Factors Influencing the Progression Trend of Early Lung Cancer and CT Findings. *Zhongguo Fei Ai Za Zhi* **2018**, *21*, 793–799. [CrossRef]
37. Kakinuma, R.; Ashizawa, K.; Kuriyama, K.; Fukushima, A.; Ishikawa, H.; Kamiya, H.; Koizumi, N.; Maruyama, Y.; Minami, K.; Nitta, N.; et al. Measurement of focal ground-glass opacity diameters on CT images: Interobserver agreement in regard to identifying increases in the size of ground-glass opacities. *Acad. Radiol.* **2012**, *19*, 389–394. [CrossRef]
38. Han, D.; Heuvelmans, M.A.; Oudkerk, M. Volume versus diameter assessment of small pulmonary nodules in CT lung cancer screening. *Transl. Lung Cancer Res.* **2017**, *6*, 52–61. [CrossRef]
39. Liang, X.; Liu, M.; Li, M.; Zhang, L. Clinical and CT Features of Subsolid Pulmonary Nodules with Interval Growth: A Systematic Review and Meta-Analysis. *Front. Oncol.* **2022**, *12*, 929174. [CrossRef]
40. Travis, W.D.; Asamura, H.; Bankier, A.A.; Beasley, M.B.; Detterbeck, F.; Flieder, D.B.; Goo, J.M.; MacMahon, H.; Naidich, D.; Nicholson, A.G.; et al. The IASLC Lung Cancer Staging Project: Proposals for Coding T Categories for Subsolid Nodules and Assessment of Tumor Size in Part-Solid Tumors in the Forthcoming Eighth Edition of the TNM Classification of Lung Cancer. *J. Thorac. Oncol.* **2016**, *11*, 1204–1223. [CrossRef]
41. Zhang, Z.; Zhou, L.; Yang, F.; Li, X. The natural growth history of persistent pulmonary subsolid nodules: Radiology, genetics, and clinical management. *Front. Oncol.* **2022**, *12*, 1011712. [CrossRef]
42. Gao, C.; Li, J.; Wu, L.; Kong, D.; Xu, M.; Zhou, C. The Natural Growth of Subsolid Nodules Predicted by Quantitative Initial CT Features: A Systematic Review. *Front. Oncol.* **2020**, *10*, 318. [CrossRef]
43. Wu, F.-Z.; Wu, Y.-J.; Chen, C.-S.; Tang, E.-K. Prediction of Interval Growth of Lung Adenocarcinomas Manifesting as Persistent Subsolid Nodules $\leq$ 3 cm Based on Radiomic Features. *Acad. Radiol.* **2023**. [CrossRef]
44. Morgan, H.; O'Dowd, E.L.; Nair, A.; Baldwin, D.R. New fissure-attached nodules in lung cancer screening: More practical implications from the NELSON study? *Transl. Lung Cancer Res.* **2020**, *9*, 2161–2164. [CrossRef]
45. Liu, M.; Wigle, D.; Wampfler, J.A.; Dai, J.; Stoddard, S.M.; Xue, Z.; Nichols, F.C.; Jiang, G.; Yang, P. T category of non-small cell lung cancer invading the fissure to the adjacent lobe. *J. Thorac. Cardiovasc. Surg.* **2017**, *154*, 1777–1783.e1773. [CrossRef]
46. Van Schil, P.E. Non-small cell lung cancer transgressing an adjacent fissure: Does one T category fit all? *J. Thorac. Dis.* **2018**, *10*, S3290–S3291. [CrossRef]
47. Song, Y.S.; Park, C.M.; Park, S.J.; Lee, S.M.; Jeon, Y.K.; Goo, J.M. Volume and mass doubling times of persistent pulmonary subsolid nodules detected in patients without known malignancy. *Radiology* **2014**, *273*, 276–284. [CrossRef]
48. Qi, L.L.; Wu, B.T.; Tang, W.; Zhou, L.N.; Huang, Y.; Zhao, S.J.; Liu, L.; Li, M.; Zhang, L.; Feng, S.C.; et al. Long-term follow-up of persistent pulmonary pure ground-glass nodules with deep learning-assisted nodule segmentation. *Eur. Radiol.* **2020**, *30*, 744–755. [CrossRef]
49. Xu, X.; Wu, K.; Zhao, Y.; Mei, L. Stage I lung adenocarcinoma: The value of quantitative CT in differentiating pathological subtypes and predicting growth of subsolid nodules. *Medicine* **2017**, *96*, e6595. [CrossRef]
50. Shin, K.E.; Lee, K.S.; Yi, C.A.; Chung, M.J.; Shin, M.H.; Choi, Y.H. Subcentimeter lung nodules stable for 2 years at LDCT: Long-term follow-up using volumetry. *Respirology* **2014**, *19*, 921–928. [CrossRef]
51. Scholten, E.T.; de Jong, P.A.; de Hoop, B.; van Klaveren, R.; van Amelsvoort-van de Vorst, S.; Oudkerk, M.; Vliegenthart, R.; de Koning, H.J.; van der Aalst, C.M.; Vernhout, R.M.; et al. Towards a close computed tomography monitoring approach for screen detected subsolid pulmonary nodules? *Eur. Respir. J.* **2015**, *45*, 765–773. [CrossRef]
52. He, Y.; Xiong, Z.; Tian, D.; Zhang, J.; Chen, J.; Li, Z. Natural progression of persistent pure ground-glass nodules 10 mm or smaller: Long-term observation and risk factor assessment. *Jpn. J. Radiol.* **2023**, *41*, 605–616. [CrossRef]
53. Shewale, J.B.; Nelson, D.B.; Rice, D.C.; Sepesi, B.; Hofstetter, W.L.; Mehran, R.J.; Vaporciyan, A.A.; Walsh, G.L.; Swisher, S.G.; Roth, J.A.; et al. Natural History of Ground-Glass Lesions among Patients with Previous Lung Cancer. *Ann. Thorac. Surg.* **2018**, *105*, 1671–1677. [CrossRef]
54. De Margerie-Mellon, C.; Gill, R.R.; Monteiro Filho, A.C.; Heidinger, B.H.; Onken, A.; VanderLaan, P.A.; Bankier, A.A. Growth Assessment of Pulmonary Adenocarcinomas Manifesting as Subsolid Nodules on CT: Comparison of Diameter-Based and Volume Measurements. *Acad. Radiol.* **2020**, *27*, 1385–1393. [CrossRef]
55. Oudkerk, M.; Devaraj, A.; Vliegenthart, R.; Henzler, T.; Prosch, H.; Heussel, C.P.; Bastarrika, G.; Sverzellati, N.; Mascalchi, M.; Delorme, S.; et al. European position statement on lung cancer screening. *Lancet Oncol.* **2017**, *18*, e754–e766. [CrossRef]
56. Han, D.; Heuvelmans, M.A.; Vliegenthart, R.; Rook, M.; Dorrius, M.D.; de Jonge, G.J.; Walter, J.E.; van Ooijen, P.M.A.; de Koning, H.J.; Oudkerk, M. Influence of lung nodule margin on volume- and diameter-based reader variability in CT lung cancer screening. *Br. J. Radiol.* **2018**, *91*, 20170405. [CrossRef]
57. Xie, X.; Zhao, Y.; Snijder, R.A.; van Ooijen, P.M.; de Jong, P.A.; Oudkerk, M.; de Bock, G.H.; Vliegenthart, R.; Greuter, M.J. Sensitivity and accuracy of volumetry of pulmonary nodules on low-dose 16- and 64-row multi-detector CT: An anthropomorphic phantom study. *Eur. Radiol.* **2013**, *23*, 139–147. [CrossRef]
58. Lee, J.H.; Hwang, E.J.; Lim, W.H.; Goo, J.M. Determination of the optimum definition of growth evaluation for indeterminate pulmonary nodules detected in lung cancer screening. *PLoS ONE* **2022**, *17*, e0274583. [CrossRef]

59. Gao, C.; Yan, J.; Luo, Y.; Wu, L.; Pang, P.; Xiang, P.; Xu, M. The Growth Trend Predictions in Pulmonary Ground Glass Nodules Based on Radiomic CT Features. *Front. Oncol.* **2020**, *10*, 580809. [CrossRef]
60. Sun, Y.; Ma, Z.; Zhao, W.; Jin, L.; Gao, P.; Wang, K.; Huang, X.; Duan, S.; Li, M. Computed tomography radiomics in growth prediction of pulmonary ground-glass nodules. *Eur. J. Radiol.* **2022**, *159*, 110684. [CrossRef]
61. Yoon, H.J.; Park, H.; Lee, H.Y.; Sohn, I.; Ahn, J.; Lee, S.H. Prediction of tumor doubling time of lung adenocarcinoma using radiomic margin characteristics. *Thorac. Cancer* **2020**, *11*, 2600–2609. [CrossRef] [PubMed]
62. Tan, M.; Ma, W.; Sun, Y.; Gao, P.; Huang, X.; Lu, J.; Chen, W.; Wu, Y.; Jin, L.; Tang, L.; et al. Prediction of the Growth Rate of Early-Stage Lung Adenocarcinoma by Radiomics. *Front. Oncol.* **2021**, *11*, 658138. [CrossRef]
63. Wu, Y.J.; Wu, F.Z.; Yang, S.C.; Tang, E.K.; Liang, C.H. Radiomics in Early Lung Cancer Diagnosis: From Diagnosis to Clinical Decision Support and Education. *Diagnostics* **2022**, *12*, 1064. [CrossRef]
64. Moskowitz, C.S.; Welch, M.L.; Jacobs, M.A.; Kurland, B.F.; Simpson, A.L. Radiomic Analysis: Study Design, Statistical Analysis, and Other Bias Mitigation Strategies. *Radiology* **2022**, *304*, 265–273. [CrossRef] [PubMed]
65. Nardone, V.; Reginelli, A.; Grassi, R.; Boldrini, L.; Vacca, G.; D'Ippolito, E.; Annunziata, S.; Farchione, A.; Belfiore, M.P.; Desideri, I.; et al. Delta radiomics: A systematic review. *La Radiol. Medica* **2021**, *126*, 1571–1583. [CrossRef] [PubMed]
66. Altorki, N.K.; Markowitz, G.J.; Gao, D.; Port, J.L.; Saxena, A.; Stiles, B.; McGraw, T.; Mittal, V. The lung microenvironment: An important regulator of tumour growth and metastasis. *Nat. Rev. Cancer* **2019**, *19*, 9–31. [CrossRef]
67. Lee, G.; Park, H.; Bak, S.H.; Lee, H.Y. Radiomics in Lung Cancer from Basic to Advanced: Current Status and Future Directions. *Korean J. Radiol.* **2020**, *21*, 159–171. [CrossRef]
68. Wu, F.-Z.; Wu, Y.-J.; Tang, E.-K. An integrated nomogram combined semantic-radiomic features to predict invasive pulmonary adenocarcinomas in subjects with persistent subsolid nodules. *Quant. Imaging Med. Surg.* **2022**, *13*, 654–668. [CrossRef]
69. Bastos, P.A.D.; Barbosa, R. The tip of the iceberg for diagnostic dilemmas: Performance of current diagnostics and future complementary screening approaches. *Eur. J. Med. Genet* **2020**, *63*, 104089. [CrossRef]
70. Wilson, D.O.; Ryan, A.; Fuhrman, C.; Schuchert, M.; Shapiro, S.; Siegfried, J.M.; Weissfeld, J. Doubling times and CT screen–detected lung cancers in the Pittsburgh Lung Screening Study. *Am. J. Respir. Crit. Care Med.* **2012**, *185*, 85–89. [CrossRef]
71. Last, J.M.; Adelaide, D.P. The iceberg: 'completing the clinical picture' in general practice. 1963. *Int. J. Epidemiol.* **2013**, *42*, 1608–1613. [CrossRef] [PubMed]
72. Welch, H.G.; Black, W.C. Overdiagnosis in cancer. *J. Natl. Cancer Inst.* **2010**, *102*, 605–613. [CrossRef] [PubMed]
73. Healey, T.T.; Shepard, J.-A.O. Biopsy of Subsolid Nodules Suspicious for Adenocarcinoma: Point—CT-Guided Biopsy of Subsolid Nodules Is a Safe and Effective Means to Establish a Definitive Preoperative Diagnosis. *Am. J. Roentgenol.* **2021**, *217*, 813–814. [CrossRef] [PubMed]
74. Kiranantawat, N.; McDermott, S.; Petranovic, M.; Mino-Kenudson, M.; Muniappan, A.; Sharma, A.; Shepard, J.O.; Digumarthy, S.R. Determining malignancy in CT guided fine needle aspirate biopsy of subsolid lung nodules: Is core biopsy necessary? *Eur. J. Radiol. Open* **2019**, *6*, 175–181. [CrossRef] [PubMed]
75. Silva, M.; Prokop, M.; Jacobs, C.; Capretti, G.; Sverzellati, N.; Ciompi, F.; van Ginneken, B.; Schaefer-Prokop, C.M.; Galeone, C.; Marchianò, A.; et al. Long-Term Active Surveillance of Screening Detected Subsolid Nodules is a Safe Strategy to Reduce Overtreatment. *J. Thorac. Oncol.* **2018**, *13*, 1454–1463. [CrossRef]
76. Ricciardi, S.; Booton, R.; Petersen, R.H.; Infante, M.; Scarci, M.; Veronesi, G.; Cardillo, G. Managing of screening-detected sub-solid nodules-a European perspective. *Transl. Lung Cancer Res.* **2021**, *10*, 2368–2377. [CrossRef]

diagnostics

MDPI

Systematic Review

Predicting the Invasiveness of Pulmonary Adenocarcinomas in Pure Ground-Glass Nodules Using the Nodule Diameter: A Systematic Review, Meta-Analysis, and Validation in an Independent Cohort

Jieke Liu †, Xi Yang †, Yong Li, Hao Xu, Changjiu He, Peng Zhou * and Haomiao Qing *

Department of Radiology, Sichuan Clinical Research Center for Cancer, Sichuan Cancer Hospital and Institute, Sichuan Cancer Center, Affiliated Cancer Hospital of University of Electronic Science and Technology of China, Chengdu 610041, China; liu.jieke@uestc.edu.cn (J.L.); m17726362884@163.com (X.Y.); muzi5969@foxmail.com (Y.L.); xu378531592@foxmail.com (H.X.); hechangjiou@sina.com (C.H.)

* Correspondence: zhoupeng@scszlyy.org.cn (P.Z.); qinghaomiao@scszlyy.org.cn (H.Q.)

† These authors contributed equally to this work.

Abstract: The nodule diameter was commonly used to predict the invasiveness of pulmonary adenocarcinomas in pure ground-glass nodules (pGGNs). However, the diagnostic performance and optimal cut-off values were inconsistent. We conducted a meta-analysis to evaluate the diagnostic performance of the nodule diameter for predicting the invasiveness of pulmonary adenocarcinomas in pGGNs and validated the cut-off value of the diameter in an independent cohort. Relevant studies were searched through PubMed, MEDLINE, Embase, and the Cochrane Library, from inception until December 2022. The inclusion criteria comprised studies that evaluated the diagnostic accuracy of the nodule diameter to differentiate invasive adenocarcinomas (IAs) from non-invasive adenocarcinomas (non-IAs) in pGGNs. A bivariate mixed-effects regression model was used to obtain the diagnostic performance. Meta-regression analysis was performed to explore the heterogeneity. An independent sample of 220 pGGNs (82 IAs and 128 non-IAs) was enrolled as the validation cohort to evaluate the performance of the cut-off values. This meta-analysis finally included 16 studies and 2564 pGGNs (761 IAs and 1803 non-IAs). The pooled area under the curve, the sensitivity, and the specificity were 0.85 (95% confidence interval (CI), 0.82–0.88), 0.82 (95% CI, 0.78–0.86), and 0.73 (95% CI, 0.67–0.78). The diagnostic performance was affected by the measure of the diameter, the reconstruction matrix, and patient selection bias. Using the prespecified cut-off value of 10.4 mm for the mean diameter and 13.2 mm for the maximal diameter, the mean diameter showed higher sensitivity than the maximal diameter in the validation cohort (0.85 vs. 0.72, $p < 0.01$), while there was no significant difference in specificity (0.83 vs. 0.86, $p = 0.13$). The nodule diameter had adequate diagnostic performance in differentiating IAs from non-IAs in pGGNs and could be replicated in a validation cohort. The mean diameter with a cut-off value of 10.4 mm was recommended.

Keywords: pure ground-glass nodule; invasive adenocarcinoma; diameter; computed tomography; meta-analysis

1. Introduction

Lung cancer remains the most common cause of cancer-related mortality worldwide [1,2]. The detection of subsolid nodules, including pure ground-glass nodules (pGGNs) and mixed ground-glass nodules (mGGNs)/part-solid nodules (PSNs), has expanded enormously with the popularization of low-dose computed tomography (LDCT) in lung cancer screening, particularly in Eastern Asians [3–7]. Most pathologically confirmed subsolid nodules were pulmonary adenocarcinomas [8–10], which were categorized into precursor glandular lesions (atypical adenomatous hyperplasia (AAH) and adenocarcinoma

in situ (AIS)), minimally invasive adenocarcinomas (MIAs), and invasive adenocarcinomas (IAs) [11–13]. The precursor glandular lesions and MIAs were classified as non-invasive adenocarcinomas (non-IAs) because their 5-year recurrence-free survival (RFS) rate was 100% [14,15]. In comparison, the 5-year RFS rate of IAs ranged from 22.0% to 94.4% due to different differentiation grades [16,17].

Although pGGNs tend to be non-IAs and solid components within nodules correspond to invasive patterns in pathology, this association is not absolute [12,18]. In previous literature, a number of pGGNs were pathologically diagnosed as IAs, and the proportion ranged from 18.0% to 53.0% [19–23]. The current recommendations and guidelines maintain conservative attitudes and suggest annual screening with LDCT for pGGNs, as they tend to be stable or grow slowly during surveillance [18,24–27]. However, previous studies also found that over 50% of pGGNs progressed during the follow-up surveillance [28,29]. The invasiveness may be an indication that the pulmonary adenocarcinoma transitions from an indolent stage to a growth period. Hence, early differentiation of IAs from non-IAs in pGGNs is important for thoracic surgeons and radiologists when choosing surgical intervention or conservative surveillance.

Generally, radiologists evaluate the invasiveness of pGGNs by interpreting the morphological and quantitative characteristics using chest computed tomography (CT). As there is inherent subjectivity and inter-observer heterogeneity of the morphological features, most studies used the nodule size, usually the maximal or mean diameter, to distinguish IAs from non-IAs in pGGNs. However, the diagnostic performance of the nodule diameter was inconsistent. The area under the curve (AUC) ranged from 0.70 to 0.93, and the corresponding cut-off value ranged from 8.5 to 17.2 mm [20,30–34]. The heterogeneity of these results may be underlying the clinical characteristics of the sample, the acquisition parameters, and the measure of the maximal or mean diameter.

Therefore, this study aimed to assess the diagnostic performance of the nodule diameter for predicting invasiveness in pGGNs by performing a meta-analysis and to explore the potential heterogeneity. We also investigated whether the results of our meta-analysis could be validated in an independent cohort from a lung cancer screening.

2. Materials and Methods

2.1. Search Strategy and Selection Criteria

This meta-analysis was reported according to the preferred reporting items for systematic reviews and meta-analyses (PRISMA) guidelines [35]. We identified potentially eligible studies through electronic literature searches on PubMed, MEDLINE, Embase, and the Cochrane Library, from inception until December 2022. The following medical subject headings and keywords were used as search terms: ("computed tomography") and ("adenocarcinoma") and ("invasive *") and ("ground-glass nodule *" or "ground glass nodule *" or "ground-glass opacity" or "ground glass opacity" or "non-solid nodule *" or "nonsolid nodule *" or "sub-solid nodule *" or "subsolid nodule *"). Further eligible studies were identified by screening the references in the retrieved original papers, review articles, and meta-analyses. The inclusion criteria were as follows: (1) using nodule maximal or mean diameter to differentiate IAs from non-IAs in pGGNs; (2) using histopathological examination as the gold standard of diagnosis; (3) reporting the sensitivity and specificity to calculate the true positive (TP), false positive (FP), false negative (FN), and true negative (TN). The exclusion criteria were as follows: (1) case reports or reviews; (2) duplicate publications or data; (3) studies including benign nodules; (4) studies unrelated to the nodule diameter; (5) insufficient data reporting; (6) differentiation between the AAH/AIS and MIA/IA; (7) studies including mGGNs.

2.2. Data Extraction

Two reviewers (J.L. and X.Y.) independently collected the following data from each included study: first author name, publication year and journal, the country of study, sample size, mean or median age, number of males, number of smokers, measure of the

diameter, the cut-off value, and the acquisition parameters of the CT, including the slice thickness and reconstruction matrix. The following diagnostic performance measurements were calculated from the sensitivity and specificity: TP, FP, FN, and TN. Disagreement between the two reviewers was resolved by consulting a third reviewer (P.Z.).

2.3. Quality Assessment

The quality of the selected studies and the potential bias were assessed using the Quality Assessment of Diagnostic Accuracy Studies (QUADAS-2) tool [36]. This quality assessment procedure was independently performed by two reviewers (J.L. and X.Y.) and was checked by a third reviewer (P.Z.). Any disagreements were resolved through a discussion involving all the reviewers.

2.4. Meta-Analysis

The meta-analyses of the pooled sensitivity and specificity were performed using the MIDAS package in STATA (version 17.0), with a bivariate mixed-effect regression model. A summary receiver operating characteristic (SROC) plot was constructed to calculate the pooled AUC.

A meta-regression analysis was further conducted to explore the causes of heterogeneity using several potential covariates, including the percentage of males, percentage of smokers, measure of the diameter (maximal or mean), slice thickness (all < 1.5 mm or not), and reconstruction matrix (1024 × 1024 or 512 × 512). The patient selection of QUADA-2 was targeted as an additional covariate.

The heterogeneity of the included studies was assessed using a forest plot and the corresponding inconsistency index (I^2). Moreover, I^2 > 50% indicated a high degree of heterogeneity [37,38]. Publication bias was assessed with Egger's funnel plot and with a regression test for funnel plot asymmetry [39].

2.5. Validation Using an Independent Sample

To verify the results from the meta-analysis, we conducted a validation study using an independent cohort from a lung cancer screening. The validation study was approved by the Ethics Committees at Sichuan Cancer Hospital, and individual consent for this retrospective study was waived. Our previous study, which included an eligible sample from March 2018 to December 2020, was also included in the meta-analysis [40], thus our validation cohort was enrolled from January 2021 to December 2022. Finally, a total of 210 pathologically confirmed pGGNs (82 IAs and 128 non-IAs) were consecutively enrolled from our institution to construct the validation cohort.

All the patients underwent chest LDCT scans using a second-generation dual-source CT system (Somatom Definition Flash, Siemens Healthcare, Forchheim, Germany). The acquisition parameters of the LDCT were as follows: tube voltage, 100 kV; tube current, 10 to 30 mA; pitch, 1.0; collimation, 64 × 0.625 mm; rotation time, 0.33 s; field of view, 350 mm × 350 mm; iterative reconstruction algorithm (SAFIRE, strength level 5, Siemens Healthcare) with a soft reconstruction kernel (B); slice thickness, 0.5 mm; slice increment, 0.5 mm; reconstruction matrix, 512 × 512. All the patients had an LDCT scan within 1 month before surgical resection.

The uAI platform (United Imaging Healthcare, Shanghai, China), an artificial intelligence (AI) software based on deep learning methods [41,42], was used to automatically detect and segment pGGNs in three dimensions. The segmentation results were assessed by two radiologists (J.L. and H.Q.) in the lung window (window -500 HU, width 1500 HU). As all the segmentation results were satisfactory to both radiologists, no manual adjustments of the segmentation results were conducted to avoid inter- and intra-observer variability. Both the maximal diameter and mean diameter were recorded. To evaluate the consistency of the diameters produced by the AI software and the radiologist, 63 nodules (30% of 210) were randomly selected and measured by a third radiologist (P.Z.) who was blinded to the records of the AI software.

Statistical analysis was performed with MedCalc (version 18.2.1). The categorical variables were analyzed using Fisher's test and the continuous variables were analyzed using the independent sample t-test. The agreement of the diameters produced by the AI software and the radiologist was evaluated using the intra-class correlation coefficient (ICC). To validate the diagnostic performance of the nodule diameter for differentiating IAs from non-IAs, we prespecified the cut-off value by calculating the average of the cut-off values from the included studies in the meta-analysis, weighting by the sample size. The comparisons of sensitivity and specificity were performed using the McNemar test [43].

3. Results

3.1. Characteristics of the Included Studies

The literature search and study selection included 16 studies in the meta-analysis (Figure 1). One study measured both the maximal diameter and mean diameter in the same sample [44], and another one used both the manual method and an automatic algorithm to measure the mean diameter in the same sample [45]. In these conditions, the measurement with a higher AUC was included in the pooled meta-analysis. In addition, one study conducted subgroup analysis with a duplicate sample and, thus, the subgroup with **a** larger sample was included [46]. The details of the study characteristics are presented in Table 1.

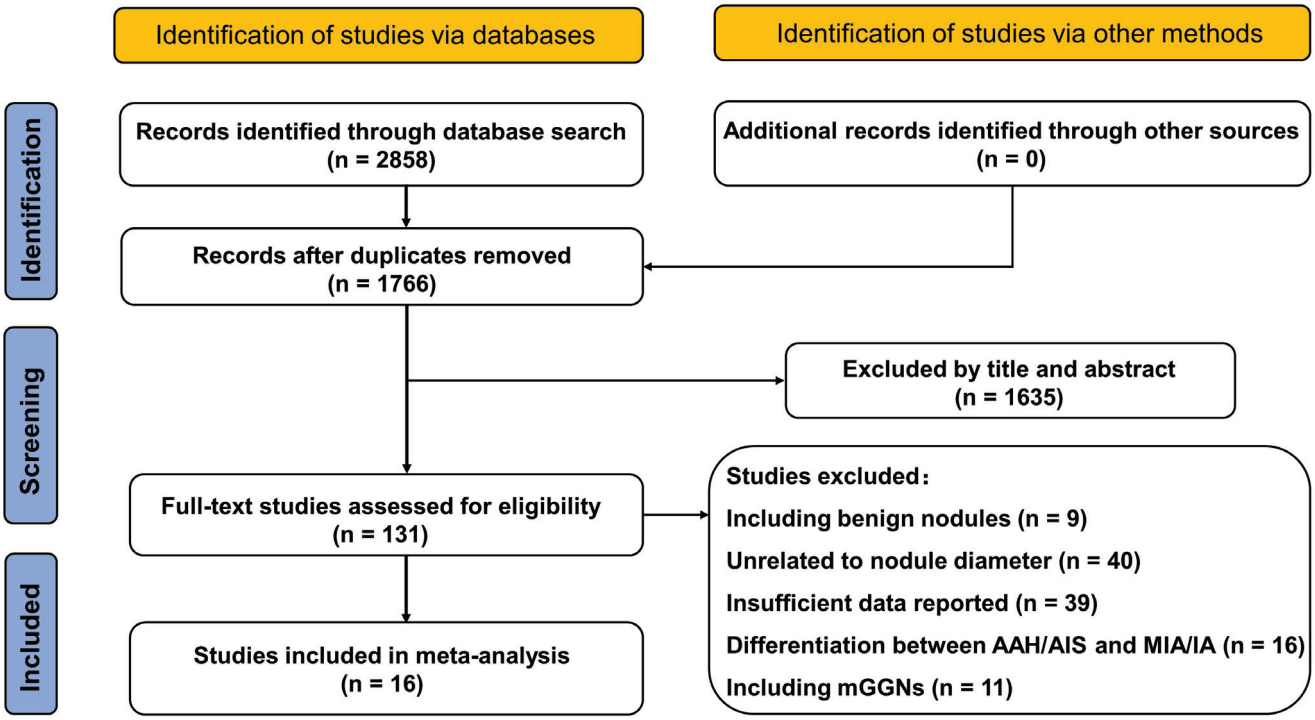

Figure 1. The flowchart of literature search and study selection. AAH: atypical adenomatous hyperplasia; AIS: adenocarcinoma in situ; MIA: minimally invasive adenocarcinoma; IA: invasive adenocarcinoma; mGGNs: mixed ground-glass nodules.

Table 1. Characteristics of the studies included in the meta-analysis.

Study (Year)	Country	No. of Patients	No. of pGGNs		Age (Years)	No. of Males (%)	No. of Smokers (%)	Measure of Diameter	Slice Thickness (mm)	Matrix
			IA	non-IA						
Lim et al. (2013) [20]	Korea	46	18	28	61.4	26 (56.5)	14 (30.4)	maximal	0.75–2.5	NA
Eguchi et al. (2014) [29]	Japan	98	24	77	64.3	39 (38.6)	31 (30.7)	maximal	1.25	NA
Moon et al. (2016) [47]	Korea	83	17	66	58.4	31 (37.3)	19 (22.9)	maximal	NA	NA
Ding et al. (2017) [32]	China	NA	86	275	54.5	125 (34.6)	NA	maximal	1.0	NA
Zhang et al. (2017) # [31]	China	53	15	40	59.0 *	13 (24.5)	0 (0)	maximal	1.25	NA
Han et al. (2018) # [34]	China	154	61	102	55.2	52 (33.8)	NA	maximal	1.25	NA
Kim et al. (2018) [46]	Korea	86	27	59	NA	41 (47.7)	NA	mean	0.625–1.25	NA
Chu et al. (2020) [22]	China	161	31	141	53.4	48 (27.9)	29 (16.9)	mean	0.625	NA
Wang et al. (2020) [30]	China	44	19	25	NA	NA	NA	maximal	0.9	1024 × 1024
Yang et al. (2020) [44]	China	641	136	523	NA	200 (30.3)	309 (46.9)	mean	NA	1024 × 1024
Yu et al. (2020) # [48]	China	62	25	41	55.4	19 (30.6)	4 (6.5)	maximal	1.25	NA
Hu et al. (2021) [33]	China	309	133	211	53.4	98 (28.5)	NA	mean	1.0	NA
Jiang et al. (2021) [23]	China	100	53	47	60.5 *	29 (29.0)	8 (8.0)	maximal	1.0–1.5	512 × 512
Liu et al. (2022) [40]	China	160	64	96	51.4	54(33.8)	NA	mean	0.625	512 × 512
Yu et al. (2022) # [49]	China	42	20	23	56.4	8 (19.1)	NA	maximal	1.0	NA
Zuo et al. (2023) # [45]	China	68	32	49	52.6	18(26.5)	NA	maximal	0.625–1.25	NA

The median or mean age, percentage of males, and percentage of smokers in the studies are calculated according to the number of patients, and those of the others are calculated according to the number of nodules. * The ages are shown as the median, and the others as the mean. pGGNs: pure ground-glass nodules; IA: invasive adenocarcinoma; non-IA: non-invasive adenocarcinoma; NA: not available.

A total of 2564 pGGNs (761 IAs and 1803 non-IAs) were finally included in our meta-analysis. The TP, FP, FN, TN, and cut-off value from each report are presented in Table 2.

Table 2. TP, FP, FN, TN, and cut-off value from the reports included in the meta-analysis.

Study	TP	FP	FN	TN	Cut-off (mm)
Lim et al. (2013) [20]	11	6	7	22	16.4
Eguchi et al. (2014) [29]	23	41	1	36	11.0
Moon et al. (2016) [47]	13	14	4	52	15.0
Ding et al. (2017) [32]	77	45	9	230	12.0
Zhang et al. (2017) [31]	10	9	5	31	16.1
Han et al. (2018) [34]	50	33	11	69	17.2
Kim et al. (2018) [46]	23	21	4	38	10.4
Chu et al. (2020) [22]	27	41	4	100	10.5
Wang et al. (2020) [30]	16	8	3	17	8.5
Yang et al. (2020) [44]	117	131	19	392	10.1
Yu et al. (2020) [48]	21	13	4	28	9.4
Hu et al. (2021) [33]	114	39	19	172	9.8
Jiang et al. (2021) [23]	42	21	11	26	13.9
Liu et al. (2022) [40]	45	26	19	70	10.0
Yu et al. (2022) [49]	13	2	7	21	14.0
Zuo et al. (2023) [45]	28	15	4	34	NA

TP: true positive; FP: false positive; TN: true negative; FN: false negative.

3.2. Quality Assessment

The QUADAS-2 results from the included studies are summarized in Table 3. Regarding patient selection, five studies had high risk of bias and applicability concerns as they did

not include pGGNs of all sizes [20,31,49] or locations [23], or excluded pGGNs that were diagnosed with AAHs [44]. Regarding the index test, three studies did not report whether the readers were blinded to the results reference standard [30,31,46]. In addition, the cut-off values from all the studies were not prespecified, which might lead to overestimation of the diagnostic performance. However, few variations were found in the test technology, execution, or interpretation among these studies and, thus, their overall applicability was sufficient. As for the reference standard, five studies had an unclear risk of bias as they did not report the details of the histopathological assessment [22,31,32,34,48]. In regard to flow and timing, seven studies had an unclear risk of bias as they did not report the time interval between the CT scan and surgery [20,29,31,33,34,44,48].

Table 3. Quality assessment of the studies included in the meta-analysis.

Study	Risk of Bias				Applicability Concerns		
	Patient Selection	Index Test	Reference Standard	Flow and Timing	Patient Selection	Index Test	Reference Standard
Lim et al. (2013) [20]	-	-	+	?	-	+	+
Eguchi et al. (2014) [29]	+	-	+	?	+	+	+
Moon et al. (2016) [47]	+	-	+	+	+	+	+
Ding et al. (2017) [32]	+	-	?	+	+	+	?
Zhang et al. (2017) [31]	-	-	?	?	-	+	?
Han et al. (2018) [34]	+	-	?	?	+	+	?
Kim et al. (2018) [46]	+	-	?	+	+	+	+
Chu et al. (2020) [22]	+	-	?	+	+	+	?
Wang et al. (2020) [30]	+	-	?	+	+	+	+
Yang et al. (2020) [44]	-	-	+	?	-	+	+
Yu et al. (2020) [48]	+	-	?	?	+	+	?
Hu et al. (2021) [33]	+	-	+	?	+	+	+
Jiang et al. (2021) [23]	-	-	+	+	-	+	+
Liu et al. (2022) [40]	+	-	+	+	+	+	+
Yu et al. (2022) [49]	-	-	+	+	-	+	+
Zuo et al. (2023) [45]	+	-	+	+	+	+	+

Index: + low risk, - high risk, ? unclear risk.

3.3. Meta-Analysis of Diagnostic Performance

The sensitivity and specificity of the individual studies varied widely, ranging from 0.61 to 0.96 and 0.47 to 0.91. The pooled sensitivity and specificity were 0.82 (95% confidence interval (CI), 0.78–0.86) and 0.73 (95% CI, 0.67–0.78). The forest plots for all the included studies are shown in Figure 2. The AUC of the SROC was 0.85 (95% CI, 0.82–0.88) (Figure 3).

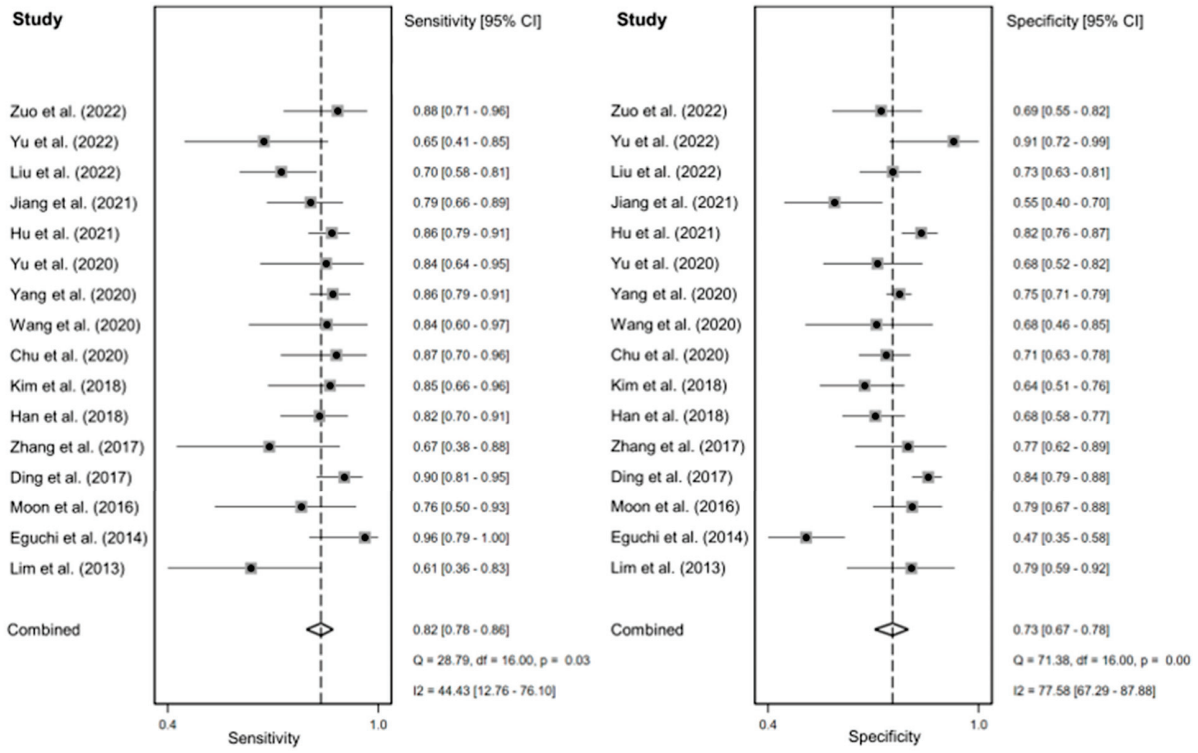

Figure 2. Forest plots on the sensitivity and specificity of the nodule size in predicting the invasiveness of pulmonary adenocarcinomas in pure ground-glass nodules. [20,22,23,29–34,40,44–49]. CI: confidence interval.

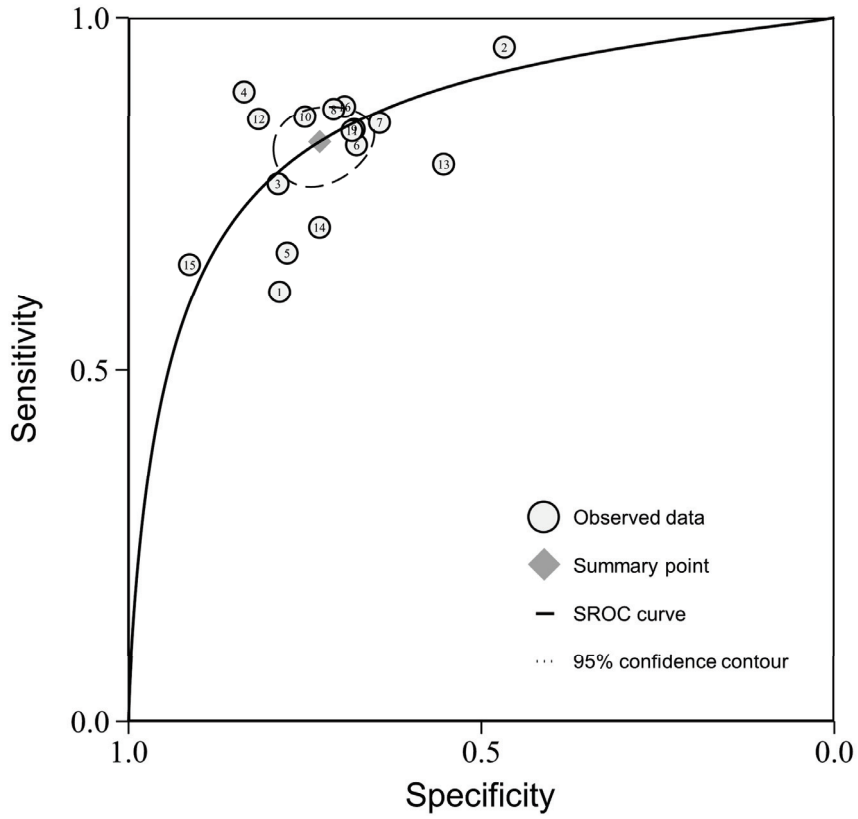

Figure 3. The summary receiver operating characteristic curve (SROC) plot on the diagnostic performance of the nodule size in predicting the invasiveness of pulmonary adenocarcinomas in pure ground-glass nodules.

The results of the meta-regression analysis are shown in Table 4. The percentage of males, percentage of smokers, and slice thickness had no effect on the sensitivity or specificity (all $p > 0.05$). The mean diameter showed higher sensitivity and specificity compared with the maximal diameter (both $p < 0.01$). The reconstruction matrix of 1024 × 1024 showed higher specificity than that of 512 × 512 ($p = 0.01$), but no significant difference in the sensitivity was found between the two reconstruction matrices ($p = 0.11$). A high risk of patient selection was associated with significantly lower sensitivity but higher specificity than a low risk of patient selection ($p = 0.04$ and $p < 0.01$).

Table 4. Meta-regression analysis of related covariates.

Covariates	No. of Reports		Sensitivity (95% CI)	*p*	Specificity (95% CI)	*p*
Percentage of males	16		0.73 (0.06–0.99)	0.77	0.38 (0.02–0.95)	0.38
Percentage of smokers	16		0.96 (0.60–1.00)	0.22	0.76 (0.22–0.97)	0.81
Measure of diameter	11	Maximal diameter	0.82 (0.76–0.87)	<0.01	0.72 (0.66–0.79)	<0.01
	5	Mean diameter	0.84 (0.77–0.90)		0.74 (0.66–0.82)	
Slice thickness	12	All < 1.5 mm	0.84 (0.79–0.88)	0.58	0.73 (0.67–0.79)	0.58
	2	Not all < 1.5 mm	0.73 (0.57–0.88)		0.67 (0.49–0.85)	
Reconstruction matrix	2	1024 × 1024	0.86 (0.80–0.91)	0.11	0.75 (0.71–0.78)	0.01
	2	512 × 512	0.74 (0.66–0.82)		0.67 (0.59–0.75′)	
Patient selection	11	Low risk	0.85 (0.81–0.89)	0.04	0.72 (0.66–0.78)	<0.01
	5	High risk	0.76 (0.67–0.85)		0.76 (0.67–0.85)	

CI: confidence interval.

The I^2 for sensitivity and specificity were 44.43% and 77.58%, indicating moderate to high heterogeneity among the included studies. The regression test for funnel plot asymmetry was insignificant ($p = 0.54$), suggesting a lack of publication bias.

3.4. Validation Using an Independent Sample

The characteristics of the pGGNs in the independent cohort are presented in Table 5. The age, maximal diameter, and mean diameter of the IA group were significantly higher than those of the non-IA group (all $p < 0.01$). No significant difference was found in regard to gender between the groups ($p = 0.88$). The ICCs of the maximal diameter and mean diameter between the AI software and the radiologist were 0.97 (0.96–0.98) and 0.98 (0.96–0.99), suggesting an excellent agreement.

Table 5. Characteristics of pGGNs in the independent sample.

Characteristics	IA (n = 82)	Non-IA (n = 128)	*p*
Gender (male/female)			0.88
Female	53	84	
Male	29	44	
Age	59.6 ± 10.5	49.2 ± 11.8	<0.01
Maximal diameter	16.7 ± 5.6	9.6 ± 3.4	<0.01
Mean diameter	14.8 ± 4.7	8.6 ± 2.9	<0.01

pGGNs: pure ground-glass nodules; IA: invasive adenocarcinoma; non-IA: non-invasive adenocarcinoma.

As the meta-regression results showed that the measure of the diameter affected the diagnostic accuracy, we conducted validation tests using the maximal diameter and the mean diameter, respectively. The prespecified cut-off value was 13.2 mm for the maximal diameter and 10.4 mm for the mean diameter in the pGGNs. In the validation tests,

the sensitivity was 0.72 (0.61–0.81) and the specificity was 0.86 (0.79–0.91) when using the maximal diameter. The sensitivity was 0.85 (0.78–0.91) and the specificity was 0.83 (0.75–0.89) when using the mean diameter (Table 6). The McNemar test further showed the mean diameter had higher sensitivity than the maximal diameter ($p < 0.01$), but no significant difference in the specificity was found between the two measures of the diameter ($p = 0.13$).

Table 6. Diagnostic performance of the nodule size for predicting the invasiveness of pulmonary adenocarcinomas in pGGNs in the independent sample.

Measures	Sensitivity (95% CI)	Specificity (95% CI)	Cut-off
Maximal diameter	0.72 (0.61–0.81)	0.86 (0.79–0.91)	> 13.2 mm
Mean diameter	0.85 (0.78–0.91)	0.83 (0.75–0.89)	> 10.4 mm

pGGNs: pure ground-glass nodules; CI: confidence interval.

4. Discussion

This meta-analysis evaluated the diagnostic performance of the nodule diameter in predicting the invasiveness of pulmonary adenocarcinomas in pGGNs. We found that the pooled AUC, sensitivity, and specificity were 0.85, 0.82, and 0.73. Using the prespecified cut-off value of 13.2 mm for the maximal diameter and 10.4 mm for the mean diameter, our validation cohort of pGGNs showed that the sensitivity and specificity are 0.72 and 0.86 for the maximal diameter, and 0.85 and 0.83 for the mean diameter. Further comparisons showed the mean diameter had higher sensitivity than the maximal diameter. These results suggested that discriminating IAs from non-IAs in pGGNs was feasible using the nodule diameter, and the mean diameter with a cut-off value of 10.4 mm was recommended.

Radiologists usually assess the invasive probability of subsolid nodules using morphological and quantitative features via chest CT. Many morphological features were found to be related to the invasiveness of pGGNs. For example, lobulation was more frequently seen in IAs than Non-IAs [22,50], which was attributed to different rates of growth. The vacuole sign, with histological characteristics of collapse and dilated bronchioles, was highly suggestive of the invasiveness of pGGNs [40,50]. However, previous meta-analysis demonstrated that morphological features, such as the vacuole, speculation, lobulation, and pleural indentation, had inadequate diagnostic value for predicting invasiveness in subsolid nodules [51]. The AUCs, sensitivities, and specificities ranged from 0.60 to 0.67, 0.41 to 0.52, and 0.56 to 0.63. Besides, the morphological features had inter-observer heterogeneity, which was dependent on the subjectivity and experience of the radiologists.

Compared with the morphological features, the quantitative features had better reproducibility with the application of computer-aided diagnosis. As one of the quantitative features, the mean CT value showed a sensitivity of 0.75 and a specificity of 0.81 in predicting invasiveness in subsolid nodules according to a recent meta-analysis, and the optimal cut-off value was −557 HU [52]. However, this meta-analysis included only six studies that contained both pGGNs and mGGNs, which might limit the use of the optimal cut-off value. In recent years, many studies have employed CT-derived radiomic features to differentiate IAs from non-IAs in subsolid nodules, and these radiomic models have shown excellent diagnostic performance [53–57]. The maximal AUC was 0.98 [54]. As radiomics requires additional software, the complexity of this approach limited its integration into clinical practice. Therefore, the nodule diameter, with the balance of objectivity and simplicity, may have diagnostic utility in predicting the invasiveness of pulmonary adenocarcinomas in pGGNs.

Regarding the Lung Imaging Reporting and Data System (Lung-RADS, v2022) and the Fleischner guideline, the diameter was a key feature for the management of pGGNs [18,58]. However, there were discrepancies in management strategies, including the cut-off value of the mean diameter and the interval of screening. Lung-RADS recommends that pGGNs with a mean diameter of < 30 mm should be annually screened. According to the Fleischner

guideline, pGGNs with a mean diameter of < 6 mm require no routine screening, and those with a mean diameter of ≥6 mm should be screened at 6 to 12 months to confirm persistence and then be screened every 2 years. Our results indicated that the mean diameter of 10.4 mm might be the cut-off value between indolence and invasiveness, which could be a potential marker to determine the management strategy for pGGNs. In addition, biopsy was not recommended for pGGNs due to inadequate sampling and false-negative results [18].

According to the results of the meta-regression, the mean diameter showed higher sensitivity and specificity compared with the maximal diameter. In our validation test, the mean diameter showed higher sensitivity than the maximal diameter, which was similar to a previous study [44], and no significant difference was found in regard to the specificity. The current guidelines also recommend using the mean diameter to stratify the risk of the pulmonary nodules [18,25,27,58]. According to our results, the optimal cut-off value for the mean diameter was 10.4 mm for predicting invasiveness in pGGNs. However, as no previous studies conducted statistical comparisons between the diagnostic performance of the mean diameter and the maximal diameter in the same cohort, our results needed further validation using a large sample. The meta-regression results also demonstrated that a larger reconstruction matrix size was associated with higher specificity, which might result from a less partial volume effect, higher spatial resolution, and more accurate measurement of the nodule size [59]. However, this meta-regression result should be taken with caution, being driven by only four studies.

A high risk of patient selection was associated with lower sensitivity but higher specificity than a low risk of patient selection. Not enrolling all eligible pGGNs in the analysis had inherent bias and limited the diagnostic utility in the clinical workflow. Specifically, three of the five studies with a high risk of patient selection excluded small pGGNs (<8 or 10 mm) and resulted in a relatively high cut-off value for the maximal diameter, ranging from 14.0 to 16.4 mm [20,31,49]. The increase in the cut-off value might lead to an increase in missed diagnosis and a decrease in the FP rate for IAs. In addition, all included studies had a high risk of index test as the cut-off values were not prespecified. Therefore, the cut-off values were various, ranging from 8.5 to 17.2 mm for the maximal diameter and 9.8 to 10.8 mm for the mean diameter. In our validation test, we used the prespecified cut-off values derived from previous studies to avoid the risk of bias regarding the index test.

There were several limitations. First, one study with a relatively small sample (81 pGGNs) did not report the cut-off value for the maximal diameter [45], which might slightly affect the prespecified cut-off value used in our validation cohort. Second, the reconstruction matrix was fixed to 512 × 512 in the validation cohort. Further study to validate the effect of this acquisition parameter on diagnostic performance is required.

5. Conclusions

In conclusion, this meta-analysis showed that the nodule diameter had adequate diagnostic performance in differentiating IAs from non-IAs in pGGNs and could be replicated in a validation cohort. The mean diameter with a cut-off value of 10.4 mm was recommended.

Author Contributions: Conceptualization, P.Z. and H.Q.; methodology, J.L. and X.Y; investigation and data collection, Y.L., H.X. and C.H.; statistical analysis, J.L. and X.Y.; writing—original draft preparation, J.L., X.Y. and H.Q.; writing—review and editing, J.L. and H.Q.; project administration, J.L.; funding acquisition, P.Z. and H.Q. All authors have read and agreed to the published version of the manuscript.

Funding: This study was funded by the National Natural Science Foundation of China (grant number 82202141), the Fundamental Research Funds for the Central Universities (grant number ZYGX2021YGCX017), and the Sichuan Science and Technology Program (grant number 2022YFSY0006).

Institutional Review Board Statement: The validation part of this study involving human data and materials was conducted in accordance with the Declaration of Helsinki and approved by the Ethics Committees at Sichuan Cancer Hospital (protocol code SCCHEC-02-2020-055).

Informed Consent Statement: The informed consent requirement was waived by the Ethics Committees at Sichuan Cancer Hospital due to the retrospective nature of the validation part of this study.

Data Availability Statement: The data presented in the validation part of this study are available on request from the corresponding author. The data are not publicly available due to privacy.

Conflicts of Interest: The authors declare no conflicts of interest.

References

1. Sung, H.; Ferlay, J.; Siegel, R.L.; Laversanne, M.; Soerjomataram, I.; Jemal, A.; Bray, F. Global Cancer Statistics 2020: GLOBOCAN Estimates of Incidence and Mortality Worldwide for 36 Cancers in 185 Countries. *CA A Cancer J. Clin.* **2021**, *71*, 209–249. [CrossRef]
2. Siegel, R.L.; Miller, K.D.; Fuchs, H.E.; Jemal, A. Cancer statistics, 2022. *CA A Cancer J. Clin.* **2022**, *72*, 7–33. [CrossRef] [PubMed]
3. Aberle, D.R.; Adams, A.M.; Berg, C.D.; Black, W.C.; Clapp, J.D.; Fagerstrom, R.M.; Gareen, I.F.; Gatsonis, C.; Marcus, P.M.; Sicks, J.D. Reduced lung-cancer mortality with low-dose computed tomographic screening. *N. Engl. J. Med.* **2011**, *365*, 395–409. [CrossRef] [PubMed]
4. Aberle, D.R.; DeMello, S.; Berg, C.D.; Black, W.C.; Brewer, B.; Church, T.R.; Clingan, K.L.; Duan, F.; Fagerstrom, R.M.; Gareen, I.F.; et al. Results of the two incidence screenings in the National Lung Screening Trial. *N. Engl. J. Med.* **2013**, *369*, 920–931. [CrossRef]
5. Lee, C.T. What do we know about ground-glass opacity nodules in the lung? *Transl. Lung Cancer Res.* **2015**, *4*, 656–659. [CrossRef] [PubMed]
6. Pedersen, J.H.; Saghir, Z.; Wille, M.M.; Thomsen, L.H.; Skov, B.G.; Ashraf, H. Ground-Glass Opacity Lung Nodules in the Era of Lung Cancer CT Screening: Radiology, Pathology, and Clinical Management. *Oncology* **2016**, *30*, 266–274. [PubMed]
7. Zhang, Y.; Jheon, S.; Li, H.; Zhang, H.; Xie, Y.; Qian, B.; Lin, K.; Wang, S.; Fu, C.; Hu, H.; et al. Results of low-dose computed tomography as a regular health examination among Chinese hospital employees. *J. Thorac. Cardiovasc. Surg.* **2020**, *160*, 824–831.e824. [CrossRef]
8. Kobayashi, Y.; Mitsudomi, T.; Sakao, Y.; Yatabe, Y. Genetic features of pulmonary adenocarcinoma presenting with ground-glass nodules: The differences between nodules with and without growth. *Ann. Oncol.* **2015**, *26*, 156–161. [CrossRef]
9. Cheng, T.Y.; Cramb, S.M.; Baade, P.D.; Youlden, D.R.; Nwogu, C.; Reid, M.E. The International Epidemiology of Lung Cancer: Latest Trends, Disparities, and Tumor Characteristics. *J. Thorac. Oncol.* **2016**, *11*, 1653–1671. [CrossRef]
10. Yang, W.; Sun, Y.; Fang, W.; Qian, F.; Ye, J.; Chen, Q.; Jiang, Y.; Yu, K.; Han, B. High-resolution Computed Tomography Features Distinguishing Benign and Malignant Lesions Manifesting as Persistent Solitary Subsolid Nodules. *Clin. Lung Cancer* **2018**, *19*, e75–e83. [CrossRef]
11. Travis, W.D.; Brambilla, E.; Nicholson, A.G.; Yatabe, Y.; Austin, J.H.M.; Beasley, M.B.; Chirieac, L.R.; Dacic, S.; Duhig, E.; Flieder, D.B.; et al. The 2015 World Health Organization Classification of Lung Tumors: Impact of Genetic, Clinical and Radiologic Advances Since the 2004 Classification. *J. Thorac. Oncol.* **2015**, *10*, 1243–1260. [CrossRef] [PubMed]
12. Travis, W.D.; Asamura, H.; Bankier, A.A.; Beasley, M.B.; Detterbeck, F.; Flieder, D.B.; Goo, J.M.; MacMahon, H.; Naidich, D.; Nicholson, A.G.; et al. The IASLC Lung Cancer Staging Project: Proposals for Coding T Categories for Subsolid Nodules and Assessment of Tumor Size in Part-Solid Tumors in the Forthcoming Eighth Edition of the TNM Classification of Lung Cancer. *J. Thorac. Oncol.* **2016**, *11*, 1204–1223. [CrossRef] [PubMed]
13. Nicholson, A.G.; Tsao, M.S.; Beasley, M.B.; Borczuk, A.C.; Brambilla, E.; Cooper, W.A.; Dacic, S.; Jain, D.; Kerr, K.M.; Lantuejoul, S.; et al. The 2021 WHO Classification of Lung Tumors: Impact of Advances Since 2015. *J. Thorac. Oncol.* **2022**, *17*, 362–387. [CrossRef] [PubMed]
14. Liu, S.; Wang, R.; Zhang, Y.; Li, Y.; Cheng, C.; Pan, Y.; Xiang, J.; Zhang, Y.; Chen, H.; Sun, Y. Precise Diagnosis of Intraoperative Frozen Section Is an Effective Method to Guide Resection Strategy for Peripheral Small-Sized Lung Adenocarcinoma. *J. Clin. Oncol.* **2016**, *34*, 307–313. [CrossRef]
15. Yotsukura, M.; Asamura, H.; Motoi, N.; Kashima, J.; Yoshida, Y.; Nakagawa, K.; Shiraishi, K.; Kohno, T.; Yatabe, Y.; Watanabe, S.I. Long-Term Prognosis of Patients With Resected Adenocarcinoma In Situ and Minimally Invasive Adenocarcinoma of the Lung. *J. Thorac. Oncol.* **2021**, *16*, 1312–1320. [CrossRef]
16. Deng, C.; Zheng, Q.; Zhang, Y.; Jin, Y.; Shen, X.; Nie, X.; Fu, F.; Ma, X.; Ma, Z.; Wen, Z.; et al. Validation of the Novel International Association for the Study of Lung Cancer Grading System for Invasive Pulmonary Adenocarcinoma and Association With Common Driver Mutations. *J. Thorac. Oncol.* **2021**, *16*, 1684–1693. [CrossRef]
17. Hou, L.; Wang, T.; Chen, D.; She, Y.; Deng, J.; Yang, M.; Zhang, Y.; Zhao, M.; Zhong, Y.; Ma, M.; et al. Prognostic and predictive value of the newly proposed grading system of invasive pulmonary adenocarcinoma in Chinese patients: A retrospective multicohort study. *Mod. Pathol.* **2022**, *35*, 749–756. [CrossRef]
18. MacMahon, H.; Naidich, D.P.; Goo, J.M.; Lee, K.S.; Leung, A.N.C.; Mayo, J.R.; Mehta, A.C.; Ohno, Y.; Powell, C.A.; Prokop, M.; et al. Guidelines for Management of Incidental Pulmonary Nodules Detected on CT Images: From the Fleischner Society 2017. *Radiology* **2017**, *284*, 228–243. [CrossRef]

19. Lee, S.M.; Park, C.M.; Goo, J.M.; Lee, H.J.; Wi, J.Y.; Kang, C.H. Invasive pulmonary adenocarcinomas versus preinvasive lesions appearing as ground-glass nodules: Differentiation by using CT features. *Radiology* **2013**, *268*, 265–273. [CrossRef]
20. Lim, H.J.; Ahn, S.; Lee, K.S.; Han, J.; Shim, Y.M.; Woo, S.; Kim, J.H.; Yie, M.; Lee, H.Y.; Yi, C.A. Persistent pure ground-glass opacity lung nodules ≥ 10 mm in diameter at CT scan: Histopathologic comparisons and prognostic implications. *Chest* **2013**, *144*, 1291–1299. [CrossRef]
21. Liang, J.; Xu, X.Q.; Xu, H.; Yuan, M.; Zhang, W.; Shi, Z.F.; Yu, T.F. Using the CT features to differentiate invasive pulmonary adenocarcinoma from pre-invasive lesion appearing as pure or mixed ground-glass nodules. *Br. J. Radiol.* **2015**, *88*, 20140811. [CrossRef]
22. Chu, Z.G.; Li, W.J.; Fu, B.J.; Lv, F.J. CT Characteristics for Predicting Invasiveness in Pulmonary Pure Ground-Glass Nodules. *AJR. Am. J. Roentgenol.* **2020**, *215*, 351–358. [CrossRef]
23. Jiang, Y.; Che, S.; Ma, S.; Liu, X.; Guo, Y.; Liu, A.; Li, G.; Li, Z. Radiomic signature based on CT imaging to distinguish invasive adenocarcinoma from minimally invasive adenocarcinoma in pure ground-glass nodules with pleural contact. *Cancer Imaging* **2021**, *21*, 1. [CrossRef]
24. Bai, C.; Choi, C.M.; Chu, C.M.; Anantham, D.; Chung-Man Ho, J.; Khan, A.Z.; Lee, J.M.; Li, S.Y.; Saenghirunvattana, S.; Yim, A. Evaluation of Pulmonary Nodules: Clinical Practice Consensus Guidelines for Asia. *Chest* **2016**, *150*, 877–893. [CrossRef]
25. Christensen, J.; Prosper, A.E.; Wu, C.C.; Chung, J.; Lee, E.; Elicker, B.; Hunsaker, A.R.; Petranovic, M.; Sandler, K.L.; Stiles, B.; et al. ACR Lung-RADS v2022: Assessment Categories and Management Recommendations. *J. Am. Coll. Radiol.* **2023**, *9*, S1546-1440(23)00761-5. [CrossRef]
26. Mazzone, P.J.; Silvestri, G.A.; Souter, L.H.; Caverly, T.J.; Kanne, J.P.; Katki, H.A.; Wiener, R.S.; Detterbeck, F.C. Screening for Lung Cancer: CHEST Guideline and Expert Panel Report. *Chest* **2021**, *160*, e427–e494. [CrossRef]
27. Wood, D.E.; Kazerooni, E.A.; Aberle, D.; Berman, A.; Brown, L.M.; Eapen, G.A.; Ettinger, D.S.; Ferguson, J.S.; Hou, L.; Kadaria, D.; et al. NCCN Guidelines®Insights: Lung Cancer Screening, Version 1.2022. *J. Natl. Compr. Cancer Netw.* **2022**, *20*, 754–764. [CrossRef]
28. Kodama, K.; Higashiyama, M.; Yokouchi, H.; Takami, K.; Kuriyama, K.; Kusunoki, Y.; Nakayama, T.; Imamura, F. Natural history of pure ground-glass opacity after long-term follow-up of more than 2 years. *Ann. Thorac. Surg.* **2002**, *73*, 386–392. [CrossRef]
29. Eguchi, T.; Kondo, R.; Kawakami, S.; Matsushita, M.; Yoshizawa, A.; Hara, D.; Matsuoka, S.; Takeda, T.; Miura, K.; Agatsuma, H.; et al. Computed tomography attenuation predicts the growth of pure ground-glass nodules. *Lung Cancer* **2014**, *84*, 242–247. [CrossRef]
30. Wang, H.; Weng, Q.; Hui, J.; Fang, S.; Wu, X.; Mao, W.; Chen, M.; Zheng, L.; Wang, Z.; Zhao, Z.; et al. Value of TSCT Features for Differentiating Preinvasive and Minimally Invasive Adenocarcinoma From Invasive Adenocarcinoma Presenting as Subsolid Nodules Smaller Than 3 cm. *Acad. Radiol.* **2020**, *27*, 395–403. [CrossRef]
31. Zhang, Y.; Tang, J.; Xu, J.; Cheng, J.; Wu, H. Analysis of pulmonary pure ground-glass nodule in enhanced dual energy CT imaging for predicting invasive adenocarcinoma: Comparing with conventional thin-section CT imaging. *J. Thorac. Dis.* **2017**, *9*, 4967–4978. [CrossRef]
32. Ding, H.; Shi, J.; Zhou, X.; Xie, D.; Song, X.; Yang, Y.; Liu, Z.; Wang, H. Value of CT Characteristics in Predicting Invasiveness of Adenocarcinoma Presented as Pulmonary Ground-Glass Nodules. *Thorac. Cardiovasc. Surg.* **2017**, *65*, 136–141. [CrossRef]
33. Hu, F.; Huang, H.; Jiang, Y.; Feng, M.; Wang, H.; Tang, M.; Zhou, Y.; Tan, X.; Liu, Y.; Xu, C.; et al. Discriminating invasive adenocarcinoma among lung pure ground-glass nodules: A multi-parameter prediction model. *J. Thorac. Dis.* **2021**, *13*, 5383–5394. [CrossRef]
34. Han, L.; Zhang, P.; Wang, Y.; Gao, Z.; Wang, H.; Li, X.; Ye, Z. CT quantitative parameters to predict the invasiveness of lung pure ground-glass nodules (pGGNs). *Clin. Radiol.* **2018**, *73*, 504.e501–504.e507. [CrossRef]
35. Page, M.J.; McKenzie, J.E.; Bossuyt, P.M.; Boutron, I.; Hoffmann, T.C.; Mulrow, C.D.; Shamseer, L.; Tetzlaff, J.M.; Akl, E.A.; Brennan, S.E.; et al. The PRISMA 2020 statement: An updated guideline for reporting systematic reviews. *BMJ* **2021**, *372*, n71. [CrossRef]
36. Whiting, P.F.; Rutjes, A.W.; Westwood, M.E.; Mallett, S.; Deeks, J.J.; Reitsma, J.B.; Leeflang, M.M.; Sterne, J.A.; Bossuyt, P.M. QUADAS-2: A revised tool for the quality assessment of diagnostic accuracy studies. *Ann. Intern. Med.* **2011**, *155*, 529–536. [CrossRef]
37. Vamvakas, E.C. Meta-analyses of studies of the diagnostic accuracy of laboratory tests: A review of the concepts and methods. *Arch. Pathol. Lab. Med.* **1998**, *122*, 675–686.
38. Higgins, J.P.; Thompson, S.G. Quantifying heterogeneity in a meta-analysis. *Stat. Med.* **2002**, *21*, 1539–1558. [CrossRef]
39. Egger, M.; Davey Smith, G.; Schneider, M.; Minder, C. Bias in meta-analysis detected by a simple, graphical test. *BMJ* **1997**, *315*, 629–634. [CrossRef]
40. Liu, J.; Yang, X.; Li, Y.; Xu, H.; He, C.; Qing, H.; Ren, J.; Zhou, P. Development and validation of qualitative and quantitative models to predict invasiveness of lung adenocarcinomas manifesting as pure ground-glass nodules based on low-dose computed tomography during lung cancer screening. *Quant. Imaging Med. Surg.* **2022**, *12*, 2917–2931. [CrossRef]
41. Mu, G.; Chen, Y.; Wu, D.; Zhan, Y.; Zhou, X.; Gao, Y. *Relu Cascade of Feature Pyramid Networks for CT Pulmonary Nodule Detection*; Springer International Publishing: Cham, Switzerland, 2019; pp. 444–452.

42. Wang, Q.; Zhou, X.; Wang, C.; Liu, Z.; Huang, J.; Zhou, Y.; Li, C.; Zhuang, H.; Cheng, J.Z.J.I.A. WGAN-Based Synthetic Minority Over-Sampling Technique: Improving Semantic Fine-Grained Classification for Lung Nodules in CT Images. *IEEE Access* **2019**, *7*, 18450–18463. [CrossRef]
43. Hawass, N.E. Comparing the sensitivities and specificities of two diagnostic procedures performed on the same group of patients. *Br. J. Radiol.* **1997**, *70*, 360–366. [CrossRef]
44. Yang, H.H.; Lv, Y.L.; Fan, X.H.; Ai, Z.Y.; Xu, X.C.; Ye, B.; Hu, D.Z. Factors distinguishing invasive from pre-invasive adenocarcinoma presenting as pure ground glass pulmonary nodules. *Radiat. Oncol.* **2020**, *15*, 186. [CrossRef]
45. Zuo, Z.; Wang, P.; Zeng, W.; Qi, W.; Zhang, W. Measuring pure ground-glass nodules on computed tomography: Assessing agreement between a commercially available deep learning algorithm and radiologists' readings. *Acta Radiol.* **2023**, *64*, 1422–1430. [CrossRef]
46. Kim, H.; Goo, J.M.; Park, C.M. Evaluation of T categories for pure ground-glass nodules with semi-automatic volumetry: Is mass a better predictor of invasive part size than other volumetric parameters? *Eur. Radiol.* **2018**, *28*, 4288–4295. [CrossRef]
47. Moon, Y.; Sung, S.W.; Lee, K.Y.; Sim, S.B.; Park, J.K. Pure ground-glass opacity on chest computed tomography: Predictive factors for invasive adenocarcinoma. *J. Thorac. Dis.* **2016**, *8*, 1561–1570. [CrossRef]
48. Yu, Y.; Cheng, J.J.; Li, J.Y.; Zhang, Y.; Lin, L.Y.; Zhang, F.; Xu, J.R.; Zhao, X.J.; Wu, H.W. Determining the invasiveness of pure ground-glass nodules using dual-energy spectral computed tomography. *Transl. Lung Cancer Res.* **2020**, *9*, 484–495. [CrossRef]
49. Yu, Y.; Fu, Y.; Chen, X.; Zhang, Y.; Zhang, F.; Li, X.; Zhao, X.; Cheng, J.; Wu, H. Dual-layer spectral detector CT: Predicting the invasiveness of pure ground-glass adenocarcinoma. *Clin. Radiol.* **2022**, *77*, e458–e465. [CrossRef]
50. Hsu, W.C.; Huang, P.C.; Pan, K.T.; Chuang, W.Y.; Wu, C.Y.; Wong, H.F.; Yang, C.T.; Wan, Y.L. Predictors of Invasive Adenocarcinomas among Pure Ground-Glass Nodules Less Than 2 cm in Diameter. *Cancers* **2021**, *13*, 3945. [CrossRef]
51. Dai, J.; Yu, G.; Yu, J. Can CT imaging features of ground-glass opacity predict invasiveness? A meta-analysis. *Thorac. Cancer* **2018**, *9*, 452–458. [CrossRef]
52. He, S.; Chen, C.; Wang, Z.; Yu, X.; Liu, S.; Huang, Z.; Chen, C.; Liang, Z.; Chen, C. The use of the mean computed-tomography value to predict the invasiveness of ground-glass nodules: A meta-analysis. *Asian J. Surg.* **2023**, *46*, 677–682. [CrossRef]
53. Fan, L.; Fang, M.; Li, Z.; Tu, W.; Wang, S.; Chen, W.; Tian, J.; Dong, D.; Liu, S. Radiomics signature: A biomarker for the preoperative discrimination of lung invasive adenocarcinoma manifesting as a ground-glass nodule. *Eur. Radiol.* **2019**, *29*, 889–897. [CrossRef]
54. Wu, G.; Woodruff, H.C.; Shen, J.; Refaee, T.; Sanduleanu, S.; Ibrahim, A.; Leijenaar, R.T.H.; Wang, R.; Xiong, J.; Bian, J.; et al. Diagnosis of Invasive Lung Adenocarcinoma Based on Chest CT Radiomic Features of Part-Solid Pulmonary Nodules: A Multicenter Study. *Radiology* **2020**, *297*, 451–458. [CrossRef]
55. Wu, L.; Gao, C.; Ye, J.; Tao, J.; Wang, N.; Pang, P.; Xiang, P.; Xu, M. The value of various peritumoral radiomic features in differentiating the invasiveness of adenocarcinoma manifesting as ground-glass nodules. *Eur. Radiol.* **2021**, *31*, 9030–9037. [CrossRef]
56. Li, Y.; Liu, J.; Yang, X.; Xu, H.; Qing, H.; Ren, J.; Zhou, P. Prediction of invasive adenocarcinomas manifesting as pure ground-glass nodules based on radiomic signature of low-dose CT in lung cancer screening. *Br. J. Radiol.* **2022**, *95*, 20211048. [CrossRef]
57. Kao, T.N.; Hsieh, M.S.; Chen, L.W.; Yang, C.J.; Chuang, C.C.; Chiang, X.H.; Chen, Y.C.; Lee, Y.H.; Hsu, H.H.; Chen, C.M.; et al. CT-Based Radiomic Analysis for Preoperative Prediction of Tumor Invasiveness in Lung Adenocarcinoma Presenting as Pure Ground-Glass Nodule. *Cancers* **2022**, *14*, 5888. [CrossRef]
58. American College of Radiology. Lung CT Screening Reporting and Data System (Lung-RADS, v2022). Available online: https://www.acr.org/Clinical-Resources/Reporting-and-Data-Systems/Lung-Rads (accessed on 29 December 2023).
59. Goo, J.M.; Tongdee, T.; Tongdee, R.; Yeo, K.; Hildebolt, C.F.; Bae, K.T. Volumetric measurement of synthetic lung nodules with multi-detector row CT: Effect of various image reconstruction parameters and segmentation thresholds on measurement accuracy. *Radiology* **2005**, *235*, 850–856. [CrossRef]

MDPI AG
Grosspeteranlage 5
4052 Basel
Switzerland
Tel.: +41 61 683 77 34

Diagnostics Editorial Office
E-mail: diagnostics@mdpi.com
www.mdpi.com/journal/diagnostics

Academic Open
Access Publishing

mdpi.com

ISBN 978-3-7258-4484-5